

THE ROLE OF MEMBRANE POTENTIAL
DYNAMICS IN CELL BEHAVIOURS:
INVESTIGATING THE MEMBRANE
POTENTIAL DYNAMICS IN THE JURKAT
AND HMEC-1 CELL LINES USING THE
CONTINUOUS WAVELET TRANSFORM

Shakil Patel, MSc
Division of Biomedical and Life Sciences
Lancaster University

This thesis is submitted in partial fulfilment of the requirements for the degree of
Doctor of Philosophy
November 2016

DECLARATION

I, Shakil Patel confirm that the work presented in this thesis is my own and has not been submitted in substantially the same form for the award of a higher degree elsewhere. Where information has been derived from other sources, I confirm this has been indicated in the thesis.

Signed: _____

Date: _____

Shakil Patel (MSc)

Shakil Patel, MSc

Lancaster University, September 2015

ABSTRACT

The role of the plasma membrane potential is most commonly associated with the generation of action potentials in excitable cells, however, experimental evidence suggests that this membrane potential is also linked to various behaviours in all cells (Blackiston et al., 2009). These cell behaviours include cell proliferation, cell migration and even cell survival. The membrane potential has been thought to influence these cell behaviours upstream of the classical transduction pathways. Recent evidence suggests that the membrane potential is dynamic rather than static and this dynamic behaviour may encode information on cell behaviours. The whole cell patch clamping technique coupled with the continuous wavelet transform (CWT) technique was used to investigate the presence of fluctuations and oscillations in the membrane potential of Jurkat cells and HMEC-1 cells. The underlying nature of the membrane potential dynamics of Jurkat cells was investigated by perturbing the extracellular concentration of either K^+ , Na^+ or Cl^- . The membrane potential dynamics of proliferating, non-proliferating and activated Jurkat cells was investigated by either varying the culture medium or treating the cells with the concavalin A mitogen. The membrane potential dynamics of HMEC-1 endothelial cells was also investigated. The magnitude of the static membrane potential of proliferating Jurkat cells was significantly more depolarised than non-proliferating Jurkat cells – a trend which has been observed in a wide range of cell types. The membrane potential dynamics appear to be driven by the conductance of ions rather than the magnitude of the static membrane potential per se. In summary, this thesis has proven that the membrane potential varies with cell state and the CWT technique can be used to interrogate recordings of the membrane potential to ascertain information on the membrane potential dynamics that cannot be currently determined by other techniques.

ACKNOWLEDGEMENTS

I would like to thank my supervisors, Professor Jane Owen-Lynch, Dr. Stephen Roberts and Professor Aneta Stefanovska for their help and support throughout my PhD. Without their help, support and time I would not be in the position I currently am. I would also like to thank Michelle Bates and Dr. Matt Hodges who helped me with problems and difficulties in the lab. I would like to thank my fellow PhD students who provided me with support during the PhD. Finally, I would like to thank Lancaster University and Leese Bequest for funding my PhD research.

LIST OF TABLES

| | |
|-----------------|-----|
| TABLE 1.1 | 5 |
| TABLE 1.2 | 9 |
| TABLE 1.3 | 13 |
| TABLE 1.4 | 21 |
| TABLE 1.5 | 31 |
| TABLE 1.6 | 41 |
| TABLE 1.7 | 43 |
| TABLE 2.1 | 57 |
| TABLE 2.2 | 58 |
| TABLE 2.3 | 59 |
| TABLE 2.4 | 62 |
| TABLE 2.5 | 63 |
| TABLE 2.6 | 65 |
| TABLE 4.1 | 145 |
| TABLE 4.2 | 150 |

LIST OF FIGURES

| | |
|-------------------|-----|
| FIGURE 1.1 | 3 |
| FIGURE 1.2 | 5 |
| FIGURE 1.3 | 8 |
| FIGURE 1.4 | 13 |
| FIGURE 1.5 | 26 |
| FIGURE 1.6 | 28 |
| FIGURE 1.7 | 34 |
| FIGURE 1.8 | 35 |
| FIGURE 2.1 | 51 |
| FIGURE 2.2 | 55 |
| FIGURE 3.1 | 73 |
| FIGURE 3.2 | 75 |
| FIGURE 3.3 | 77 |
| FIGURE 3.4 | 79 |
| FIGURE 3.5 | 81 |
| FIGURE 3.6 | 83 |
| FIGURE 3.7 | 84 |
| FIGURE 3.8 | 85 |
| FIGURE 3.9 | 87 |
| FIGURE 3.10 | 90 |
| FIGURE 3.11 | 92 |
| FIGURE 3.12 | 95 |
| FIGURE 3.13 | 97 |
| FIGURE 3.14 | 100 |
| FIGURE 3.15 | 103 |
| FIGURE 3.16 | 105 |
| FIGURE 4.1 | 120 |
| FIGURE 4.2 | 121 |
| FIGURE 4.3 | 123 |
| FIGURE 4.4 | 125 |
| FIGURE 4.5 | 128 |
| FIGURE 4.6 | 131 |

| | |
|-------------------|-----|
| FIGURE 4.7 | 133 |
| FIGURE 4.8 | 135 |
| FIGURE 4.9 | 136 |
| FIGURE 4.10 | 141 |
| FIGURE 4.11 | 146 |
| FIGURE 4.12 | 148 |
| FIGURE 4.13 | 149 |
| FIGURE 5.1 | 166 |
| FIGURE 5.2 | 172 |
| FIGURE 5.3 | 173 |
| FIGURE 5.4 | 179 |
| FIGURE 5.5 | 181 |
| FIGURE 5.6 | 183 |
| FIGURE 5.7 | 185 |
| FIGURE 5.8 | 189 |
| FIGURE 5.9 | 193 |
| FIGURE 5.10 | 195 |
| FIGURE 5.11 | 197 |
| FIGURE 6.1 | 212 |
| FIGURE 6.2 | 215 |
| FIGURE 6.3 | 220 |
| FIGURE 6.4 | 224 |
| FIGURE 6.5 | 225 |
| FIGURE 6.6 | 228 |
| FIGURE 6.7 | 231 |
| FIGURE 6.8 | 235 |
| FIGURE 6.9 | 237 |
| FIGURE 6.10 | 241 |
| FIGURE 6.11 | 242 |

LIST OF ABBREVIATIONS AND ACRONYMS

- 4-AP = 4-Aminopyridine
ACh = acetylcholine
ConA = concanavlin A
CWT= continuous wavelet transform
 E_{rev} = reversal potential
HMEC-1 = Human microvascular endothelial cell-1
HUVEC = Human umbilical vein endothelial cells
IL-2 = interleukin 2
IV = current voltage
KV = channels = Voltage-gated K channels
L-NMMA = N(G)-monomethyl arginine
MES = 2-ethanosulfonic acid
NPC= neural precursor cells
NPPB = 5-nitro-2-(3-phenylpropylamino)-benzoic acid
NRSF = neuron-restrictive silencer factor
PBS = phosphate buffered saline
PHA phytohaemagglutinin
ROS = reactive oxygen species
shRNA = short hairpin RNA
siRNA = small interference RNA
SNP = sodium nitroprusside
TEA = tetraethylammonium
VSP = voltage sensitive phosphate

CONTENTS

| | |
|---|----------|
| 1 INTRODUCTION | 1 |
| 1.1 OVERVIEW | 1 |
| 1.2 THE RESTING MEMBRANE POTENTIAL..... | 4 |
| 1.2.1 The resting plasma membrane potential | 4 |
| 1.2.2 Overview of ion channels, pumps and carriers..... | 6 |
| 1.2.3 Selectivity and gating properties of membrane transport proteins | 10 |
| 1.3 THE FUNCTIONAL ROLE OF THE MEMBRANE POTENTIAL IN CELL BEHAVIOUR.... | 11 |
| 1.3.1 Introduction..... | 11 |
| 1.3.2 Overview of the cell cycle | 11 |
| 1.3.3 The role of specific membrane transport proteins in the regulation of proliferation..... | 16 |
| 1.3.4 The membrane potential and ion channels in disease states | 22 |
| 1.3.5 The effects of cell signalling mechanisms and cell cycle progression on ion channel activity and the membrane potential | 22 |
| 1.4 COMPONENTS OF THE PATHWAYS ASSOCIATED WITH BIOELECTRIC CONTROL OF CELL BEHAVIOURS..... | 24 |
| 1.4.1 Introduction..... | 24 |
| 1.4.2 Mechanisms of Bioelectric signalling in cell behaviours involving Ca^{2+} | 27 |
| 1.4.3 Mechanisms of bioelectric signalling in cell behaviours associated with intracellular ions | 29 |
| 1.4.4 Components linking ion channel activity and cell cycle regulators | 30 |
| 1.5 INTRODUCTION TO THE DYNAMIC BEHAVIOUR WITHIN HUMAN BIOLOGY | 32 |
| 1.5.1 The dynamic nature of the membrane potential | 35 |
| 1.6 RECORDING THE PLASMA MEMBRANE POTENTIAL..... | 37 |
| 1.6.1 Optical techniques to measure the membrane potential | 37 |
| 1.6.2 Electrophysiological techniques to record the membrane potential | 38 |
| 1.7 MODEL CELL SYSTEMS TO INVESTIGATE MEMBRANE POTENTIAL DYNAMICS.... | 39 |
| 1.7.1 Jurkat cells – T-lymphocytes | 39 |
| 1.7.2 HMEC-1 endothelial cells..... | 39 |
| 1.8 HYPOTHESIS AND AIMS OF THE CURRENT PROJECT | 44 |

| | |
|--|-----------|
| 2 MATERIALS AND METHODS | 45 |
| 2.1 MATERIALS | 45 |
| 2.2 METHODS..... | 45 |
| 2.2.1 Cell culture..... | 45 |
| 2.2.2 Trypsinising HMEC-1 Cells | 46 |
| 2.2.3 Cell viability and proliferation assays..... | 47 |
| 2.2.4 Cell cycle analysis..... | 48 |
| 2.2.5 Interluekin-2 secretion assay..... | 49 |
| 2.3 PATCH CLAMPING..... | 50 |
| 2.3.1 Patch clamping measurements..... | 50 |
| 2.3.2 Procedure for patch clamping | 53 |
| 2.3.3 Intracellular and extracellular solutions used in the patch clamping experiments | 56 |
| 2.4 STIMULATION PROTOCOLS | 66 |
| 2.5 DATA ANALYSIS | 66 |
| 2.5.1 Analysis of the whole cell currents | 66 |
| 2.5.2 Nonlinear analysis of the membrane potential using continuous wavelet transform..... | 67 |
| 2.5.3 Statistical Analysis..... | 68 |
| 3 ELECTROPHYSIOLOGICAL CHARACTERISATION OF JURKAT CELLS IN THE LOG PHASE OF GROWTH | 70 |
| 3.1 INTRODUCTION..... | 70 |
| 3.2 RESULTS..... | 72 |
| 3.2.1 Ascertaining culture conditions required to yield Jurkat cells in an actively proliferating state..... | 72 |
| 3.2.2 The membrane potential of actively proliferating Jurkat cells | 74 |
| 3.2.3 The resting membrane potential of actively proliferating Jurkat cells | 76 |
| 3.2.4 Whole cell currents observed in Jurkat cells cultured in standard culture conditions..... | 78 |
| 3.2.5 The time dependent activating current with slow inactivation was carried by K ⁺ | 80 |
| Channel recovery and inactivation kinetics of the time dependent K ⁺ current | 82 |

| | |
|---|------------|
| Gating and activation kinetics of the time dependent K ⁺ current | 86 |
| Pharmacology of the time dependent K ⁺ current..... | 89 |
| 3.2.6 Instantaneously activating outward currents..... | 94 |
| 3.2.7 Slow activating currents..... | 104 |
| 3.3 DISCUSSION..... | 106 |
| 4 EFFECT OF CELL STATUS ON THE ELECTROPHYSIOLOGICAL CHARACTERISATION OF JURKAT CELLS | 115 |
| 4.1 INTRODUCTION..... | 115 |
| 4.2 RESULTS..... | 118 |
| 4.2.1 Ascertaining the culture conditions required for achieving Jurkat cells in a non-proliferative state | 118 |
| 4.2.2 The effect of ConA and PHA on the activation of Jurkat cells | 122 |
| 4.2.3 The effect of ConA treatment on the cell viability of Jurkat cells cultured in medium containing varying concentrations of FBS | 124 |
| 4.2.4 The effect of PHA treatment on the cell viability of Jurkat cells cultured in medium containing varying concentrations of FBS | 127 |
| 4.2.5 The role of extracellular ions on mitogen induced activation of the Jurkat cells | 130 |
| 4.2.6 The effect of ConA and PHA treatment on the viability of Jurkat cells with altered concentrations of either K ⁺ . Na ⁺ or Cl ⁻ | 132 |
| 4.2.7 The effect of FBS and ConA on the cell cycle distribution in Jurkat cells | 134 |
| 4.2.8 Electrophysiological characterisation of Jurkat cells in either a non-proliferating or an activated state..... | 139 |
| 4.2.9 The whole cell currents of Jurkat cells either in a non-proliferative state or a ConA activated state..... | 143 |
| 4.3 DISCUSSION..... | 152 |
| 5 ANALYSIS OF THE MEMBRANE POTENTIAL DYNAMICS OF JURKAT CELLS USING THE CONTINUOUS WAVELET TRANSFORM | 161 |
| 5.1 INTRODUCTION..... | 161 |
| 5.2 RESULTS..... | 164 |

| | |
|---|-----|
| 5.2.1 Investigating the application of the wavelet transform technique – can the technique discriminate between physiological and non-physiological electrical signals? | 164 |
| 5.2.2 Longitudinal analysis of the membrane potential recording from Jurkat cells in the frequency domain (using histograms)..... | 168 |
| 5.2.3 Investigating the effect of ionic changes on the static resting membrane potential..... | 169 |
| 5.2.4 Investigating the membrane potential of Jurkat cells in the time-frequency domain using the continuous wavelet transform | 176 |
| 5.2.5 Investigating the role of voltage-gated K ⁺ channels on the membrane potential dynamics of Jurkat cells..... | 188 |
| 5.2.6 Investigating the influence of intracellular Ca ²⁺ on the static membrane potential..... | 191 |
| 5.2.7 Investigating the effect of intracellular Ca ²⁺ on the membrane potential of Jurkat cells in the time domain | 192 |
| 5.2.8 Investigating the effect of intracellular Ca ²⁺ on the membrane potential of Jurkat cells in the time-frequency domain using the continuous wavelet transform..... | 194 |
| 5.2.9 Investigating the membrane potential of Jurkat cells in different states in time-frequency domain using the continuous wavelet transform..... | 196 |
| 5.3 DISCUSSION..... | 199 |

| | |
|---|------------|
| 6 ELECTROPHYSIOLOGICAL CHARACTERISATION AND ANALYSIS OF THE MEMBRANE POTENTIAL DYNAMICS OF HMEC-1 ENDOTHELIAL CELLS | 207 |
| 6.1 INTRODUCTION..... | 207 |
| 6.2 RESULTS..... | 210 |
| 6.2.1 The membrane potential of proliferating HMEC-1 cells | 210 |
| 6.2.2 Ionic conductance's regulating the membrane potential of the HMEC-1 cells | 213 |
| 6.2.3 Analysis of the whole cell currents of proliferating HMEC-1 cells | 218 |
| 6.2.4 Investigating the effect of K ⁺ conductance on the membrane potential of HMEC-1 cells in the presence of elevated concentrations of intracellular Ca ²⁺ | 230 |

| | |
|--|------------|
| 6.2.5 Analysis of the whole cell currents of HMEC-1 cells in response to elevated concentrations of intracellular Ca ²⁺ | 232 |
| 6.2.6 Analysis of the membrane potential dynamics of HMEC-1 cells..... | 240 |
| 6.3 DISCUSSION..... | 244 |
| 7 CONCLUSION | 253 |
| 8 GLOSSARY | 258 |
| 9 REFERENCES | 260 |

1 INTRODUCTION

1.1 Overview

As early as 1969, based on a series of experiments investigating the effects of the plasma membrane potential of somatic cells on cell cycle progression, it was hypothesised that variations in the membrane potential were associated with proliferation (Cone, 1969, 1971). Subsequent studies have provided strong evidence for a regulatory role of the membrane potential in proliferation. The membrane potential has also been suggested to be an indicator of the proliferative state of a cell (Figure 1.1). The influencing role of the membrane potential has also been observed in other cell behaviours such as migration, differentiation and survival (Blackiston et al., 2009; Sundelacruz et al., 2009; Yang and Brackenbury, 2013). The role of the membrane potential in cell behaviours is sometimes described as a bioelectric signal whereby the electrical properties of a cell affect cell behaviour (Blackiston et al., 2009). Bioelectric control mechanisms have been described in single cells through to complex multi-cellular systems (Blackiston et al., 2009; Sundelacruz et al., 2009). The influencing role of the membrane potential in cell behaviours has generally been considered in terms of a single static value under different conditions. There is also, however, evidence suggesting that the membrane potential is a dynamic property of a cell, in other words, the membrane potential has temporal variation. This dynamic membrane potential may also have a functional role in bioelectric signalling. In the introduction of this thesis, the role of the static and dynamic membrane potential in proliferation and activation of cells will be discussed.

One of the central questions concerning the regulatory role of the membrane potential in cell behaviours is whether the membrane potential is essential in regulating cell behaviours or if the membrane potential is just a consequence of downstream mechanisms. This question will also be explored in the introduction in light of the experimental data available on the role of bioelectric signalling in cellular proliferation.

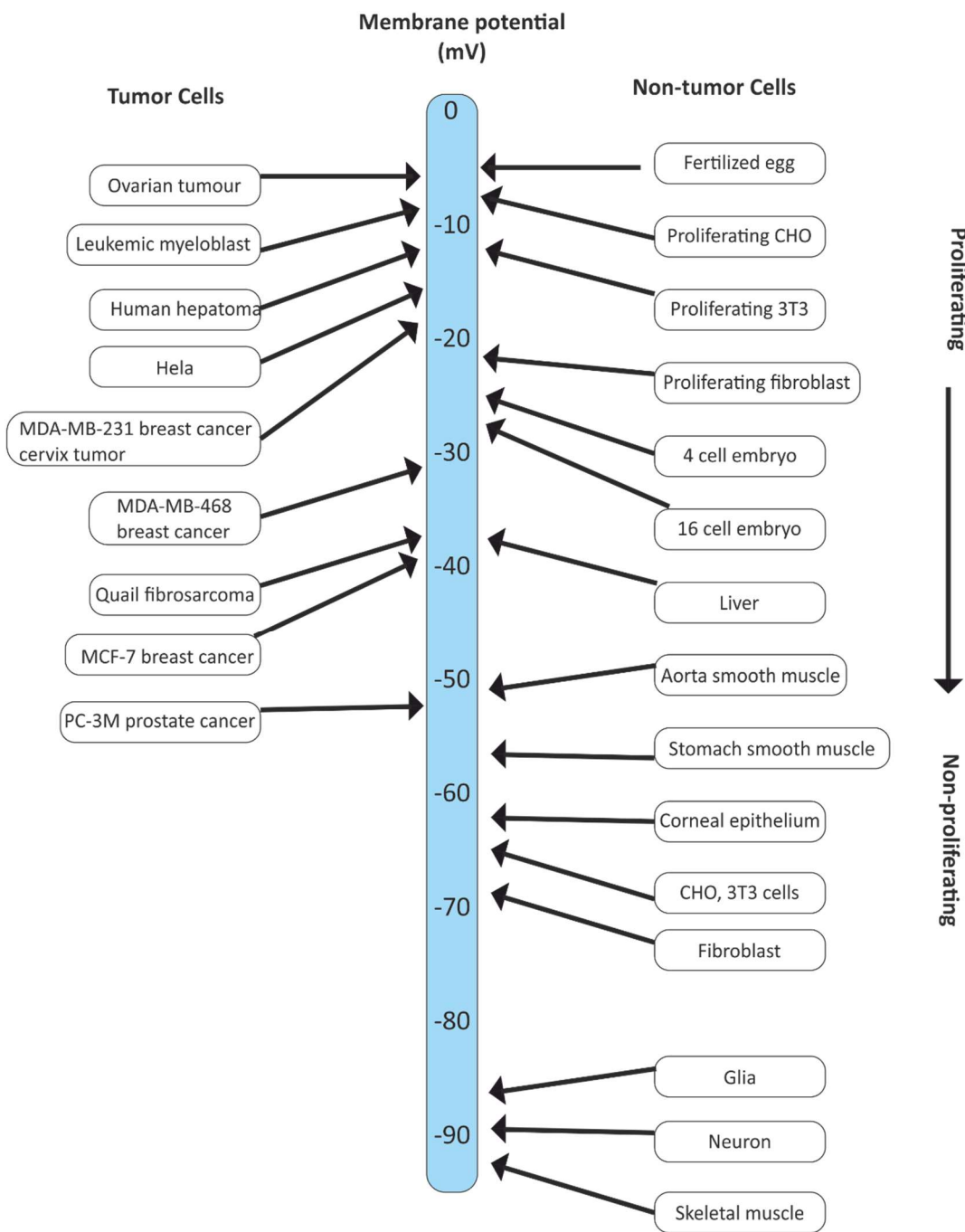


Figure 1.1

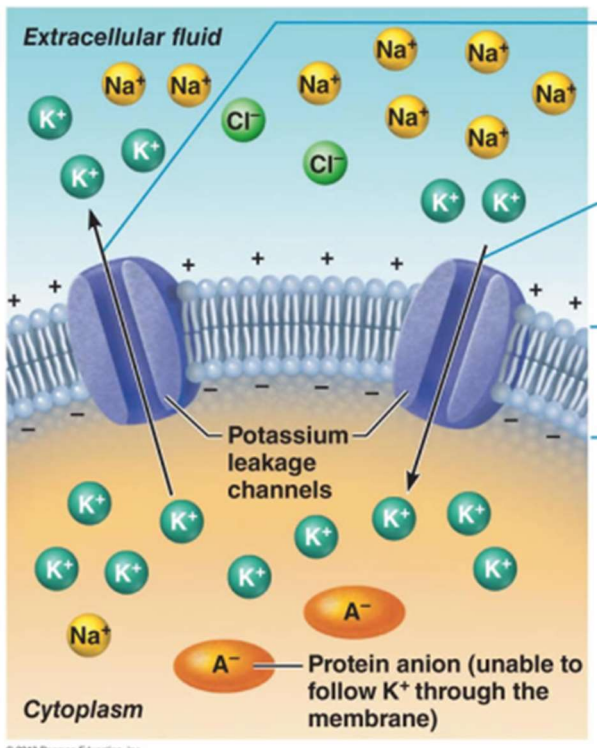
The membrane potential of proliferating and non-proliferating cells. The membrane potential of proliferating cells is depolarised whilst the membrane potential of non-proliferating (quiescent) cells is hyperpolarised. The figure is adapted from Yang and Brackenbury (2013).

1.2 The resting membrane potential

1.2.1 The resting plasma membrane potential

The membrane potential is a fundamental physiological parameter found in all cells and refers to the voltage difference across the plasma membrane (Lodish, 2004; Wright, 2004). The plasma membrane acts as a capacitor due to its electrically insulating characteristics where it is surrounded by electrical conductors in the form of the cytoplasm and the extracellular fluid. In a similar way, a membrane potential can be observed across the membrane of different intracellular organelles such as the mitochondria and the nucleus which is linked with the electrochemical gradients of ions (Gottlieb et al., 2003; Jang et al., 2015). The work in this thesis concentrates on the plasma membrane potential and is referred to as the membrane potential hereon in.

The membrane potential of mammalian cells is “non-zero” due to the semi-permeable nature of the plasma membrane. This allows the movement of specific ions through it due to the presence of membrane transport proteins (ion channels, pumps and carriers) within the membrane (Sundelacruz et al., 2009; Wright, 2004). The movement of ions between the cytoplasm and the extracellular space is governed by electrochemical gradients. These electrochemical gradients drive ion movement based on chemical concentration gradients (i.e. movement of an ion from an area of high concentration to an area of low concentration) and electrical gradients (i.e. movement of an ion based on the attraction to the opposite charge) (Wright, 2004). The resting membrane potential is achieved when the electrochemical gradient either side of the plasma membrane is balanced and thus equilibrium is reached and the net flux of ions is zero (Reuss, 2011; Sundelacruz et al., 2009) (Figure 1.2). The activity of ion channels, pumps and carriers on the plasma membrane of cells maintains the characteristic ionic concentrations of the inside of a cell i.e. high $[K^+]$ and low $[Na^+]$ relative to the outside of the cell (Table 1.1).



1) Ions diffuse down their concentration gradient. In the case of K^+ ions, they diffuse out of the cell leaving the intracellular solution negatively charged.

2) Ions are also attracted to their opposite charge causing ions to move between the cytosol and extracellular fluid. In the case of K^+ ions, they are attracted back to the cytosol due to the negative charge of the cytosol.

3) The resting membrane potential is established when the concentration of an ion exactly opposes the electrical gradient. Net movement of ions ceases. In the case of K^+ ions, the resting membrane potential is reached when K^+ efflux due to the concentration gradient equals K^+ influx due to the electrical gradient.

Figure 1.2

Schematic diagram outlining the generation of the resting membrane potential. The figure is adapted from Pearson (2010).

| Ion | Intracellular Concentration (mM) | Extracellular Concentration (mM) |
|------------------|---|---|
| K^+ | 139 | 4 |
| Na^+ | 12 | 145 |
| Cl^- | 4 | 116 |
| Mg^{2+} | 0.8 | 1.5 |
| Ca^{2+} | <0.0002 | 1.8 |

Table 1.1

Ionic concentrations of a mammalian cell. Typical values of the ionic concentrations in the intracellular cytoplasm and the extracellular fluid in mammalian cells. The values are taken from Lodish (2004).

1.2.2 Overview of ion channels, pumps and carriers

Ion channels, pumps and carriers are integral transmembrane proteins involved in the movement of ions, molecules and even macromolecules between the cytosol and the extracellular fluid (Sukul and Sukul, 2006) (Figure 1.3). Ion channels are selective pores that allow the movement of ions across the plasma membrane by providing a hydrophilic route for the ion when the gating mechanism of the channel opens in response to the appropriate stimulus (Table 1.2) (Reuss, 2011). Ion channels are passive transporters and the net flow of the ion movement is always down its electrochemical gradient (Dahl et al., 2004). On the other hand, pumps are active transporters that have more complex gating mechanisms than ion channels. As active transporters, pumps use energy that is usually released from the hydrolysis of ATP to move an ion across the membrane against its electrochemical gradient. Pumps can also be driven by light or the redox potential (Gadsby, 2009; Lodish, 2004).

Carriers, like ion channels and pumps, facilitate the movement of molecules across the plasma membrane and three primary types of carriers have been identified (Figure 1.3B). These different carriers are defined by the energy source used for the moment of ions and the number of ions transported at each point. A uniporter is a passive carrier whilst a symporter and an antiporter are secondary active carriers. A uniporter mediates the movement of a single ion whilst a symporter and an antiporter are coupled carriers and thus facilitate the transport of two ions. A symporter and antiporter use the energy stored in the electrochemical gradient of the driver ion to move the coupled substrate (osmolytes, nutrients and neurotransmitters) against its electrochemical gradient (Gadsby, 2009). The driver ion in secondary active transporters is usually either Na^+ or H^+ and is transported down its electrochemical gradient (Loo et al., 2002).

Pumps can generally be distinguished from ion channels based on several factors such as the speed of ion transport and whether or not the membrane transport protein is capable of thermodynamic uphill movement of an ion, in other words, moving an ion against its electrochemical gradient (Gadsby, 2009). In principle at least, ion channels and pumps can also be distinguished by the number of gates; ion channels only require one gate whilst pumps require a minimum of two gates. This clear distinction in the gating mechanisms of ion channels and pumps is apparent in the crystal structures of

bona fide ion channels (KcsA K⁺ channel) and pumps (Na⁺/K⁺ ATPase pump). The distinction between ion channels and pumps, however, is sometimes blurred. For instance, the CFTR Cl⁻ ion channel has characteristics of pumps (Gadsby et al., 2006; Morais-Cabral et al., 2001; Morth et al., 2007; Vasiliou et al., 2009). Similarly, it has recently become evident that there is also overlap between the characteristics of ion channels and carriers. For example, Cl⁻ channels from the CLC family of transporters, act as both, Cl⁻ channels and proton pumps (Lim et al., 2012; Lisal and Maduke, 2008; Picollo and Pusch, 2005). The distinction between the different types of membrane transport proteins is not always obvious, even at the atomic level. As a prime example, ClC-ec1 was initially assumed to be a Cl⁻ channel ion channel but subsequent studies showed this apparent Cl⁻ channel was in fact a Cl⁻/H⁺ carrier protein. This transporter was considered as a channel despite the availability of its crystal x-ray structure (Accardi and Miller, 2004; Dutzler et al., 2002).

Nomenclature of the membrane transport proteins. The name of ion channels which have a principle permeant ion usually contain the symbol of the permeant ion. This symbol is followed by the symbol of the ligand molecule, if indeed, the ion channel is gated by a ligand or V, if the ion channel is voltage-gated (Catterall et al., 2003; Sterratt, 2014). The subsequent name of the channel contains the type and subtype of the channel in the form of digits. The subtype of the channel is usually determined by the sequence homology of the hydrophobic transmembrane core. For example, the KV1.3 is a voltage-gated K⁺ channel belonging to the Shaker channel family (KV1). Often each ion channel has a number of different names, for instance, the voltage-gated K⁺ channel is sometimes referred to as a delayed-rectifier K⁺ channel due to the characteristics of the whole cell current. It also has to be noted that occasionally, this nomenclature is not always accurate, for example, the Kca4.2 channel is activated by Na⁺ rather than Ca²⁺ as the name suggest (Fleming et al., 2013). Similar to ion channels, pumps and carriers also contain the symbol of the permeant ion (or ions in the case of coupled carriers e.g. Na⁺/K⁺ ATPase pump) in addition to the symbol of the activating molecule.

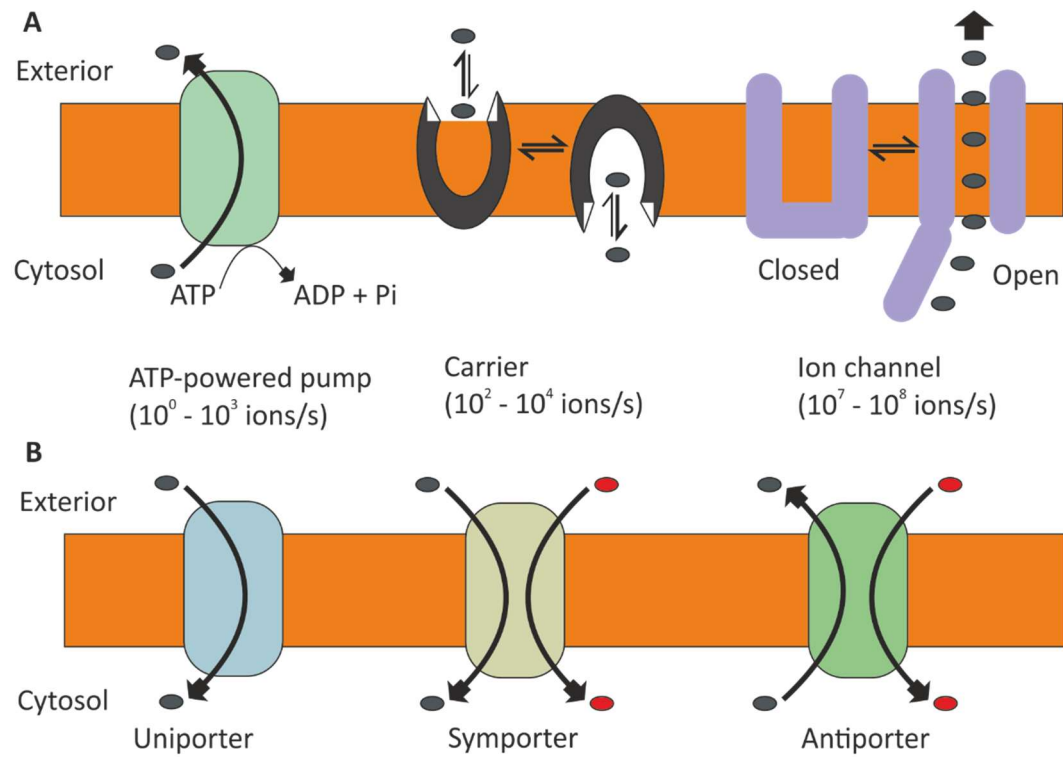


Figure 1.3

Schematic diagram illustrating the action of membrane transport proteins. **(A)** The three types of transport proteins are either pumps, transporters or ion channels. Pumps are driven by either light, redox state or use the energy released by the hydrolysis of ATP to power the movement of specific ions (black circles) through the plasma membrane. Carriers facilitate the movement of specific ions or small molecules whilst ion channels provide a hydrophilic pathway to allow movement of specific ions through the plasma membrane. **(B)** The different types of carrier proteins. A uniporter facilitates the movement of a single molecular species down its electrochemical gradient whilst a symporter facilitates the movement of two or more molecular species (black and red circles) down their electrochemical gradients. Antiporters facilitate the movement of two or more molecular species in opposite directions. The schematic diagram is adapted from Lodish (2004).

| Gating Mechanism | Permeating ionic species or type of ligand sensitivity | Examples of specific ion channels | Reference |
|------------------|--|---|------------------------------|
| Voltage | K ⁺ | KV1.3 Channel | (Dupuis et al., 1989) |
| | H ⁺ | Voltage-gated proton channel | (DeCoursey and Cherny, 1996) |
| | Ca ²⁺ | Voltage-gated Ca ²⁺ channel | (Catterall, 2011) |
| Ligand | ATP channels | ATP sensitive K ⁺ channels | (Craig et al., 2008) |
| | Glutamate channels | N-methyl-D-Aspartate (NMDA) receptors | (Petrenko et al., 2003) |
| Light | Non-selective cations | Channels rodopsin-2 | (Lin, 2011) |
| Mechanosensitive | Cl ⁻ | Volume sensitive Cl ⁻ channels | (Jentsch et al., 1999) |
| Temperature | Cations | TRPV1 | (Vay et al., 2012) |

Table 1.2

Some examples of the different types of ion channels based on their gating mechanisms.
KV1.3 channel = Voltage-gated K⁺ Channel, TRPV1 = Transient receptor potential vanilloid subfamily, member 1.

1.2.3 Selectivity and gating properties of membrane transport proteins

Ion channels show a preference for a specific ion, however, they may allow other ionic species to travel through the channel. For example, K⁺ leak channels show a preference to conduct K⁺ over Na⁺ by a ratio of 10000 to 1, respectively (Doyle et al., 1998). Ion channels can also be selective for either cations or anions with little or no selectivity for the ionic species (Hille, 1992). The mechanism involved in ion channel selectivity is not completely understood, however, a significant amount of knowledge on K⁺ selectivity was derived from resolving the atomic structure of a K⁺ channel from *Streptomyces lividans* (Doyle et al., 1998). Such was the importance of this, Roderick MacKinnon was awarded with the Nobel Prize in Chemistry in 2003 for his work on resolving the atomic structure of the K⁺ channel. The selectivity filter of the K⁺ channel is a highly conserved GYG amino acid sequence termed the “K⁺ channel signature sequence” (Heginbotham et al., 1994). Four carbonyl oxygen atoms line this selectivity filter and are involved in the dehydration of the impinging permeant K⁺ (MacKinnon, 2003). Despite the important developments in understanding aspects of K⁺ channel conductance, there is still continued debate about the mechanism(s) involved in allowing movement of K⁺ but not Na⁺ i.e. the selectivity (Nimigean and Allen, 2011). Different degrees of Na⁺ permeability have also been observed with K⁺ channels, despite the conserved “K⁺ channel signature sequence” (Callahan and Korn, 1994; Korn and Ikeda, 1995; Wang et al., 2009b; Zhu and Ikeda, 1993). Some voltage-gated K⁺ channels have also been reported to become more permeable to Na⁺ after becoming inactivated, which indicates a potential link between selectivity and gating mechanisms (the process from sensing the initial signal through to opening the channel allowing ion conduction) (Beckstein, 2004; Starkus et al., 1997).

Gating Mechanism. A number of different gating stimuli controlling the conductance of ions through ion channels have been identified and a summary of these are presented in Table 1.2. The stimuli to activate the gate is transduced by a sensor which in turn causes a conformational change in the ion channel, thereby controlling the conductance state of the channel (Bezanilla and Perozo, 2003). Ion channels which are voltage sensitive respond to changes in voltage through voltage sensor domains, whilst ligand gated ion channels contain ligand binding sites. These are usually attached to the pore near the plasma membrane on the extracellular side (Bezanilla, 2000; Schreiber and Salkoff, 1997; Zagotta and Siegelbaum, 1996). Several

theoretical models for the gating mechanisms have been proposed such as blockage of the site by a single side chain or steric occlusion which prevents ion movement through the channel pore (Beckstein, 2004). It is thought that the gating mechanism of the inwardly rectifying K⁺ channel works through a steric mechanism (Nanazashvili et al., 2007).

1.3 The functional role of the membrane potential in cell behaviour

1.3.1 Introduction

The membrane potential is not just a physiological phenomenon that arises due to the separation of ions between the intracellular and extracellular milieu. A number of studies have suggested that the membrane potential is important for several aspects of cell behaviour such as proliferation, differentiation, migration, activation, maturation and the survival of the cell. Thus, the membrane potential is vital for living systems (Blackiston et al., 2009; Bortner and Cidlowski, 2004; Pardo, 2004; Sundelacruz et al., 2009). This section will discuss the influence of the membrane potential on cell behaviours, in particular, proliferation. In addition, the opposite scenario, wherein cell behaviours that induce changes in the membrane potential and the activity of ion channels will also be touched on. Moreover, the role of the membrane potential and ion channels in diseases states such as cancer will also be discussed. The next section will discuss the eukaryotic cell cycle followed by the current knowledge of the mechanisms involved in the relationship between the membrane potential and the cell cycle.

1.3.2 Overview of the cell cycle

Cell proliferation is the replication of a mother cell to yield daughter cells and involves a series of phases which combine to make the cell cycle (Pardo, 2004; Rao et al., 2015) (Figure 1.4). The different phases of the cell cycle include the G1, S, G2 and M phase. Cells which are not undergoing proliferation reside in the G0 phase in a quiescent state and the majority of non-proliferating cells *in vivo* reside in this phase (Rao et al., 2015). Some cells can be activated to proceed to the next stage of the cell

cycle. For example, lymphocytes can be activated by an antigen which triggers the lymphocyte to enter the G1 phase of the cell cycle (Lea et al., 2003). G1 is the first gap phase and prepares the cell for DNA replication whilst the S phase is the phase wherein DNA synthesis occurs and chromosome replication is achieved. G2 is the second gap phase and the cell is prepared for mitosis in G2. The M phase is the mitosis phase and comprises of the prophase, metaphase, anaphase and telophase and the daughter cells are produced during this M phase. After the completion of the M phase, the daughter cells can continue through to another cell cycle or enter G0 (Vermeulen et al., 2003). Progression of the cell cycle from one phase to the next occurs in a tightly regulated manner (Golias et al., 2004). This regulation is dependent regulatory mechanisms and the important regulators in the cell cycle are checkpoints and proteins. These regulatory proteins include cyclin dependent kinases (CDK), cyclins, CDK inhibitors (CKI), tumour suppressor gene products p53 and pRb (Galimuttasib and Bakkar, 2002). The CDK's are activated by forming a complex with cyclins which occurs during specific phases of the cell cycle, for example, during G1 to S transition, CDK2 is activated by forming a complex with cyclin E (Gerard and Goldbeter, 2014). Table 1.3 shows the different CDK's, their activating cyclins and the phase of the cell cycle at which the CDK's are activated. Checkpoints control progression through the cell cycle and ensure critical cell events such as chromosome segregation are completed to a high degree of accuracy (Elledge, 1996). For instance, the tumour suppressor gene P53 activates the transcription of P21 in response to DNA damage which ultimately causes cycle arrest during G1 (Kastan et al., 1992).

In addition to the aforementioned regulatory proteins and mechanisms, it is increasingly evident that the membrane potential of a cell can also influence and regulate cell cycle progression (Blackiston et al., 2009). Studies have shown that the membrane potential is an indicator of the proliferative state of a cell. In general, proliferating cells are depolarised (the membrane potential is less negative) whilst the membrane potential of quiescent and non-proliferating cells is hyperpolarised (the membrane potential is negative) (see Figure 1.1) (Binggeli and Weinstein, 1986; Yang and Brackenbury, 2013).

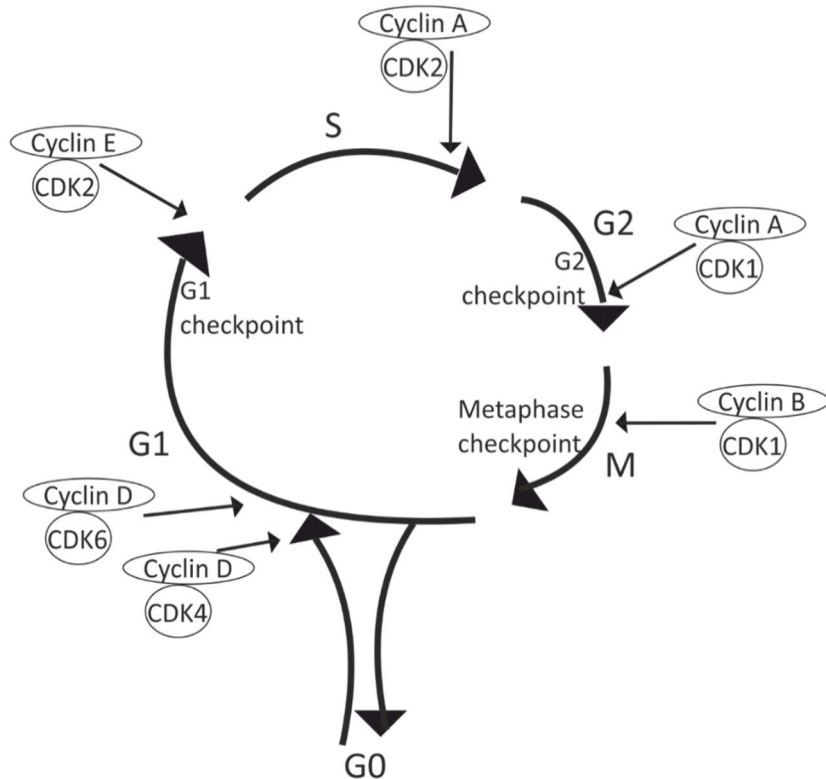


Figure 1.4

Overview of the different stages of the eukaryotic cell cycle. The different phases of the cell cycle together with the sites of the cyclins/CDK complexes and the different checkpoints. The figure is adapted from Vermeulen et al., (2003).

Cyclins, their associated cyclin dependent kinases (CDK's) and the phase of the cycle in which they act

| Cyclin | CDK | Cell cycle phase activity |
|-------------------|------|---------------------------|
| Cyclin D1, D2, D3 | CDK4 | G1 phase |
| Cyclin D1, D2, D3 | CDK6 | G1 phase |
| Cyclin E | CDK2 | G1/S transition |
| Cyclin A | CDK2 | S phase |
| Cyclin A | CDK1 | G2/M transition |
| Cyclin B | CDK1 | Mitosis |
| Cyclin H | CDK7 | All cell cycle phases |

Table 1.3

1.3.2.1 The effects of the membrane potential on cell cycle progression and proliferation

A role for the membrane potential in cell proliferation has been observed as early as the 1970's when studies showed that a reversible block on proliferation could be achieved by merely manipulating the membrane potential to a highly negative value by altering the ionic concentration of the culture medium (Cone, 1971; Cone and Tongier, 1971). The rationale for manipulating the membrane potential to hyperpolarised levels was based on the observations of quiescent fully differentiated neurons which have a hyperpolarised membrane potential (Cone and Cone, 1976). Subsequent studies by Cone's group showed that a sustained depolarisation of the membrane potential of mature quiescent neurons led to neuronal proliferation (Cone and Cone, 1976; Stillwel et al., 1973). In this section of their studies, the membrane potential was manipulated to depolarised levels by treating the neurons with different compounds to alter their membrane permeability. Gramicidin; a K^+ ionophore was used to alter K^+ permeability, veratridine, a Na^+ channel activator was used to alter Na^+ permeability and ouabain was used to alter both, Na^+ and K^+ permeability by inhibiting the Na^+/K^+ ATPase pump. The same effect on cell proliferation was observed with all three different approaches to manipulating the membrane potential.

Since Cone's seminal experiments, it has become generally accepted that the membrane potential of cells varies during the different phases of the cell cycle. For example, using electrical impalements to measure the membrane potential, it was observed that MCF-7 breast cancer cells have a hyperpolarised membrane potential during the G1 to S and G2 to M transition whilst cells that are arrested in G0/G1 and M phase have depolarised membrane potentials (Wonderlin et al., 1995). In line with these observations, studies where the membrane potential was manipulated to depolarising levels (thus preventing hyperpolarisation) caused inhibition of the G1 to S transition in numerous cell types including lymphocytes, astrocytes, fibroblasts and Schwann cells (Freedman et al., 1992; Wang et al., 1992; Wilson and Chiu, 1993).

The role of the membrane potential in the control of proliferation in cancer cells has also been observed. These cancer cell lines have a depolarised membrane potential in comparison to their non-proliferating counterparts (see Figure 1.1). For example, fibrosarcoma cells which are proliferating fibroblasts have a membrane potential of -

14 mV whilst non-proliferating fibroblasts exhibit a relatively hyperpolarised membrane potential of -43 mV (Binggeli and Cameron, 1980). Likewise, non-invasive *in vivo* measurements of breast tissue showed a similar trend in the difference in polarity of the surface electrical potentials between normal and the site of the breast tumour in the same individual (Marino et al., 1994). The degree of the difference in the potentials between normal and cancer cells was not as large as the differences observed in other cell types, however, this likely reflects the non-invasive *in vivo* measurement technique.

The role of the membrane potential in proliferation has also been studied in stem cells and precursor cells. Depolarisation of the membrane potential of neural precursor cells (NPC) and embryonic stem cells using inhibitors of membrane transport proteins caused an increase in the rate of proliferation (Wang et al., 2005; Yasuda et al., 2008). In the study conducted by Yasuda et al., (2008), the inhibition of the voltage-gated K⁺ channels (KV channels) with tetraethylammonium (TEA) failed to significantly alter the membrane potential of NPC's despite inhibiting currents mediated by KV channels in whole cell patch clamp studies. Nevertheless, treatment with the same KV channel inhibitor dramatically reduced NPC proliferation suggesting that the role of KV channels in NPC proliferation is not mediated solely through a change in the membrane potential.

In the vast majority of studies wherein ion channel activity is reduced through ion channel inhibitors or ion channel knockdown, the membrane potential is not measured but there are a few studies where the membrane potential is measured. For example, endothelin-1, which can regulate proliferation caused significant changes in the activity of Cl⁻ channels and dramatically altered the membrane potential in epithelial cells suggesting endothelin-1-induced proliferation involves Cl⁻ channel activity (Mair et al., 1998; Murlas et al., 1995).

In summary, a regulatory role of the membrane potential has been observed in proliferating and quiescent cells, normal and cancer cells and even stem cells across a range of species. In general, a depolarisation of the membrane potential is associated with proliferation whilst a hyperpolarisation inhibits proliferation. Due to the underlying mechanisms governing the generation of the membrane potential (refer to

section 1.2), changes in the membrane potential have to be linked to changes in the permeability of ion channels, pumps and carriers. The following section will give an overview of the different channel types linked to proliferation with a focus on K⁺, Cl⁻ and Na⁺ selective membrane transport proteins as these are the primary determinants of the membrane potential (Wright, 2004).

1.3.3 The role of specific membrane transport proteins in the regulation of proliferation

1.3.3.1 The role of K⁺ channels in proliferation

A number of different types of ion channels have been implicated in proliferation with the most common ion channels belonging to the K⁺ channel family. In fact, K⁺ channels represent the largest group of ion channels associated with proliferation (Blackiston et al., 2009; Urrego et al., 2014) (Table 1.4). K⁺ channel activity is usually associated with proliferation by causing a depolarisation in the membrane potential whilst an inhibition of K⁺ channel activity leads to membrane potential hyperpolarisation and is generally associated with cell cycle arrest (Blackiston et al., 2009).

The voltage-gated KV1.3 channel was the first channel to be implicated in proliferation wherein lymphocyte activation was inhibited in cells treated with either 4-aminopyridine (4-AP) or quinine (DeCoursey et al., 1984). The activity of specific K⁺ channel types fluctuates during the different stages of the cell cycle (Arcangeli et al., 1995; Day et al., 1993; Huang et al., 2012; Lenzi et al., 1991; Takahashi et al., 1994). For example, in oocytes, K⁺ channel activity increases through the M and G1 phases whilst K⁺ channel activity is reduced during the S and G2 phases and these changes correlate with changes in the membrane potential (Day et al., 1993). In support of a role for K⁺ channel activity in cell cycle progression, treatment with K⁺ channel blockers induced cell cycle arrest of B cells and MCF-7 breast cancer cells in the G1 phase (Amigorena et al., 1990; Ouadid-Ahidouch et al., 2004). Experimental evidence also suggests that K⁺ channel activity does not always stimulate proliferation. For example, the colon carcinoma cell line, T84 cells, Caco-2 cells and NPC inhibition of K⁺ channel activity (Ca²⁺-activated K⁺ and Kir channels) either resulted in accelerated proliferation or had no effect on proliferation at all (Abdullaev

et al., 2010; Lotz et al., 2004; Yasuda et al., 2008). Nevertheless, as a result of the observations on the role of K⁺ channels in proliferation, it has been postulated that K⁺ channels are key components in cell cycle progression with MacFarlane and Sontheimer (2000b) even hypothesising that K⁺ channels act as an additional layer of checkpoints.

The most common K⁺ channels associated with proliferation are the voltage-gated and Ca²⁺-activated K⁺ channels (KV1.3, KV10.1 and Kv11.1 channel). The KV10.1 channel (also called ether-a-go-go K⁺ channel, EAG or EAG1) has been strongly implicated with proliferation (Farias et al., 2004; Meyer and Heinemann, 1998; Meyer et al., 1999; Ouadid-Ahidouch et al., 2001). For example, CHO cells transfected to overexpress KV10.1 channels exhibited faster growth than wild type CHO cells. (Pardo et al., 1999). In addition, all of the severe combined immune deficiency mice transplanted with CHO cells overexpressing the EAG mRNA transcript for KV10.1 channel had tumours. These results suggest that constitutive expression of the KV10.1 channel can drive transformation of cells to a cancerous phenotype. In this study, only mRNA transcript levels were measured, rather than actual KV10.1 channel activity. Therefore, it is impossible to prove if proliferation was related to bioelectric mechanisms associated with KV10.1 channel activity. In fact, other studies have shown ion channels can influence cell behaviour without the channel conducting ions (Downie et al., 2008; Millership et al., 2011).

Another factor to consider is the presence of compensatory mechanisms which could mask the effects of specific ion channel activity. For example, the activity of voltage-gated K⁺ channels are vital to proliferation which in turn is critical to an effective immune response (DeCoursey et al., 1984). KV1.3 knockout mice, however, failed to show an impaired immunological response (Koni et al., 2003). It was postulated that Cl⁻ channels or other K⁺ channels compensated for the absence of the KV1.3 channels.

Despite the plethora of evidence implicating a role of K⁺ channels in proliferation, there is no consensus on either the precise role of K⁺ channels in proliferation or the specific K⁺ channel types involved. In most cases, K⁺ channel activity is associated with proliferation whilst K⁺ channel block is generally associated with the inhibition of proliferation.

1.3.3.2 The role of Cl⁻ channels in proliferation

Two different Cl⁻ channels (volume-activated Cl⁻ channels and Ca²⁺- activated Cl⁻ channels) have been implicated to play a role in proliferation in several different cell types such as glial derived tumour cells and nasopharyngeal carcinoma cells (Ullrich, 1999; Xu et al., 2010). Generally Cl⁻ channel activity is increased during the G2 and M phases of the cell cycle (Blackiston et al., 2009; Habela et al., 2008; Zheng et al., 2002).

Inhibition of Cl⁻ channels using non-specific Cl⁻ channel inhibitors (flufenemic acid, tamoxifen and NPPB) or Cl⁻ channel silencing using small interference RNA (siRNA) caused a concomitant reduction in proliferation in several cell types e.g. rat aortic smooth muscle cell, human T-lymphocytes and human adipocytes (Hu et al., 2010; Nilius et al., 1997a; Schlichter et al., 1996; Schumacher et al., 1995; Tang et al., 2008). On the contrary, (and similar to the role of K⁺ channels in proliferation) the inhibition of Cl⁻ channels in Schwann cells, astrocytoma's and B lymphocytes caused increased proliferation (Deane and Mannie, 1992; Ullrich and Sontheimer, 1996; Wilson and Chiu, 1993).

Unexpectedly, Cl⁻ channel block of Schwann cells from rabbit and rat species using the same Cl⁻ channel blocker at similar concentrations exhibited two different responses on proliferation. In rat Schwann cells, Cl⁻ channel block appeared to stimulate proliferation whilst in rabbit Schwann cells, Cl⁻ channel block reduced proliferation (Pappas and Ritchie, 1998; Wilson and Chiu, 1993). The seemingly contradictory findings could be due to the difference in the experimental designs; Wilson and Chiu treated the Schwann cells with a mitogen in the form of glial growth factor, whilst Pappas and Ritchie conducted experiments on untreated Schwann cells.

1.3.3.3 The role of Na⁺ channels in proliferation

A few studies have shown a relationship between inhibition of Na⁺ flux and proliferation (Koch and Leffert, 1979; Ousingsawat et al., 2008). Proliferation of neuroblastoma-glioma hybrid cells and fibroblasts was inhibited in response to Na⁺ channel blockers such as amiloride and benzamil (O'Donnell et al., 1983). Based on the findings from these studies it could be speculated that Na⁺ channels were involved in

proliferation. The concentration of amiloride (a Na^+ channel blocker) used by Koch and Leffert (1979), however, has also been shown to suppress the citric acid cycle in dog kidney cells (Taub, 1978). In addition, the concentration of amiloride used in these studies was significantly higher than the concentration required to inhibit Na^+ channel activity which points towards nonspecific effects of the channel inhibitor (O'Donnell et al., 1983). In support against a role of Na^+ channels in proliferation, inhibition of Na^+ channels failed to affect cell cycle progression. (Macfarlane and Sontheimer, 2000a).

Examples of the effect of inhibiting ion channels on proliferation in different cell types

| Cell line/ cell type | Channel type | Effect of channel block on proliferation | Reference |
|---|--|--|---|
| Brown Fat cells | KV | reduced proliferation | (Pappone and Ortiz-Miranda, 1993) |
| A549 (Human lung cell line) | KV1.3 | reduced proliferation | (Jang et al., 2011) |
| Bovine pulmonary endothelial cells | Cl ⁻ _{Ca} , Cl ⁻ _{Vol} | reduced proliferation | (Nilius et al., 1997a) |
| Human T-lymphocyte cells | K ⁺ , Cl ⁻ | Inhibited activation and reduced proliferation | (DeCoursey et al., 1984; Phipps et al., 1996) |
| Several melanoma cell lines | KV10.1 | reduced proliferation | (Meyer et al., 1999) |
| MCF-7 (Breast cancer cell line) | KV10.1 | reduced proliferation | (Ouadid-Ahidouch et al., 2001) |
| LNNCaP, PC-3, DU-145 (Prostate cancer cell lines) | KCa3.1 | reduced proliferation | (Lallet-Daher et al., 2009) |
| Microglia | Kir, Cl ⁻ | reduced proliferation | (Schlichter et al., 1996) |
| Retinal glial cells | K ⁺ | reduced proliferation | (Puro et al., 1989) |
| O-2A (Cortical oligodendrocyte progenitor cells) | KV1.3 | reduced proliferation | (Gallo et al., 1996) |
| Bone marrow derived macrophages | KV1.3 | Inhibited proliferation | (Vicente et al., 2005) |
| Rat Schwann cells | Cl ⁻ | enhanced proliferation | (Pappas and Ritchie, 1998) |
| Rabbit Schwann cells | Cl ⁻ | reduced proliferation | (Wilson and Chiu, 1993) |
| B cells derived | Cl ⁻ | stimulated proliferation | (Deane and |

| | | | |
|---------------------------------|-----------------|---------------------------|----------------------------|
| from rat splenocytes | | | Mannie, 1992) |
| LoVo (human colon cell line) | KCa3.1 | reduced proliferation | (Lai et al., 2011) |
| T84 Colon (carcinoma cell line) | K _{Ca} | accelerated proliferation | (Lotz et al., 2004) |
| Caco-2 cells | K _{Ca} | accelerated proliferation | (Lotz et al., 2004) |
| U251, U87 (Glioma cell lines) | Kir6.2 | reduced proliferation | (Huang et al., 2009) |
| Mouse colonic epithelial | ENaC | reduced proliferation | (Ousingsawat et al., 2008) |

Table 1.4

KV = voltage-gated K⁺ channels, KCa = Ca²⁺-activated K⁺ channels, Kir = Inwardly rectifying K⁺ channel, ENaC = Na⁺ epithelial channel, Cl⁻_{Ca} = Ca²⁺-activated Cl⁻ channel, Ca Vol = volume activated Cl⁻ channel.

1.3.4 The membrane potential and ion channels in disease states

The discussion thus far provides strong evidence for a regulatory role of either ion channel activity and/or the membrane potential in cell proliferation. Therefore, disruptions in cell proliferation due to insults in these underlying regulators could contribute to disease states that are intrinsically linked to proliferation such as cancers (Rao et al., 2015). Despite the heterogeneity of cancer, the basic characteristics of carcinogenesis are uncontrolled cell proliferation and dysregulated apoptosis, ultimately allowing disease progression (Evan and Vousden, 2001; Fulda, 2010; Stern et al., 1999).

The aberrant expression of various channel types have been observed in several cancers such as lymphomas, breast and pancreas tissue (Bose et al., 2015; Ousingsawat et al., 2007; Preussat et al., 2003). Abnormal ion channel expression has also been implicated to confer apoptotic resistance in cells through changes in the intracellular volume (Bortner et al., 1997). In support for a role of the membrane potential and ion channel activity, inhibition of ion channels, in particular, voltage-gated K⁺ channels has been shown to reduce and even inhibit tumour cell proliferation in *in vivo* and *in vitro* models (Pardo, 2004; Pardo et al., 1999) In addition to K⁺ channels, Cl⁻ channel blockers have also been shown to reduce cancer proliferation implicating Cl⁻ channels in cancer (Fernandez-Salas et al., 2002; Suh et al., 2005). From the findings showing partial inhibition of tumour cell proliferation, it seems as though aberrant expression of a single channel type is not enough to trigger tumorigenesis, rather, a number of factors are associated with carcinogenesis.

1.3.5 The effects of cell signalling mechanisms and cell cycle progression on ion channel activity and the membrane potential

The role of the membrane potential and the underlying ion channels have been discussed in terms of their influencing role in proliferation but it is possible that downstream mechanisms and cellular signalling mechanisms feedback to alter either the membrane potential and/or ion channel activity. Indeed, a number of in different cell types have been shown to be modulated by proliferation in a feedback loop (Arcangeli et al., 1995; Lin et al., 2011; Ouadid-Ahidouch et al., 2004; Urrego et al., 2014).

The transient receptor potential channel (TRP) has been found to be modulated by enzymes such as PKC and calmodulin which are involved in cellular signalling cascades (Bhave et al., 2003; Rosenbaum et al., 2004). PKC increases the activity of TRP channel resulting in an increase in the influx of Ca^{2+} . It is possible that this increase in intracellular Ca^{2+} activates other channels ultimately resulting in a change in the membrane potential. Similar to the TRP channels, cyclic nucleotide-gated channels are activated by molecules involved in signalling mechanism e.g. cAMP and cGMP (Kaupp and Seifert, 2002). The activation of ion channels by components of signal transduction pathways highlights the potential complexities of identifying the initial component of bioelectric signalling in cell behaviours. It is possible that changes in ion channel activity and the membrane potential could be secondary to signalling transduction mechanisms.

In addition to signalling transduction mechanisms, downstream cell behaviours could also modulate ion channel activity and thus the membrane potential. *Xenopus* oocytes are reside in the G2 phase of cell cycle and treatment with progesterone induces the activation of mitosis promoting factor which ultimately leads to the G2 to M transition (Stanford et al., 2003). Mitosis promoting factor activity leads to the modulation of KV10.1 channel activity causing a decrease in the current (Bruggemann et al., 1997). Furthermore, in MCF-7 breast cancer cells, KV10.1 channel activity was increased after treatment of the cells with insulin-like growth-factor (IGF-1), and IGF-1 treatment causes G1 to S phase progression via the PI3K/Akt pathway (Borowiec et al., 2007). Similarly, the neuron-restrictive silencer factor (NRSF) (also known as RE-silencing transcription factor) which is considered to be an important transcriptional regulator has been shown to modulate membrane transport protein expression and activity (Gao et al., 2011; Schoenherr and Anderson, 1995). The gene expression of a specific voltage-gated Na^+ channel is restricted to neurons by the activity NRSF and reduced expression of NRSF has been shown to increase the transcription levels of Ca^{2+} -activated K^+ channels (KCa3.1) in vascular smooth muscle cells (Cheong et al., 2005; Chong et al., 1995). The gene encoding the specific Ca^{2+} -activated K^+ channel in question (KCNN4) contains binding sites for NRSF suggesting a direct link between NRSF and KCa3.1 channels. In the same study, mRNA levels of NRSF was significantly less (approximately 50% less) in proliferating smooth muscle cells in

comparison to quiescent muscle cells. The mRNA levels of the KCNN4 and presence of KCa3.1 channels was significantly less in quiescent cells whilst mRNA levels and the presence of KCa3.1 channels was significantly increased in proliferating cells. Moreover, KCa3.1 channel inhibition with TRAM-34 reduced hyperplasia of the human saphenous vein providing further support for a role of KCa3.1 channel activity in proliferation. Taken together, ion channel activity could be mediated by downstream effectors of the proliferative responses.

Despite the apparent importance of bioelectric signalling in proliferation, studies have focussed on the classical signal transduction pathways and largely neglected the molecular mechanisms associated with bioelectric signalling. The next section will discuss the limited amount of knowledge of the molecular elements in the potential pathways involved between ion channel activity and cell behaviours.

1.4 Components of the pathways associated with bioelectric control of cell behaviours

1.4.1 Introduction

The pathways involved in cell behaviour influenced by bioelectric signalling are poorly understood, however, experimental evidence has identified various components that could be involved (Ouadid-Ahidouch and Ahidouch, 2013). These components have been outlined in Figure 1.5 and some of these components are involved feedback loops to modulate membrane transport proteins (as discussed previously). It is possible that various elements associated with ion channel activity and cell behaviours feed into aspects of the classical signal transduction pathways. For example, the membrane potential could affect transcription factors, such as NRF-2 transcription factor. Depolarisation in the membrane potential can cause nuclear translocation of the NRF-2 and intracellular NRF-2 accumulation is favourable for proliferation (Jaramillo and Zhang, 2013; Yang et al., 2004). In the earlier section the link between progression through the cell cycle and the membrane potential in a feedback loop was discussed. The potential molecular mediators involved in this feedback loop will also be discussed in this section.

The components implicated to be involved in the bioelectric signalling mechanisms include Ca^{2+} mediated mechanisms, voltage-sensitive proteins such as voltage-sensitive phosphatases (VSP's) and transporters e.g. SERT and the ions themselves (Figure 1.5) (Blackiston et al., 2009; Fukumoto et al., 2005). The SERT transporter catalyses the influx of serotonin which has been implicated in proliferation (Azmitia, 2001). VSP's are activated in response to depolarisations in the membrane potential have recently been discovered and VSP's from *Ciona intestinalis* have dephosphorylating abilities (Lacroix et al., 2011; Murata et al., 2005; Ooms et al., 2009). It is therefore, also possible that mammalian VSP's could be involved in proliferation and various other cell behaviours regulated by the membrane potential.

Ion channel mediated control of cell behaviour has also been observed through mechanisms independent of conducting ions which cannot be considered as a bioelectric signal (Arcangeli and Becchetti, 2006; Denker and Barber, 2002). For example, fibroblasts transfected with a non-conducting mutant KV10.1 channel that is incapable of conducting K^+ had the same strong stimulating effect on proliferation as fibroblasts with wild type KV10.1 channels that were capable of conducting K^+ (Hegle et al., 2006).

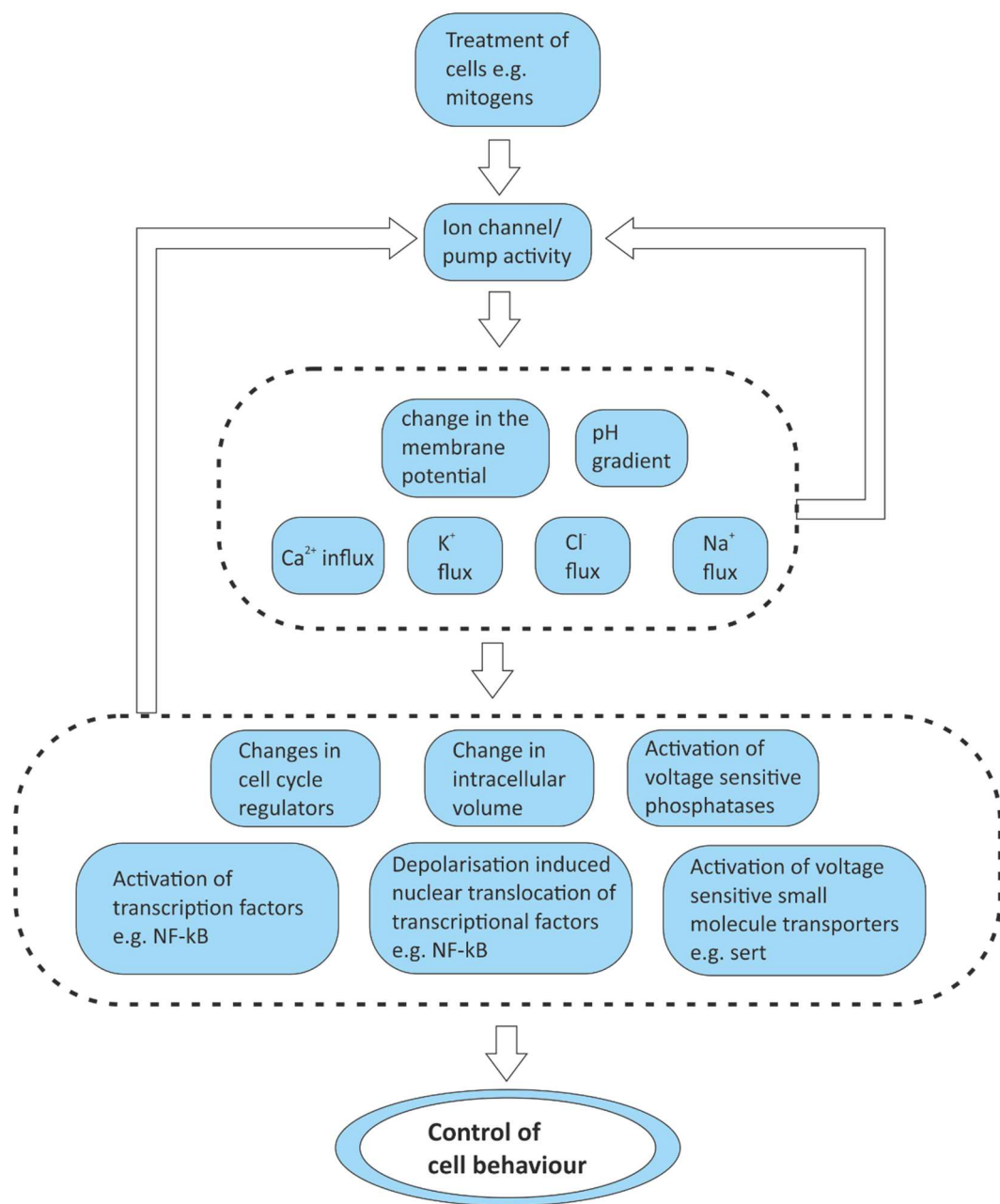


Figure 1.5

Potential mechanisms associated with cell behaviour influenced by bioelectric signalling. A change in the membrane potential can occur due to changes in ion channel activity causing a flux of K⁺, Cl⁻, Na⁺ and Ca²⁺. Changes in the flux of these ions could affect cell behaviour through changes in the intracellular volume or activation of transcription factors such as NFκB. Changes in the membrane potential could also activate small transporters such as SERT which can transport serotonin to the cytosol that in turn can act as a mitogen. Depolarisation of the membrane potential could also cause nuclear translocation of the NRF-2 transcriptional factor. This diagram is adapted from Sundelacruz et al., (2009) and Blackiston et al., (2009).

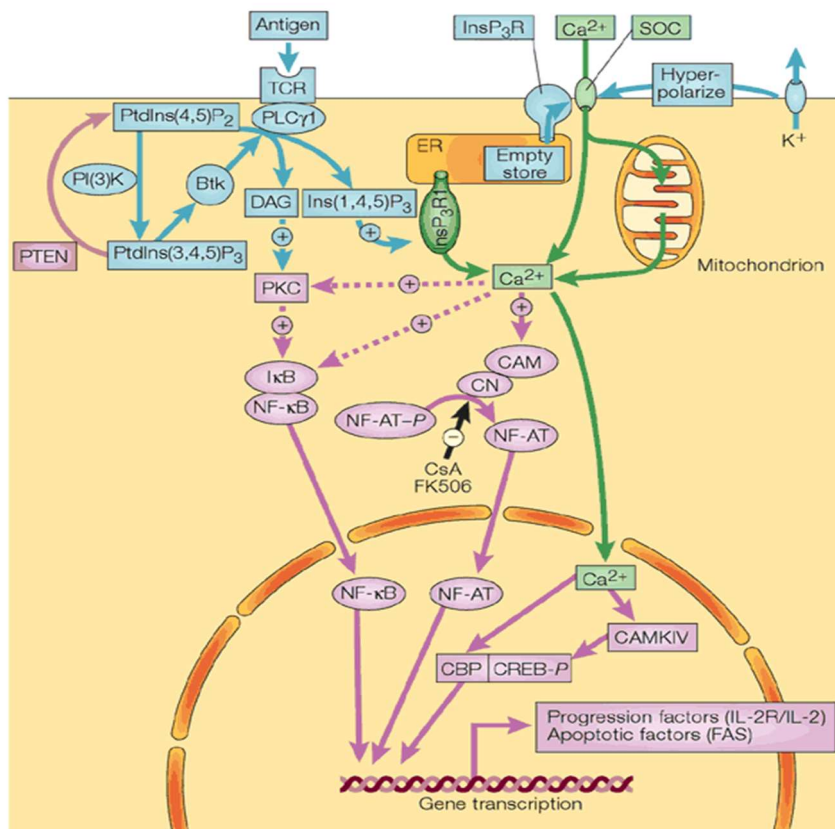
1.4.2 Mechanisms of Bioelectric signalling in cell behaviours involving Ca^{2+}

One important downstream mechanism of bioelectric signalling involves Ca^{2+} which is unsurprising due to the extensive role of Ca^{2+} signalling in cell behaviours (Berridge et al., 2003; Bootman, 2012). For example, proliferation that is inhibited by manipulating the membrane potential to depolarised levels was reversed by increasing intracellular $[\text{Ca}^{2+}]$ using ionomycin (Gelfand et al., 1987). This study suggests the membrane potential could provide a driving force favouring Ca^{2+} entry.

The intracellular Ca^{2+} can activate cytosolic targets such as calmodulin and $\text{I}\kappa\text{Ba}$ which activate nuclear factor of activated cells (NFAT) and $\text{NF}\kappa\text{Ba}$, respectively (Hogan et al., 2003; Sen et al., 1996) (Figure 1.6). Activation of these two proteins cause them to translocate to the nucleus where they are involved in proliferation (Berridge et al., 2003; Macian, 2005). In addition, Ca^{2+} can also accumulate in the nucleus where it activates CAMKII, CAMKIV and CREB binding protein (CBP) (Bading, 2013; Berridge et al., 2003; Lipskaia and Lompre, 2004; O'Malley, 1994).

A prolonged Ca^{2+} signal is required for proliferation and the cytosolic $[\text{Ca}^{2+}]$ is maintained from a combination of Ca^{2+} from the extracellular space and Ca^{2+} from intracellular stores resulting in oscillations in the concentration of intracellular Ca^{2+} (Berridge, 1995; Bootman, 2012; Lechleiter and Clapham, 1992). Studies on CHO cells and Jurkat cells showed that a Ca^{2+} signal was required for a period of two hours for proliferation. Gene transcription was abated in cells with defective Ca^{2+} channel activity, specifically the CRAC channel, this channel is involved in store operated Ca^{2+} entry i.e. Ca^{2+} influx from the extracellular space (Akagi et al., 1999; Fanger et al., 1995; Timmerman et al., 1996).

Ca^{2+} has also been found to play a role in cell death through apoptosis. Studies have shown an increase in the concentration of cytosolic Ca^{2+} during the early stages of apoptosis. Consequently, studies which investigating the role of Ca^{2+} through mechanisms which cause dysregulation could be complicated by apoptosis (Lynch et al., 2000; Pinton et al., 2008; Rizzuto and Pozzan, 2006)



Nature Reviews | Molecular Cell Biology

Figure 1.6

The bioelectric signalling pathway involving Ca^{2+} in a lymphocytic cell. Ca^{2+} can enter the cell through voltage-gated Ca^{2+} channels in response to changes in the membrane potential. The cytosolic Ca^{2+} binds calmodulin and calcineurin to activate NFAT. The Ca^{2+} also plays a role to activate NF κ B. Ca^{2+} in the nucleus activates CBP which binds to CREB and the Ca^{2+} also activates CAMKIV. Ca^{2+} is also involved in the canonical transduction pathways which is initiated by an antigen binding with the T-Cell receptor which recruits phospholipase C γ 1 which leads to the generation of diacylglycerol and inositol-1,4,5-triphosphate (Ins(1,4,5)P₃). This leads to the release of Ca^{2+} from the endoplasmic reticulum to cause the initial rise in intracellular Ca^{2+} . The depletion of Ca^{2+} from the endoplasmic reticulum goes to activate capacitive Ca^{2+} entry through the activation of Orai by STIM1. The figure is copied from Berridge et al., (2000).

1.4.3 Mechanisms of bioelectric signalling in cell behaviours associated with intracellular ions

Although Ca^{2+} signalling is important in bioelectric signalling and cell behaviours, studies have highlighted other components independent of Ca^{2+} signalling that are potentially involved in bioelectric signalling. For example, a number of studies have shown that apoptosis is averted in the presence of either the non-specific K^+ channel blocker, TEA or an increase in the extracellular $[\text{K}^+]$ implicating the importance of intracellular K^+ in apoptosis (Thompson et al., 2001; Yu et al., 1999). Moreover, in lymphocytes, intracellular K^+ was found to be inhibitory to apoptotic enzymes such as active nuclease and caspases during apoptosis, thus providing protection against apoptosis, albeit through poorly understood mechanisms (Hughes et al., 1997). However, subsequent studies on neuronal apoptosis induced by K^+ efflux using a K^+ channel opener and an K^+ ionophore was inhibited by cycloheximide (an inhibitor of protein synthesis). This study hints at a potential link between K^+ and gene transcription in the bioelectric control of apoptosis. Indeed, a subsequent study by Tao et al., (2006) showed that apoptosis induced by serum deprivation was inhibited by K^+ channel blockers (TEA and cesium) and the TEA also blocked de novo gene transcription of Bcl-X_s, a pro-apoptotic protein. Furthermore, using an assay to investigate the binding ability of transcription factors to their consensus DNA sequences, they also showed the transcriptional activity of NF- κ B is directly up-regulated by a decrease in the concentration of intracellular K^+ .

Changes in the intracellular concentrations of K^+ and Cl^- are also associated with apoptosis through a dramatic decrease in cell volume (Chen et al., 2002; Chen et al., 2007; Yu and Choi, 2000). Several different hypotheses have been made attempting to link changes in cell volume with proliferation and these include changes in intracellular pH, size of the cell and changes in the cytoskeleton (Chen et al., 2007; Dubois and Rouzaire-Dubois, 2004; Urrego et al., 2014). It is also well established that the size of the cell changes during the progression of the cell cycle (Vermeulen et al., 2003).

1.4.4 Components linking ion channel activity and cell cycle regulators

Some of the regulatory factors involved in ion channel mediated effects on the cell cycle have been investigated across a range of cell types. From Table 1.5 it appears that the activity of different channel types, even from the same channel family i.e. voltage-gated K⁺ channel family (KV10.1 and KV1.3) can affect different regulators of the cell cycle.

Mitogenic stimulation of MCF-7 breast cancer cells causes an increase of KV10.1 channel activity and ultimately cell cycle progression whilst inhibition of this channel causes cell cycle arrest in the G1 phase (Borowiec et al., 2011; Ouadid-Ahidouch et al., 2001). MCF-7 breast cancer cells arrested in the G1 phase of the cell cycle could be re-entered into the cell cycle through IGF-1 treatment (as previously discussed, IGF-1 causes G1 to S phase progression and a concomitant increase in the activity of KV10.1) and the effects of IGF-1 are thought to be partly mediated by an increase in cyclin D1. The role of cyclin D1 in the progression of MCF-7 breast cancer cells through G1 is well established (Bartkova et al., 1994). Similarly, aberrant changes in the expression of cyclin D1 and cyclin E were also observed with cell cycle arrest at G1 in MG-63 osteosarcoma cells and mesenchymal stem cells when the KV10.1 channel was knockdown using shRNA (short hairpin RNA) (Wu et al., 2014; Zhang et al., 2014).

Knockdown of Cl⁻ channels using small interference RNA (siRNA) caused cell cycle arrest of endothelin-1-induced proliferation of smooth muscle cells at the G1/S checkpoint together with the downregulation of cyclin D1 and cyclin E and the upregulation of p21^{Waf1/Cip1} p27^{Kip1} (Tang et al., 2008). Cyclin D1 and cyclin E are associated with cell cycle progression whilst p21^{Waf1/Cip1} and p27^{Kip1} restricts the transition between G1 and S. It has to be remembered that knockdown models of ion channels assume a role of the ion channels and thus, bioelectric signalling. As discussed earlier, it is possible that ion channels can exert influence on cell behaviours without passing current.

The effect of ion channel inhibition on cell cycle regulatory proteins.

| Cell line/cell type | Channel type | Cell cycle phase affected by the channel | Cell cycle regulators affected by the channel | Reference |
|---|--------------------------|--|--|-----------------------------|
| MCF-7 (Breast cancer cell line) | KV10.1 | G1 & G1/S | Cyclin D1 Cyclin E pRb | (Borowiec et al., 2007) |
| LoVo (Human colon cell line) | KCa3.1 | G2/M | p-Cdc2 | (Lai et al., 2011) |
| A549 (Human lung cell line) | KV1.3 | G1 | p2Waf1/Cip1 CDK4 Cyclin D3 | (Jang et al., 2011) |
| U87 & U251 (Human glioma cell lines) | Kir6.2 | G1 | p-ERK | (Huang et al., 2009) |
| LNCaP PC-3 DU-145 (Prostate cancer cell line) | KCa3.1 | G1/S | p2Cip1 | (Lallet-Daher et al., 2009) |
| MD (medulloblastoma) CNS tumour | KV10.2 | G2 | Cyclin B1 p38 MAPK | (Huang et al., 2012) |
| HL-60 (Leukaemia cell line) | KV11.1 | G1 | B-catenin Cyclin D1 c-myc | (Zheng et al., 2011) |
| Aortic smooth muscle cells | Cl ⁻ channels | G1 | Cyclin D1 Cyclin E p21Waf1/Cip1 p27Kip1 | (Tang et al., 2008) |

Table 1.5

The table is adapted from Ouadid-Ahidouch and Ahidouch (2013).

In summary, despite advances in understanding the mechanisms involved in the control of proliferation through bioelectric signalling, it seems unlikely that the bioelectric signal controls cell behaviour through a simple binary mechanism. This binary mechanism suggests that a membrane potential depolarisation results in cell proliferation. Conversely, a hyperpolarisation results in the inhibition of proliferation. This raises questions regarding the nature of the bioelectric signal itself and how information bearing instructive roles is encoded in either the membrane potential and/or ion channel activity.

One mechanism that this bioelectric signalling could influence proliferation is through the dynamic nature of the membrane potential in the form of oscillations and fluctuations. It is hypothesised that this dynamic characteristic of the membrane potential can be investigated using the continuous wavelet transform technique.

1.5 Introduction to the dynamic behaviour within human biology

The human body and in fact, all living organisms exhibit dynamic changes in their behaviour and/or physiology which arises from biological clocks (Vitaterna et al., 2001). This biological clock gives rise to rhythms such as the circadian rhythm, ultradian rhythm and the infradian rhythm. The circadian rhythm is approximately 24 hours and determines several behavioural and physiological factors such as patterns of hormone secretion e.g. melatonin and blood pressure (Czeisler and Klerman, 1999; Giles, 2006). These inherent rhythms involve complex interactions between the biological clocks and external cues such as light exposure, behaviour and neuroendocrine feedback mechanisms (Czeisler and Klerman, 1999).

In addition to circadian rhythms, the human body has several other dynamic components, namely, organ systems wherein there are continuous changes that are sometimes oscillatory and these systems are interdependent on each other (Cherif et al., 2012; Stefanovska, 2007b). A primary example of the dynamic behaviour within the human body is the heart beat which pumps blood around the body and this heart beat is manifested as the pulse which is easily measured. In addition to the single entity of the pulse, the cardiovascular system contains other dynamic aspects which

are not as easily measured as the pulse. Complex measurement techniques such as the laser Doppler flowmetry (to measure blood flow) coupled with analytical methods to investigate the time-frequency domain have been used to appreciate the full range of dynamic activity within this cardiovascular system (Kvandal et al., 2006; Stefanovska and Bracic, 1999). Distinct oscillations with frequency intervals ranging from 0.005 Hz to 2 Hz were observed in the analysis of the blood flow recordings in the time-frequency domain using the continuous wavelet transform (CWT) technique (Kvandal et al., 2006; Stefanovska, 2007b). These oscillations correspond to the dynamic activity of different physiological processes feeding into the cardiovascular system which are synchronised to function efficiently (Figure 1.7) (Stefanovska, 2007b). For example, the oscillatory process which has a frequency interval of 0.6 to 2 Hz corresponds to the heart beat (Stefanovska and Bracic, 1999).

The two lowest oscillatory bands have frequency intervals of either 0.005 – 0.0095 Hz or 0.0095 – 0.021 Hz. Both frequency intervals correspond to oscillatory components associated with endothelial cell activity within the cardiovascular system (Bernjak et al., 2008; Kvandal et al., 2006; Kvernmo et al., 1999). The assignment of these frequencies to the activity of endothelial cells was ascertained through studies on blood flow in the presence of endothelial dependent vasodilators using acetylcholine (ACh), sodium nitroprusside (SNP) and N(G)-monomethyl arginine (L-NMMA) (Kvandal et al., 2003; Kvernmo et al., 1999). The application of both ACh and SNP caused a significant increase in the amplitude of the low frequency oscillations, whilst application of L-NMMA in the presence of these two compounds allowed assignment of the dynamic properties to either NO dependent or NO independent endothelial activity. It is possible that these low frequency oscillations arise due to a degree of synchrony between the endothelial cells in the cardiovascular system as vasodilation or vasoconstriction spreads along the vessel and this is associated with changes in ion flow across the cells (Segal et al., 1999). Oscillations related to the activity of endothelial cells could therefore be considered as oscillations in a multicellular context.

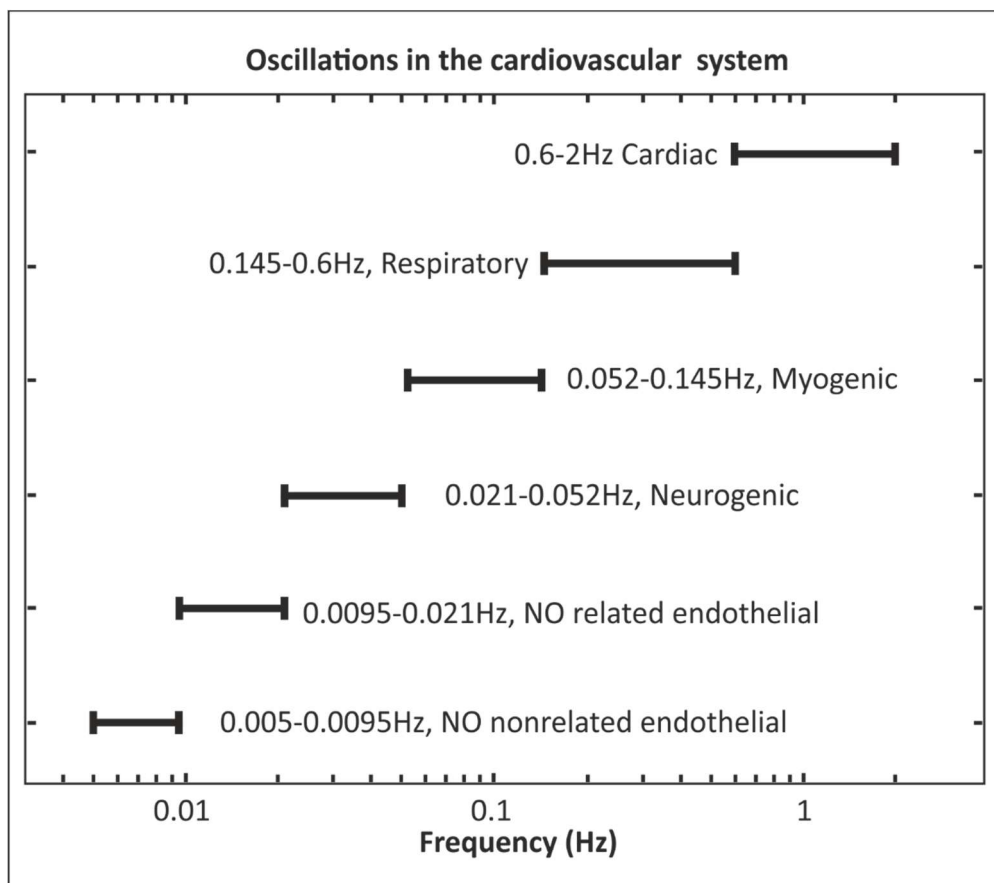


Figure 1.7

Schematic diagram highlighting different oscillatory frequencies identified in the blood flow signal. The blood flow signal was measured using laser Doppler flowmetry and subsequently analysed using the continuous wavelet transform to identify the oscillations. Oscillations with distinct frequency intervals are associated with different aspects of the human body. The figure is adapted from Stefanovska (2007a).

1.5.1 The dynamic nature of the membrane potential

In addition to the oscillatory activity within multicellular systems, oscillations have also been observed in a single cellular context, for example, in recordings of the membrane potential (Lang et al., 1991). A dynamic membrane potential with persistent oscillations has been observed in neurons (Yoshida et al., 2011), fibroblasts (Ince et al., 1984; Lang et al., 1991; Okada et al., 1979), pancreatic β -cells (Goehring et al., 2012), macrophages (Hanley et al., 2004) and mammary epithelial cells (Enomoto et al., 1986). The frequency of the oscillations in the membrane potential of these cells ranged from approximately 0.01 to 0.05 Hz and these oscillations were visible within the recordings themselves. The oscillatory activity of the membrane potential was obvious by eye mainly due to the large degree of change in the membrane potential. For example, the membrane potential of fibroblasts recorded by Lang et al., (1991) changed by approximately 20 mV with a frequency of roughly 0.016 Hz (oscillatory cycle lasting 1 minute) (Figure 1.8). It is possible that the oscillatory behaviour observed in the cardiovascular system using laser Doppler flowmetry coupled with the CWT technique is manifested in the membrane potential.

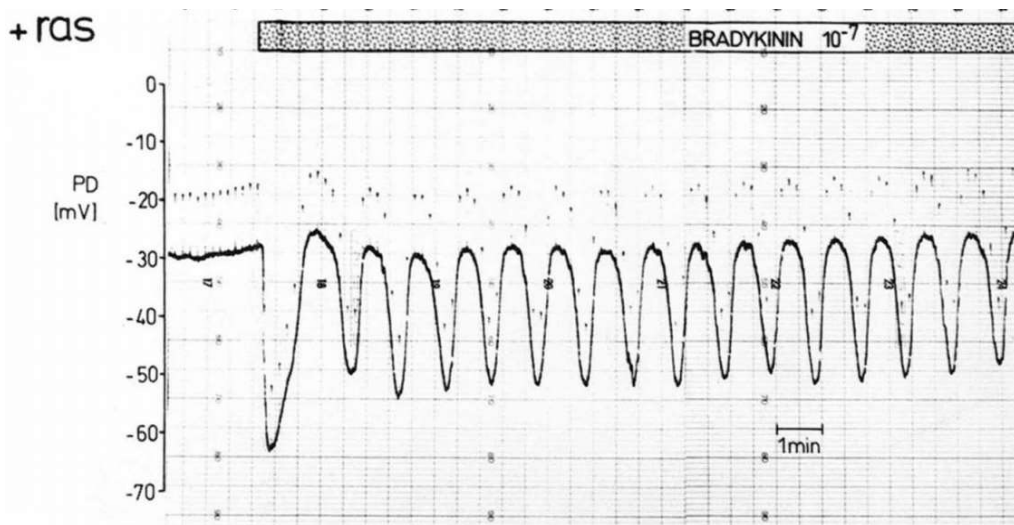


Figure 1.8

The oscillations in the membrane potential of a fibroblast cell. The oscillations in the membrane potential of a fibroblast cell was induced with bradykinin and recorded using the electrical impalement technique. The figure is copied from Lang et al., (1991).

The oscillations in the membrane potential could be important in the context of bioelectric signalling in proliferation due to a number of reasons. Oscillations in the membrane potential of fibroblasts (overexpressing the EGF receptor) and mammary epithelial cells were observed upon treatment with EGF (Enomoto et al., 1986; Pandiella et al., 1989). Activation of the EGF receptor is known to induce a number of intracellular signalling pathways leading to an increase in cytosolic $[Ca^{2+}]$ which in turn plays a role in proliferation (Berridge et al., 2003; Berridge et al., 2000). Oscillations in the membrane potential induced by EGF treatment in mammary gland cells was blocked by inhibitors of the Na^+/K^+ ATPase pump and the K^+ channel, (ouabain and quinine, respectively) (Grinstein and Foskett, 1990; Kuriyama et al., 1995; Moller et al., 1990). Both of these membrane transport protein inhibitors have been shown to block proliferation raising the possibility that oscillations in the membrane potential maybe an important signal for proliferation (Glavinovic and Trifaro, 1988; Pappone and Ortiz-Miranda, 1993). Bradykinin-induced oscillations of the membrane potential of fibroblasts were only observed in cells transfected with a mutated Ha-ras oncogene and mutations in the Ha-ras have been implicated to confer a hyper-proliferative phenotype to cells (Lang et al., 1991; Prior et al., 2012). This again hints at the possible importance of the dynamic membrane potential in encoding a regulatory signal.

The membrane potential oscillations discussed up to this point described oscillations that were induced by perturbing the cells through transfections or treatment with compounds. Furthermore, the oscillations in the membrane potential recordings were easily observed by eye due to the large change in the magnitude of the membrane potential. It is possible that oscillations with a smaller change in the magnitude of the membrane potential were overlooked as more complex analytical techniques were not used. Given the evidence that low frequency oscillations exist in the cardiovascular system and these low frequency oscillations are linked to the activity of endothelial cells, it is possible that there is novel oscillatory behaviour in the membrane potential that is associated with cell behaviours. Consequently, we asked this question and decided to investigate the presence of oscillations and fluctuations in the membrane potential of endothelial cells using the CWT technique.

1.6 Recording the plasma membrane potential

The following section will discuss the techniques available to record the membrane potential. The current techniques available to record the membrane potential of cells are based on either optical methods or electrophysiological methods.

1.6.1 Optical techniques to measure the membrane potential

Optical methods to measure the membrane potential utilise voltage sensitive dyes, also known as potentiometric dyes. The standard potentiometric dyes are based on either oxonols, cyanines or mercocyanines e.g. di-8-ANEEPS, RH421 and DiBAC₄(3), whilst the more advanced dyes use coupled dyes or fluorescence resonance energy transfer (Clarke and Kane, 1997; Gonzalez and Tsien, 1997; Miller et al., 2012; PromoKine, 2015; Whiteaker et al., 2001). These potentiometric dyes relay information of the membrane potential by either an electrochromic or an electrophoretic effect. The dyes which operate through electrophoretic effects traverse the plasma membrane in response to a change in the membrane potential (Sundelacruz et al., 2009). Dyes operating through electrochromic effects relay changes in the membrane potential through a shift in their spectral properties upon coupling between their molecular electronic states with the electric field across the membrane (Loew, 2010).

The dyes are often categorised according to the speed at which they respond to changes in the membrane potential. Some dyes are very slow. For example, the DiBAC₄(3) dye takes more than a minute to reach 90% of its maximum signal. On the other hand, other dyes are classed as fast dyes (the FRET based system takes five seconds to reach 90% of its maximum signal), therefore, the temporal resolution of these dyes varies greatly (Wolff et al., 2003). Furthermore, additional calibration using electrophysiological methods are needed if absolute membrane potential values need to be ascertained (Adams and Levin, 2012). As the aims of the current project include investigating the absolute membrane potential and temporal changes in the membrane potential across a range of frequencies, optical methods to record the membrane potential may not be suitable.

1.6.2 Electrophysiological techniques to record the membrane potential

Electrophysiological methods utilise microelectrodes to record the membrane potential and are considered as the gold standard technique and the information obtained is far superior in comparison to the optical methods (Gonzalez et al., 1999; Harrison et al., 2015). Electrophysiological techniques can be grouped into either intracellular impalements or patch clamping technologies. Intracellular impalements are conducted using a sharp glass microelectrode which impales the cell membrane to make contact with the cytoplasm. Simultaneously, another electrode is positioned in the extracellular solution surrounding the impaled cell. The membrane potential is calculated from the difference in the potential between the cytoplasm of the impaled cell and the electrode in the extracellular solution (Ling and Gerard, 1949).

The patch clamp technique utilises a similar glass microelectrode, however, unlike the impalement technique, this tip of the glass microelectrode is blunt allowing a high resistance seal (usually above $1\text{ G}\Omega$) with a minuscule region of the cell membrane. Subsequently, suction or a short pulse of electricity is applied to remove this region of the plasma membrane to yield access to the cytosol and produce the whole cell configuration (Molleman, 2003). Similar to the impalement technique, a second electrode is positioned in the bath solution and the difference in the electric potential between the two electrodes is considered as the membrane potential.

Despite being the gold standard in measuring the membrane potential, the electrophysiological methods are laborious, time consuming and have a low throughput due to measurements being obtained from individual cells (Stuart and Palmer, 2006). The electrophysiological techniques do however, allow continuous long term recordings with a high accuracy of reporting the membrane potential. Both of these aspects are essential for this project.

1.7 Model cell systems to investigate membrane potential dynamics

1.7.1 Jurkat cells – T-lymphocytes

One of the aims of the current project was to investigate the membrane potential dynamics in cell behaviours such as proliferation and activation. The Jurkat cell line is an established model of T-lymphocytes and allows different aspects of cell behaviour to be investigated. Jurkat cells can also be easily activated by treating them with a mitogen and this activation process can be monitored through assays of IL-2 secretion (Gillis and Watson, 1980; R&D systems, 2015). There is also general consensus that this mitogen-induced activation results in a homogeneous population of activated Jurkat cells. Furthermore, there is evidence that this activation process is related to bioelectric signalling (DeCoursey et al., 1984).

The Jurkat cell line also provides a well characterised model of T-lymphocytes *in vivo*, however, unlike T-lymphocytes *in vivo*, the cells proliferate rapidly *in vitro* with a population doubling time of 24 hours in serum containing growth medium (ATCC, 2015). The Jurkat cells do not require any special conditions to grow in culture, therefore, it is envisaged that the proliferation rate of the cells can be manipulated easily. Moreover, T-lymphocytes *in vivo* are activated upon encountering an antigen which prepares them for proliferation. This aspect of lymphocyte behaviour can also be replicated *in vitro* using a number of different mitogens. As such, Jurkat cells provide the possibility to investigate the membrane potential dynamics in different aspects of proliferation and activation in a single model cell line.

1.7.2 HMEC-1 endothelial cells

As discussed earlier, low frequency oscillations in the cardiovascular system related to the activity of endothelial cells have been identified (Bernjak et al., 2008; Kvandal et al., 2006; Kvernmo et al., 1999). Little however, is known about the origin of these oscillations besides being associated with the activity of microvascular endothelial cells. In addition, as the membrane potential has been shown to influence cell behaviours, the questions were asked if the low frequency oscillations could be manifested in the membrane dynamics of microvascular endothelial cells and if these

low frequency oscillations are related to cell behaviours. Consequently, a human microvascular endothelial cell line similar to endothelial cells *in vivo* suitable for this aspect of the work was identified. Several characteristics and markers of microvascular endothelial cells have been identified and these can be used for comparing the resemblance of *in vitro* cell models with *in vivo* endothelial cells (Table 1.6).

The human umbilical vein endothelial cell (HUVEC) was one of the first model systems to used study endothelial cells (Gimbrone et al., 1974; Jaffe et al., 1973). They are primary cells, therefore, the results obtained from experiments using HUVEC cells are physiologically relevant, however, these cells have a short life span and the phenotype of these cells can vary depending on the source (Koch et al., 1995). To address these limitations several immortalised endothelial cell models have been produced (Figure 1.7). From the available cell lines, the HMEC-1 cell line best reflects the *in vivo* situation of endothelial cells. The immortalized HMEC-1 (CDC/EU.HMEC-1) cell line was established by transfecting human dermal microvascular cells with the pSVT vector. The pSVT vector is a PBR-322 based plasmid encoding the large T antigen of the simian virus 40 (Ades et al., 1992).

In contrast to the Jurkat cells, the HMEC-1 cells are a much less tractable cell system and consequently, are more difficult to manipulate. The work in this thesis, therefore, was undertaken on Jurkat cells and HMEC-1 cells to accomplish the aims of the project.

Markers and characteristics of microvascular endothelial cells and their relevance in endothelial cells.

| Marker/Characteristics | Relevance | Reference |
|---|---|---|
| Cobblestone morphology | Microvascular endothelial cells have a cobblestone morphology | (Ades et al., 1992) |
| Weibel-Palade Bodies | Weibel-Palade bodies store von Willebrand factor multimers for rapid release during vessel injury. Weibel-Palade bodies are specific to endothelial cells. | (Bouis et al., 2001; Sumpio et al., 2002) |
| von Willebrand Factor | Endothelial cells and platelets secrete von Willebrand factor but the vast majority is synthesized by endothelial cells. Von Willebrand factor is instrumental in blood coagulation | (Sumpio et al., 2002) |
| Adhesion molecules | Adhesion molecules include ICAM, VCAM, and E-Selectin. E-selectin is only expressed by endothelial cells. ICAM and VCAM are present in leukocytes and endothelial cells in small numbers but all three adhesion molecules are upregulated to play an important role in the inflammatory response. | (Sumpio et al., 2002) |
| Ulexeuropaeuslectin Agglutinin 1 Binding | Ulexeuropaeuslectin Agglutinin 1 binds selectively to human microvascular endothelial cells. | (Jackson et al., 1990) |
| Acetylated low density lipoprotein uptake | Acetylated low density lipoproteins are taken up by macrophages and endothelial cells. | (Voyta et al., 1984) |
| Tubule Formation | Although not a defining trait, tubule formation is considered important for angiogenesis studies i.e. the expansion of the vascular system from existing vessels. | (Cines et al., 1998) |

Table 1.6

The characteristics of microvascular endothelial model cell lines

| Cell Line | Origin | Morphology | Life span | Weibel-Palade-bodies | von Willibrand Factor | Adhesion molecules | bind Ulexeuropaeus lectinaglutinin I | Uptake of acetylated low density lipoproteins | Tube like structures on matrigel | Reference |
|---------------|----------------|-------------|-----------|----------------------|-----------------------|--------------------|--------------------------------------|---|----------------------------------|-----------------------------------|
| HMEC-1 | Dermal | Cobblestone | Immortal | x | ✓ | ✓ | ✓ | ✓ | ✓ | (Ades et al., 1992) |
| HPEC-A1 | Placenta | | Extended | | ✓ | ✓ | ✓ | ✓ | | (Schutz et al., 1997) |
| hTERT-HDMEC | Dermal | | | | | ✓ | | ✓ | ✓ | (Yang et al., 1999) |
| HPMEC -ST1.6R | Pulmonary | Cobblestone | Immortal | | ✓ | ✓ | | ✓ | | (Krump-Konvalinkova et al., 2001) |
| SV-HCEC | Microvessels | Cobblestone | Immortal | x | ✓ | ✓ | | ✓ | ✓ | (Muruganandam et al., 1997) |
| iHDME 1 | Dermal | | Immortal | | | | | | ✓ | (Jiang et al., 2010) |
| RF24 | Umbilical cord | | Immortal | | ✓ | ✓ | | | | (Fontijn et al., 1995) |
| iSEC | Fetal sinusoid | | Immortal | x | ✓(diffus) | | | | | (Hering et al., |

| | | | | | | | | | | |
|-------------|---------------|-------------|----------|--|-----|--|---|---|---|-----------------------------|
| | | | | | ed) | | | | | 1991) |
| HMVEC | Microvascular | | Immortal | | | | | | ✓ | (Shao and Guo, 2004) |
| HADM EC-5 | Adipose | | Immortal | | ✓ | | ✓ | ✓ | ✓ | (Flynn et al., 1997) |
| hTERT-HDLEC | Lymphatic | Cobblestone | Extended | | * | | | | ✓ | (Nisato et al., 2004) |
| TIME | Microvascular | Cobblestone | Immortal | | | | | ✓ | ✓ | (Venetsanakos et al., 2002) |

Table 1.7

Different microvascular endothelial cell models and their characteristics. The table highlights different characteristics observed in a number of different immortalised models of endothelial cells. Note, the blank fields indicate unknown characteristics.

1.8 Hypothesis and Aims of the current project

It is hypothesised that the membrane potential is a dynamic property of a cell and the static membrane potential influences cell behaviours such as proliferation and activation. The dynamic membrane potential will be investigated using the continuous wavelet transform to highlight oscillations and fluctuations not observed by eye.

As described in this introduction, it is widely accepted that a complex array of ion channels, pumps and carriers play a role in various cell behaviours such as proliferation and activation. Although the static value of the membrane potential is usually associated with the proliferative state of the cell, it is hypothesised that oscillations and dynamic changes in the membrane potential may also play a role. Thus the aims of the project are:

- to continuously record the plasma membrane potential of a single Jurkat cell or a HMEC-1 cell for either 10 or 30 minutes to investigate the presence of fluctuations and oscillations
- to investigate the feasibility of applying the CWT technique to investigate the membrane potential dynamics of Jurkat cells and HMEC-1 cells
- to investigate the presence of low frequency oscillations in the membrane potential of HMEC-1 cells
- to investigate the role of specific ions in the membrane potential dynamics of Jurkat cells
- to investigate the influence of the static membrane potential on mitogen induced activation of Jurkat cells
- to ascertain the culture conditions required to alter Jurkat cell behaviour i.e. alter the proliferative state of Jurkat cells and yield a population of non-proliferating Jurkat cells
- to investigate changes in the membrane potential dynamics of Jurkat cells with altered cell behaviours, focussing on proliferation and activation
- to determine the static membrane potential and the underlying ion channels of Jurkat cells with altered cell behaviours
- to determine the static membrane potential and the underlying ion channels present on the plasma membrane of HMEC-1 cells.

2 MATERIALS AND METHODS

2.1 Materials

Jurkat E6.1 cells were purchased from the American Type Culture Collection (ATCC) and the HMEC-1 cells (termed CDC/EU.HMEC-1) were a kind gift from Dr. Victoria Heath from the University of Birmingham (Kaur et al., 2011).

2.2 Methods

2.2.1 Cell culture

Culturing actively proliferating Jurkat cells. Jurkat E6.1 cells a widely used human T-lymphocyte cell line was used as a model of T-lymphocytes. These cells were cultured in 25 cm³ flasks (Nunc) at 37°C with 95% air and 5% CO₂. The Jurkat cells were cultured in RPMI-1640 medium (Sigma Aldrich) supplemented with 10% foetal bovine serum (FBS) (Life Technologies) and 100 units/ml penicillin and streptomycin (Sigma Aldrich). The cells were subcultured in fresh culture medium at a dilution ratio of 1:10 (1 ml of cells in 10 ml of new culture medium) every 2-3 days by centrifuging the medium containing the Jurkat cells at 600RPM for 5 minutes, removing the supernatant and resuspending the cell pellet in a new T25 culture flask containing 7 ml of warm RPMI-1640 medium. The cells were maintained at a density between 1x10⁵

and 1.2×10^6 cells/ml. The new T25 flask was incubated at 37°C with 95% air and 5% CO₂.

Culturing viable Jurkat cells in a state of inactive proliferation. In experiments where Jurkat cells that were viable but not in a proliferative state, the cells were cultured in RPMI-1640 medium supplemented with 1% FBS and 100 units/ml penicillin and streptomycin and used at 48 hours. Briefly, the cells were subcultured from the T25 flask containing the main stock of Jurkat cells by centrifuging the cells at 600RPM for 5 minutes. The supernatant was removed and the pellet was resuspended in warm RPMI-1640 medium. Trace amounts of FBS was removed by centrifuging the cell suspension at 600RPM for 5 minutes. The cell pellet was then resuspended in warm RPMI-1640 and the volume of medium containing 2×10^5 cells/ml was transferred to a T25 flask containing fresh new RPMI-1640 medium supplemented with 1% FBS and 100 units/ml penicillin and streptomycin. These cells were used at 48 hours.

Culturing HMEC-1 cells. HMEC-1 cells were cultured in Medium 199 (Sigma Aldrich) supplemented with 10% FBS, 10% Glutamax (Life Technologies), 100 units/ml penicillin and streptomycin antibiotic and large vessel endothelial cell growth supplement (TCS Cellworks). The cells were cultured in T25 culture flasks at 37°C with 95% air and 5% CO₂. The HMEC-1 cells were subcultured at a ratio of 1:10 every 5-7 days.

2.2.2 Trypsinising HMEC-1 Cells

The HMEC-1 cell line is an adherent cell line, consequently, to maintain a healthy population of cells, the cells needed to be disassociated from the bottom of the T25 culture flask before each subculture. The HMEC-1 cells were subcultured at a ratio of 1:10. The medium from the T25 culture flask containing the HMEC-1 cells was removed and the cells were washed three times with Dulbecco's Phosphate-Buffered Saline (DPBS) without Ca²⁺ and Mg²⁺ (Gibco). 500 µl of Trypsin-EDTA (Gibco) was added to the T25 flask and the flask was incubated for 5 minutes at 37°C. After which, the flask was removed from the incubator and gently tapped on the side to ensure the HMEC-1 cells had detached from the surface of the flask. 7 ml of fresh complete medium was added to the flask and 700 µl volume of the cell suspension was

transferred to the new T25 flask containing pre-warmed complete medium. The flask was then incubated at 37°C with 95% air and 5% CO₂ until required.

2.2.3 Cell viability and proliferation assays

Cell viability and proliferation was determined using either the trypan blue exclusion dye (Sigma Aldrich) or the PrestoBlue cell viability reagent (Invitrogen). Cell viability determined with the trypan blue exclusion dye was completed by mixing 20 µl of trypan blue with an equal volume of RPMI-1640 medium containing the Jurkat cells. 20 µL of the suspension containing the trypan blue and Jurkat cells was then loaded on a haemocytometer and the viable and non-viable cells were counted. The Jurkat cells which were unstained were considered as viable whilst the Jurkat cells which were stained blue were considered non-viable. Proliferation of the Jurkat cells was determined as cells per ml using the calculation below

$$\text{Cells (x}10^4 \text{ per ml)} = \text{Number of cells} \times \left(\frac{\text{dilution factor}}{\text{Numer of large squared counted}} \right)$$

The % cell viability was ascertained using the following formula

$$\text{Viability (\%)} = \frac{\text{Number viable cells}}{\text{Total number of cells}} \times 100$$

Cell viability established using the PrestoBlue cell viability reagent was completed by adding PrestoBlue at a ratio of 1:10 to each well on the 96 well plate. The rate of proliferation was ascertained by incubating a known density of Jurkat cells which ranged from 1x10⁵ cells/ml to 5x10³ cells/ml and the PrestoBlue cell viability reagent added at the same time as incubating the test wells with the PrestoBlue reagent. The 96 well plate was then incubated at 37°C for 10 minutes and the fluorescence was read at 560 nm on a plate reader (Tecan Infinite 200). The fluorescence from the known concentration of cells was plotted as the function of the cell density. The cell density of the Jurkat cells present in the test wells was interpolated from this graph.

Investigating proliferation and cell viability of the Jurkat cells cultured in a range of FBS concentrations. Jurkat cells cultured in RPMI-1640 medium were supplemented with FBS concentrations ranging from 0% to 10%. These Jurkat cells were incubated in a T25 flask for 24, 48 or 72 hours at 37°C with 95% air and 5% CO₂. After the required time lapsed, the cells were counted using the same method used for the trypan blue exclusion dye to determine viability and the rate of proliferation. The rate of proliferation and cell viability of Jurkat cells cultured in identical conditions was also ascertained using the PrestoBlue cell viability reagent. In these experiments, the Jurkat cells were cultured in 96 well plates and the seeding density of the Jurkat cells was 2x10⁵ cells/ml. These experiments were repeated three times in triplicate.

Investigating proliferation and cell viability of Jurkat cells stimulated with mitogens and cultured in a range of FBS concentrations. Jurkat cells were cultured in RPMI-1640 medium supplemented with a range of FBS concentrations with and without the presence of either the concanavlin A (ConA) (Sigma Aldrich) or phytohaemagglutinin (PHA) (Sigma Aldrich) mitogen were seeded in 96 well plates at a density of 2x10⁵ cells/ml. These 96 well plates were incubated at 37°C with 95% air and 5% CO₂ between 24 and 72 hours. After the required culturing time lapsed, the cell viability was determined by adding PrestoBlue. A negative control containing RPMI-1640 medium rather than cells was added into each plate. Each condition in the ConA experiment was performed in triplicates and each triplicate repeated three times. Each condition in the PHA experiment was obtained in triplicates and repeated twice. The required concentration of either ConA or PHA was made by diluting the required concentration in dH₂O and then sterile filtered prior to freezing in aliquots until needed.

2.2.4 Cell cycle analysis

Cell suspension containing 1.5x10⁶ Jurkat cells/ml was centrifuged and the supernatant was removed. The cell pellet was resuspended in phosphate buffered saline (PBS) (Sigma Aldrich) and fixed in ice cold absolute ethanol for 30 minutes. The cells were then centrifuged and the supernatant removed. The cell pellet was then resuspended in 480 µL of PBS. RNase A (Thermo Scientific) and propidium iodide (Cambridge Bioscience) was added to the cell suspension at a final concentration of

20 µg/ml and 50 µg/ml, respectively. The cells were then analysed by flow cytometry using PE detection. The data was captured using the FACSDiva software (BD Biosciences) and subsequently analysed using ModFit LT 4.1 (Verity Software House) to ascertain the percentage of cells in the G0/G1, S, G2, and M phase of the cell cycle.

2.2.5 Interluekin-2 secretion assay

Jurkat cells secrete interleukin-2 (IL-2) when activated with mitogens (ATCC, 2015). To investigate the activating effects of ConA and PHA, the IL-2 concentration was measured using the Human IL-2 Quantikine ELISA kit (R&D systems). Jurkat cells were seeded at 2×10^6 cells/ml in RPMI-1640 supplemented with a final concentration of 10% FBS with either 20 µg/ml ConA, 20 µg/ml PHA or 20 µl RPMI. The experiments were conducted on 96 well plates. In a series of experiments, the same conditions were used with the addition of RPMI-1640 culture medium supplemented with either 6 mM or 30 mM K⁺, Na⁺, Cl⁻, K⁺ and Na⁺ or 0.5 mM 4-aminopyridine (4-AP). A sorbitol control was included to ascertain the effect of osmolarity changes caused by the elevated ions. In another series of experiments the Jurkat cells were seeded with RPMI-1640 medium supplemented with 1% FBS in the presence and absence of 20 µg/ml PHA. The assay incorporated known IL-2 standards to interpolate the concentration of the IL-2 concentration of the test wells.

The IL-2 Quantikine assay was completed by adding 100 µl of the assay diluent which contained a buffered protein base to the test wells followed by 100 µl of either the human IL-2 standard or the test sample. The solution was left to incubate for 2 hours at room temperature, after which the wells were washed with the Wash buffer three times. Subsequently, 200 µl of a polyclonal antibody specific for human IL-2 conjugated to horseradish peroxidase was added to the wells and left to incubate for 2 hours at room temperature. The wells were then washed again with the Wash buffer three times and the 200 µl of substrate solution was added to the wells and left to incubate for 20 minutes at room temperature. The substrate solution contained hydrogen peroxide and the chromogen, tetramethylbenzidine. After 20 minutes, 50 µl of the Stop solution which contained 2 N sulphuric acid was added and the color was measured immediately at 540 nm. The known human IL-2 standard solution and wash

buffer were made one hour before completing the assay whilst the substrate solution was made 5 minutes prior to its use as per the manufacturer's instructions.

2.3 Patch clamping

The patch clamping technique was used to investigate the whole cell currents and the membrane potential of the Jurkat cells and the HMEC-1 cells.

2.3.1 Patch clamping measurements

Equipment. The patch clamping rig is shown in Figure 2.1. The patch pipette was positioned in a standard pipette holder (Warner Instruments, Hamden) which in turn was attached to an Axon CV201 headstage (Axon, USA). The pipette holder contained a silver/silver chloride wire and was connected to a 1 ml syringe. The syringe allowed for pressure to be applied to the patch pipette and was used to achieve a $G\Omega$ seal. The headstage was connected to the Axopatch 200B amplifier (Axon, USA). The headstage was also connected to another pipette holder containing a silver/silver chloride pellet electrode containing 3 M KCl with a 5% agar bridge. This agar bridge was positioned in the bath solution. The headstage was mounted on a bracket attached to a micromanipulator allowing coarse and fine movements. To reduce the electrical noise, the cells were patched inside a faraday cage as shown in Figure 2.1. In addition, all of the different pieces of equipment were grounded. The cells were continually perfused with the required extracellular solution. The inlet of the perfusion system was based on a gravity fed system whilst the outlet of the perfusion was based on a peristaltic pump.

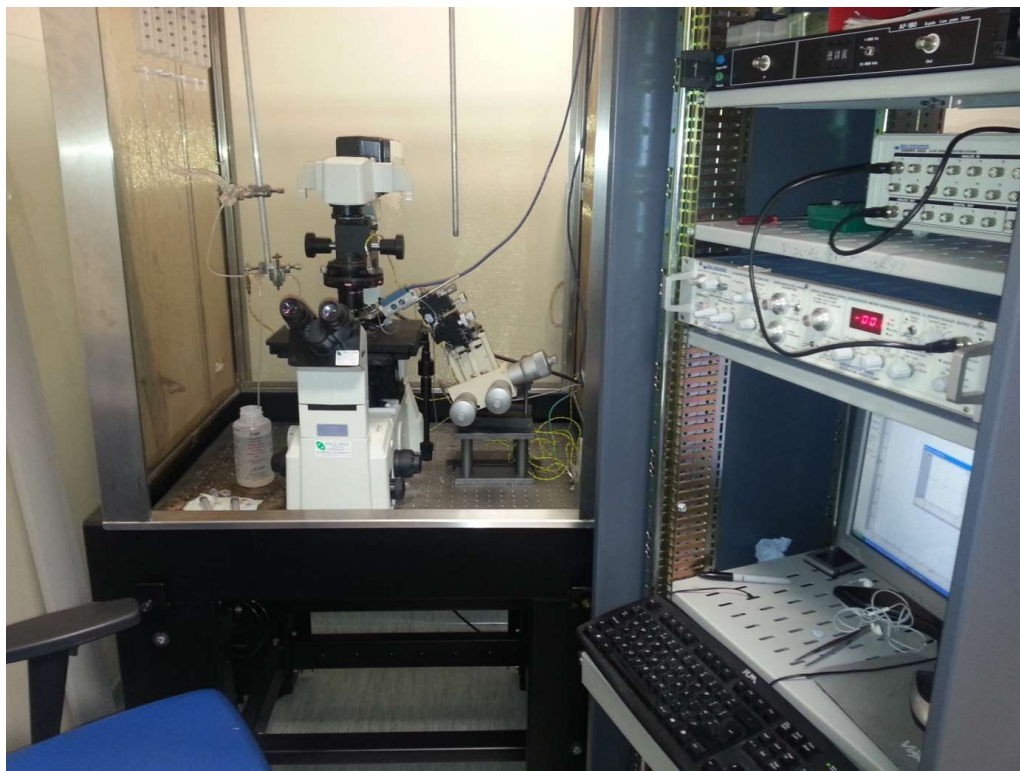


Figure 2.1

A picture of the patch clamping rig. The microscope, micromanipulator, headstage and the gravity fed perfusion system were kept in a faraday cage to reduce electrical noise. These pieces of equipment together with the amplifier were also grounded to a thick copper wire inside the faraday cage to further reduce electrical noise.

Cell handling. On the day of experiments on Jurkat cells, 200 µl of Jurkat cells were removed from the culture flask and kept at room temperature. 50 µl of the cell suspension was then placed on 35mm culture dishes for patching. These cells were left for 5 minutes to settle before the perfusion system was switched on. This settling time allowed the Jurkat cells to loosely adhere to the bottom of the culture dish. The Jurkat cells were kept on the culture dish for a maximum of 60 minutes before being replaced. The cells were kept at room temperature for a maximum time of 2 hours before being replaced by a fresh 200 µl cell suspension from the cell culture flask (see Section 2.2.1).

For experiments using HMEC-1 cells, an aliquot of HMEC-1 cells taken from the T25 culture flask containing HMEC-1 cells were seeded on a 35mm culture dish 24 hours before patch clamping experiments. The confluence of the HMEC-1 cells in these culture dishes was not allowed to exceed 60% confluency (determined visually). If required, the confluency was diluted by adding fresh Medium 199. On the day of the experiments, a culture dish containing the HMEC-1 cells was placed on the microscope and the cells were perfused for 10 minutes to remove trace amounts of the culture medium before being patched. The culture dish was used for a maximum of 90 minutes before being replaced by another culture dish containing fresh new cells.

The culture dish containing the cells was positioned on the stage of the Nikon Diaphot inverted microscope (Nikon, Japan). The microscope and the micromanipulator were positioned on a floating table which was kept in a Faraday cage to provide electrical insulation. The microscope, perfusion system and micromanipulator were earthed to the Faraday cage. The patch clamping measurements were conducted using the Axopatch 200B amplifier. The stimulation protocols were set up using Clampex 8.1 software (Molecular devices, USA) and was visualised on a computer monitor. The sampling frequency was 10 KHz and the recorded currents were saved directly to the computer.

Recording conditions. The electrophysiological experiments were conducted using the patch clamping technique in the whole cell configuration (Hamill et al., 1981). All electrophysiology experiments were carried out between 20-22°C with borosilicate glass pipettes. The borosilicate glass had an external diameter of 1.5-1.8 mm. The

pipettes had a resistance between 3-5 M Ω . The patch pipettes were fabricated using a 2 stage pipette puller (Narishige, Japan). The pipette tip was filled by placing the pipette by drawing up the required intracellular solution using a 1 ml syringe. The remainder of the pipette was back filled with the required intercellular pipette solution using an adapted pipette tip with a fine elongated end attached to a 1 ml syringe.

2.3.2 Procedure for patch clamping

In order to patch a cell, positive pressure was applied to the patch pipette using a 1 ml syringe attached to the patch pipette holder to prevent debris contaminating the patch pipette tip. This pipette was then positioned in the culture dish containing the cells using the coarse micromanipulator. The seal test function on the Clampex software was selected and the junction potential was adjusted to zero using the pipette offset dial on the amplifier when the patch pipette was close to the target cell. A square pulse was also observed at this point (Figure 2.2). The seal test was programmed to deliver a 2 mV pulse at a holding potential of 0 mV. The patch pipette was then positioned such that it was touching the cell membrane of the target cell using the fine controls on the micromanipulator. Contact between the tip of the patch pipette and the cell membrane was confirmed with an increase in the seal resistance by approximately 0.5 M Ω on the seal test function. At this point, gentle negative pressure was applied to the back of the patch pipette using the syringe. The negative pressure was locked and the seal resistance was left to form a G Ω seal. During this sealing process, the holding potential was gradually hyperpolarised from 0 mV to -60 mV to help achieve a G Ω seal. The seal formation was monitored using the seal test function in Clampex. A G Ω seal was confirmed by an increase in pipette capacitance together with the increase in the seal resistance. The pipette capacitance was minimized using the fast capacitance dial on the amplifier.

The whole cell configuration was achieved by applying gentle suction using the 1 ml syringe. Successful break-in was confirmed by an increase in the transient capacitance due to the series resistance, that is the combination of the cell capacitance and the series resistance of the pipette and access. Immediately upon achieving the whole cell configuration, the membrane voltage of the cell was noted by changing to the current clamp mode. The amplifier was then switched back to the voltage clamp mode and the capacitance was reduced using the fast and slow pipette capacitance compensation

together with the whole cell capacitance and series resistance capacitance compensation on the amplifier. The cytosolic solution and the intracellular pipette solution were allowed to equilibrate for 10 minutes before any stimulation protocols were applied. The membrane voltage recordings were made in current clamp mode. The stimulation protocols used in the voltage clamp mode are described in the figure legends in the results chapters.

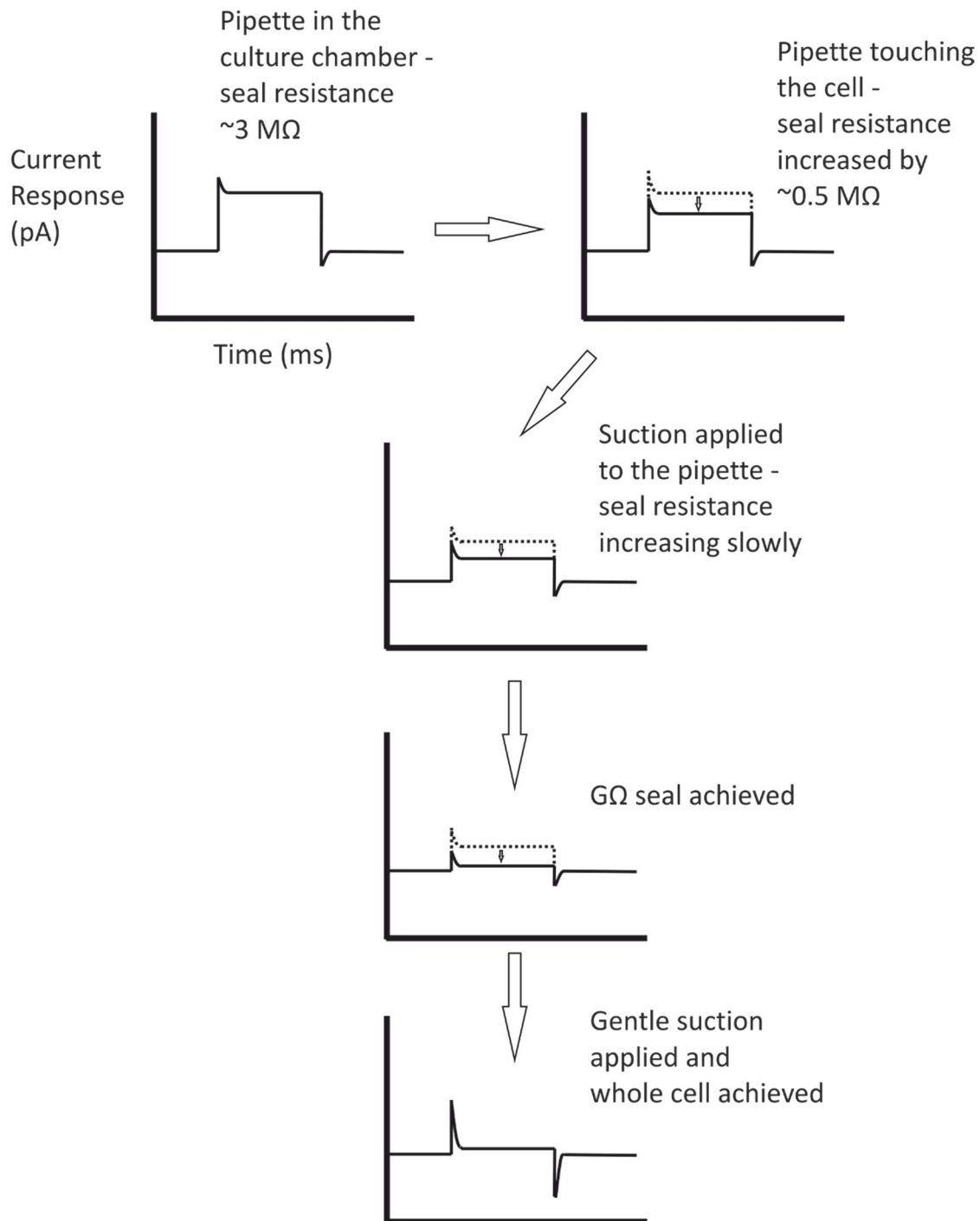


Figure 2.2

Schematic diagram showing the current response during the different steps of achieving a whole cell configuration. The low resistance shown whilst the pipette is in the solution but not touching the cell indicates the resistance of the pipette tip. An increase in the resistance indicates contact between the pipette tip and the plasma membrane of the target cell. Gentle suction usually results in an increase in the resistance and further sealing between the pipette and the membrane. Suction is stopped when the seal resistance exceeds a giga Ω . Further suction is applied to achieve the whole cell configuration.

2.3.3 Intracellular and extracellular solutions used in the patch clamping experiments

Solutions used in patch clamping experiments of Jurkat cells. Electrophysiology experiments to investigate the membrane potential and the whole cell currents of Jurkat cells were undertaken in various extracellular and intracellular solutions. Table 2.1 details the standard intracellular solution used. The osmolarity of the solutions was between 280 mOsm and 310 mOsm and was measured using a Vapro osmometer (Wescor, USA).

The composition of the standard intracellular and extracellular solutions used to patch Jurkat cells

| Constituent | E1 Standard extracellular solution (mM) | I1 Standard intracellular solution (mM) | E1K Elevated extracellular K ⁺ solution (mM) | E1Cl Low extracellular Cl ⁻ solution (mM) | E1Na Low extracellular Na ⁺ solution (mM) | I1Ca Elevated intracellular Ca ²⁺ solution (mM) |
|-------------------|---|---|---|--|--|--|
| KCl | 6 | 120 | 6 | - | 6 | 120 |
| NaCl | 150 | 20 | 150 | - | 10 | 20 |
| MgCl ₂ | 1 | - | 1 | 1 | 1 | - |
| CaCl ₂ | 2 | - | 2 | 2 | 2 | 1µM |
| Hepes | 10 | 10 | 10 | 10 | 10 | 10 |
| Glucose | 10 | - | 10 | 10 | 10 | - |
| EGTA | - | 11 | - | - | - | 11 |
| K gluconate | - | - | 54 | 6 | - | - |
| Na gluconate | - | - | - | 150 | - | - |
| Choline Cl | - | - | - | - | 140 | - |
| pH | 7.4 | 7.2 | 7.4 | 7.4 | 7.4 | 7.2 |

Table 2.1

The constituents of the standard extracellular and intracellular pipette solutions used in patch clamping experiments on Jurkat cells. The solutions were made by adding each of the constituents from stock solutions prepared in advance. The bath solutions were made up to 450ml with dH₂O. The pH of the solutions was then adjusted to 7.4 with NaOH and then dH₂O was added to make the volume of the solution 500ml. The intracellular solution I1 was made to a final volume of 100 ml but the pH was adjusted to 7.2 with KOH. The concentration of CaCl₂ in solution I1Ca is the free concentration of Ca²⁺. The intracellular solution was frozen in aliquots of 1 ml and frozen until required. Solutions E1K and I2 were designed to isolate K⁺ currents.

In a series of experiments, solutions were designed to isolate chloride currents. KCl in the extracellular and intracellular solutions was replaced with equimolar concentrations of CsCl to avoid contamination of the whole cell currents with the conductance of K^+ . To investigate the Cl^- selectivity of these currents, extracellular solution E2Cl which contained 12 mM Cl^- rather than the 162 mM Cl^- in solution E2 was used. Table 2.2 shows the constituents of the solutions used in this series of experiments.

The composition of the K^+ free intracellular and extracellular solutions used to investigate Cl^- selective currents in Jurkat cells

| Constituent | E2Cl extracellular solution (mM) | E2.1 K^+ Free extracellular solution (mM) | E2.1Cl K^+ Free reduced extracellular Cl^- solution (mM) | I2 K^+ free intracellular solution (mM) | I2Ca K^+ free intracellular solution (mM) |
|-------------------|---|---|---|---|---|
| CsCl | - | - | 6 | 120 | 120 |
| NaCl | - | 150 | - | 20 | 20 |
| MgCl ₂ | 1 | 1 | 1 | - | - |
| CaCl ₂ | 2 | 2 | 2 | - | 5 μ M |
| Hepes | 10 | 10 | 10 | 10 | 10 |
| Glucose | 10 | 10 | 10 | 10 | 10 |
| Na Gluconate | 150 | - | 150 | - | - |
| K Gluconate | 6 | - | - | - | - |
| EGTA | - | - | - | 11 | 5 |

Table 2.2

Solutions designed to isolate Cl^- currents. The concentration of CaCl₂ in solution I2Ca is the free concentration of Ca²⁺. The pH of the extracellular solutions was 7.4 whilst the pH of the intracellular solutions was 7.2. The solutions were made up as described in Table 2.1.

To isolate slow activating currents present in Jurkat cells, solutions were designed to eliminate the conductance of K⁺, Na⁺, and Cl⁻. Solutions with different pH were made as shown in Table 2.3.

The composition of intracellular and extracellular solutions used to investigate slow activating currents observed in Jurkat cells

| Constituent | E3 extracellular solution (mM) | I3 intracellular solution (mM) |
|-------------------|--------------------------------------|--------------------------------------|
| D-Gluconic acid | 100 | 100 |
| CaCl ₂ | 1 | - |
| MgCl ₂ | - | 2 |
| EGTA | - | 1 |
| Buffer | 100 MES 100 Hepes 100 Tricine | 100 MES |
| pH | 6.5 7.5 8.5 | 6.4 |

Table 2.3

The constituents of the extracellular and intracellular pipette solution designed to isolate the slow activating currents. The solutions were made by adding each of the constituents from stock solutions. The pH of the solutions was adjusted using chlorine hydroxide. When the pH of the extracellular solution was 6.5, the buffer 2-ethanosulfonic acid (MES) was used in the solution. HEPES was used as the buffer in the extracellular solution with a pH of 7.5. When the pH of the extracellular was 8.5 tricine was used as the buffer in the solution. The solutions were made as described in Table 2.1.

Solutions used in patch clamping experiments of HMEC-1 cells. Patch clamping experiments investigating the whole cell currents and the membrane potential of HMEC-1 cells were undertaken in various extracellular and intracellular solutions. The intracellular and extracellular solutions are detailed in Table 2.4. These solutions were altered depending on the experimental requirements. The osmolarity of the solutions was between 280 mOsm and 310 mOsm.

The composition of standard intracellular and extracellular solutions used to patch HMEC-1 cells

| Constituent | HE1 extracellular solution (mM) | HI1 intracellular solution (mM) | HI1.2 intracellular solution (mM) | HI1.3 intracellular solution (mM) | HE1Cl Reduced extracellular Cl ⁻ solution (mM) | HE1Na Reduced extracellular Na ⁺ solution (mM) | HE1K Elevated extracellular K ⁺ solution (mM) |
|-------------------|---------------------------------------|---------------------------------------|---|---|---|---|--|
| KCl | 6 | 40 | 40 | 40 | - | 6 | 6 |
| K gluconate | - | 100 | 100 | 100 | 6 | - | 24 |
| NaCl | 150 | - | - | - | - | 10 | 150 |
| MgCl ₂ | 1 | 1 | 1 | 1 | 1 | 1 | 1 |
| EGTA | - | 1 | 1 | 1 | - | - | - |
| HEPES | 10 | 10 | 10 | 10 | 10 | 10 | 10 |
| Na-ATP | - | 4 | - | 4 | - | - | - |
| CaCl ₂ | 2 | - | 1 μM | 1 μM | 2 | 2 | 2 |
| Glucose | 10 | - | - | - | 10 | 10 | 10 |
| Na Gluconate | - | - | - | - | 150 | - | - |
| HCl | - | - | - | - | - | 140 | - |

| | | | | | | | |
|----|-----|-----|-----|-----|-----|-----|-----|
| pH | 7.4 | 7.2 | 7.2 | 7.2 | 7.4 | 7.4 | 7.4 |
|----|-----|-----|-----|-----|-----|-----|-----|

Table 2.4

The constituents of the extracellular and intracellular pipette solutions used to investigate the currents from HMEC-1 cells. The solutions were made up as described in Table 2.1. The concentration of CaCl₂ in solution H1.2 and HI1.3 is the free concentration of Ca²⁺. The pH of the intracellular solutions were adjusted to 7.2 using KOH whilst the pH of the extracellular solutions were adjusted to 7.4 using NaOH with the exception of solution HE1Na which was adjusted to pH 7.4 using NMDG.

The composition of the intracellular and extracellular solutions used to investigate the K⁺ selectivity of the currents recorded from HMEC-1 cells

| Constituent | HE2 Redesigned extracellular solution (mM) | HI2 Redesigned intracellular solution (mM) | HE2KCl Elevated extracellular K ⁺ solution (mM) | HE2MgCl Elevated extracellular Mg ²⁺ solution (mM) | HE2KG Elevated extracellular K ⁺ solution (mM) | HI2.1 intracellular solution (mM) |
|-------------------|--|--|--|--|---|--|
| KCl | 10 | 140 | 110 | 10 | 10 | 140 |
| K gluconate | - | - | - | - | 100 | - |
| NaCl | 40 | - | 40 | 40 | 40 | - |
| MgCl ₂ | 1 | 1 | 1 | 101 | 1 | 1 |
| EGTA | - | 1 | - | - | - | 1 |
| HEPES | 10 | 10 | 10 | 10 | 10 | 10 |
| Na-ATP | - | 4 | - | - | - | 4 |
| CaCl ₂ | 2 | - | 2 | 2 | 2 | 100nM |
| Glucose | 10 | - | 10 | 10 | 10 | - |

Table 2.5

The constituents of the redesigned solutions used to investigate K⁺ selectivity of the whole cell currents recorded from HMEC-1 cells. The solutions were made up as described in Table 2.1. The concentration of CaCl₂ in solution HI2.1 is the free concentration of Ca²⁺. The pH of the intracellular solutions was adjusted to 7.2 using KOH whilst the pH of the extracellular solutions was adjusted to 7.4 using NaOH.

The composition of the intracellular and extracellular solutions used to investigate the selectivity and Ca^{2+} sensitivity of the currents recorded from HMEC-1 cells

| Constituent | HE3 Extra-cellular solution (mM) | HE3.1 Extra-cellular solution (mM) | HE3.1K Extra-cellular solution (mM) | HE3.1Cs Extra-cellular solution (mM) | HE3.1KG Extra-cellular solution (mM) | HI3 Intra-cellular solution (mM) | HI3.1 Intra-cellular solution (mM) | HI3.2 Intra-cellular solution (mM) | HI3.3 Intra-cellular solution (mM) | HI3.4 Intra-cellular solution (mM) | HI3.5 Intra-cellular solution (mM) |
|-------------------|-------------------------------------|---------------------------------------|--|---|---|-------------------------------------|---------------------------------------|---------------------------------------|---------------------------------------|---------------------------------------|---------------------------------------|
| KCl | 10 | 10 | 110 | - | 10 | 140 | 140 | 140 | 140 | 140 | 140 |
| CsCl | - | - | - | 100 | - | - | - | - | - | - | - |
| NaCl | 40 | - | - | - | - | - | - | - | - | - | - |
| MgCl ₂ | 1 | 1 | 1 | 1 | 101 | 1 | 1 | 1 | 1 | 1 | 1 |
| EGTA | - | - | - | 1 | 1 | 1 | 1 | - | - | - | 1 |
| HEPES | 10 | 10 | 10 | 10 | 10 | 10 | 10 | 10 | 10 | 10 | 10 |
| Na-ATP | - | - | - | - | - | 4 | 4 | 4 | 4 | | 4 |
| CaCl ₂ | 2 | 2 | 2 | 2 | 2 | - | 100 nM | 200 nM | 600 nM | 600 nM | 1 μ M |
| Glucose | 10 | 10 | 10 | 10 | 10 | 10 | 10 | 10 | 10 | 10 | 10 |
| Mg-ATP | - | - | - | - | - | - | - | - | - | 4 | - |
| Mg-ATP | 4 | 4 | 4 | 4 | 4 | 4 | 4 | 4 | 4 | - | 4 |
| NMDG | | 40 | 40 | 40 | 40 | - | - | - | - | 40 | - |
| K gluconate | - | - | - | - | 10 | - | - | - | - | - | - |

| | | | | | | | | | | |
|----|-----|-----|-----|-----|-----|-----|-----|-----|-----|-----|
| pH | 7.4 | 7.4 | 7.4 | 7.4 | 7.4 | 7.2 | 7.2 | 7.2 | 7.2 | 7.2 |
|----|-----|-----|-----|-----|-----|-----|-----|-----|-----|-----|

Table 2.6

The constituents of solutions used to investigate K⁺ selectivity and Ca²⁺ sensitivity of the whole cell currents. The solutions were made up as described in Table 2.1. The pH of extracellular solutions containing Na⁺ was adjusted using NaOH whilst the pH of the intracellular solutions containing Na⁺ was adjusted with KOH. The pH of the solutions containing NMDG was adjusted with HCl. The concentration of CaCl₂ in solutions HI3.1, HI3.2, HI3.3, HI3.4 and HI3.5 is the free concentration of Ca²⁺.

2.4 Stimulation protocols

The standard protocol to study whole cell currents had test potentials ranging from +80 mV to -100 mV with -20 mV steps from a holding voltage of -80 mV. The time interval between each voltage step ranged between 1 second and 60 seconds depending on the experiment.

2.5 Data analysis

2.5.1 Analysis of the whole cell currents

Selectivity of the currents. Whole cell currents obtained were analysed by constructing a current-voltage (IV) plot. The selectivity of the instantaneous currents was characterized by using the same stimulating protocol in solutions containing different concentrations of the ion in question. An IV plot of the currents was constructed and the reversal voltages (E_{rev}) i.e. the membrane voltage at which there is no net flow of ions was noted for both extracellular solutions. The E_{rev} was then compared to the calculated E_{rev} for the ion in question using the Nernst equation (Hille, 1992).

In some experiments the current is presented as the chord conductance. The chord conductance was defined by

$$G = \left(\frac{I_{max}}{(V - E_{rev})} \right)$$

Where G is the conductance, I_{max} is the peak current, V is the test potential at which the peak current was measured and E_{rev} is the reversal voltage.

Characterizing the activation and inactivation kinetics of the time dependent current with rapid activation with slow inactivating properties. Kinetic analysis of the activation and the inactivation phase of this time dependent current were undertaken using the single exponential function

$$F(t) = \sum_{i=1}^n A_i \left(1 - e^{-t/t_i} \right) A + C$$

Where A_i is the maximum outward current amplitude of the current, t_i is the decay time constant.

Characterizing the effect of channel blockers on currents. In experiments investigating the effect of channel blockers, various approaches were used. In one series of experiments investigating either the TEA or 4-AP blockers on the current thought to be conducted by K^+ , a range of blocker concentrations were used to produce a dose response curve. The dose response curve was constructed as the % inhibition and was calculated by

$$\% \text{ Inhibition} = \left(\frac{\text{Peak current in the presence of TEA}}{\text{Peak current in the absence of TEA}} \right) \times 100.$$

The data was fitted with the Hill function and the K_d value and Hill coefficient was noted.

In experiments investigating the instantaneous outward current, NPPB was used at a single concentration of 100 μM and an IV plot of the currents in the presence and absence of this blocker was plotted.

2.5.2 Nonlinear analysis of the membrane potential using continuous wavelet transform

The presence of fluctuations and oscillations was investigated using the CWT. The technique highlights the power, the frequency and the time at which the fluctuations occur (Figure 2). This technique is capable of highlighting fluctuations and oscillations of a lower power which would not be observed by eye.

The membrane potential was recorded for either 10 minutes or 30 minutes using the current clamp mode of the patch clamping technique. The recorded membrane potential was analysed for nonlinear dynamics using the CWT technique, more specifically, the Morlet wavelet transform. The Morlet wavelet transform is an adaption of the Fourier transform. The Fourier transform investigates the time series of a given recording by identifying the amplitude, frequency and phase of the sine and cosine functions. Components in the Fourier transform with higher amplitude than the

background noise indicate the existence of periodic fluctuations or oscillations in the signal. The frequency of the fluctuations can then be determined from the amplitude of the components in the Fourier transform. The resolution of the frequency is limited by the length of the time series. The Fourier transform in its simplest form is inaccurate for non-stationary time series i.e. time series which contain time dependent changes in the frequency.

To transform a non-stationary signal accurately, the signal has to be divided into multiple time windows covering both short windows and long windows. The short windows allows for a high resolution of low frequency fluctuations whilst the long windows allow for high frequency fluctuations to be resolved. The changing frequencies can be analysed using Morlet wavelets in which each frequency has a wavelet constructed with its optimal frequency resolution. The wavelet transform is then calculated from a convolution between each wavelet and the time series i.e. comparing the fit of the data with the wavelets.

Signal pre-processing for non-linear analysis of the membrane potential. The patch clamping recordings were conducted in the Faraday cage to minimise electrical interference, however, electrical interference in the form of large spikes was still evident. In order to remove these artificial spikes, the trend of the time series recording was ascertained using a 3rd order polynomial and spikes were identified if they were more than 5σ away from the trend of the time-series.

2.5.3 Statistical Analysis

All the data was plotted as the mean \pm SEM unless otherwise states. The statistical significance of the data was analysed using a Student's T-test, one-way ANOVA, mixed models ANOVA, a three-way mixed model ANOVA, a Wilcoxon signed-rank test, Mann-Whitney U test or Chi-square test for association.

The mixed models ANOVA allowed for a comparison between the within-subject factors in addition to between-subjects. The mixed models ANOVA consisted of a univariate ANOVA and repeated measures ANOVA with *post hoc* tests in the form of either a Tukey's HSD test or a Bonferroni correction to account for the multiple

comparisons (Seltman, 2012). The three-way mixed models ANOVA was similar to mixed models ANOVA but allowed for more comparisons of the between-subjects. Prior to completing the statistical tests, the following tests were undertaken to ensure the assumptions required for the tests were met and thus the results of the chosen statistical tests were valid. Box plots were constructed to ensure the data had no outliers. Shapiro-Wilk's test was used to test the data for normal distribution. Homogeneity of variances and covariance's were tested using Levene's test and Box's test, respectively. Mauchly's test of sphericity was used to ensure the assumption of sphericity had been met. Sphericity is an equal difference between the data in individual groups of data. In cases wherein the assumption of sphericity was violated, then the Greenhouse-Geisser correction was applied and the statistical significance of these interactions was based on these corrections. In data sets where the assumption of sphericity had been violated, a one-way ANOVA rather than a mixed model ANOVA was used to test significance. This was because of the critical importance of the assumption of sphericity in the repeated measured ANOVA.

Similar to the mixed models ANOVA, several assumptions were tested before conducting the one-way ANOVA statistical. The data was tested to ensure that there were no outliers in the dataset. The normal distribution and homogeneity of variances was tested. If the assumption of homogeneity of variances was violated, then the Welch test was used and the Games-Howell post Hoc test was used for multiple comparisons since the Games-Howell test does assume homogeneity in the variance within the data.

The significance of the results from the different statistical tests was considered significant by a *p*-value below 0.05. Where possible, the *p*-value less than 0.05 is presented as * in figures whilst a *p*-value less than 0.005 and 0.0005 is presented as ** and ***, respectively.

3 ELECTROPHYSIOLOGICAL CHARACTERISATION OF JURKAT CELLS IN THE LOG PHASE OF GROWTH

3.1 Introduction

The membrane potential is the difference in the electric potential between the cytosolic and extracellular solution and the difference in the electric potential is generated due to the semi-permeable nature of the plasma membrane. This semi-permeable property of the plasma membrane is conferred by ion channels, carriers and ATP-powered pumps which are embedded within the plasma membrane. Through these transport mechanisms, a combination of the concentration gradient and the electric gradient drive the movement of the principal cellular ions i.e. K^+ , Na^+ , Cl^- and Ca^{2+} . Although the combined effect of the membrane transport proteins produce the separation of ions across the plasma membrane, the activity of ion channels and pumps primarily determine the membrane potential of cells (Lodish, 2004).

The Na^+-K^+ -ATPase pump and the resting K^+ channels are the primary contributors of the membrane potential during the resting state. The Na^+-K^+ -ATPase pump is a P class pump which transports three molecules of Na^+ from the cytosol whilst pumping

two molecules of K^+ into the cytosol. The intracellular K^+ then move to the extracellular space through the resting K^+ channels leaving the cytosol with a negative potential (Lodish, 2004; Wright, 2004). Although the Na^+-K^+ -ATPase pump and the resting K^+ channels are the major determinants of the membrane potential, the permeability of ions through various other pumps, channels and transporters can also contribute to the generation of the membrane potential. In fact, the Goldman-Hodgkin-Katz equation shows that the membrane potential is dependent on the permeability of K^+ , Cl^- and Na^+ ions, therefore, the membrane potential of cells should reflect the complement of ion channels and pumps permeable to these three ions (Hodgkin and Katz, 1949).

Aims of the chapter

In this chapter, the culture conditions required to achieve Jurkat cells in the log phase of proliferation are ascertained. The membrane potential and the underlying ion channels setting the resting membrane potential of these cells are also investigated.

3.2 Results

3.2.1 Ascertaining culture conditions required to yield Jurkat cells in an actively proliferating state

The aim of this chapter was to investigate the link between the membrane potential of actively proliferating Jurkat cells and the underlying ion channels determining this membrane potential. Consequently, the rate of proliferation of Jurkat cells cultured in RPMI-1640 medium supplemented with FBS concentrations ranging from 0-10% was investigated by staining the cells with trypan blue stain and manually counting the viable cells. Figure 3.1 shows that the Jurkat cells were in an actively proliferating state when cultured in RPMI-1640 medium supplemented with 10% FBS. As a result, Jurkat cells were cultured in RPMI-1640 medium supplemented with 10% and this composition of culture medium was considered as the standard growth medium.

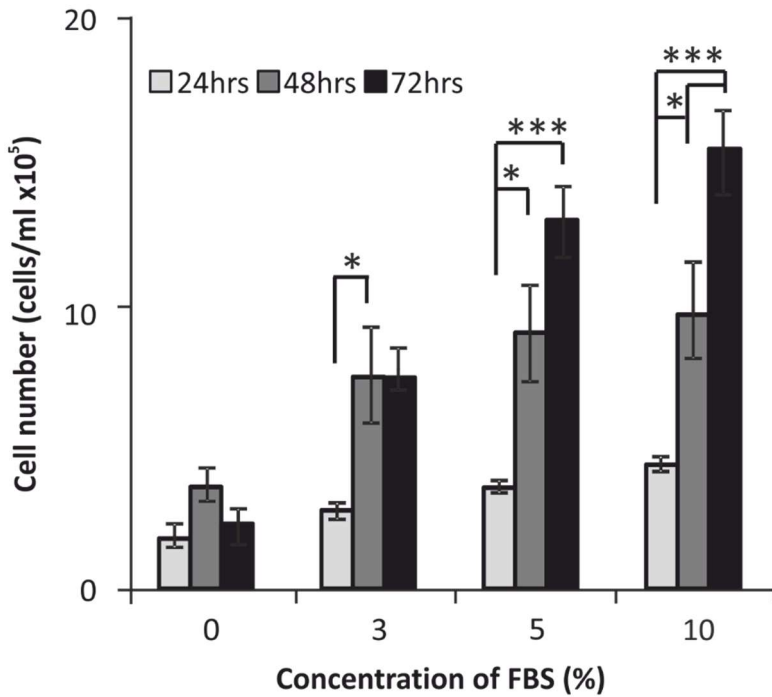


Figure 3.1

The effect of FBS on proliferation over 72 hours. Jurkat cells were seeded at 2×10^5 cells/ml in T25 flasks in RPMI culture medium supplemented between 0 - 10% FBS as shown and incubated between 24 hrs and 72 hrs at 37°C. Thereafter, the rate of proliferation was assayed by manually counting the number of viable Jurkat cells i.e. cells which excluded the trypan blue dye on a haemocytometer after being stained with trypan blue. The number of cells was determined by the formula $Cell\ Number\left(\frac{Cells}{ml} \times 10^5\right) = \frac{Number\ of\ large\ square\ counted}{Dilution\ factor\ in\ trypan\ blue} / 10$. Each experiment was repeated 3 times in triplicates and the average plotted with the SEM. A one-way ANOVA was used to ascertain the statistical significance of the differences within the groups. * represents $p < 0.05$ whilst ** and *** represent $p < 0.005$ and $p < 0.0005$, respectively.

3.2.2 The membrane potential of actively proliferating Jurkat cells

The membrane potential is determined in part by the complement of active ion channels on the plasma membrane (Kurachi et al., 2001). Variations in the expression of ion channels and the time after subculture have been observed in cells (Ypey and Clapham, 1984). Consequently, the possibility that the membrane potential of the Jurkat cells varied with time after subculture was investigated. As such, the current clamp mode in the whole cell configuration of the patch clamping technique was used to investigate the distribution of the membrane potential in actively proliferating Jurkat cells.

The average immediate membrane potential of the Jurkat cells was measured within two seconds of achieving the whole cell mode. This immediate measurement of the membrane potential was considered to reflect the membrane potential of the actively proliferating Jurkat cells during growth in the culture medium (see Chapter 2 for information on the handling of cells).

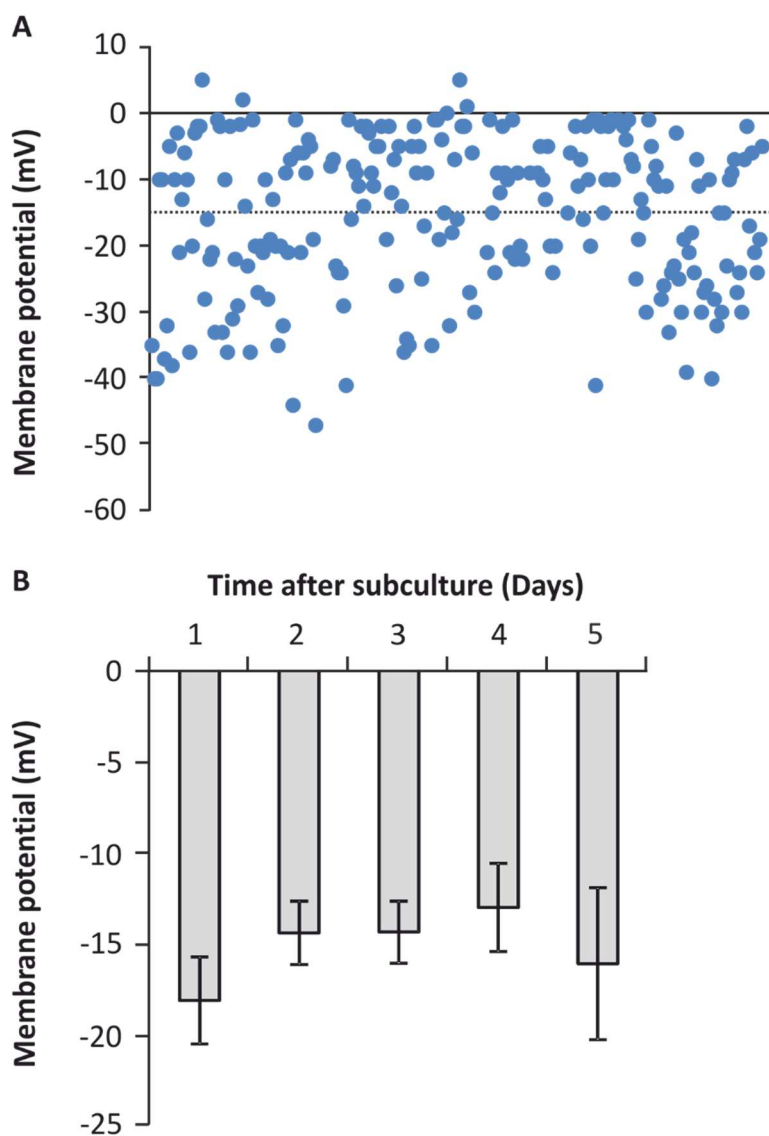


Figure 3.2

Distributions of the membrane potential of Jurkat cells cultured in standard culture conditions, i.e. RPMI supplemented with 10% FBS. (A) The distribution of the membrane potential of Jurkat cells measured within 2 seconds after establishing the whole cell configuration. Each dot represents the membrane potential of an individual Jurkat cell. The data from 243 Jurkat cells aged between 1 and 5 days after subculture is shown. The dashed grey line indicates the mean membrane potential of the 243 cells. (B) The distribution of the membrane potential of Jurkat cells according to the age of cells after subculture ($n=243$). The data is plotted as the average \pm SEM. The Jurkat cells were patched in extracellular solution E1 and the intracellular solution was I1. A paired Student's T-test was used to ascertain the degree of statistical significance between the different groups.

3.2.3 The resting membrane potential of actively proliferating Jurkat cells

After achieving the whole cell configuration, the cytosolic components of a cell are replaced with the pipette solution causing the membrane potential to be in a state of flux. During this cytosolic washout process the complement of active membrane transport proteins could change, which in turn could affect the membrane potential as the complement of active ion channels play a role in determining the membrane potential. Consequently, the resting membrane potential of the Jurkat cells was measured after 15 minutes to allow equilibration of the cytosolic and the intracellular solution. Figure 3.3 shows the difference in the average resting membrane potential and immediate membrane potential of 30 Jurkat cells was not significantly different.

As there are Ca^{2+} -gated ion channels on the plasma membrane of Jurkat cells, the free intracellular concentration of Ca^{2+} was increased from nominally free to 1 μM and the resting membrane potential of the cells was recorded. The mean immediate membrane potential and the mean resting membrane potential of Jurkat cells patched with a free intracellular Ca^{2+} concentration of 1 μM failed to significantly differ ($n=17$) (Figure 3.3). The mean immediate membrane potential of cells patched in the presence of 1 μM free Ca^{2+} , however, was significantly different to the membrane potential of Jurkat cells patched with nominally free intracellular Ca^{2+} .

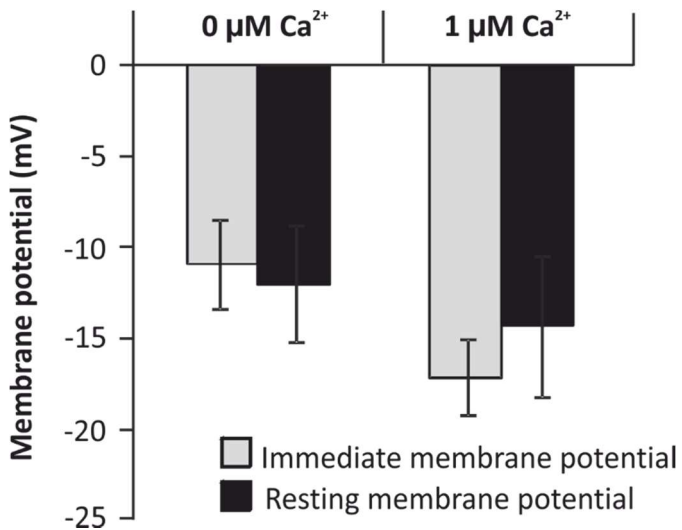


Figure 3.3

The membrane potentials of Jurkat cells with intracellular solution containing either nominally free or 1 μM free Ca^{2+} . The immediate membrane potential was recorded within 2 seconds of achieving the whole cell configuration whilst the resting membrane potential was recorded after 15 minutes of achieving the whole cell configuration. The Jurkat cells were patched in extracellular solution E1 and the intracellular solution was either I1 or I1Ca. The concentration of intracellular free CaCl_2 , was nominally free in solution I1 whilst it was a free concentration of 1 μM in solution I1Ca. The data is plotted as the average \pm SEM whilst the sample size was a minimum of 17. A paired Student's T-test was used to ascertain the degree of statistical significance between the different groups.

3.2.4 Whole cell currents observed in Jurkat cells cultured in standard culture conditions

In an attempt to understand the role of ion channels in determining the membrane potential of the actively proliferating Jurkat cells, the patch clamping technique was used in voltage clamp mode to measure the whole cell currents of the cells. In this whole cell configuration, from a holding potential of -80 mV, the Jurkat cells exhibited outwardly rectifying currents which could be grouped according to kinetics of the currents (Figure 3.4). A current exhibiting rapid activation with slow inactivating kinetics was observed in 77% (146 of the 190 cells) of the cells. The current density of the peak activated current exhibited wide variation when induced by test potentials between -20 and +80 mV. At test potentials of +80 mV, the average current density was 95.6 pA/pF with a standard deviation of 36 pA/pF. Furthermore, in some Jurkat cells, this current exhibited rapid rundown with time within the first few minutes of achieving the whole cell configuration. As such, where possible, subsequent analysis of this time dependent K⁺ current was undertaken in cells exhibiting a large conductance without significant rundown of the current within the first six minutes of achieving the whole cell configuration.

An instantaneous current which developed into a large current after 4 minutes and subsequently exhibited gradual rundown with time was also observed in 14% (27 out of 190 cells) of the cells. This instantaneous current was often coactivated with the rapidly activating current exhibiting slow inactivation. This resulted in the partial inactivation of the rapidly activating current. In addition, a current with slow activating characteristics was observed in 9% of cells (17 out of 190 cells). This slow time dependent activating current was observed immediately after achieving the whole cell configuration in some of the cells whilst in other cells the slow activating current eventually developed over the course of an experiment, ultimately dominating the existing current.

A series of biophysical characterisations of these whole cell currents was performed to define their gating, selectivity and pharmacological properties.

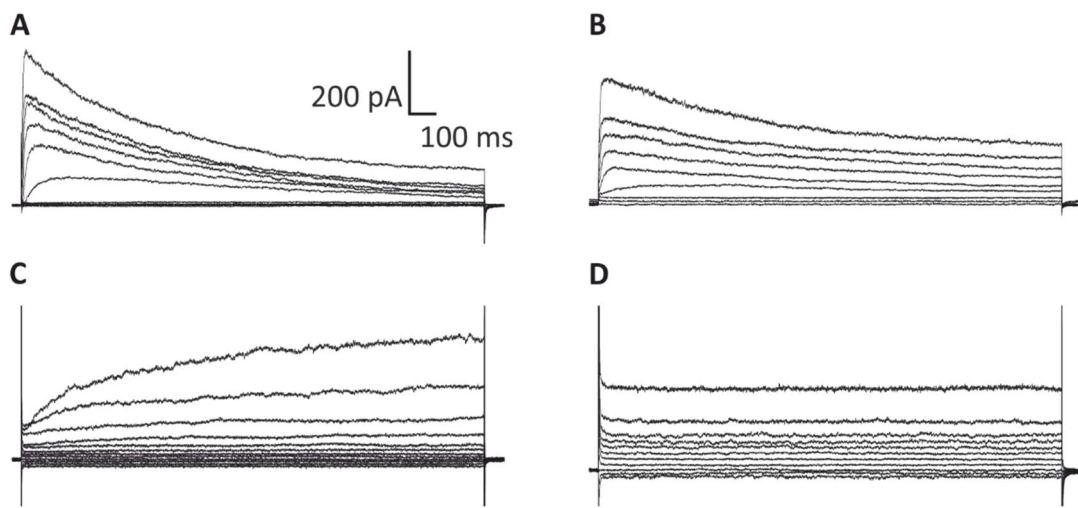


Figure 3.4

Whole cell currents observed in Jurkat cells. Representative current traces observed in four different Jurkat cells in the whole cell configuration. **(A)** Time dependent activating current with slow complete inactivation, **(B)** time dependent activating current with slow partial inactivation, **(C)** slow time dependent activating current and **(D)** an instantaneous current. The currents were measured in response to test potentials between +80 mV and -12 mV from a holding potential of -80 mV with -20 mV steps. These currents were recorded in extracellular solution E1 whilst the intracellular solution was solution I1.

3.2.5 The time dependent activating current with slow inactivation was carried by K⁺

Tail current analysis was used to determine the selectivity of the time dependent current. These tail currents were evoked by stepping the membrane potential from a holding voltage of -80mV to an activating voltage of +60 mV for 10 msecounds followed by stepping the membrane potential between -50 mV to -90 mV in -10 mV intervals (Figure 3.5). The potential at which the tail currents reversed was determined by plotting the current ‘X’ against the current at ‘Y’ (Figure 3.5B) and interpolating the potential against the current amplitude ($x-y=0$ current). The tail current reversal potential followed changes in the theoretical E_K values. More specifically, the average observed E_{rev} of the tail currents in the standard extracellular solution (E1) which contained 6 mM KCl was -70 ± 1 mV (n=12). This was close to the theoretical E_K of -75mV. Increasing the extracellular concentration of KCl to 60 mM shifted the reversal potential of the tail currents to -11 ± 1 mV (n=9). This shift followed the change in the theoretical E_K (-17.5 mV) rather than the change in the theoretical E_{Cl} (E_{Cl} changed from -3 mV to -9 mV). Consequently, these results confirmed that the time dependent outward current was carried predominantly by K⁺.

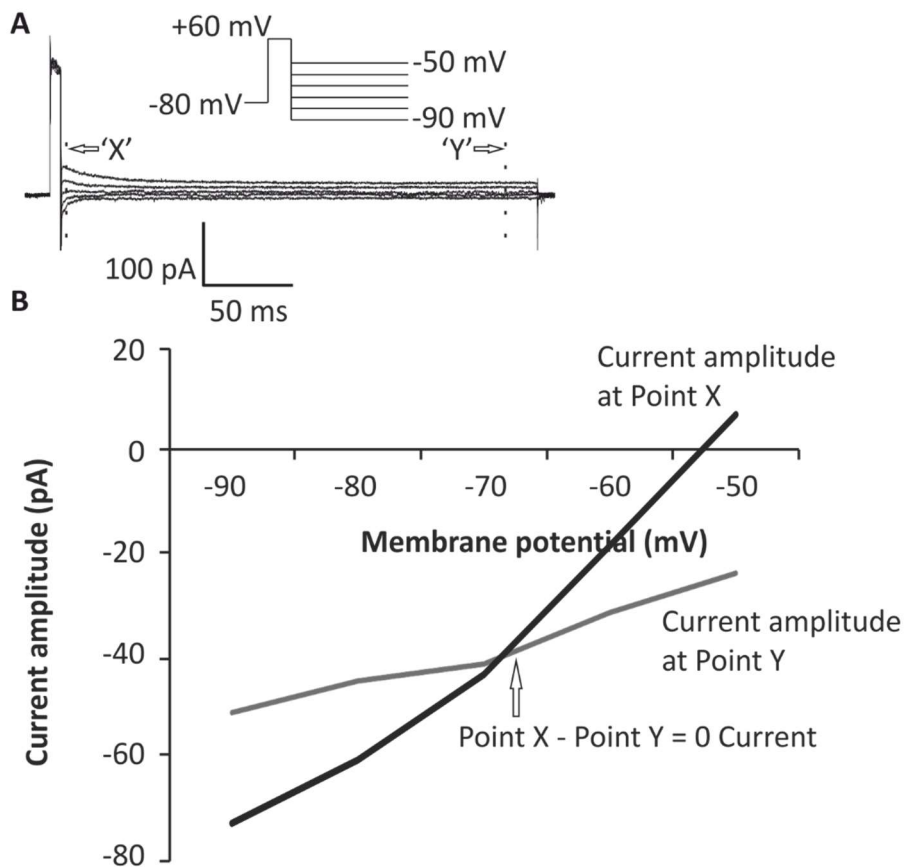


Figure 3.5

Tail currents of the time dependent outward current in Jurkat cells showed the current was carried by K⁺. (A) Representative current traces of the tail currents in bath solution containing 6mM K⁺. The initial pulse to +60 mV was followed by repolarizing test potentials between -50 and -90 mV in -10 mV steps with 60 second intervals between each test potential. The repolarizing test potentials in bath solution containing 60mM K⁺ ranged between +10 and -20 mV in -5 mV steps with 60 seconds between each test potential. (B) The zero current of the tail current was ascertained by plotting the current at 'X' and 'Y' and identifying the membrane voltage at which the two points cross. The extracellular solution was either E1 or E1K. Solution E1 contained 6mM KCl and solution E1K was similar to solution E1 but contained 60mM KCl. The intracellular solution was solution I1. The data is plotted as the average ± SEM of a minimum of 9 experiments.

Channel recovery and inactivation kinetics of the time dependent K⁺ current

Channel recovery. The outward K⁺ current exhibited slow time dependent inactivation after the initial rapid activation during the first test potential. The subsequent test potentials, however, failed to completely activate the outward current (Figure 3.4B). These findings indicate that a recovery period was necessary before channel reactivation. The recovery period associated with this channel was investigated by varying the time interval between test potentials. Figure 3.6 shows that the recovery period required to enable full activation of the time dependent K⁺ current was 60 seconds.

Inactivation Kinetics. The time dependent outward K⁺ current exhibited slow inactivation kinetics which became apparent with test potentials lasting more than 100 msec. As described earlier, some Jurkat cells exhibiting the time dependent K⁺ current showed complete inactivation whilst other Jurkat cells exhibited partial inactivation. The partial inactivation was thought to be a result of coexisting currents, therefore, the inactivation kinetics were only investigated on Jurkat cells exhibiting the time dependent K⁺ current exhibiting complete inactivation. The inactivation phase of this current was fitted with an exponential function. The results showed that the time of inactivation ranged from 200 msec at -20 mV to 327 msec at +80 mV (Figure 3.7).

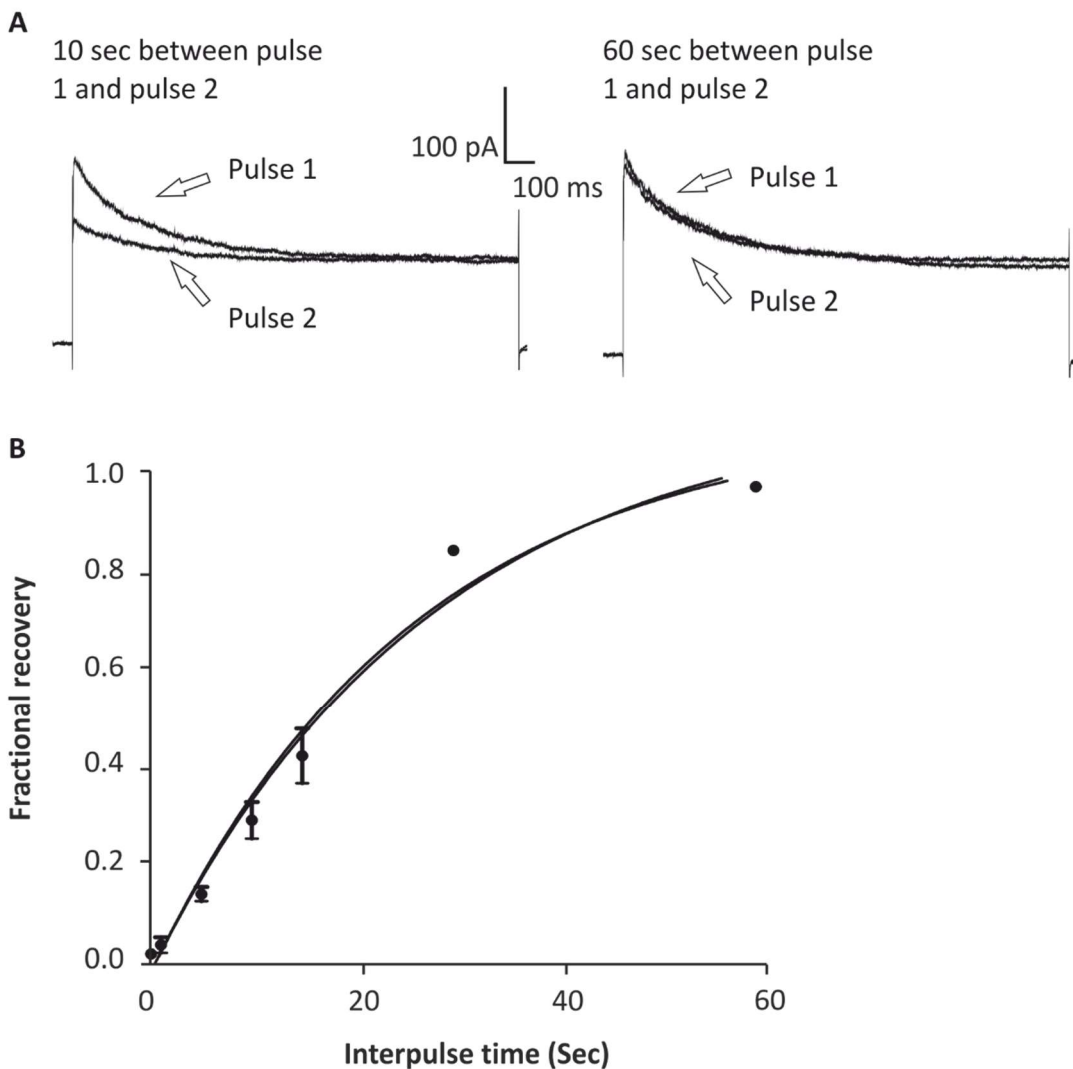


Figure 3.6

Recovery of the time dependent outward K^+ current. (A) Representative current traces from the same cell following a two pulse protocol. The time dependent current was activated by voltage step from -80 mV to +60 mV with varying times of 1, 10 and 60 seconds between the two test potentials. (B) Fractional recovery of the current is plotted as a function of the interpulse time, i.e. the two pulses to +60 mV. The fractional recovery was calculated using $\text{Fractional Recovery} = \frac{I_{\text{peak } 2} - I_{\text{mi}}}{I_{\text{peak } 1} - I_{\text{mi}}}$. The time course of the recovery was fit with the single exponential equation $F(t) = \sum_{i=1}^n A_i (1 - e^{-t/t_i}) A + C$ Where A_1 is the maximum outward current amplitude of the, t_1 is the decay time constant. The extracellular solution was E1 and the intracellular solution was I1. The data is plotted as the average \pm SEM of 5 experiments.

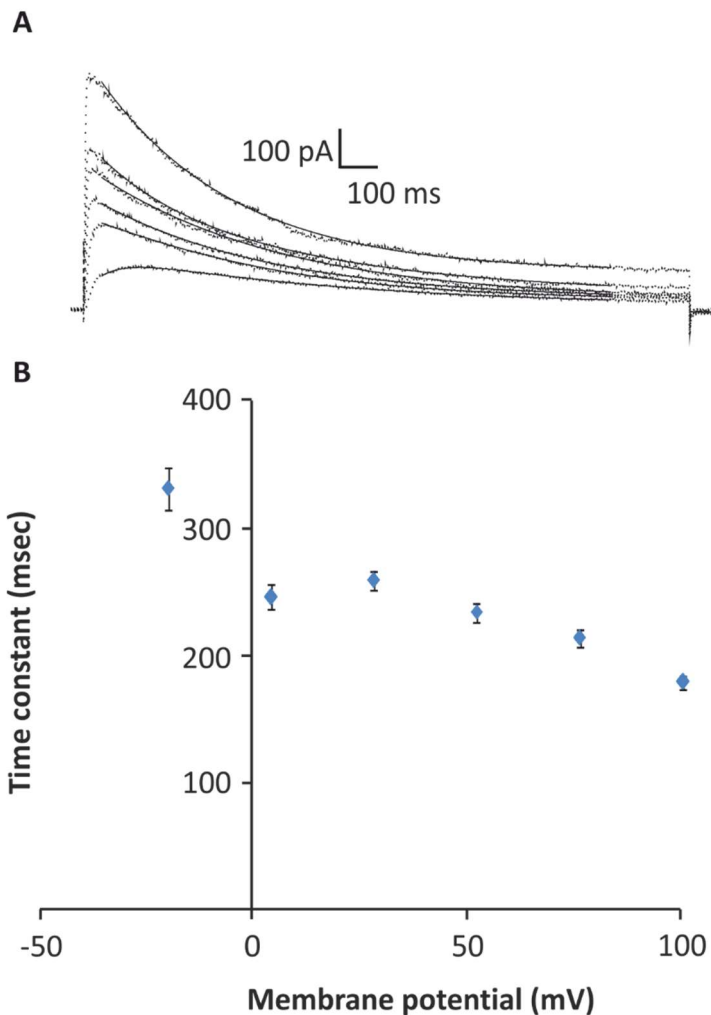


Figure 3.7

The inactivation phase of the time dependent K⁺ current. **(A)** The inactivation phase of the time-dependent currents fit with the exponential equation $(t) = \sum_{i=1}^n ie^{-\frac{t}{\tau_i}} + C$ here A1 is the maximum outward current amplitude of the, $t1$ is the decay time con. **(B)** The time constants of the inactivation phase of the currents as a function of the membrane potential. Each point is the mean of 5 experiments and the error bars represent the SEM. The extracellular solution was E1 whilst the intracellular solution was I1.

Cumulative inactivation. Several types of voltage-gated K⁺ currents exhibiting different properties have been found in lymphocytes (Lewis and Cahalan, 1988). Differentiation of these K⁺ currents can be done based on the kinetics of the currents in response to a single depolarising test potential several times in rapid succession. In response to such a pulse protocol, the K⁺ current recorded from the Jurkat cells exhibited cumulative inactivation (Figure 3.8), that is, the current failed to fully activate after the initial test potential. This cumulative inactivation is consistent with the time dependent outward current being carried by the *N*-Type voltage-gated K⁺ channel.

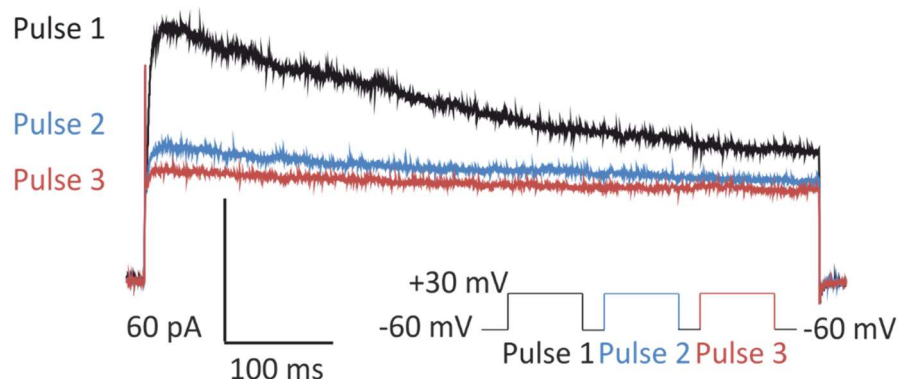


Figure 3.8

Cumulative inactivation of the outwardly rectifying time dependent K⁺ current in Jurkat cells. Current traces in response to repeated stimulations to an activation potential of +30 mV in a single Jurkat cell. The holding potential was -80 mV whilst the interval between activating potentials was 1 second. The Jurkat cells were patched with extracellular solution E1 and intracellular solution I1.

Gating and activation kinetics of the time dependent K⁺ current

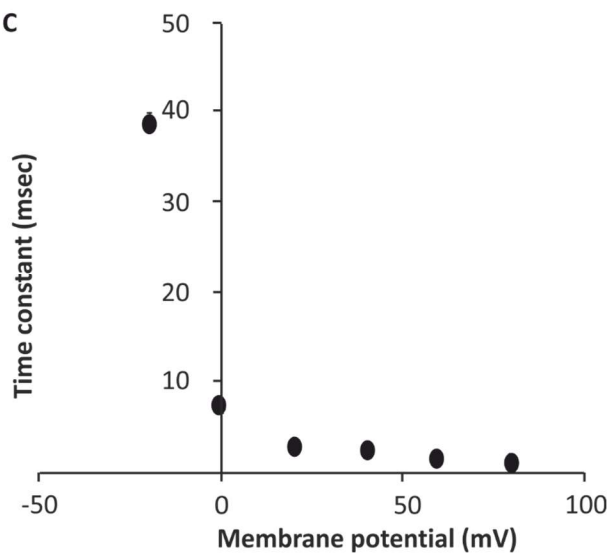
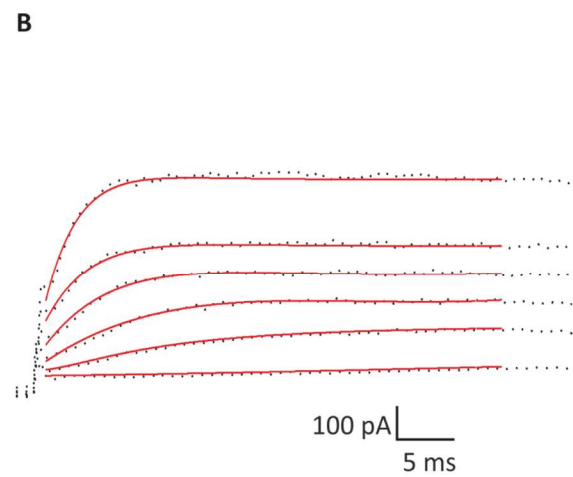
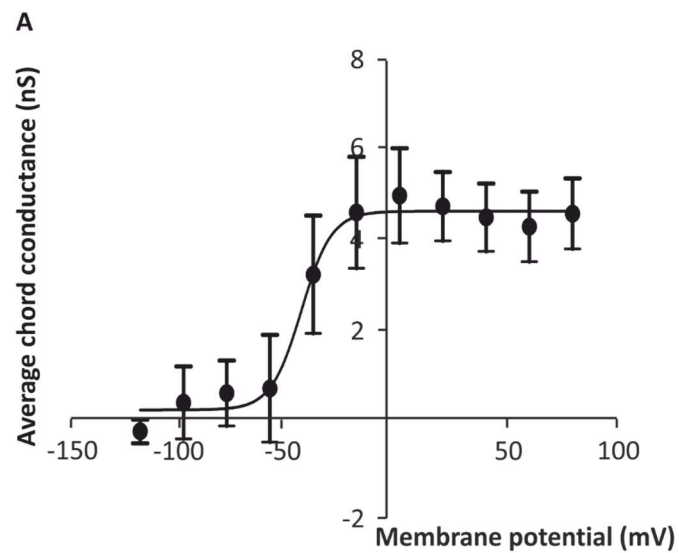
Voltage gating. The voltage dependency of the gating was investigated by plotting the average conductance against the voltage of the test potential as shown in Figure 3.9A. Applying a Boltzmann function to this plot revealed that the current was indeed voltage dependent.

Activation Kinetics. The rapid activation of the voltage-gated K⁺ current had a sigmoidal curve when observed on an expanded time scale. Kinetic analysis of this activation phase was undertaken using the exponential power function. The activation phase was voltage dependent and the tau ranged from 3 msec at +80 mV to 38 msec at -20 mV.

Figure 3.9

Voltage dependency and activation kinetics of the K⁺ current observed in Jurkat cells.

(A) Average conductance voltage relationship of Jurkat cells (n=10). The plot was constructed by plotting the chord conductance of the peak outward current induced by test potentials between +80 and -120 mV in -20 mV steps every 60 seconds. The chord conductance was calculated using the equation $G = \frac{I}{(V_m - E_k)}$ Where G is the chord conductance, I is the maximum outward current, V_m is the activation potential and E_k is the theoretical reversal potential for K⁺. The data was fitted with a Boltzmann fit, $G_k = \frac{G_{k,\max}}{1 + e^{(V - V_m)/K_n}}$ Where G_{k,max} is the maximum conductance, V_m is the voltage midpoint of the curve, K_n is the steepness of the voltage dependence and x is 1. The G_{k,max} was 5.6 ± 0.3, V_m was -41.1 ± 0.3 mV and the K_n was 9.46. (B) The activation phase of the currents overlaid with the exponential function $(t) = \sum_{i=1}^n A e^{-t/\tau_i} + C$ Where A is the maximum outward current, C is the exponent of the activation phase, t is activation time constant. The best fit of the data for C was 4. The time constants are plotted as a function of the test potentials on (C). The currents in (A) were induced by activating potentials ranging from +80 mV to -120 mV whilst the currents in (B) were induced by test potentials ranging from +80 mV to -20 mV with -20 mV steps from a holding potential of -80 mV. The time interval between the test potentials was 60 seconds. The data (A) and (C) are plotted as the mean ± SEM. The extracellular solution was E1 whilst the intracellular solution was I1.



Pharmacology of the time dependent K⁺ current

Sensitivity to tetraethylammonium. The sensitivity of the time dependent outward current to the broad spectrum channel blocker, TEA was investigated to gain further insight into the identity of this outward current. TEA inhibited the time dependent outward current with a determined Kd of 9.6 mM at +60 mV (Figure 3.10). The mechanism of action of TEA was not voltage dependent. Furthermore, inhibition of the time dependent current was only partial and this was likely due to a TEA insensitive component of the current.

Sensitivity to 4-aminopyridine. The sensitivity of the time dependent outward current to extracellular 4-AP was also investigated. The outward current was sensitive to 4-AP at concentrations above 1 µM with noticeably greater inhibition of the current at +40 mV compared to +60 mV. For example, in the presence of 50 µM 4-AP, the peak inhibited current amplitude at +60 mV was 90 ± 0.3% in comparison to unblocked current. On the other hand, the peak inhibited current during +40 mV i.e. the second pulse was 50 ± 0.1 % (n= minimum of 3). Consequently, the Kd value of 4-AP at +60 mV was 831 µM and decreased to 128 µM during the second test potential (+40 mV). It is unclear if this is a voltage dependent effect of 4-AP or if it reflects uptake of 4-AP into the cytosolic side as a result of the initial depolarising pulse at +60 mV.

Figure 3.10

Dose response curve for externally applied TEA. **(A)** Representative current traces in the presence of varying concentrations of TEA. **(B)** The % inhibition of the K⁺ current was plotted as a function of the concentration of TEA on a log₁₀ scale for currents induced at +80 mV, +60 mV and +40 mV. The % inhibition was calculated by % Inhibition = $\left(\frac{\text{Peak current in the presence of TEA}}{\text{Peak current in the absence of TEA}} \right) \times 100$. The data was fitted with a Hill function. The Kd value for TEA at +80 mV was 8.9 mM and a Hill coefficient of -0.93. The Kd value for TEA at +60 mV was as 9.6 mM with a Hill coefficient of -0.88. The Kd value for TEA at +40 mV was as 10.90 mM with a Hill coefficient of -0.85. The data is plotted as the mean ± SEM. Inset, current response of a Jurkat cell at test potentials of +60 mV superimposed in the presence of 0, 10 and 50 mM TEA. The K⁺ current was induced by test potentials ranging from +80 mV to -20 mV with a time interval of 60 seconds between each pulse. Each experiment was repeated a minimum of 4 times. The Jurkat cells were patched in intracellular solution I1 and extracellular solution E1.

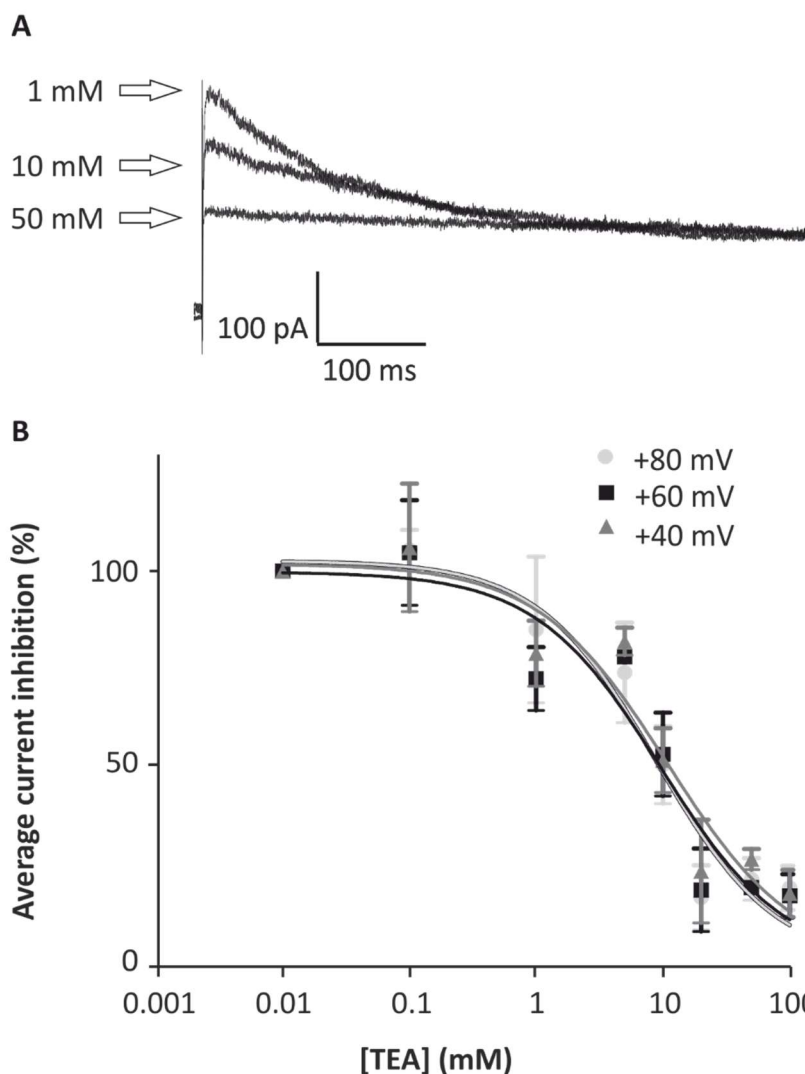
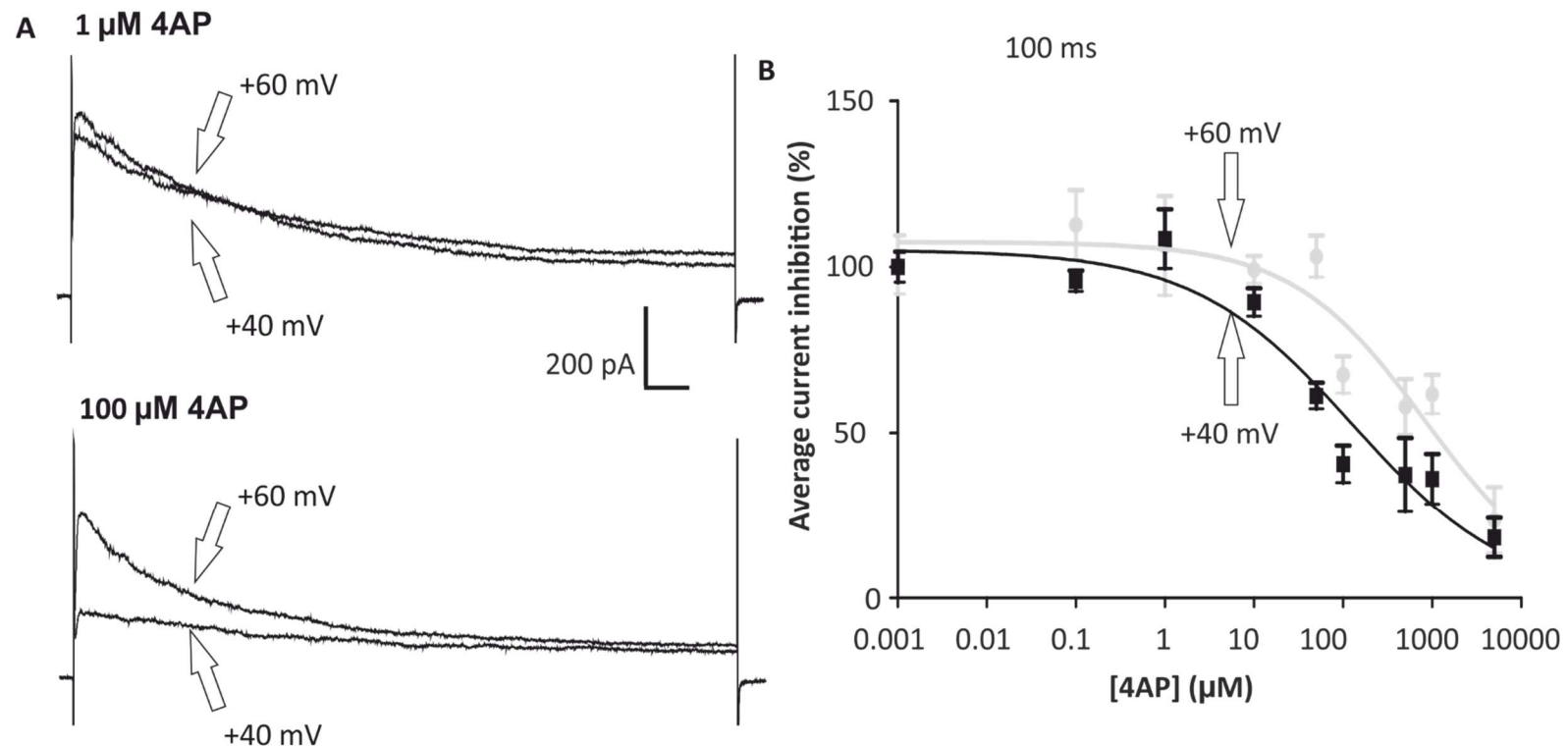


Figure 3.11

Dose response curve for exogenously applied 4-AP. (A) The % inhibition of the K⁺ current was plotted as a function of the concentration of 4-AP plotted on a log₁₀ scale. The effect of 4-AP was recorded at +40 mV and +60 mV. The % inhibition was calculated by % Inhibition = $\left(\frac{\text{Peak current in the presence of 4AP}}{\text{Peak current in the absence of 4AP}} \right) \times 100$. The data was fitted with a Hill function. The Kd value for 4-AP at +60 mV was 831 μM and a Hill coefficient of -0.6. The Kd value for 4-AP at +40 mV was as 128 μM with a Hill coefficient of -0.5. The data is plotted as the mean ± SEM. Each experiment was repeated a minimum of 3 times. (B) Representative current traces from a Jurkat cell in response to varying extracellular concentrations of 4-AP at test potentials of +60 and +40 mV with a time interval of 60 seconds between each pulse. The Jurkat cells were patched in intracellular solution I1 and extracellular solution E1.



3.2.6 Instantaneously activating outward currents

Cl⁻ selectivity of the whole cell current

The ion carrying the instantaneous current was investigated by varying the extracellular [Cl⁻] from 162 mM to 6 mM (Figure 3.12). This decrease in the extracellular [Cl⁻] shifted the average observed E_{rev} of the whole cell instantaneous current from -8.6 ± 3 mV to +31.0 ± 8 mV (n=7). The change in this observed E_{rev} followed the change in the theoretical E_{Cl} which is consistent with at least some of the current being carried by Cl⁻ ions. The observed E_{rev} of the whole cell currents, however, remained less than the theoretical E_{cl} when the extracellular solution contained 162 mM Cl⁻ indicating permeability of other ions. As expected, when the external [Cl⁻] was reduced to 6 mM, the magnitude of the inward whole cell currents increased with a concomitant decrease in the magnitude of the outward currents. This could reflect either the change in the driving force for Cl⁻ or altered gating whereby a decrease in the extracellular [Cl⁻] could inactivate the whole cell outward current.

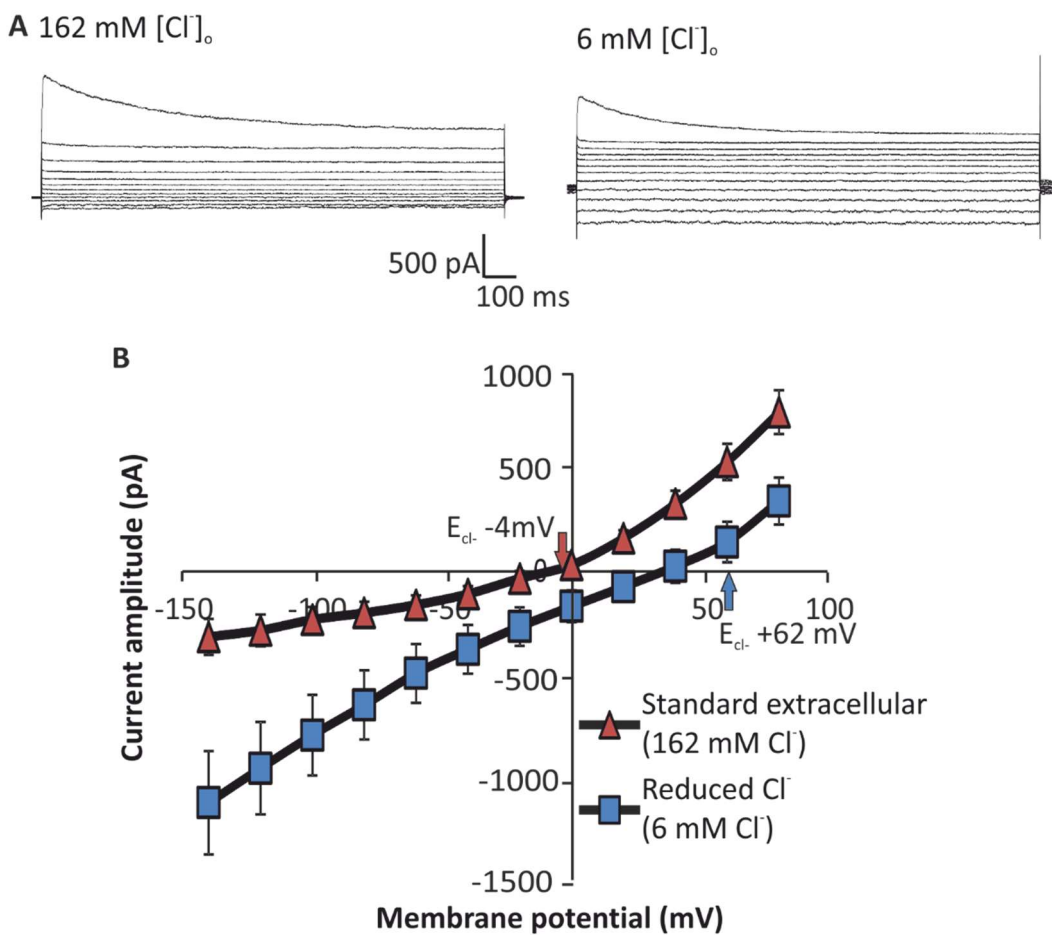


Figure 3.12

Cl^- selectivity of the instantaneous outward whole cell current. (A) Representative current traces of the instantaneous whole cell currents measured in extracellular solutions containing either 162 mM or 6 mM Cl^- . The whole cell currents in the extracellular solution containing 162 mM Cl^- were recorded after 4 minutes of achieving the whole cell configuration whilst the whole cell currents in the extracellular solution containing 6 mM Cl^- were recorded after 90 seconds of perfusing the solution containing the reduced $[Cl^-]$. The currents were induced by test potentials between +80 and -140 mV in -20 mV steps from a holding potential of -80 mV with a 1 second interval between test pulses. The 1 second pulse interval was used to eliminate contamination from the voltage-gated K^+ currents described earlier. (B) The average current amplitude of the varying extracellular solutions is plotted as a function of the membrane potential between +80 and -100 mV. The current amplitude of the whole cell instantaneous current from each cell was the average between 400 and 800 msec from each test pulse. The extracellular solution was either E1 or E2Cl. Solution E2Cl was similar to solution E1 but contained 6mM total Cl^- rather than 162mM $^-$. The intracellular solution was solution I1. The data is plotted as the average \pm SEM of a minimum of 7 experiments.

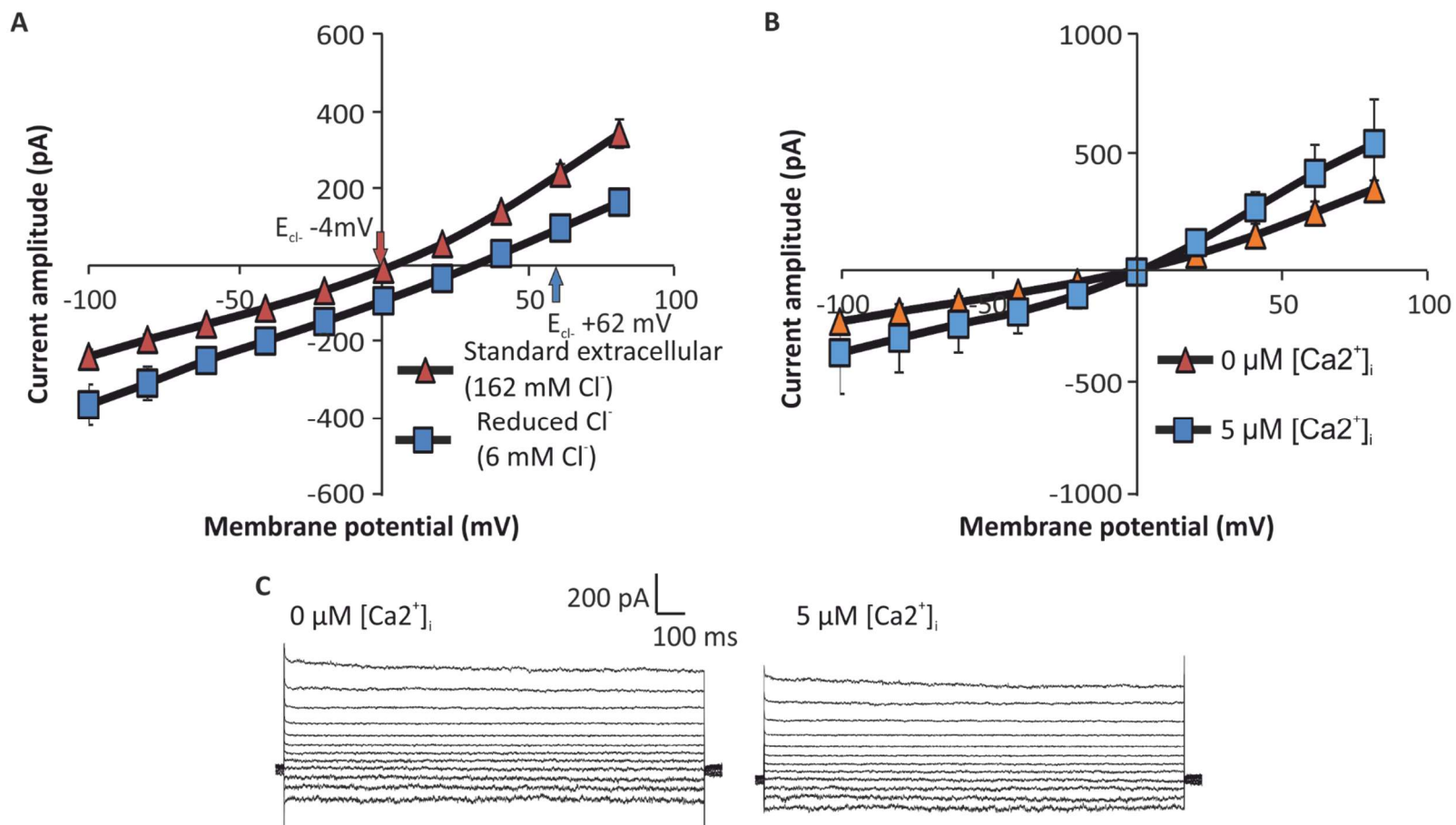
Ca²⁺ sensitivity of the instantaneous Cl⁻ current

Ca²⁺-activated Cl⁻ channels have been observed in Jurkat cells (Nishimoto et al., 1991). Therefore, the Ca²⁺ sensitivity of the whole cell instantaneous Cl⁻ current was characterised in the presence of 5 μM free intracellular Ca²⁺. As was evident from Figure 3.12A, the whole cell Cl⁻ current was contaminated with the time dependent K⁺ current exhibiting rapid activation and slow inactivating kinetics. Moreover, Ca²⁺-activated K⁺ currents have also been described in lymphocytes (Grissmer et al., 1993). Consequently, K⁺ was replaced with equimolar [Cs⁺] in the extracellular and intracellular solutions.

Due to the introduction of Cs⁺ to the solutions, Cl⁻ selectivity of the remaining whole cell instantaneous current was investigated in a similar manner to the investigation of Cl⁻ selectivity in the presence of K⁺ solutions (see Figure 3.12). In response to the reduction of the extracellular [Cl⁻] from 162 mM to 12 mM in the K⁺ free intracellular solution containing 0 mM Ca²⁺, the change in the observed E_{rev} of the whole cell currents was consistent with the change in the theoretical E_{Cl}. In addition, the magnitude of both, the inward and the outward whole cell instantaneous currents also changed in response to the reduction in extracellular Cl⁻ confirming at least part of the whole cell currents were carried by Cl⁻ (Figure 3.13A). Similar results were observed with Cl⁻ selectivity experiments carried out with a free concentration of 5 μM Ca²⁺ in the intracellular solution. Figure 3.13B shows the magnitude of the whole cell instantaneous currents were not significantly different in the presence of 5 μM Ca²⁺. Taken together, these results suggest that the whole cell instantaneous Cl⁻ currents were not Ca²⁺ dependent.

Figure 3.13

Cl⁻ selectivity and Ca²⁺ sensitivity of the whole cell instantaneous currents. **(A)** The average current amplitude in varying extracellular Cl⁻ solution of 7 Jurkat cells is plotted as function of the membrane voltage between +80 and -100 mV. The current amplitude of the whole cell instantaneous current from each cell was the average between 400 and 800 milliseconds from each test pulse. The instantaneous currents were induced by test potentials ranging from +80 and -100 mV from a holding potential of -80 mV. The whole cell currents were either recorded in extracellular solution E2.1 (final [Cl⁻] was 162 mM) or solution E2.1Cl (final [Cl⁻] concentration 12 mM). The intracellular solution was solution I2. **(B)** Same as (A) but the currents were recorded in either intracellular solution I2 or I2Ca. Solution I2 had nominally free intracellular Ca²⁺ whilst solution I2Ca had 5 μM free intracellular Ca²⁺. **(C)** Representative current traces of the instantaneous whole cell currents measured in either extracellular solution E2.1 or E2.1Cl. The currents recorded in extracellular solution E2.1 were recorded after eight minutes of achieving the whole cell configuration whilst the whole cell currents in extracellular solution E2.1Cl were recorded after 90 seconds of perfusing the solution containing the reduced [Cl⁻]. The currents were induced by test potentials between +80 and -100 mV in -20 mV steps from a holding potential of -80 mV with 1 second intervals between test pulses. The data is plotted as the average ± SEM of a minimum of 5 experiments.

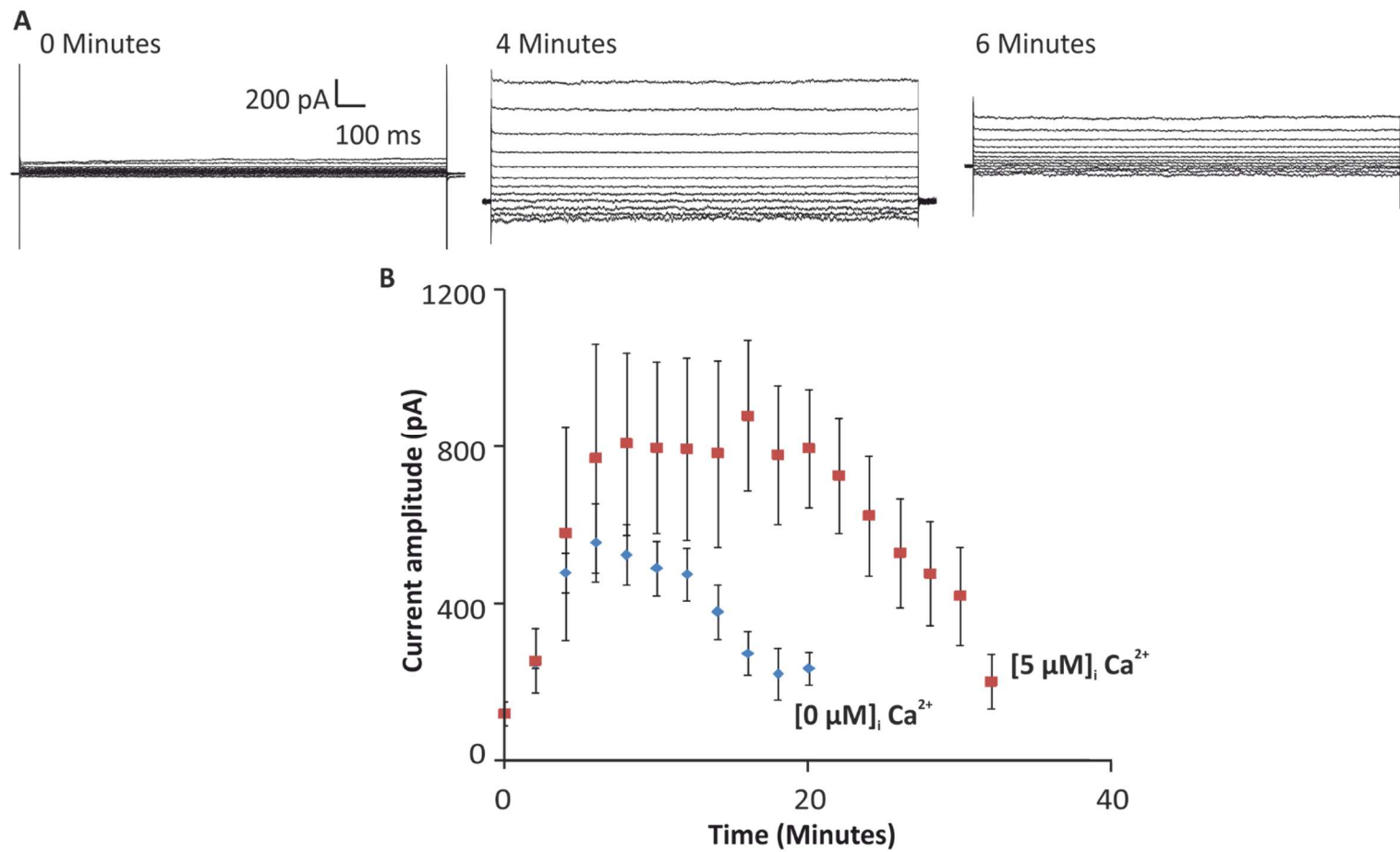


Time course of the instantaneous Cl⁻ current

The whole cell instantaneous currents exhibited rundown with time, therefore, the time course of the currents induced by test potentials of +80 mV was characterised in the absence and presence of intracellular Ca²⁺ as shown in Figure 3.14. The time course of these Cl⁻ currents showed that the instantaneous current developed after an average of eight minutes of achieving the whole cell configuration. Within two minutes of achieving the maximal current at +80 mV, the Cl⁻ current exhibited rundown in all the Jurkat cells investigated. Interestingly, rundown of the instantaneous current was abated in the presence of 5 μM intracellular Ca²⁺.

Figure 3.14

Time course of the instantaneous whole cell currents in the absence and presence of 5 μ M free intracellular Ca^{2+} . (A) Time course of the average instantaneous whole cell currents in the absence and presence of 5 μM intracellular Ca^{2+} . The whole cell currents were elicited by test potentials of +80 mV from a holding potential of -80 mV every two minutes. The data is plotted as the average \pm SEM of 6 experiments. (B) Representative current traces from the same Jurkat cell patched in Ca^{2+} free intracellular solution at the specified time. The instantaneous currents were induced by test potentials to +80 mV from a holding potential of -80 mV every two minutes. The Jurkat cells were patched in extracellular solution E2.1 and the intracellular solution was either I2 or I2Ca. Solution I2Ca was the same as solution I2 but contained a concentration of 5 μM free Ca^{2+} rather than nominally free Ca^{2+} .



Pharmacology of the instantaneous Cl⁻ current

NPPB Sensitivity. The whole cell instantaneous currents in Figure 3.12 showed Cl⁻ selectivity, therefore, the sensitivity of the instantaneous whole cell Cl⁻ current to extracellular NPPB, a broad spectrum Cl⁻ channel inhibitor was investigated. Figure 3.15 shows exogenous applications of 100 μM NPPB caused a significant decrease in the magnitude of the whole cell currents. The amplitude of the whole cell current decreased by 72% at test potential of +80 mV ($p<0.05$). The NPPB block was reversible, however, the instantaneous whole cell currents only partially returned to pre-treatment levels. This partial recovery of the current amplitude could be due to current rundown described in Figure 3.14.

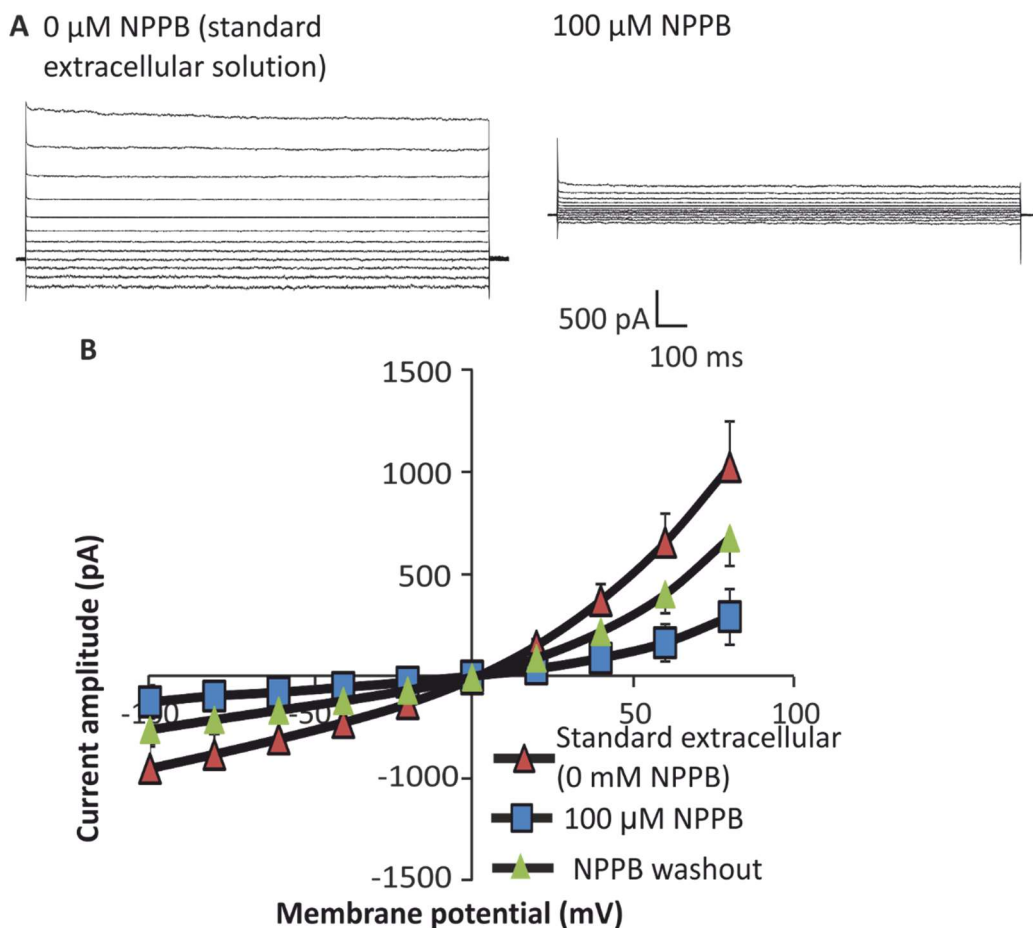


Figure 3.15

NPPB sensitivity of the whole cell instantaneous outward currents. (A) Whole cell instantaneous currents in the absence and presence of extracellular 100 μM NPPB. The instantaneous currents were induced by test potentials between +80 and -100 mV from a holding potential of -80 mV with a pulse interval of 1 second. (B) The current amplitude of the whole cell currents in the absence and presence of 100 μM NPPB applied externally and after washout of NPPB. The extracellular solution was E2.1 and the intracellular solution was solution I2. The data is plotted as the average \pm SEM of a minimum of 4 experiments.

3.2.7 Slow activating currents

In the whole cell configuration, 9% (17 out of 190 cells) of Jurkat cells that were in a state of active proliferation exhibited a slow time dependent activating outward current. This current developed immediately after achieving the whole cell configuration. Figure 3.16A-D shows the variability of the activation kinetics of this slow activating outward current from four different Jurkat cells.

Several lines of evidence suggested that this slow activating outward current was carried by protons. Firstly, tail current analysis of the current showed that the observed E_{rev} was around 0 mV (Figure 3.16F). This observed E_{rev} is close to the theoretical E_{Cl^-} , however, the tail currents did not respond to a decrease in extracellular $[Cl^-]$. Secondly, the slow activating current was still present in recording solutions lacking K^+ , Na^+ , Ca^{2+} , Mg^{2+} or ATP (Figure 3.16E). Thirdly, slow activating currents in Jurkat cells have been shown to be carried by protons (DeCoursey and Cherny, 1996; Schilling et al., 2002). The solutions designed to isolate the proton current resulted in slow activating currents that were very small making its characterisation very difficult (Figure 3.16E). Nevertheless, the slow activating kinetic properties together with the insensitivity to extracellular Cl^- and occurrence in solutions lacking K^+ , Na^+ , Ca^{2+} , Mg^{2+} or ATP suggest that this current was a proton current.

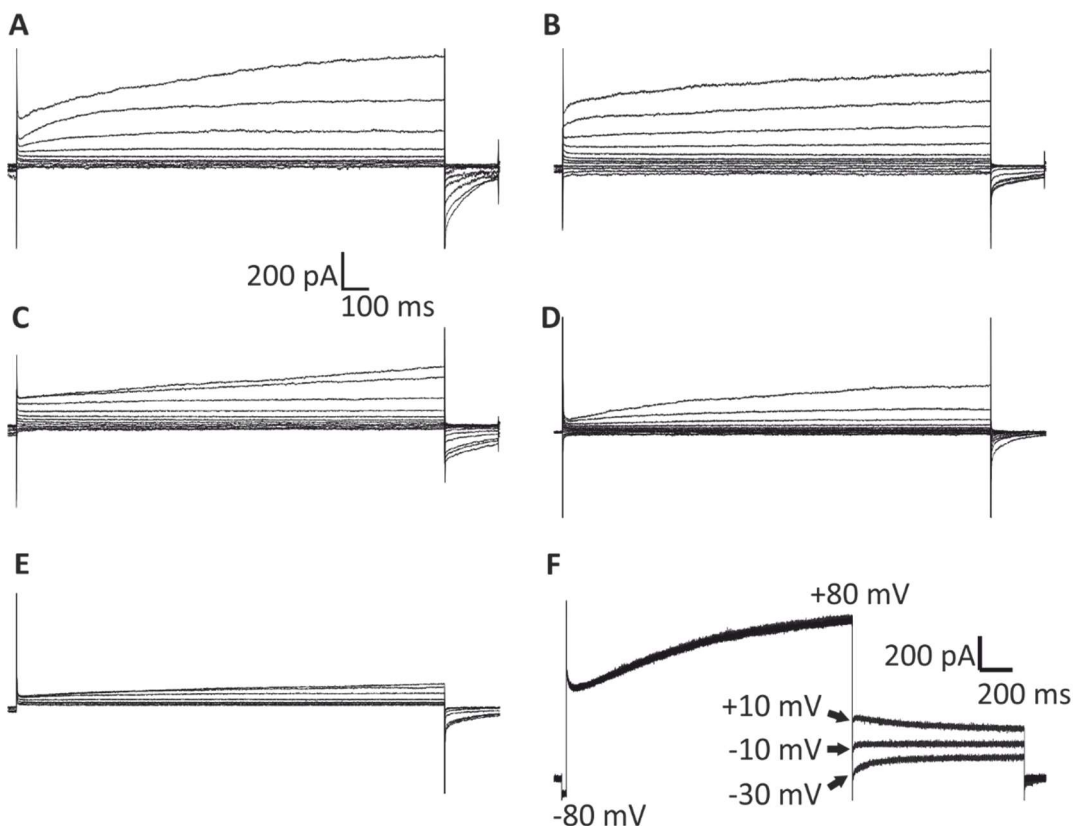


Figure 3.16

Slow time dependent activating outward current. (A-E) Representative current traces showing the slow activating outward current with different activating properties from five different Jurkat cells. The currents were induced by test potentials between +80 and -100mV from a holding potential of -80 mV with a pulse interval of 1 second. (F) Representative current trace of tail currents from a Jurkat cell. The initial activating pulse to +80 mV was followed by repolarizing test potentials between +50 and -30 mV in -10 mV steps with 1 second intervals between each pulse. Only repolarizing pulses to +10, -10 and -30 mV is shown for clarity. The currents from Jurkat cells shown in (A-D) were patched in extracellular solution E1 and intracellular solution I1. The currents shown in (E and F) were patched in extracellular solution E3 and. intracellular solution I3.

3.3 Discussion

The aim of the current project was to investigate the membrane potential dynamics of Jurkat cells in different proliferative states, ultimately, working towards elucidating the underlying mechanisms and the physiological relevance of any fluctuations and oscillations in the membrane potential. As a starting point, it was first necessary to characterise the membrane potential with regards to its magnitude and the underlying ion channels governing this membrane potential in Jurkat cells in the log phase of growth. To this end, the mean immediate membrane potential of the Jurkat cells was -15 ± 1 mV. The results from investigations on selectivity, pulse protocols and the degree of sensitivity to exogenously applied 4-AP, TEA and NPPB suggests that the Jurkat cells expressed the *N*-type voltage-gated K⁺ channel, a Cl⁻ channel and a slow time dependent activating current. In one population of the Jurkat cells, both, the K⁺ and Cl⁻ channel were coexpressed whilst in other populations either the K⁺ or the Cl⁻ channels were expressed. In addition, a slow time dependent activating current which was considered to be carried by protons was also observed in the Jurkat cells either immediately upon going whole cell or the current developed with time.

The aim of this chapter was to characterise the electrophysiology of Jurkat cells in the log phase of growth. This proliferative state was achieved by culturing the Jurkat cells in RPMI-1640 medium supplemented with 10% FBS. These are also the conditions recommended by ATCC, the source of the Jurkat cells used in this study (ATCC, 2015).

The membrane potential of the Jurkat cells. The mean membrane potential of the actively proliferating Jurkat cells in this study was recorded within two seconds of achieving the whole cell configuration. The mean resting membrane potential of the Jurkat cells was significantly depolarised in comparison to observations of lymphocytes in published literature which was between -50 and -70mV (Lewis and Cahalan, 1995; Sarkadi et al., 1990). The discrepancy in the membrane potentials could be associated with several factors. The membrane potential described in the literature were based on indirect measurements of the membrane potential using fluorescent dyes. Nevertheless, as a number of different published studies report

similar membrane potentials of lymphocytes using fluorescent dyes, the difference in the membrane potential as a result of the measurement parameter can be overlooked.

The treatment of the cells from the culture flask to the recording chamber in the present study involved leaving 50 µl of the Jurkat cell suspension in the culture dish at room temperature to settle for five minutes before being patched. It is possible that the membrane potential began changing during the five minute settling period due to the difference in ionic composition of the patch clamping solutions and the culture medium during the cell culture. Consequently, this could have driven the membrane potential to the depolarised potentials recorded.

The change in the temperature from 37°C to room temperature could have also altered the gating properties of channels causing a change in the membrane potential. Indeed, a temperature change from 20 to 40°C affected CRAC channels in Jurkat cells within five minutes causing a calcium influx (Xiao et al., 2011). Likewise, the temperature could also affect other channels and thus cause a change in the membrane potential. The malleability of the cells to the culture conditions could have also affected ion channel activity and in turn, the membrane potential. Jow and colleagues (1999) showed altered expression of ion channels in endothelial cells merely as a result of using conditioned growth medium. Sarkadi et al., (1990) failed to mention the cell culturing regime for the Jurkat cells used in their study. The culturing regime could have also produced differences in the membrane potential of the Jurkat cells between this study and study conducted by Sarkadi et al., (1990). Nevertheless, if the immediate membrane potential of the Jurkat cells was determined by their treatment and handling, the membrane potential of the Jurkat cells irrespective of their proliferative state could still be compared as all cells were treated in the same manner.

The immediate membrane potential of the Jurkat cells used in the present study exhibited significant variation and ranged from -50 mV to +5 mV. It is possible that this large deviation in the membrane potentials was due to cells being in different stages of the cell cycle (Yang and Brackenbury, 2013). This could be overcome by synchronising the Jurkat cell population to a specific stage of the cell cycle prior to measuring the membrane potential. For example, the cells could have been serum starved or treated with chemical inhibitors of the cell cycle such as lovastatin (Javanmoghadam-Kamrani and Keyomarsi, 2008; Rosner et al., 2013).

The membrane potential of lymphocytes is determined primarily by the activity of the voltage-gated *N*-type K⁺ channel (Lewis and Cahalan, 1995). As such, specific inhibitors of this channel, loureirin B and DPO-1 caused a significant depolarisation in the membrane potential (Yin et al., 2014; Zhao et al., 2013). Furthermore, cells expressing voltage-gated K⁺ channels have been shown to exhibit a more hyperpolarised membrane potential compared to those cells without voltage-gated K⁺ channels (Leonard et al., 1992). In the present study, however, despite 77% of the cells expressing a voltage-gated K⁺ current, the majority of the cells exhibited a membrane potential significantly more depolarised than the theoretical E_{K+}. Taken together, these results suggest that the membrane potential of the Jurkat cells in the current study was not determined solely by the activity of *N*-type voltage-gated K⁺ channels.

In support for the activity of additional ion channels types, the observed E_{rev} from IV plots of the peak activated K⁺ current failed to completely reflect the theoretical E_{K+}. Furthermore, the voltage-gated K⁺ current failed to completely inactivate during prolonged test potentials and this inactive portion of the whole cell current was also insensitive to TEA and 4-AP. The additional current was suspected to be carried by Cl⁻ for a number of reasons. First, the ubiquitous nature of Cl⁻ channels in animal cells (Jentsch et al., 1999). Second, a stimulation protocol known to induce Na⁺ currents in Jurkat cells failed to show the presence of Na⁺ currents (data not shown) (Fraser et al., 2004). Third, investigations on Cl⁻ selectivity and NPPB sensitivity of the whole cell currents showed that the Jurkat cells used in the present study also exhibited Cl⁻ channels.

As the Jurkat cells in the present study expressed three current types i.e. a K⁺ current, Cl⁻ current and potentially, a proton current, the Goldman-Hodgkin-Katz (GHK) equation could be used to delineate the membrane potential of cells expressing all three conductance's (Hille, 1992). Assuming a permeability of 1 for K⁺ and Cl⁻, and overlooking the permeability of the potential protons due to its low concentration in the solutions used, the calculated membrane potential using the GHK equation is -16.5 mV which is very close to the mean resting membrane potential of Jurkat cells in this study. If the permeability of Cl⁻ was assumed to be low at 0.1, for example, in Jurkat

cells expressing the *N*-type voltage-gated channel with complete inactivation, the GHK equation suggests that the membrane potential of the cell would be -47.4 mV. On the other hand, if the permeability of Cl⁻ was large and the permeability of K⁺ low then the membrane potential as calculated using the GHK equation would be closer to 0 mV. All three scenarios were observed in the present study. Taken together, these results suggest that the resting membrane potential of the Jurkat cells is due to the combined permeability's of K⁺ and Cl⁻ through their respective membrane transport proteins.

N-type voltage-gated K⁺ channel

Variability of the voltage-gated K⁺ channel. It was interesting to note that the magnitude of the voltage-gated K⁺ current varied significantly between the Jurkat cells patched in the present study. The mean magnitude of this voltage-gated current at activation potentials of +80 mV was 928 pA with a standard deviation of 401 pA. Several studies investigating the voltage-gated K⁺ current from lymphocytic cells of human and mouse origins have also shown considerable variability in the magnitude of this K⁺ current (Cahalan et al., 1985; Fukushima et al., 1984; Matteson and Deutsch, 1984). The variability could be a result of cell damage during the cell handling, however, Cahalan et al., (1985) suggested the variability was not due to cell damage. Rather, the variations in the K⁺ current amplitude was hypothesized to be a result of the differences in the number of voltage-gated K⁺ channels in each cell.

Inactivation kinetics. The K⁺ current exhibited cumulative inactivation upon repetitive pulses to a single depolarising potential with a 1 second interval between the pulses. This cumulative inactivation points towards a complex inactivation process (Cahalan et al., 1985). Indeed, the existence of more than one inactivation processes in the *N*-type voltage-gated K⁺ channel has been acknowledged - a slow C-type inactivation and a fast N-type inactivation (Levy and Deutsch, 1996a, b). Marom and Levitan (1994) suggested that the inactivation process is dependent on the state of the channel prior to the inactivation, however, the mechanism of inactivation is yet to be fully understood.

Pharmacology. TEA and 4-AP which are non-specific K⁺ channel blockers, blocked the voltage-gated K⁺ channel. Two binding sites for TEA have been identified, an

intracellular binding site and an extracellular binding site. The results from this study showed that the potency of 4-AP was more pronounced during the second activating pulse at +40 mV in comparison to the first pulse at +60 mV. Although this suggests that that 4-AP block is voltage dependent, Choquet and Korn (1992) showed that 4-AP block requires an initial depolarising pulse presumably to allow 4-AP to enter the channel pore. They also showed that a depolarising potential is necessary for 4-AP unblock.

The K_d value for 4-AP during the second test pulse i.e. at +40mV was 128 μM which is similar to the K_d value of 120 μM ascertained by Choquet and Korn (1992) but less than 190 μM observed by DeCoursey et al., (1984). These results suggest that 4-AP was a more potent K^+ channel than that reported by DeCoursey et al., The difference in the K_d values of this study and the study conducted by DeCoursey et al., could be related to the cell type. DeCoursey et al., used primary T-lymphocytes whilst Jurkat cells were used in the current study. Nevertheless, these results suggest the potency of 4-AP in blocking N -type voltage-gated channels varies between the type of lymphocyte.

Although variability was observed in the current amplitude of the time-dependent voltage-gated K^+ current, this does not explain the seemingly increased potency of 4-AP observed in the present study. In two different Jurkat cells, the peak amplitude of the voltage-gated K^+ current was similar at 460 and 500 pA, however, the ratio of remaining current during the second test pulse differed significantly.

4-AP block depends on the intracellular and extracellular pH and as such, the K_d value has shown to differ based on the pH. This effect of pH seems unlikely in the current study as the pH of the intracellular solution used in this study was 7.2 and was the same as the intracellular pH used by DeCoursey et al., (1984). The concentration of hepes was also 10 mM in both experiments. It is possible that the intracellular pH changed during the course of an experiment in the current study. This hypothesis is based on the development of the outwardly rectifying slow time dependent activating current during the course of some patch clamping experiments which was hypothesized to be a proton current. This, however, seems unlikely due to the

intracellular concentration of hepes used. The reason for the discrepancy in the Kd value of 4-AP remains unknown.

Cl⁻ currents. The theoretical membrane potential ascertained using the GHK equation suggested the contribution of Cl⁻ permeability. Indeed, Cl⁻ channels in the Jurkat cells were observed in the present study. Interestingly, the time course of the Cl⁻ currents showed run-up followed by rundown of the current test potentials of +80 mV. The development of the current with time hints to the Jurkat cells having a low cytosolic [Cl⁻] during the cell culture. This low [Cl⁻] was replaced by an elevated [Cl⁻] in the pipette upon achieving the whole cell configuration. In fact the cytosolic concentration of Cl⁻ has been found to be approximately 58 mM in Jurkat cells cultured in RPMI-1640 (Heimlich and Cidlowski, 2006). On the other hand, Lewis et al., (1993) also saw the development of a Cl⁻ conductance after 50 seconds of achieving the whole cell configuration despite having a low intracellular [Cl⁻] in the pipette solution. This suggests that the development of the Cl⁻ currents was not completely due to the difference in the [Cl⁻] between the cytosol of intact cells and the intracellular patch clamping solution. Rather, the development of the Cl⁻ current could be related to the volume sensitive Cl⁻ channel (Ross et al., 1994).

Although the precise Cl⁻ channel type expressed by the Jurkat cells used in the present study remains elusive, several lines of evidence suggest that the Cl⁻ current was conducted by the volume sensitive channel. Firstly, the Cl⁻ current in this study exhibited run up with time. Lewis et al., (1993) and Worell et al., (1989) also observed cell swelling with a volume sensitive Cl⁻ current that developed 50 seconds after going whole cell despite a difference of only 6% in the osmolarity of the intracellular and extracellular solutions. In the present study, the maximal difference between the osmolarity of the intracellular solution and extracellular solution was slightly higher at 10% and cell swelling in some cells was also noticed. Secondly, Lewis et al., (1993) and Ross et al., (1994) showed that ATP is required to maintain the volume sensitive Cl⁻ current. ATP was omitted from the intracellular solution, therefore the rundown in the Cl⁻ could be due to the lack of intracellular ATP. Thirdly, the volume sensitive Cl⁻ channel has been shown to be sensitive to 100 μM NPPB which was also observed in the current study (Schmid et al., 1998).

Slow activating current. In a subset of Jurkat cells, an outwardly rectifying slow time dependent activating current was observed at depolarising test potentials. This current was observed either immediately after achieving the whole cell configuration or it developed slowly with time. Based on the presence of this current in the absence of K⁺, Cl⁻, Na⁺, Ca²⁺ and ATP in the patch clamping solutions, this current was considered as a proton current. This slow activating current exhibited noticeable variations in its activation kinetics making its characterisation difficult. Four distinct types of proton current kinetics have been identified in different Jurkat cells in the current study. In the study conducted by Schilling et al., (2002), were they characterised a similar slow activating current, noticeably different activation kinetics of the proton currents can also be observed by eye. The reason for the variation in the apparent activation kinetics of this current remain elusive.

The slow time dependent activating current has been described in Jurkat cells, as well as other cell types as a proton current (DeCoursey and Cherny, 1996; Schilling et al., 2002). In the present study, this current developed slowly with time. Schilling et al., showed that the proton current amplitude increased with intracellular pH 6.0 compared with intracellular pH 7.0. This suggests that the intracellular pH in the current study changed during the course of an experiment. This seems unlikely as the pH of the intracellular solution was buffered with 10 mM hepes which was expected to keep the pH stable at pH 7.2. Furthermore, the same regime for making solutions was used throughout the entire study, therefore, the slow activating current should have developed during the course of all experiments if the concentration of hepes was inadequate.

In some Jurkat cells, the development of this slow activating current coincided with rundown in the voltage-gated K⁺ current, however, this was not always observed. Furthermore, if there was a relationship between rundown of the voltage-gated K⁺ current and the activation/observance of the slow activating current, then the slow activating current should have been observed in Jurkat cells when the K⁺ channel was blocked with either TEA or 4-AP. The reason for the development of this slow time dependent activating current with time in some Jurkat cells but no others remains unidentified.

In solutions designed to isolate this slow time dependent activating current, the current amplitude was very small. These observations disagree with the findings in published literature where the amplitude of the proton currents in Jurkat cells was large enough to characterise. These differences could be due to the solutions used. Schilling et al., and DeCoursey and Cherny (1998) used trimethylamine methosulfonate (TMA-MeSO₃) based solutions whilst Kuno et al., (1997) used K glutamate as the major intracellular ion. In the present study, D-gluconic acid was used as the major ion in the solution in an attempt to isolate the potential proton currents. It is possible that the D-gluconic acid could have reduced the amplitude of proton currents.

More likely, the voltage-gated proton channel is extremely sensitive to temperature, therefore, the differences in the amplitude of the slow time dependent current could be related to the temperature. In mast cells, the conductance of a proton current was found to increase proportionally with temperature, that is an increase in temperature from 24 to 36°C resulted in an elevated current amplitude (Kuno et al., 1997). Conversely, a decrease in the temperature by 11°C resulted in a reduced amplitude of the proton current (DeCoursey and Cherny, 1998). Similar temperature sensitive characteristics of this proton channel have been observed in several other cell types. Therefore, differences in the current properties observed in the Jurkat cells used in this study and those cited elsewhere could be attributed to differences in the temperature. The change in temperature could have also caused the development of the slow activating current with time in some Jurkat cells but not others as described earlier. This, however, seems unlikely as the room was kept air conditioned to a constant temperature between 20-22°C. To eliminate temperature related differences, stringent mechanisms to control the temperature could be used through a temperature controlled microscope stage and a heated perfusion system similar to the one used in the study by Kim et al., (2013). In addition, a temperature controlled patch clamping set-up would also overcome difficulties associated with changes in the temperature during the cell culture and patch clamping.

In summary, the membrane potential of actively proliferating Jurkat cells has been investigated and this membrane potential has been found to be determined by a contribution of *N*-type voltage-gated K⁺ channels and Cl⁻ channels. In addition, a channel exhibiting a current with slow time dependent activating kinetics was also

observed. However, its contribution to setting the membrane potential in this study was considered minimal due to the low concentration of protons in the patch clamping solutions. The membrane potential and the underlying channels determining this membrane potential in non-proliferating and activated Jurkat cells will be investigated in the next chapter.

4 EFFECT OF CELL STATUS ON THE ELECTROPHYSIOLOGICAL CHARACTERISATION OF JURKAT CELLS

4.1 Introduction

The membrane potential is the voltage difference across the plasma membrane of a cell and is generated through gradients in the ion concentration between the intracellular and extracellular solutions (Sundelacruz et al., 2009). As described in the introduction, these ionic gradients arise due to the movement of ions through ion channels and pumps. The importance of ionic homeostasis has been established in cell viability, cell excitability, the functioning of protein's such as interleukin-IB converting enzyme and gene expression (Lodish, 2004; Muto et al., 2000; Walev et al., 1995).

Recently, a functional relationship rather than a mere correlative relationship between the membrane potential and various cell behaviours has emerged. The static membrane potential of cells has been shown to vary depending on the proliferative

state of the cell. In general, the static membrane potential of quiescent cells is hyperpolarised whilst proliferating cells have a depolarised membrane potential (see Figure 1.1). Similarly, tumour cells which are in a highly proliferative state also have a depolarised membrane potential (Yang and Brackenbury, 2013). Furthermore, the membrane potential can stimulate and even inhibit cell proliferation (Cone and Tongier, 1973). Changes in the membrane potential have also been shown to modulate differentiation, maturation and migration (Sundelacruz et al., 2009; Yang and Brackenbury, 2013).

Interestingly, regulation of these cell behaviours through the membrane potential has been observed in many different cell types such as proliferative and quiescent cells, normal and cancerous cells (Sundelacruz et al., 2009). This suggests that the modulation of cell behaviours through the membrane potential is a ubiquitous and fundamental control mechanism which is not limited to specific cell type or stage in the life of the cell.

Although a functional relationship between the membrane potential and cell behaviours in a wide variety of cell types has been identified, the precise pathways from the initial change in the membrane potential to the final cell behaviour remains to be elucidated. Only a handful of studies have investigated the membrane potential in detail with a view to understanding its physiological role in cells (de Queiroz et al., 2008; Marek et al., 2010).

Aims of the chapter

In this chapter, culture conditions to inhibit proliferation of the Jurkat cells without inducing cell death are ascertained. In addition, conditions required to activate the Jurkat cells are also determined. The magnitude of the static membrane potential and the ion channels underpinning this static membrane potential is investigated in Jurkat cells in either a non-proliferative state or an activated state and compared to the static membrane potential and the ion channels identified in Jurkat cells in the log phase of growth (see Chapter 3).

The Jurkat E6-1 model cell line is a T-cell leukemic cell line derived from a 14 year old teenager (Schneider et al., 1977). Since its emergence in the late 1970's, Jurkat

cells have been widely used to investigate signalling leukaemia of T cells. Lymphocyte activation can be investigated and confirmed through the secretion of IL-2 and as Jurkat cells also secrete IL-2, this cell line provides a convenient and a well-studied model system in which the influence of the membrane potential (i.e. bioelectric control) on cell behaviours can be studied in a population of Jurkat cells in different proliferative states.

4.2 Results

4.2.1 Ascertaining the culture conditions required for achieving Jurkat cells in a non-proliferative state

Although a functional relationship between the membrane potential and cell proliferation and cell cycle progression has been shown in a wide variety of cells, the precise mechanisms and pathways are poorly understood (Blackiston et al., 2009; Sundelacruz et al., 2009; Yang and Brackenbury, 2013). The membrane potential is determined primarily by the conductance of ions through ion channels and these ion channels have been shown to vary throughout the cell cycle (see Chapter 1). As such, it was hypothesised that the electrophysiological characteristics, namely the static membrane potential i.e. the membrane potential recorded at a single time point would differ between Jurkat cells in either a non-proliferative state, an activated state or cells in the log phase of proliferation (described in Chapter 3). In addition, the activity of ion channels in the plasma membrane of the Jurkat cells was also hypothesised to differ between cells in the three different states.

Experiments were set up to ascertain culture conditions required to achieve Jurkat cells in a static proliferative state wherein proliferation was inhibited with minimal cell death. Proliferation and cell viability was ascertained using the trypan blue exclusion dye assay and the PrestoBlue cell viability assay. The PrestoBlue cell viability reagent is based on resazurin-resorufin dye. The resazurin is reduced to resorufin by the mitochondrial activity of cells which can be monitored by either by fluorescence or absorbance and thus the fluorescence/absorbance is proportional to the rate of proliferation and cell viability (Niles et al., 2009).

Cell viability and proliferation assays determined using the trypan blue reagent suggested that the Jurkat cells were in the log phase of proliferation between 24 and 48 hours when cultured in RPMI-1640 medium containing between 1 and 10% FBS (Figure 4.1). Jurkat cells cultured in medium containing less than 1% FBS also showed an increase in proliferation between 24 and 48 hours, however, the cells were not in the log phase of growth. Jurkat cell numbers continued to increase after 48 hours when the culture medium contained FBS concentrations between 2 and 10%. Jurkat cells cultured in culture medium containing less than 2% FBS showed a

decrease in the cell number at the 72 hour time point in comparison to the 48 hour time point in the same conditions. Furthermore, at the 72 hour time point, a significant decrease in Jurkat cell viability was also observed in comparison to the 48 hour time point in all the culture conditions. It has to be noted, however, that the cell viability at the 72 hour time point increased as the concentration of FBS in the culture medium was increased. For example, in cell cultures lacking FBS, Jurkat cell viability was $41 \pm 9\%$ at the 72 hour time point whilst the viability of Jurkat cells cultured with medium supplemented with 10% FBS was $88 \pm 1\%$ at the same time point.

Similar to the results obtained using the trypan blue assay, the proliferation assay using PrestoBlue showed a significant increase in the cell number between 24 and 48 hours when the culture medium contained between 1 and 10% FBS (Figure 4.2). Unlike the results from the trypan blue assay, the proliferation assay ascertained using the PrestoBlue reagent showed that the Jurkat cells were not in the log phase of growth between 24 and 48 hours in the different culture conditions investigated. In addition, the cell viability from the PrestoBlue assay did not show significant changes in the Jurkat cell viability at the 72 hour time point when cultured in RPMI-1640 medium containing between 1 and 10% FBS.

The cell viability and proliferation results obtained using the trypan blue reagent and the PrestoBlue assay suggest that the Jurkat cells used in the present study cannot be put into a completely static proliferative state without inducing cell death. Rather, these results indicate a specific time point wherein the Jurkat cells were in a static proliferative state with minimal cell death. The time point wherein the Jurkat cells were in this static proliferative state was at 48 hours when the Jurkat cells were cultured in RPMI-1640 medium supplemented with 1% FBS. This static proliferative state will be referred to as the non-proliferative state for hereon in. In line with the objectives of this chapter and the aims of this study, these conditions will be used for the electrophysiological characterisation of the Jurkat cells that were in a non-proliferative state with minimal cell death.

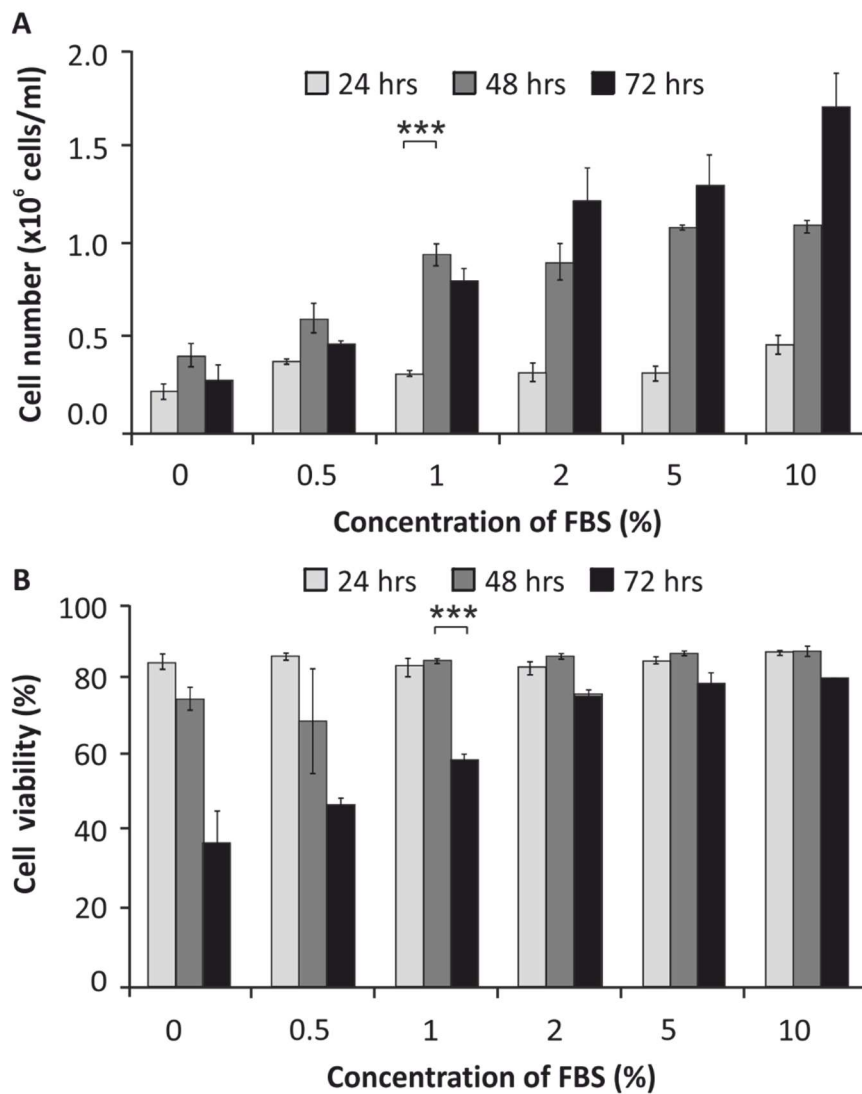


Figure 4.1

Using trypan blue to investigate the effect of FBS on cell viability and cell proliferation over 72 hours. Jurkat cells were seeded 2×10^5 cells/ml in T25 flasks in RPMI culture medium supplemented with FBS concentrations between 0 - 10% as shown and incubated between 24 hours and 72 hours at 37°C. Thereafter, the cells were stained with trypan and manually counted at 24 hours, 48 hours and 72 hours to ascertain the (A) cell number and the (B) cell viability. The cell viability was determined using the methods described in the methods section. A mixed models ANOVA was used to ascertain the statistical significance of the differences between the different conditions with the most relevant statistical differences highlighted with *** which represents $p < 0.0005$. A Bonferroni correction was applied when comparing either cell number or cell viability at the different time points within each FBS concentration group. Each experiment was repeated three times in triplicates and plotted as the mean \pm SEM.

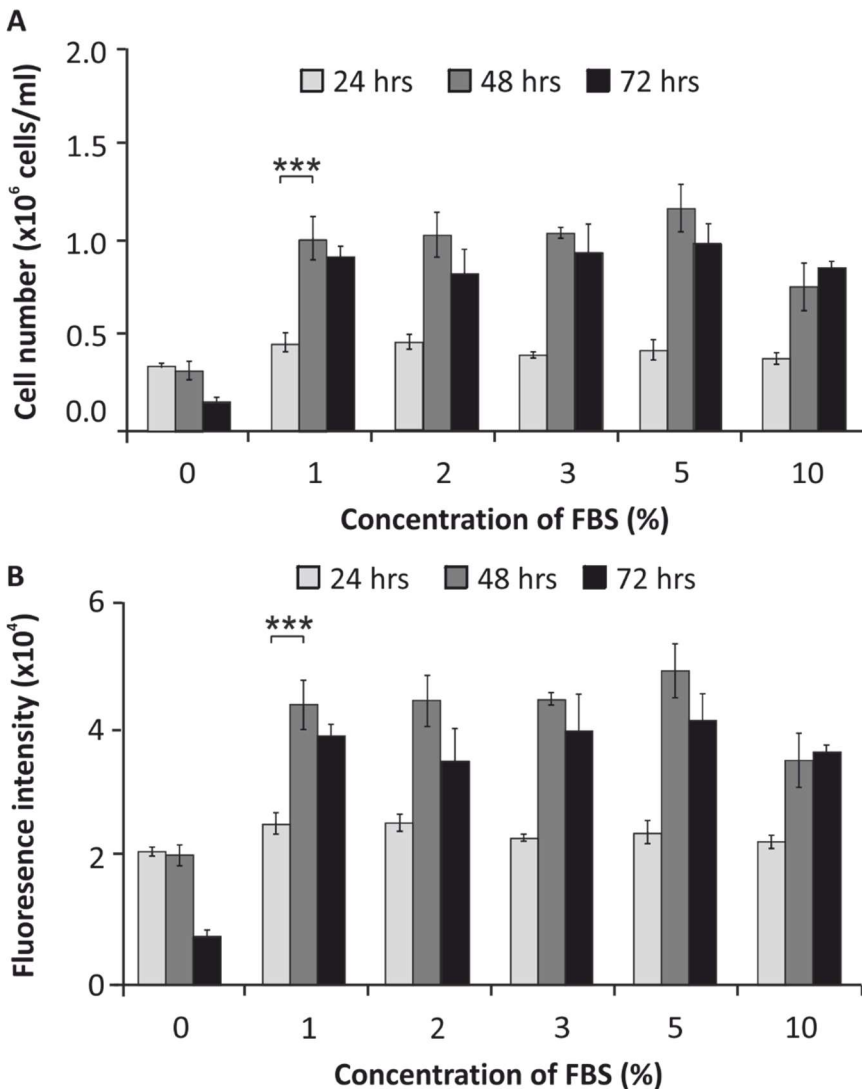


Figure 4.2

Investigating the effect of FBS on cell viability and cell proliferation over 72 hours using PrestoBlue cell Viability reagent. Jurkat cells were seeded 2×10^5 cells/ml in 96 well plates in RPMI culture medium containing between 0 - 10% FBS as shown and incubated between 24 hours and 72 hours at 37°C . Thereafter, the cells were incubated with PrestoBlue and the fluorescence measured. Jurkat cells incubated with PrestoBlue were incubated for 10 minutes at 37°C and the (A) cell number and the (B) fluorescence intensity. The cell number in (A) was ascertained by incubating between 100 and 2×10^6 cells/ml of Jurkat cells at the same time as incubating the Jurkat cells under investigation with PrestoBlue. The fluorescence intensity of the known density of cells was plotted against each and a curve of best fit of the data was added. The density of the Jurkat cells under investigation i.e. under different treatments was interpolated based on the fluorescence intensity. A mixed models ANOVA was used to ascertain the statistical significance of the differences between the different conditions. The most relevant statistical differences have been highlighted with *** which represents $p < 0.0005$. A Bonferroni correction was applied when comparing either the cell number or fluorescence intensity at the different time points within each FBS concentration group. Each experiment was repeated three times in triplicates and plotted as the mean \pm SEM.

4.2.2 The effect of ConA and PHA on the activation of Jurkat cells

Activation of T-lymphocytes results in the secretion of IL-2 and the secretion of this cytokine promotes the expansion of T cells both, *in vivo* and *in vitro* (Nelson, 2004). The Jurkat T-lymphocyte model cell line also secretes IL-2 upon activation (ATCC, 2015; Pawelec et al., 1982). Consequently, activation of the Jurkat cells can be followed by assaying the IL-2 secreted. The effect of either 20 µg/ml ConA or PHA treatment on IL-2 secretion from the Jurkat cells was investigated using this IL-2 secretion as the marker for activation. Both, PHA and ConA are lectins and are widely used mitogens in this regard (Gillis and Watson, 1980).

In the absence of the mitogens no IL-2 secretion above the minimum detectable level of 7 pg/ml was observed in either the proliferating or the non-proliferating Jurkat cells (Figure 4.3) (R&D systems, 2015). On the other hand, Jurkat cells treated with 20 µg/ml of either the ConA or the PHA mitogen showed IL-2 secretion confirming that the Jurkat cells can indeed be activated by treatment with either ConA or PHA (Figure 4.3). Interestingly, treatment with 20 µg/ml PHA induced significantly more ($p<0.005$) IL-2 secretion in comparison to 20 µg/ml ConA suggesting that PHA is the more effective mitogen for the Jurkat cells at this concentration.

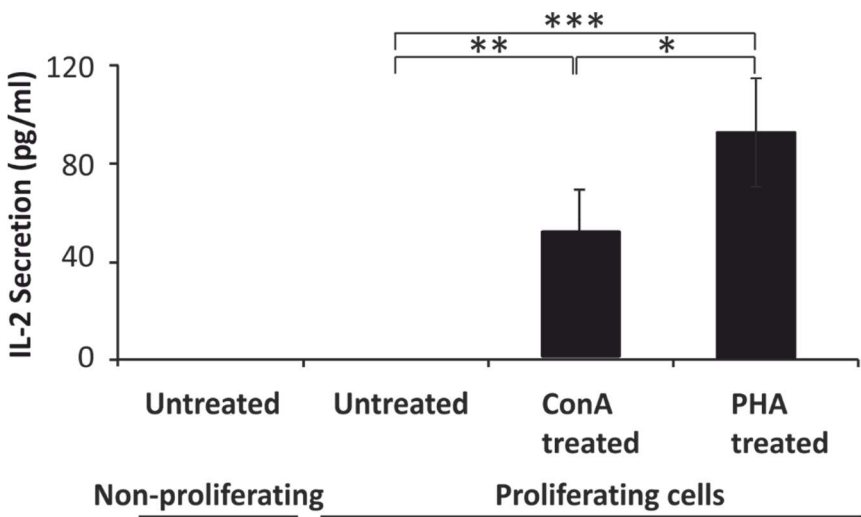


Figure 4.3

The effect of ConA or PHA treatment on IL-2 secretion from Jurkat cells either in a non-proliferative or a proliferative state. The proliferative Jurkat cells were either untreated or treated with either 20 µg/ml ConA or 20 µg/ml PHA for 24 hours. The Jurkat cells were seeded at a density of 2×10^6 cells/ml and incubated with the mitogen for 24 hours before the cell suspension was harvested, spun down and the supernatant removed for IL-2 quantification using the Human IL-2 Quantikine ELISA kit. Each experiment was repeated three times in triplicates and the bar chart is plotted as mean ± SEM. A Student's T-test was used to ascertain the degree of statistical significance between the different conditions and * represents $p < 0.05$ whilst ** and *** represents $p < 0.005$ and $p < 0.0005$, respectively.

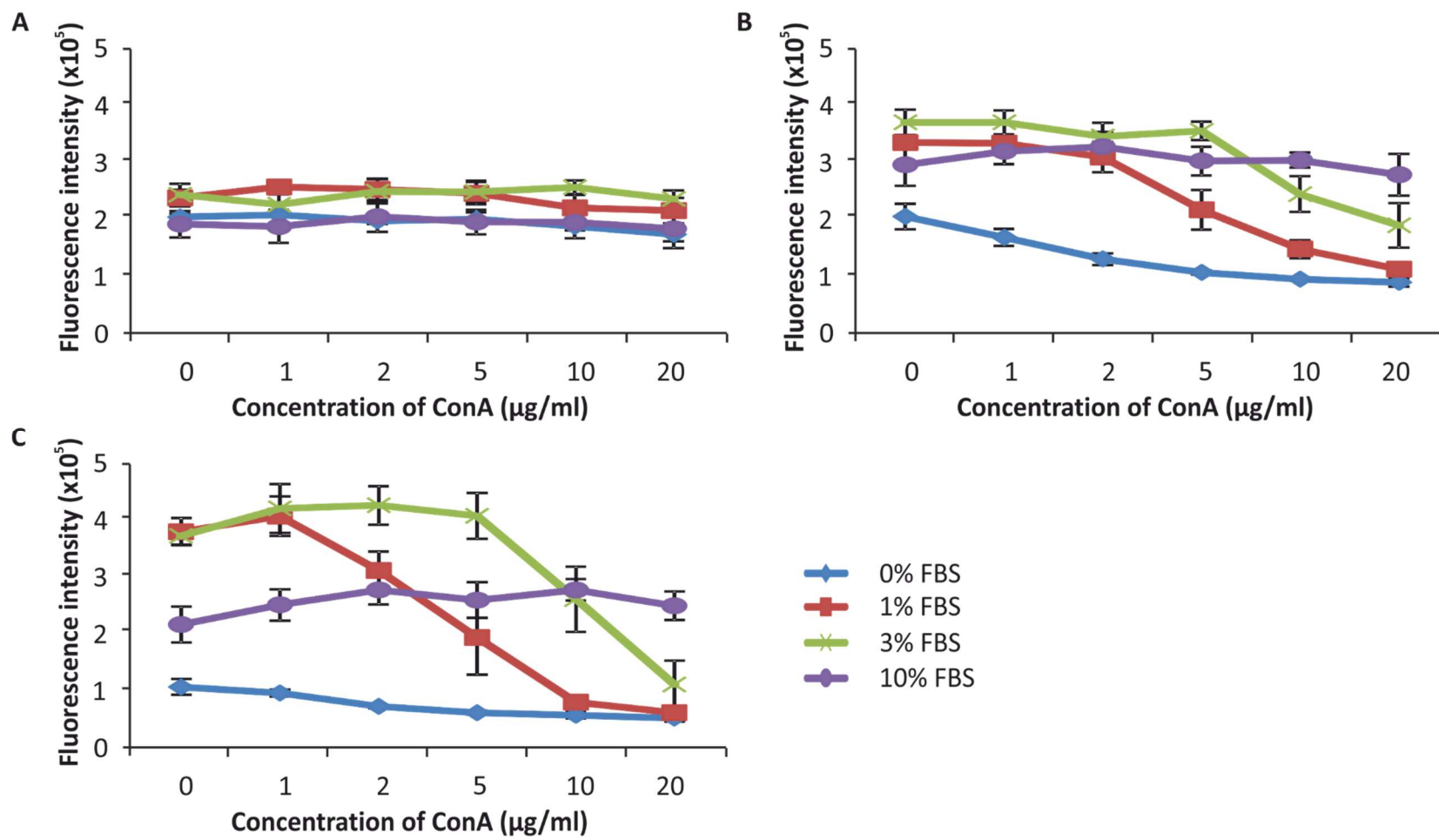
4.2.3 The effect of ConA treatment on the cell viability of Jurkat cells cultured in medium containing varying concentrations of FBS

The results thus far have shown that both, ConA and PHA treatment induced activation of the Jurkat cells. Next, the effect of either ConA or PHA treatment on the cell viability of Jurkat cells was ascertained. In addition, the effect of either ConA or PHA treatment was also investigated in the presence of different concentrations of FBS in the culture medium (Figure 4.4).

As expected, cell cultures supplemented with 0% FBS were not viable over the 72 hour time course. At the 24 hour time point, minimal effects of ConA treatment were observed but at the 48 hour time point, the higher concentrations of ConA caused a reduction in the cell viability of the Jurkat cells cultured in medium containing FBS concentrations less than 3%. This cytotoxic effect induced by ConA was even more pronounced at the 72 hour time point, however, the cytotoxic effect of ConA was abated by the addition of 10% FBS in the culture medium at both, 48 and 72 hours. At the 72 hour time point, the cytotoxic effect of ConA was most apparent in cultures containing FBS concentrations less than 10% FBS with ConA concentrations above 5 $\mu\text{g}/\text{ml}$.

Figure 4.4

The effect of ConA on the viability of the Jurkat cells. The Jurkat cells were seeded at 2.0×10^5 cells/ml in 96 well plates and incubated for either **(A)** 24 hours, **(B)** 48 hours or **(C)** 72 hours in RPMI-1640 culture medium containing either 0, 1, 3 or 10% FBS concentrations. The concentration of ConA treatment ranged from 0 to 20 $\mu\text{g}/\text{ml}$. The cell viability was measured by incubating the cells with PrestoBlue reagent for 10 minutes and the fluorescence measured as described in the methods. A mixed models ANOVA was used to ascertain the statistical significance of the differences between the different conditions. A Bonferroni correction was applied when pairwise comparisons were made between the ConA concentration and the different FBS concentrations. Although statistically significant differences of $p < 0.05$ were observed they have been omitted for clarity. Each experiment was repeated three times in triplicate. The data is plotted as the mean \pm SEM.

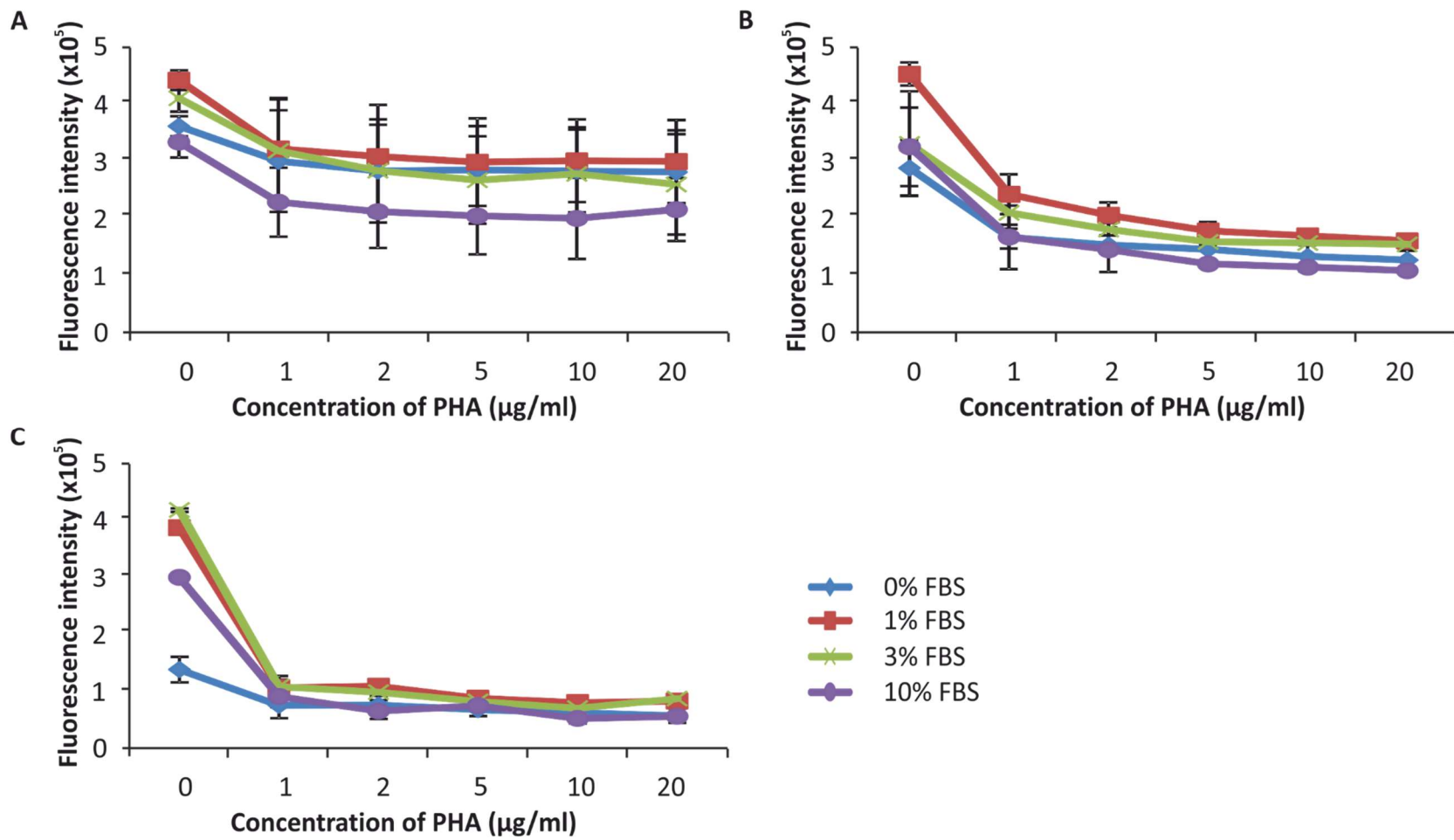


4.2.4 The effect of PHA treatment on the cell viability of Jurkat cells cultured in medium containing varying concentrations of FBS

To investigate if the cytotoxic effect was specific to the ConA mitogen, the effect of PHA on the viability of the Jurkat cells was ascertained. Consistent with the findings of Gillis and Watson (1980), PHA was a more effective activator of the Jurkat cells used in the present study in comparison to the ConA (see Figure 4.3). Similar to the cytotoxic effects of ConA on the Jurkat cells, the results showed that PHA treatment was also cytotoxic to the cells (Figure 4.5). The cytotoxic effect of PHA was apparent at 1 µg/ml at 24 hours, whereas the cytotoxicity of ConA was observed at the 48 hour time point at concentrations above 5 µg/ml. The degree of cytotoxicity of PHA failed to show a dose dependent increase at both, 48 and 72 hour time points hinting at the increased cytotoxic potency of PHA. Furthermore, increasing the concentration of FBS in the RPMI-1640 culture medium failed to prevent the cytotoxic effect of PHA unlike the counteracting effect of FBS on ConA induced cytotoxicity shown in Figure 4.4. Taken together, these results suggest that PHA is a more potent cytotoxic agent to the Jurkat cells than ConA.

Figure 4.5

The effect of PHA on the viability of the Jurkat cells. The Jurkat cells were seeded at 2.0×10^5 cells/ml in 96 well plates for either **(A)** 24 hours, **(B)** 48 hours or **(C)** 72 hours and were cultured in either 0, 1, 3 or 10% FBS concentrations with PHA treatment ranging from 0 to 20 $\mu\text{g}/\text{ml}$. Cell viability was measured by incubating the cells with PrestoBlue reagent for 20 minutes and the fluorescence measured. Each experiments was repeated two times in triplicate. The data is plotted as mean \pm SD. A mixed models ANOVA was used to ascertain the statistical significance of the differences between the different conditions. A Bonferroni correction was applied when pairwise comparisons were made between the PHA concentrations with FBS concentrations. Although statistically significant differences of $p < 0.05$ were observed they have been omitted for clarity.



4.2.5 The role of extracellular ions on mitogen induced activation of the Jurkat cells

To further investigate the activation mechanism involved with either ConA or PHA, the concentration of either K^+ , Na^+ or Cl^- was increased in the RPMI-1640 culture medium. The concentration of these ions were increased by either 6 mM or 30 mM. The $[K^+]$ was increased through the addition K gluconate, whilst the $[Na^+]$ was increased using Na gluconate. The $[Cl^-]$ was increased through the addition of ChCl.

As the concentration of IL-2 secretion differed significantly according to the mitogen used to induce the secretion of IL-2 (see Figure 4.3), the IL-2 secretion was normalised to the IL-2 secretion induced by either the ConA or PHA mitogen described in Figure 4.3. This normalisation allowed for a direct comparison between the effects of the three ions on IL-2 secretion induced by either ConA or PHA. In addition, osmolarity matched controls using sorbitol were incorporated in the assay to account for changes in the osmolarity of the RPMI-1640 culture medium due to the addition of the salts. The increase in the osmolarity did not show significant differences in the mitogen-induced IL-2 secretion relative to that in the unperturbed RPMI-1640 medium. This indicates that any effects on the mitogen-induced IL-2 secretion in the presence of the RPMI-1640 medium perturbed with salts was not caused by changes in the osmolarity.

Figure 4.6 shows that an increase in $[K^+]$ in the culture medium by only 6 mM significantly reduced ($p<0.05$) both, ConA and PHA induced IL-2 secretion in the Jurkat cells. A further increase in the $[K^+]$ in the RPMI-1640 medium by 30 mM completely abolished both, PHA and ConA induced IL-2 secretion. Interestingly, an increase in the extracellular $[Na^+]$ by 30 mM also reduced both, PHA and ConA induced IL-2 secretion albeit to a much lesser degree than the effect of elevating the $[K^+]$ of the culture medium by the same concentration.

As the increase in extracellular $[K^+]$ caused a significant decrease in mitogen induced IL-2 secretion, the role of K^+ channels in mitogen-induced activation was investigated using 4-AP. 4-AP is non-specific K^+ channel blocker which inhibited the voltage-gated K^+ channel (see Chapter 3). The presence of 0.5 mM 4-AP in the culture medium did not affect either the ConA or PHA induced IL-2 secretion.

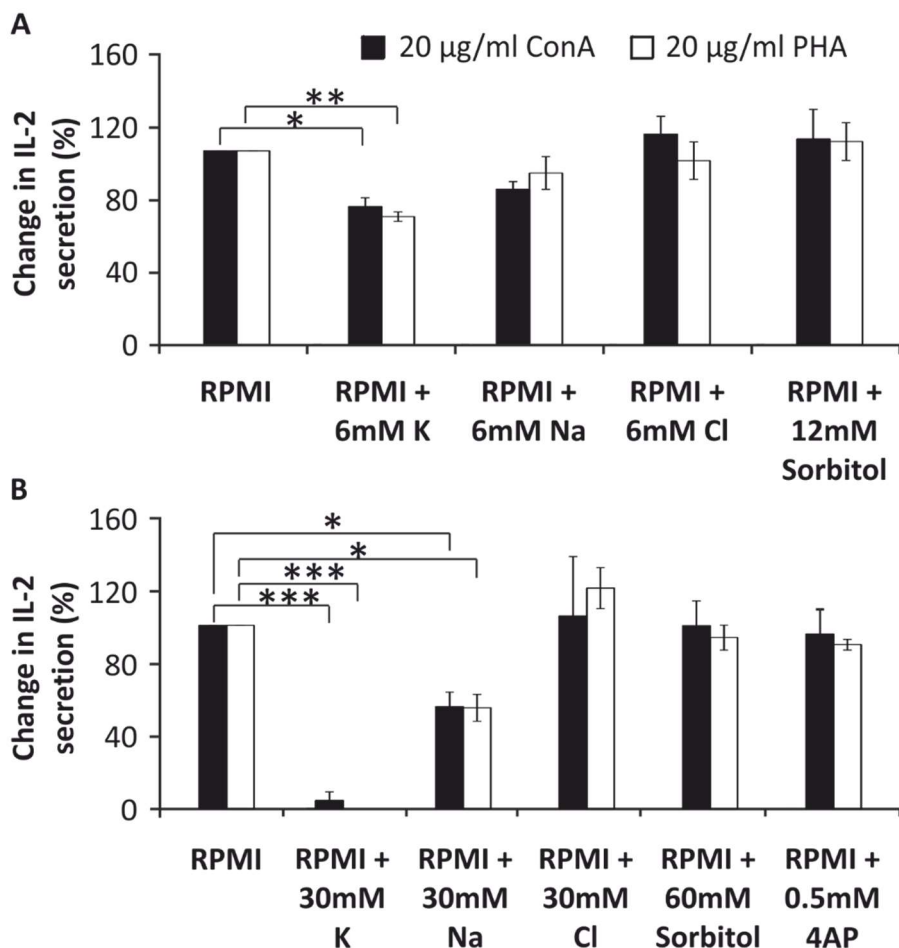


Figure 4.6

IL-2 secretion induced by either ConA or PHA in the presence of altered membrane potential by varying the ionic concentration of the RPMI culture medium. The Jurkat cells were either untreated or treated with 20 µg/ml ConA or 20 µg/ml PHA for 24 hours in RPMI-1640 culture medium containing elevated concentration of either K gluconate, Na gluconate or ChCl by (A) 6mM or (B) 30mM. Appropriate sorbitol controls were incorporated to ascertain the effect of osmolarity on IL-2 secretion. The Jurkat cells were seeded at a density of 2.0×10^6 cells/ml and incubated with the mitogen for 24 hours before the cell suspension was spun down and the supernatant removed for IL-2 quantification using the Human IL-2 Quantikine ELISA kit. The cells which were treated with either PHA or ConA in the standard RPMI culture medium were considered as the control and shown as 100% change in IL-2 secretion in the figures. The IL-2 secretion in the changed RPMI solution was compared to this control and shown as the % change between the control and the changed RPMI solution. Data represents mean \pm SEM ($n=6$). The same conditions were investigated in the absence of ConA and PHA (untreated Jurkat cells), however, as the cells did not secrete IL-2, they were omitted from (A) and (B) for clarity. A Student's T-test was used to ascertain the statistical significance between the changes in the mitogen induced IL-2 secretion in the different conditions. * represents a $p < 0.05$, whilst ** represents $p < 0.005$ and *** represents $p < 0.0005$.

4.2.6 The effect of ConA and PHA treatment on the viability of Jurkat cells with altered concentrations of either K⁺, Na⁺ or Cl⁻

The results thus far have shown that changes in the ionic concentrations of either K⁺ or Na⁺ in the RPMI-1640 medium interferes with mitogen induced IL-2 secretion in the Jurkat cells. It is possible that the decrease in the secretion of IL-2 was due to reduced cell viability as a result of the alterations in the RPMI-1640 culture medium. Therefore, the viability of the Jurkat cells was investigated with the altered ion concentrations already investigated i.e. the concentration of either K⁺, Na⁺ or Cl⁻ was increased in the culture medium by either 6 mM or 30 mM. In addition, osmolarity matched controls were also incorporated into the assay. The viability of the Jurkat cells were ascertained using the PrestoBlue cell viability reagent.

Figure 4.7 shows that the fluorescence intensity and thus the viability of the Jurkat cells did not significantly change after 24 hours in culture with the medium containing the elevated ionic concentrations by either 6 mM or 30 mM in comparison to the unaltered RPMI-1640 culture medium. These results suggest that reductions in the IL-2 secretion observed in the presence of an increase of 6 mM or 30 mM K⁺ in RPMI-1640 culture medium was not due to a reduction in Jurkat cell viability.

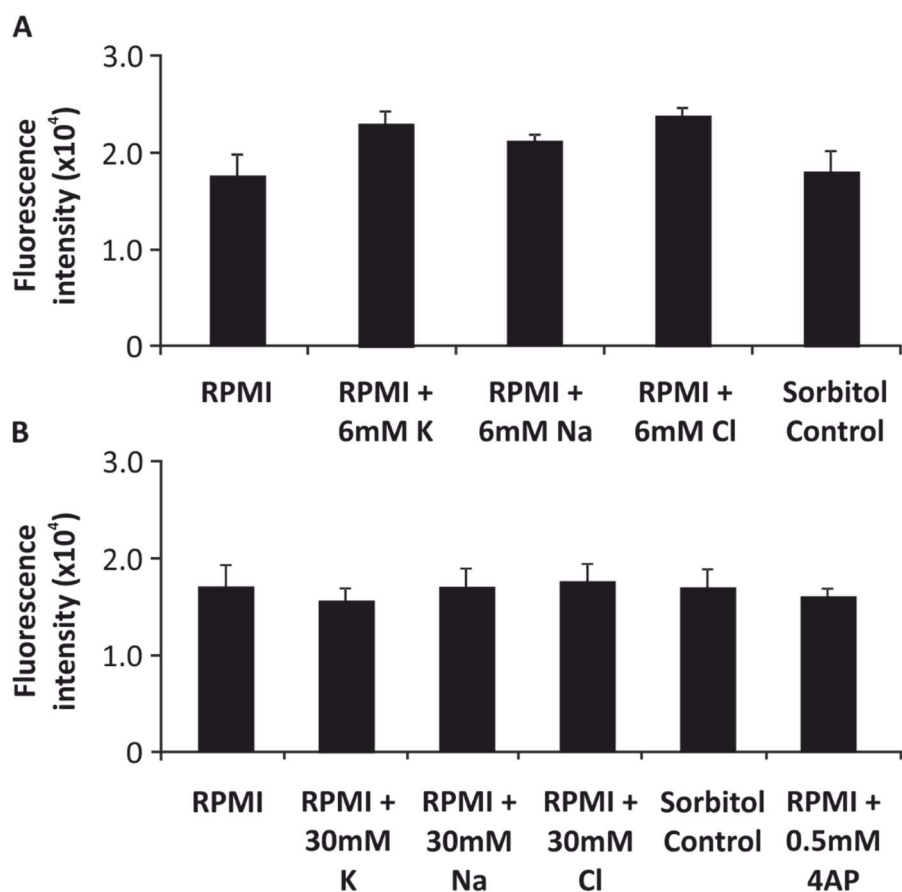


Figure 4.7

The effect of increasing the ionic concentration of the RPMI-1640 culture medium on the viability of the Jurkat cells. The Jurkat cells were seeded at 2.0×10^5 cells/ml in 96 well plates for 24 hours. The ionic concentration of the specific ions was increased by either (A) 6 mM or (B) 30 mM. The cell viability was measured by incubating the cells with PrestoBlue reagent for 10 minutes and the fluorescence measured as described in the Chapter 2. The data represents the mean \pm SEM (n=3).

4.2.7 The effect of FBS and ConA on the cell cycle distribution in Jurkat cells

The results from the trypan blue and PrestoBlue assay's showed that the Jurkat cells can be cultured to a non-proliferative state with minimal cell death from a state of active proliferation by reducing the concentration of FBS in the culture medium. In addition, the Jurkat cells can also be activated using mitogens. To further characterise the Jurkat cells the distribution of the cell cycle was investigated in the three different states i.e. Jurkat cells in the log phase of growth, Jurkat cells in a non-proliferative state and Jurkat cells in an activated state. The distribution of the cell cycle was investigated using propidium iodide staining.

The results showed that the distribution of the cell cycle of the Jurkat cells in the log phase of growth did not change significantly over the 120 hour time course (Figure 4.8). A decrease in the proportion of cells in the G2 phase was observed at 96 and 120 hours in comparison to 24 hours, however, this was not statically significant.

Previous results from the present study showed that incubation of the Jurkat cells with ConA for 24 hours caused IL-2 secretion and thus suggested that the Jurkat cells were in an activated state. Despite this change in the state of the Jurkat cells, the distribution of the cell cycle at the different phases of the cell cycle did not significantly change between proliferating Jurkat cells and the activated Jurkat cells (Figure 4.9).

The previous results suggested that the Jurkat cells were in a non-proliferative state with minimal cell death at 48 hours when cultured in RPMI-1640 medium containing 1% FBS. The distribution of the cell cycle at the 48 hour time point supported these findings and failed to show significant changes in the proportion of cells in the G2 phase of the cell cycle between Jurkat cells in the log phase of growth and Jurkat cells in a non-proliferative state (Figure 4.9). Furthermore, no significant differences in the proportion of cells in the G0/G1 phase were observed at the 48 hour time point. If proliferation was completely inhibited an accumulation of cells in the G0/G1 phase would be expected.

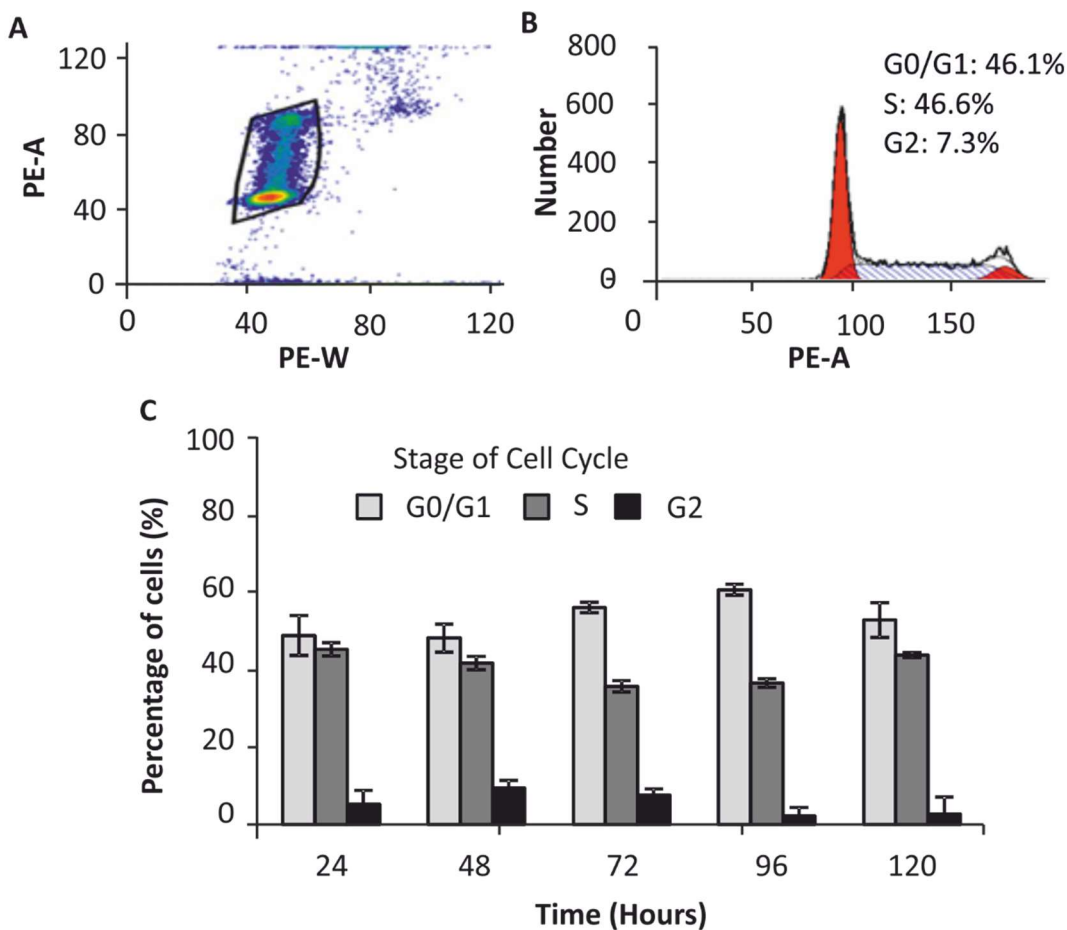
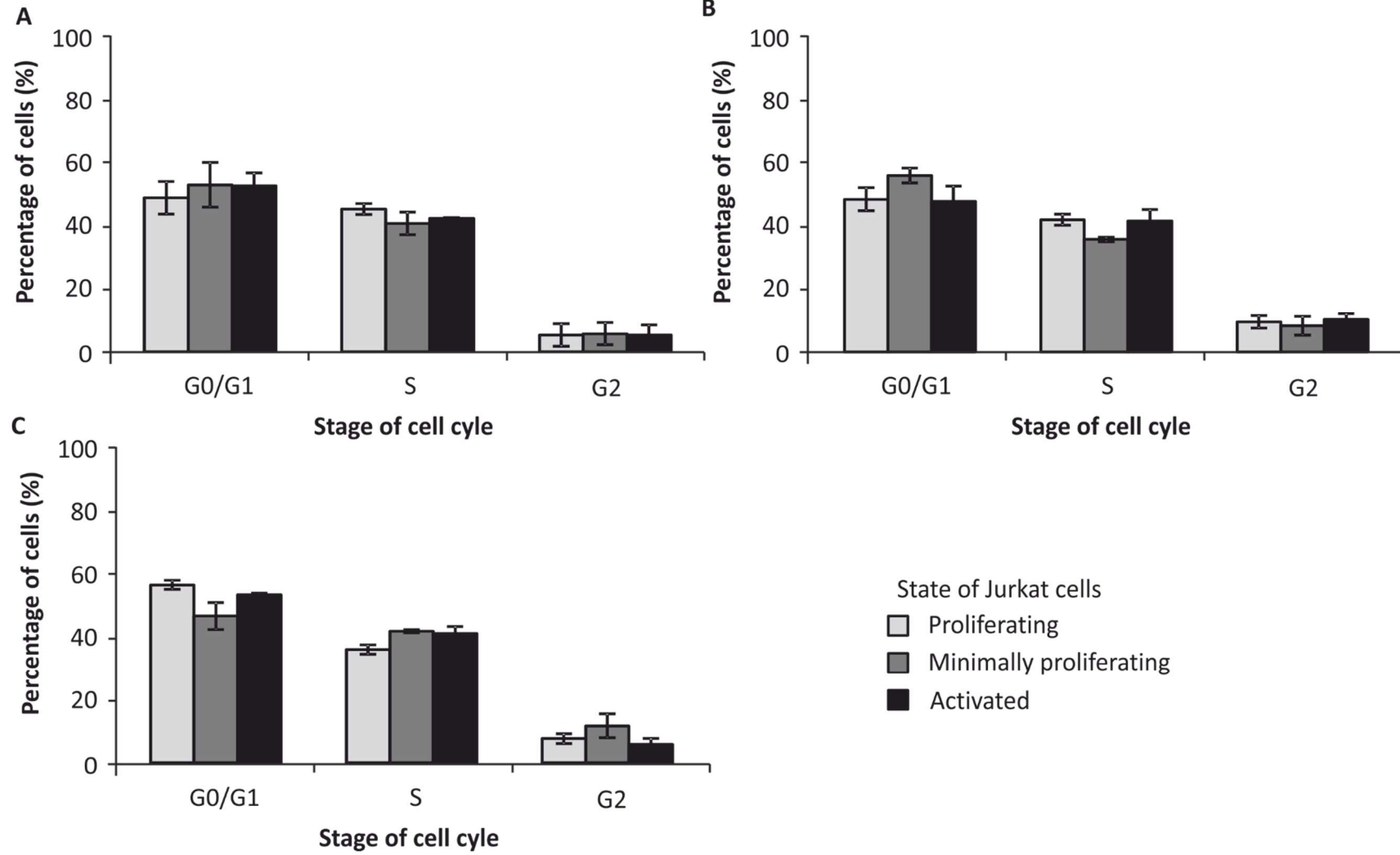


Figure 4.8

Cell cycle analysis of proliferating Jurkat cells using the propidium iodide dye. Jurkat cells were cultured in RPMI medium containing 10% FBS and harvested at time points between 24 and 120 hours for cell cycle analysis. (A) A representative dot plot highlighting the gating regime used for doublet discrimination using pulse width and pulse area. (B) A representative histogram of the cell cycle profile of Jurkat cells cultured in RPMI-1640 culture medium containing 10% FBS at 24 hours. (C) Bar chart showing the percentage of cells in the different phases of the cell cycle for Jurkat cells in the log phase of growth. The cells were harvested at the indicated time points. 1.5×10^5 cells/ml Jurkat cells were fixed in ethanol and stained with propidium iodide as described in the methods. The plot on (A) and the histogram in (B) are representative of three independent experiments. Data in (C) is presented as means \pm SEM.

Figure 4.9

Cell cycle analysis of Jurkat cells using propidium iodide dye. Jurkat cells were cultured in RPMI medium containing either 10% FBS, 1% FBS or 10% FBS with 20 µg/ml to achieve cells in either the log phase of growth, a non-proliferative state or an activated state, respectively. The Jurkat cells were harvested at time-points between 24 and 72 hours for cell cycle analysis. Bar charts showing the percentage of cells in different phases of the cell cycle for Jurkat cells in the different states and analysed at (A) 24 hours, (B) 48 hours and (C) 72 hours. The cells were harvested at the indicated time points. The Jurkat cells were counted and 1.5×10^5 cells/ml were fixed in ethanol and stained with propidium iodide as described in the methods. Cell cycle analysis of the Jurkat cells was repeated three times. The data is presented as mean \pm SEM.



In summary, the Jurkat cells used in the present study can be cultured into a static proliferative state with minimal cell death which is referred to as a non-proliferating state. This state was achieved by culturing the Jurkat cells in RPMI-1640 medium supplemented with 1% FBS for 48 hours. In addition, the Jurkat cells can also be activated treating them with either 20 µg/ml ConA or 20 µg/ml PHA for 24 hours. Next, the electrophysiology of Jurkat cells in these two states will be investigated and compared to Jurkat cells in the log phase of growth described in Chapter 3.

4.2.8 Electrophysiological characterisation of Jurkat cells in either a non-proliferating or an activated state

Increasing evidence suggests that the membrane potential plays a functional role in various cell behaviours such as proliferation (Sundelacruz et al., 2009). Therefore, the electrophysiological characteristics of Jurkat cells which were either in a non-proliferating state whilst maintaining cell viability or activated by the ConA mitogen were investigated using the whole cell configuration of the patch clamping technique. The patch clamping technique was also used to investigate the membrane potential of the Jurkat cells and the ion channels underpinning this membrane potential. In line with the aims of this chapter, the electrophysiological characteristics of Jurkat cells in the three different states i.e. Jurkat cells in a non-proliferating state, Jurkat cells in a proliferative state and cells in an activated state were compared.

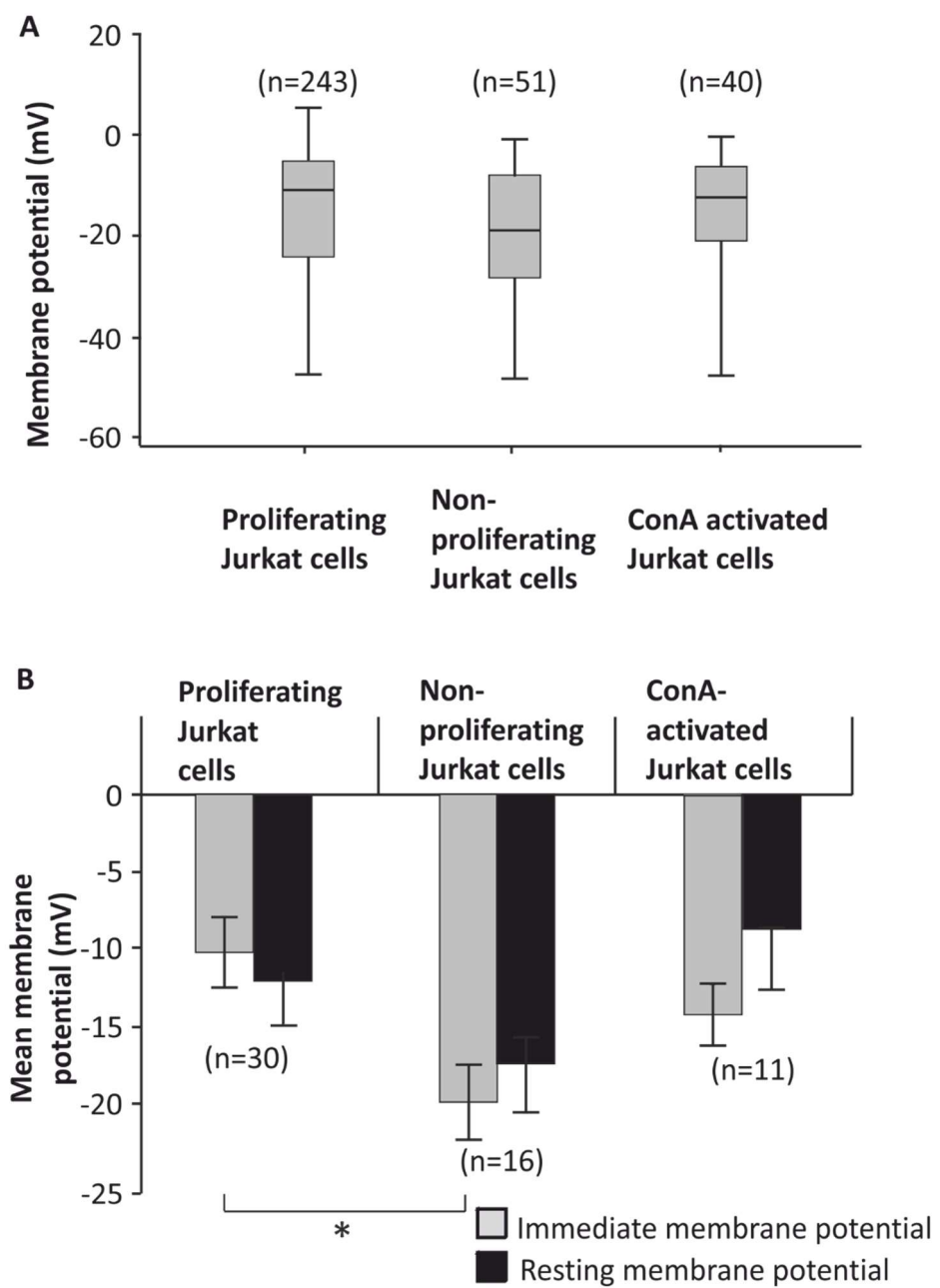
4.2.8.1 The membrane potential of the Jurkat cells in different states

Figure 4.10A shows the distributions of the immediate membrane potential (membrane potential recorded within 2 seconds of achieving the whole cell configuration) of all the Jurkat cells which were either in the log phase of proliferation, a non-proliferative state without concurrent cell death or activated by ConA treatment. The mean immediate membrane potential of the population of cells in the log phase of growth was -15 ± 1 mV ($n=243$) whilst the mean membrane potential of Jurkat cells in a non-proliferative state was -20 ± 2 mV ($n=51$) whilst the mean membrane potential of the ConA activated Jurkat cells was -14 ± 2 mV ($n=40$).

Figure 4.10B shows the mean immediate membrane potential of Jurkat cells in a non-proliferative state was significantly different to the immediate membrane potential of the proliferating Jurkat cells which was -11 ± 2 mV ($n=30$) ($p<0.05$). On the contrary, Jurkat cells which were activated by treatment with 20 µg/ml ConA for 24 hours did not show a significant difference in the mean immediate membrane potential in comparison to the proliferating Jurkat cells. Figure 4.10B also shows that the resting membrane potential (recorded after a minimum of five minutes of achieving the whole cell configuration) of the population of Jurkat cells in a state of static proliferation was -17.5 ± 3 mV ($n=16$) whilst the resting membrane potential of the activated Jurkat cells was -9 ± 4 mV ($n=11$). In both states, the resting membrane potential failed to significantly differ from the immediate membrane potential of the Jurkat cells in their respective states.

Figure 4.10

Distributions of the membrane potentials of Jurkat cells in different proliferative states. (A) Box plot showing the distribution of the membrane potential of either 243 Jurkat cells in a proliferative state, 51 Jurkat cells in a non-proliferative state or 40 ConA activated Jurkat cells measured within 2 seconds after establishing the whole cell configuration. Each point represents the membrane potential of an individual Jurkat cell. (B) The immediate and stabilised membrane potential of 30 proliferating Jurkat cells, 16 Jurkat cells in a non-proliferative state or 11 ConA activated Jurkat cells. Treatment with 20 µg/ml ConA for 24 hours was used to activate the Jurkat cells, whilst Jurkat cells were in a non-proliferative state by culturing the cells with RPMI-1640 supplemented with 1% FBS and patched at 48 hours. The data is plotted as the mean ± SEM. Note, all the cells that had their immediate membrane potential measured are shown in (A), whilst only cells that had a membrane potential measured both, immediately and at a resting state are shown in (B), consequently, the sample size of (A) and (B) is significantly different despite cells shown in (B) belonging to same populations in (A). The Jurkat cells were patched in extracellular solution E1 and intracellular solution I1. A paired Student's T-test was used to ascertain the statistical significance between the immediate and resting membrane potential within each state. An independent Student's T-test was used to ascertain the statistical significance between the immediate membrane potential of the Jurkat cells in the three different states. * represents $p < 0.05$.



4.2.9 The whole cell currents of Jurkat cells either in a non-proliferative state or a ConA activated state

The membrane potential is determined predominantly by the activity of ion channels and as the immediate membrane potential of the Jurkat cells in the non-proliferative state significantly differed from the immediate membrane potential of proliferating Jurkat cells described in Chapter 3, it was hypothesised that these two populations of Jurkat cells would also have different ion channels. On the contrary, it was envisaged that there would be no differences in the ion channels and currents observed between ConA activated Jurkat cells and proliferating Jurkat cells due to the non-significant differences in the immediate membrane potential of these two populations of cells.

In the whole cell configuration, Jurkat cells which were in a non-proliferative state exhibited three different current types (Table 4.1 and Figure 4.11). These current types exhibited similar activation and inactivation properties to the proliferating Jurkat cells in described in Chapter 3. A time dependent activating current with rapid activation followed by slow inactivating properties was observed in 83% of the Jurkat cells (45 out of 54 cells). This current was determined to be conducted by the *N*-type voltage-gated K⁺ channel in Jurkat cells in the log phase of proliferation (see Chapter 3). A current exhibiting slow time dependent activating current properties was observed in 6% of the cells (3 out of 54 cells) and an instantaneous current was also observed in 11% of the Jurkat cells in a non-proliferative state (6 out of 54 cells).

The ConA-activated Jurkat cells also exhibited similar current types that were seen in both, the proliferating Jurkat cells and Jurkat cells that were in a non-proliferative state, however, the proportion of cells expressing the current types differed (see Table 4.1). The time dependent activating current with slow inactivating properties was observed in 58% of the ConA treated Jurkat cells (23 out of 40 cells). The current exhibiting slow time dependent activating current properties was observed in 8% of the cells (3 out of 40 cells) whilst the instantaneous current was observed in 33% of the cells (13 out of 40 cells). In addition to these three current types, a voltage-dependent instant current was also observed in one ConA activated Jurkat cell wherein the current appeared to be inactivated at test potentials above +20 mV (Figure 4.11E). This current was not characterised as it was only observed in one cell, however, the

observed E_{rev} of this current was -55 mV suggesting that it could be carried by K^+ as the theoretical E_{K+} was -75 mV.

The time dependent activating current with slow inactivation properties observed in both, the non-proliferating and ConA activated Jurkat cells was suspected to be carried by K^+ as the observed E_{rev} of the peak activated current was close to the theoretical E_{K+} which was -75 mV (see Figure 4.11B). This current was also suspected to be conducted through the same voltage-gated K^+ channel described in the proliferating Jurkat cells characterised in Chapter 3 due to the manner of activation and inactivation. To confirm, if the current was indeed conducted through the same channel, the degree of cumulative inactivation of the whole cell currents of Jurkat cells in the non-proliferative state and ConA activated state was ascertained. Recall, cumulative inactivation is a defining characteristic of the N -type voltage-gated K^+ channel and the results showed that this time-dependent current exhibited cumulative inactivation (Figure 4.12). The E_{rev} of whole cell time dependent current and the cumulative inactivation in combination suggest that this current is indeed the same current type observed in the proliferating Jurkat cells.

Activation kinetics. As the time dependent current was suspected to be the same current found in the Jurkat cells in the log phase of proliferation (see Chapter 3), it was decided to investigate the activation kinetics of this current from the Jurkat cells in a non-proliferative state or an activated state. The activation phase of this voltage-gated K^+ current was fitted with an exponential function. Table 4.2 shows that tau in the proliferating Jurkat cells was voltage dependent and there were no significant differences in the tau's between Jurkat cells in either a proliferative state, non-proliferative state or an activated state.

The current types and its expression in the Jurkat cells in the three different states

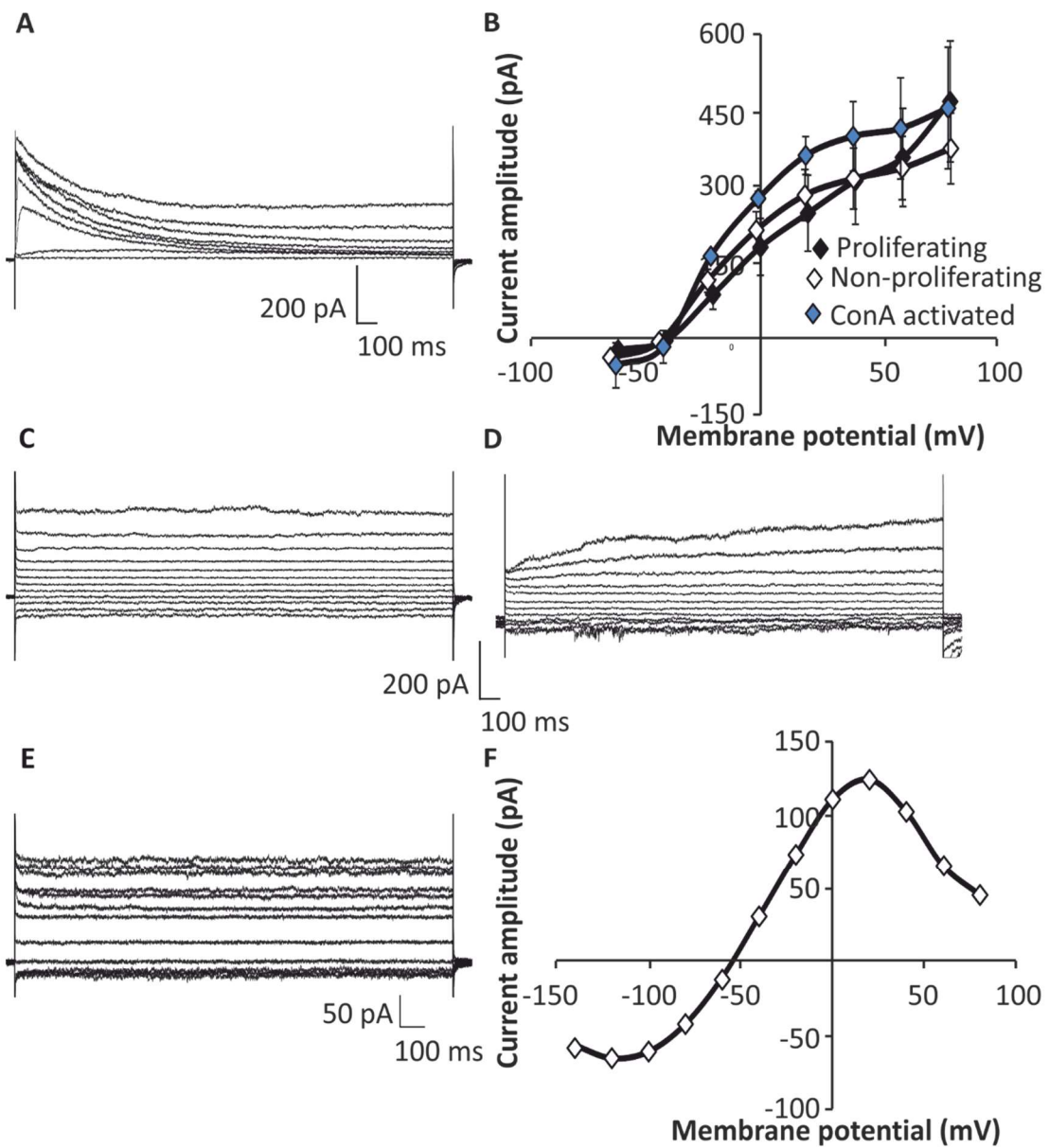
| Current Type | Number of cells (% of total cells in brackets) | | |
|-----------------------------------|---|-----------------------------------|-----------------------------|
| | Non-proliferating Jurkat cells | Proliferating Jurkat cells | ConA Activated cells |
| Instant | 6 (11) | 27 (14) | 13 (33) |
| Fast activating slow inactivating | 45 (83) | 146 (77) | 23 (58) |
| Slow activating | 3 (6) | 17 (9) | 3 (8) |
| Voltage-dependent instant | 0 | 0 | 1 (3) |
| Total number of cells | 54 | 190 | 40 |

Table 4.1

The proportion of current types observed the Jurkat cells that were in a different state.
The proportion of the Jurkat cells exhibiting the different currents types from either 190 Jurkat cells in a proliferative state, 54 Jurkat cells in a non-proliferative state or 40 ConA activated Jurkat cells. The percentage of cells of cells are shown in brackets. The currents types are described by the apparent kinetics. A Chi-Squared test was to compare the expected proportion of current types observed with the actual current types observed.

Figure 4.11

Whole cell currents observed in Jurkat cells in different states. **(A)** Representative current trace of a Jurkat cell in an activated state with a time dependent activating current with slow partial inactivation. **(B)** The average peak current amplitude of the time dependent current with slow partial inactivation in either proliferating Jurkat cells cell in the log phase of growth, non-proliferating Jurkat cells or Con-activated Jurkat cells plotted as a function of the membrane potential. **(C, D)** Representative current trace of a Jurkat in a non-proliferative state exhibiting either instant or a slow activating time dependent current, respectively. **(E)** Representative current trace of a ConA activated Jurkat cell exhibiting a voltage dependent instant current. **(F)** The average peak current amplitude of the currents in (E) plotted as a function of the membrane potential. The Jurkat cells were in a state of inactive proliferation by culturing them in RPMI-1640 medium supplemented with 1% FBS and used at 48 hours. The activated Jurkat cells were activated treating them with 20 µg/ml ConA for 24 hours. The currents in (A) were recorded in response to test potentials between +80 mV and -60 mV with -20 mV steps whilst (C), (D) and (E) were recorded in response to test potentials between +80 mV and -140 mV with -20 mV steps from a holding potential of -80 mV. These currents were recorded in extracellular solution E1 and intracellular solution I1.



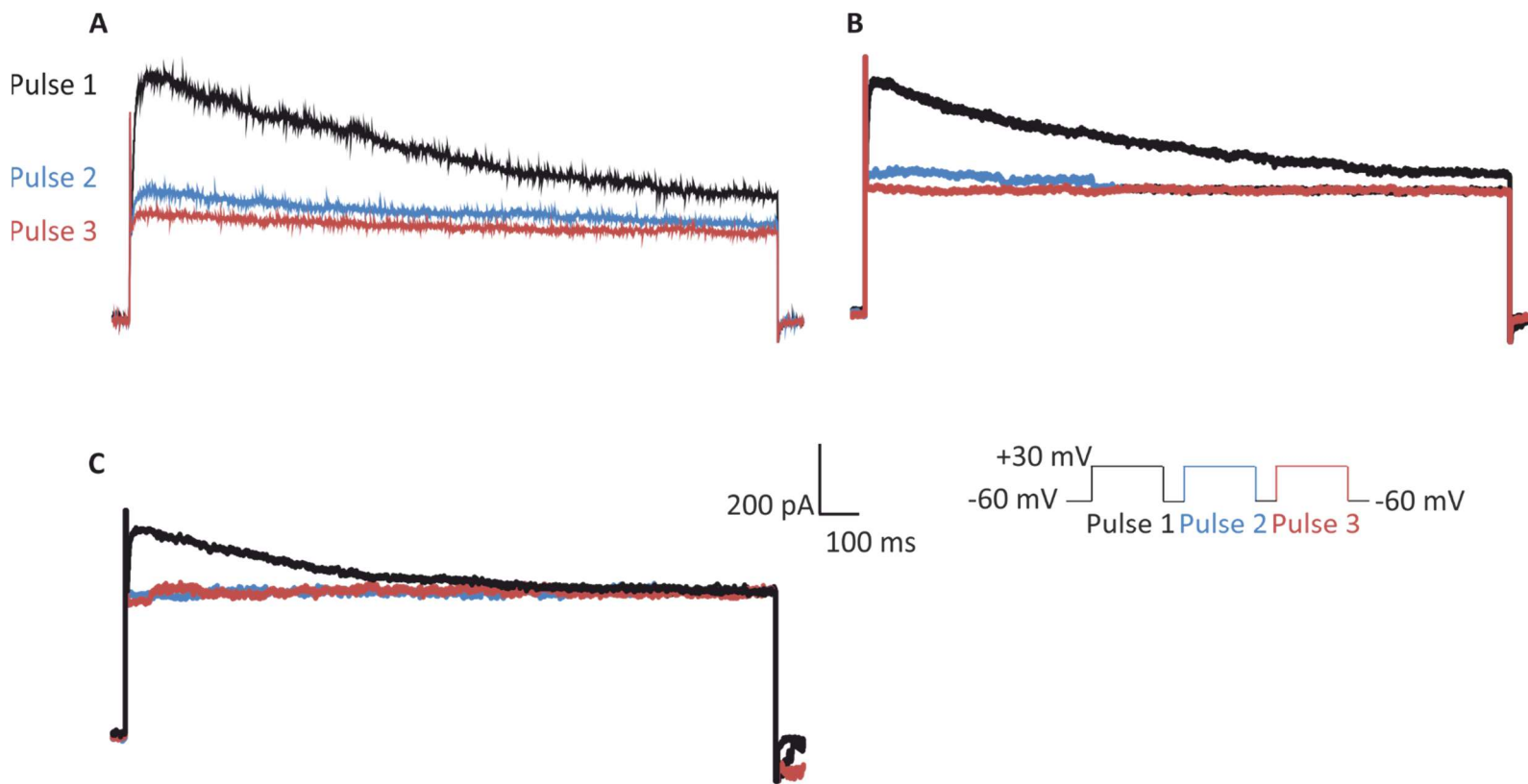


Figure 4.12

Cumulative inactivation of the outwardly rectifying time dependent K^+ current in Jurkat cells. Cumulative inactivation of the K^+ current in (A) Jurkat cells in the log phase of growth, (B) Jurkat cells in a non-proliferative state and (C) Jurkat cells activated with 20 μ g/ml for 24 hours. Current trace in response to repeated stimulations to an activation potential of +30 mV from a holding potential of -80 mV with a 1 second interval between activating pulses. The Jurkat cells were patched with extracellular solution E1 and intracellular solution I1.

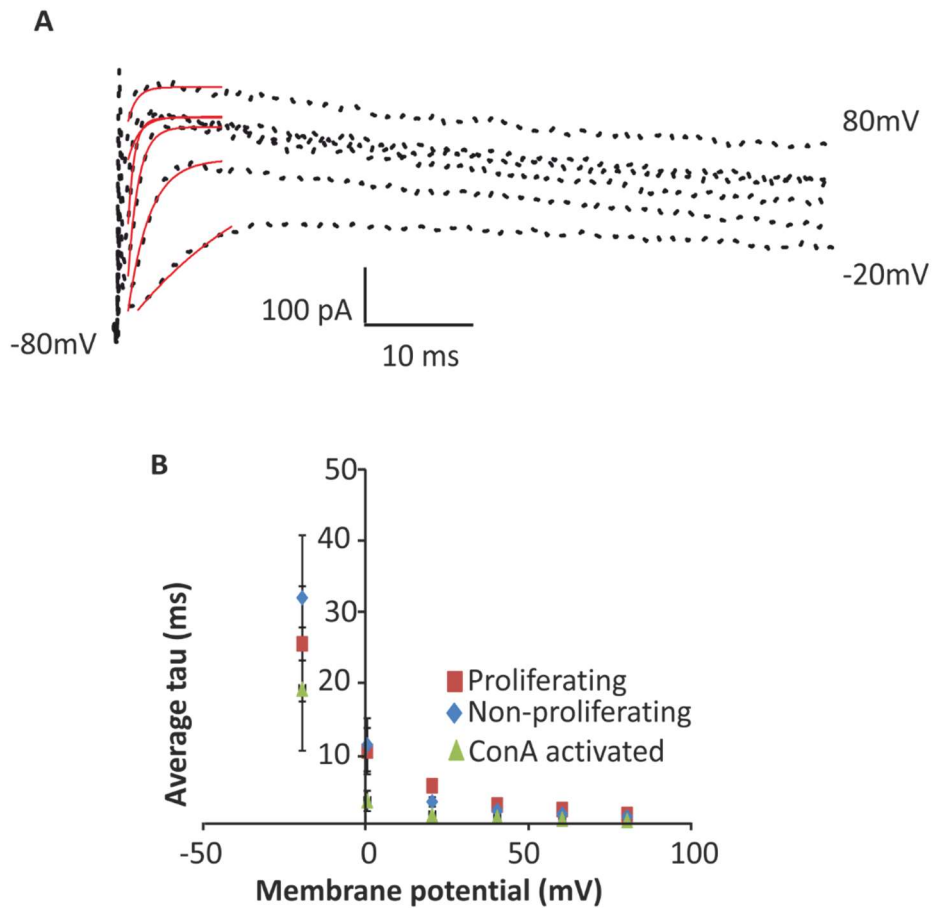


Figure 4.13

Characterising the activation kinetics of Jurkat cells in the different proliferative states.
(A) Representative current trace showing the exponential fit of the activation phase of a ConA-activated Jurkat cell ($i = \sum_{i=1}^n i e^{-\frac{t}{\tau_i}} + C$ where C is the exponent of the activation phase, t is activation time constant. The time constants are plotted as a function of the test potentials on **(B)**. The extracellular solution was E1 whilst the intracellular solution was I1. The data in **(C)** is plotted as the mean \pm SEM with a sample size of a minimum of 4.

The tau of the activation phase of the time dependent

| Holding potential (mV) | Mean τ (ms) | | |
|------------------------|--------------------------------|----------------------------|----------------------|
| | Non-proliferating Jurkat cells | Proliferating Jurkat cells | ConA Activated cells |
| +80 | 1.0 \pm 0.3 | 1.4 \pm 0.2 | 0.5 \pm 0.1 |
| +60 | 1.4 \pm 0.3 | 2.1 \pm 0.4 | 0.7 \pm 0.1 |
| +40 | 1.9 \pm 0.3 | 2.7 \pm 0.4 | 1.0 \pm 0.1 |
| +20 | 3.2 \pm 0.7 | 5.4 \pm 0.9 | 1.3 \pm 0.1 |
| 0 | 11.2 \pm 3.7 | 10.3 \pm 3.3 | 3.3 \pm 1.4 |
| -20 | 32.0 \pm 8.8 | 25.4 \pm 8.1 | 19.1 \pm 8.7 |

Table 4.2

The tau of the activation phase of the time dependent current exhibiting rapid activation and slow inactivation characteristics. This current was observed in Jurkat cells in all three different states. The data is presented as mean \pm SEM with a sample size of a minimum of 4.

In summary, the immediate static membrane potential of the Jurkat cells differed in cells which were in a non-proliferative state in comparison to Jurkat cells in the log phase of growth. The whole cell currents of Jurkat cells in the different states did not express different current types, however, non-proliferating Jurkat cells did express a higher percentage of cells expressing the *N*-type voltage-gated K⁺ channel in comparison to either the Jurkat cells in the log phase of growth or the activated Jurkat cells.

4.3 Discussion

The aim of this chapter was to ascertain the culture conditions required to achieve Jurkat cells in either a non-proliferative or an activated state. The magnitude of the static membrane potential and the whole cell currents of the Jurkat cells in these two states were also investigated and compared to the membrane potential and the whole cell currents of Jurkat cells in the log phase of growth (see Chapter 3).

Obtaining Jurkat cells in either a non-proliferative or an activated state. Investigations on the cell viability of the Jurkat cells using trypan blue and PrestoBlue dyes were undertaken to ascertain the culture conditions required to achieve Jurkat cells in a non-proliferative state wherein the rate of proliferation was reduced with minimal cell death. The proliferation assay using trypan blue suggested that the Jurkat cells stopped proliferating at 48 hours when cultured in RPMI-1640 medium supplemented with 1% FBS as seen by the static rate of the cell numbers between the 48 and 72 hour time point (see Figure 4.1). As such, the Jurkat cells were in a non-proliferative state at 48 hours when cultured with culture medium supplemented with 1% FBS. The rate of proliferation and the cell viability ascertained using the PrestoBlue assay also suggested that the Jurkat cells were in a non-proliferative state at the 48 hour time point in culture medium supplemented with 1% FBS. Unlike the trypan blue assay, the PrestoBlue assay suggested that the Jurkat cells were in a non-proliferative state between 48 and 72 hours despite increasing the concentration of FBS in the culture medium from 1% to 10%. This seems out of line with literature since most laboratories, and even the ATCC suggest using 10% FBS to culture Jurkat cells to a healthy standard (ATCC, 2015).

Differences between the trypan blue and PrestoBlue assay. The trypan blue assay and the PrestoBlue cell viability assay are based on different principles with different advantages and disadvantages. The PrestoBlue assay is based on the resazurin-resorufin dye wherein the resazurin is reduced to resorufin by the mitochondrial activity of the cells which in turn was monitored by fluorescence in the present study (Lall et al., 2013; Niles et al., 2009). On the other hand, the trypan blue requires a manual assessment of the cells to distinguishing between living and dead cells. It is therefore, possible that the cell viability and proliferation obtained using the trypan

blue method yielded results of low precision due to human error as the technique requires labour intensive examination of the cells (Kim et al., 2011). Furthermore, trypan blue exclusion assay has been shown to overestimate the cell viability of the cells in the early stages of cell death and the diminishing nutrients in the culture media after 48 hours could have induced cell death (Ming et al., 2008). Thus, at the time of the cell counts, the Jurkat cells could potentially be in the early to mid-stage of apoptosis (Koopman et al., 1994; Terri Sundquist, 2006). As the trypan blue is an exclusion dye assay, like other vital stains used as viability assays, it is based on the assumption that dead cells have a compromised cell membrane which allows the dye to permeate the membrane (Strober, 2001). Consequently, an intact plasma membrane with concurrent cell death, as is the case of a cell in the initial stages of cell death would exclude the trypan blue dye and thus, the cell would be incorrectly considered as a viable cell (Lee and Shacter, 2007).

Although the PrestoBlue assay provides rapid results of the cell viability and proliferation of cells, it is based on the same principle as the AlamarBlue assay and a high concentration of FBS has been shown to attenuate the fluorescence signal from the resorufin in the AlamarBlue assay (Voytik-Harbin et al., 1998). Both the trypan blue assay and the PrestoBlue assay were used in the present study to ascertain the cell viability and the rate of proliferation to overcome the disadvantages of each assay. Alternatively, Jurkat cell proliferation could have been assayed by measuring either DNA synthesis, ATP concentration or measuring proteins associated with proliferation i.e. Ki-67 (Defries and Mitsuhashi, 1995; Palutke et al., 1987). It is possible that a protocol measuring DNA synthesis would provide a more accurate measurement of proliferation than a metabolic assay such as PrestoBlue as DNA synthesis is directly correlated with proliferation (Madhavan, 2007). Indeed, Quent et al., (2010) found metabolic assays over-estimated cell proliferation in comparison to assays using DNA synthesis.

Obtaining Jurkat cells in a non-proliferative state. The Jurkat cells that were in a non-proliferative state without inducing cell death was achieved through the reduction of nutrients in the culture medium. It was also possible to get Jurkat cells into a non-proliferative state without inducing cell death by using antiproliferative compounds such as ciprofloxacin and SP600125 at concentrations which confers cytostatic

properties to these compounds (Du et al., 2004; Duszynski et al., 2006; Koziel et al., 2010). Although this is an alternative method to achieve Jurkat cells in a non-proliferative state, treatment with antiproliferative compounds exhibiting cytostatic effects could adversely affect important cellular mechanisms such as mitochondrial respiration, ATP synthesis and even intracellular $[Ca^{2+}]$. Indeed, all of these changes have been observed with ciprofloxacin treatment (Koziel et al., 2010). Consequently, the Jurkat cells treated with such antiproliferative compounds could potentially undergo a plethora of intracellular changes such as aberrant intracellular signalling, changes in the cytosolic [ATP] and cytosolic $[Ca^{2+}]$ in and across the cell and thus affect the membrane potential and the underlying ion channel activity of the Jurkat cells. On the other hand, primary lymphocytes which are mostly in a quiescent state could also be used as a model of non-proliferating lymphocytes (Kinet et al., 2002).

Using primary lymphocytes would have also ensured the physiological relevance of the findings from this study. Immortalised cell lines which are derived from primary cells as is the case with Jurkat cells offer several advantages over primary cell lines such as cost effectiveness and ease of culturing the cells, whilst providing a homogenous population of cells. Nevertheless, as T-lymphocytes are in a quiescent state *in vivo*, the findings obtained from Jurkat cells in a non-proliferative state should also be physiologically relevant and produce comparative data.

Electrophysiological characteristics of the Jurkat cells. The mean immediate membrane potential of the population of Jurkat cells which were in a non-proliferative state was significantly different to the mean immediate membrane potential Jurkat cells in the log phase of growth, albeit by only 6 mV. On the other hand, the immediate membrane potential of the Jurkat cells in a non-proliferative state was similar to the immediate membrane potential of the ConA activated Jurkat cells.

The cell viability assay of the Jurkat cells treated with ConA suggested that the Jurkat cells were in a non-proliferative state when treated with ConA and cultured with 10% FBS (see Figure 4.4). A proliferation assay is required to confirm this. Nevertheless, the current types observed in these two populations of Jurkat cells, although similar, were evident in different proportions. The voltage-gated K^+ current was observed in 83% of Jurkat cells which were in a state of non-proliferation whilst this current was

observed in only 58% of ConA activated Jurkat cells. As the membrane potential is determined by the activity of ion channels, the difference in the mean immediate membrane potential between non-proliferating and activated cells could be explained by the difference in the proportion of cells expressing the voltage-gated K⁺ current. The activity of the voltage-gated K⁺ channel would make the membrane of the Jurkat cells more permeable to K⁺. As a result, this increased permeability is expected to influence the membrane potential and push it towards the theoretical E_K which is -75 mV. The membrane potential, however, failed to completely reflect this theoretical E_{K+} probably due to the activity of currents carried by other ions, namely the instantaneous current which was most likely carried by Cl⁻ as was discussed in Chapter 3. The theoretical E_{Cl-} was -3 mV, thus the presence of a Cl⁻ conductance within the whole cell currents would drag the observed E_{rev} of the whole currents between theoretical E_{K+} and theoretical E_{Cl-}.

The characteristics of the ion channels from the activated Jurkat cells have been shown to express various differences in the voltage-gated K⁺ channel such as faster activation kinetics and a more hyperpolarised threshold for the activation of the currents in comparison to non-activated Jurkat cells (Cahalan et al., 1985; DeCoursey et al., 1984). In contrast, the ConA activated Jurkat cells in the present study failed to show a significant difference in the activation voltage in comparison to the Jurkat cells in the log phase of growth or Jurkat cells in a non-proliferative state. This is surprising as a change in the activation kinetics was been observed following the addition of PHA (Cahalan et al., 1985; DeCoursey et al., 1984). It is possible that the change in kinetics upon mitogenic stimulation is specific to the PHA mitogen, thus, differences in the activation kinetics from ConA-activated Jurkat cells was not observed in the current study. Interestingly, the change in the activation kinetics induced by PHA were observed within 30 seconds of the mitogen addition implying that the PHA mitogen induced local changes rather than widespread genetic changes in the voltage-gated K⁺ channel which would be expected to take longer. The increased speed of the activation phase has been postulated to be associated with an increase in the flux of K⁺ as more voltage-gated K⁺ channels would be in a recruitable state at any given time (Tsien et al., 1982).

The cell viability assay showed that both, ConA and PHA mitogens were cytotoxic to the Jurkat cells after 24 hours. The time course for the different stages of apoptosis in these Jurkat cells remains unknown, however, based on the results from the cell viability assays, the Jurkat cells were still viable at 24 hours. Nevertheless, it is possible they were in the early stages of apoptosis at this 24 hour time point. In *Xenopus* oocytes undergoing apoptosis, Englund et al., (2014) found a voltage-gated Na⁺ channel that exhibited dramatic differences in the activation voltage and gating kinetics in comparison to established voltage-gated Na⁺ channels. This could be due to the observed Na⁺ channel being a novel unidentified Na⁺ channel, however, it is likely to reflect channel properties which were altered by the process of apoptosis. Furthermore, changes in ionic homeostasis have also been observed during the early stages of apoptosis (Bortner and Cidlowski, 2004).

Jurkat cell activation. Activation of Lymphocytes *in vivo* is required for clonal expansion to mount an efficient immune response (Nelson, 2004). As discussed in the introduction, the signalling cascade leading to activation involves the secretion of IL-2 which marks a critical point past which activation is no longer dependent on an antigen (Panyi et al., 2004). Consequently, activation in Jurkat cells is manifested and easily measured by the secretion of IL-2. *In vitro* this can be mimicked using activators such as ConA or PHA.

PHA was found to be a more effective inducer of the IL-2 secretion in the present study in comparison to ConA. This is in agreement with Gillis and Watson (Gillis and Watson, 1980). These results are, however, in contrast to the findings of Dupuis and Bastin (Dupuis and Bastin, 1988) who found ConA to be a more effective activator of the Jurkat cells. The difference in the contrasting results could be due to the type of Jurkat cells used. Alternatively, the differences could be associated with the type of PHA used. PHA-L was used in the present study whilst PHA-M was used by Gillis and Watson. PHA-L is the purified form of the PHA lectin and has higher mitogenic activity in comparison to PHA-M owing to the higher affinity for the lymphocyte surface receptors (Movafagh et al., 2011). On the other hand, PHA-M is a crude form of PHA-L and is present in the form of a mucoprotein (Aldrich, 2015). It is also possible that the reduced efficiency of ConA in comparison to PHA was related to the fact that ConA's carbohydrate binding requires Ca²⁺ and manganese (Sigel, 1983).

Mitogenic stimulation using either ConA or PHA did not increase proliferation as was expected, rather, both mitogens were in fact found to be cytotoxic to the Jurkat cells with PHA being more cytotoxic than ConA in the present study. ConA-induced cell death of lymphocytes has been reported, however, this cell death was not investigated in detail in studies showing ConA-induced cytotoxicity. Nevertheless, in these studies, the cell viability upon stimulation with ConA and PHA ranged from 5% to 90% (Dupuis and Bastin, 1988; Gillis and Watson, 1980). The discrepancy of the cytotoxicity could be due to the Jurkat variant used in the experiments. The Jurkat E6.1 cell line was used in the present study whilst the Jurkat FHCRC variant was used by Gillis and Watson and Dupuis and Bastin used the Jurkat 77 variant.

Mitogen induced cell death could be due to a result of the generation of either reactive oxygen species (ROS) upon mitogen stimulation, activation of scramblase or activation induced cell death (Benichou and Leca, 1989; Maher et al., 2002). Increasing evidence suggests ROS play a pivotal role in transduction pathways that mediate apoptosis (Perl et al., 2002). An increase in the intracellular concentration of Ca^{2+} has also been shown to activate phospholipid scramblase 1 which in turn has been shown to increase phosphatidylserine on the surface of the cell. Phosphatidylserine breakdown on the surface of the cell is a hallmark of apoptosis (Zhou et al., 2002).

Activation-induced cell death is a self-inflicted apoptotic process to remove T cells after clonal expansion caused by antigenic stimulation *in vivo*. In essence, the mechanism maintains homeostasis after clonal expansion and is hypothesised to prevent autoimmune diseases (Cohen and Eisenberg, 1991; Krammer et al., 2007). Although activation-induced cell death is an *in vivo* phenomena, it can be mimicked *in vitro* by repeatedly stimulating T cells with a mitogen over a course of a few days separated by washout of the mitogen (Krammer et al., 2007; Lenardo et al., 1999). In the present study, the *in vivo* situation rather than the *in vitro* situation was mimicked as the Jurkat cells were continually stimulated with the mitogen without washout of the mitogen thus, the results are expected to be more physiologically relevant. The Jurkat cells still exhibited a reduction in cell viability which is in stark contrast to *in vitro* induction of activation-induced cell death and suggests that the Jurkat cells have

become more susceptible to activation-induced cell death, if indeed the mitogen induced cell death is activation-induced cell death. The fact that cell death was also observed with both, ConA and PHA stimulation suggests the increased susceptibility was not specific for one particular mitogen.

PHA was a more potent cytotoxic agent to the Jurkat cells in the present study in comparison to ConA. Furthermore, unlike ConA, PHA failed to show a dose dependent response in cytotoxicity. There is some disagreement whether PHA is a more potent mitogen than ConA based on IL-2 secretion, however, PHA treatment caused significantly more IL-2 secretion than ConA in the present study. It is possible that the increased cytotoxicity was due to the elevated concentrations of IL-2 secreted in response to treatment with PHA as IL-2 has been shown to enhance mitogen-induced cell death although there is some disagreement on this (Nguyen and Russell, 2001). Nevertheless, this provides further support for the hypothesis that the mitogen-induced cytotoxicity of the Jurkat cells was due to activation-induced cell death.

It was surprising to find that several studies which investigated IL-2 secretion induced by mitogens failed to investigate the cytotoxic effects of the mitogens in detail (Dupuis and Bastin, 1988; Gillis and Watson, 1980). An increased concentration of FBS provided a protective effect of ConA induced cell death in a concentration dependent manner. The protective effects of FBS was most obvious at 10%. Surprisingly, FBS did not protect against cell death elicited by PHA stimulation, possibly due to the increased cytotoxic potency of PHA. It would have been interesting to see the effects of FBS on concentrations of PHA less than 1 µg/ml or shorter incubation times. Taken together, these results suggest that FBS confers a protective effect against mitogen induced cell death whilst IL-2 could contribute to the mitogen-induced cell death. In fact, the role of IL-2 in increasing susceptibility of T-lymphocytes to mitogen-induced cell death has been previously debated (Lenardo, 1991; Pender, 1999).

The membrane potential and mitogen induced activation. The role of the membrane potential in mitogen induced activation was investigated by increasing the extracellular ionic concentration of either K⁺, Na⁺ or Cl⁻. This perturbation was expected to modulate the membrane potential of the Jurkat cells during incubation

secretion precedes activation and clonal expansion. Indeed, the membrane potential has been implicated to initiate proliferation in post-mitotic cells (Cone and Cone, 1976; Stillwel et al., 1973). Electrophysiological characterisation of the static membrane potential and the underlying ion channels in Jurkat cells which were in a non-proliferative state and Jurkat cells which were either in the log phase of growth or activated by the ConA mitogen had significantly different static membrane potentials. In the next chapter, the dynamic membrane potential of the Jurkat cells will be investigated in the time frequency domain using the continuous wavelet transform technique.

5 ANALYSIS OF THE MEMBRANE POTENTIAL DYNAMICS OF JURKAT CELLS USING THE CONTINUOUS WAVELET TRANSFORM

5.1 Introduction

The membrane potential of cells is often reported in terms of its static potential i.e. the membrane potential value at a single time point. The physiological relevance of this static membrane potential has traditionally been associated with excitable cells in the generation of action potentials and spiking behaviour (Fontaine et al., 2014; Hodgkin and Huxley, 1952; Miura, 2002). Mounting experimental evidence, however, suggests that the membrane potential plays a functional role in regulating various aspects of cell behaviours such as proliferation, differentiation and migration (Blackiston et al., 2009; Sundelacruz et al., 2009). The precise mechanisms involved in membrane potential regulated cell behaviours are ill understood but various mechanisms such as the actual change in the static membrane potential, change in the ionic concentrations

and the osmolarity have been implicated (see Chapter 1). The effect of the dynamic membrane potential i.e. the membrane potential over a longer continuous time period has been completely overlooked in relation to cell behaviours.

In support for studying membrane potential dynamics, rhythmic fluctuations have been observed in single cells through to complex multi-cellular organisms. For example, in humans, several different types of oscillations have been observed such as circadian rhythms, the heartbeat and ultradian rhythms. In the context of these fluctuations in the membrane potential, single cells often display oscillating behaviour in the membrane potential. For example, the membrane potential of mammary gland cells, fibroblasts and kidney cells were found to be oscillating after treatment with EGF (Enomoto et al., 1986; Pandiella et al., 1989). These oscillations had a large amplitude which made them easily detectable by eye, however, it is possible that smaller amplitude oscillations which are less apparent are also present in the membrane potential. The membrane potential dynamics were investigated using the continuous wavelet transform (CWT) technique. The CWT technique is an established analytical technique used to investigate the dynamic nature of a time-series. Application of the CWT technique may uncover further dynamical behaviour of the membrane potential that is potentially associated with cell behaviours or responses.

Aims of the chapter

The CWT technique was developed to investigate a time-series in the frequency domain, however, to the best our knowledge it has not been applied to investigate the dynamic behaviour, specifically oscillations in the membrane potential of mammalian cells across a time-series recorded for more than a few minutes (Huizinga et al., 2014).

In this chapter the dynamic nature of the membrane potential of Jurkat cells is investigated using the CWT technique. To gain insights in to the nature of the membrane potential dynamics, the concentrations of extracellular K^+ , Cl^- or Na^+ was varied which was also expected to alter the membrane potential of the Jurkat cells. In addition, the effect of the presence of intracellular Ca^{2+} on the membrane potential dynamics were also investigated. Finally, the membrane potential dynamics of Jurkat

cells in either the log phase of proliferation, a non-proliferative state or a ConA-activated state (described in Chapter 4) are also investigated.

5.2 Results

5.2.1 Investigating the application of the wavelet transform technique – can the technique discriminate between physiological and non-physiological electrical signals?

The patch clamping recordings were conducted in a Faraday cage to isolate electrical noise, however, some membrane potential recordings still exhibited obvious electrical interference which manifested as large spikes in these recordings. These large spikes produced artefacts in the CWT analysis, consequently, a regime to remove this obvious artificial noise during the analysis stage was implemented (described in Chapter 2). Besides the obvious noise, it was possible that less obvious electrical noise originating from the patch clamping hardware was also present in the membrane potential recordings. Consequently, to ensure the CWT technique could accurately discriminate between membrane potential dynamics of a physiological origin and noise arising from the patch clamping hardware (described simply as noise hereon in) within the time-series recording, CWT analysis was applied to the membrane potential recorded from Jurkat cells and electrical signals generated from a dummy cell was used to replicate the whole cell scenario. The dummy cell is a model cell with an in-built circuit to create a complete circuit and replicate the resistance of either the whole cell or the cell attached scenario.

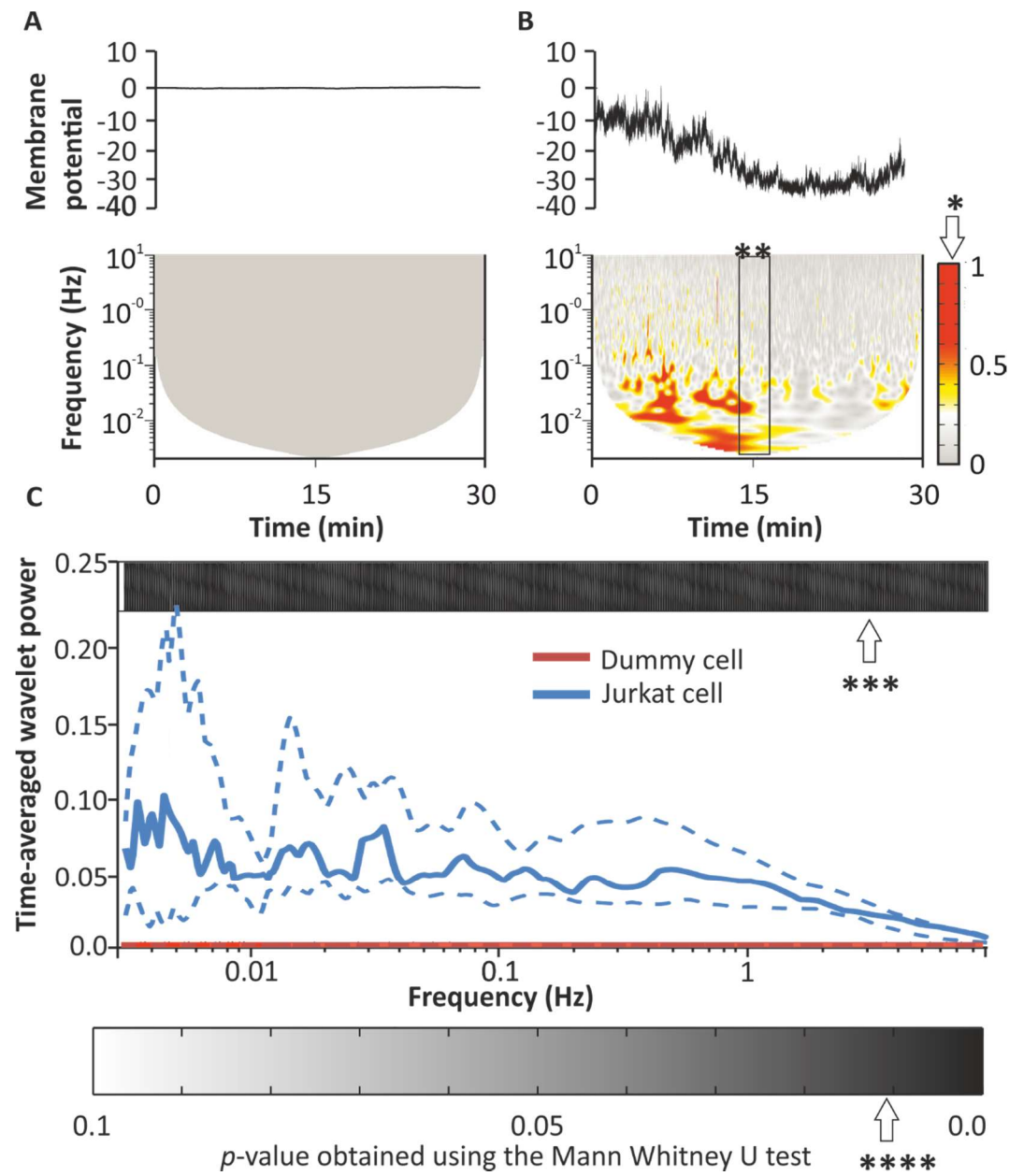
The wavelet transforms of the membrane potential recordings from the Jurkat cells and the electrical signal from the dummy cell showed significant ($p<0.05$) differences in the wavelet power across all the frequency intervals investigated (Figure 5.1). Figure 5.1A shows that the CWT technique failed to show fluctuations for the time-series recorded from the dummy cells at frequencies spanning approximately 0.1 and 5 Hz. On the other hand, CWT analysis of the Jurkat cells showed fluctuations and these fluctuations appear to be deterministic rather than stochastic (Figure 5.1B). The frequency interval of these fluctuations was approximately 0.1 and 5 Hz. The wavelet transform of the membrane potential signal also provides evidence of nonstationary dynamics in the membrane potential of the cells which is evident by the time-dependent frequency distributions within the membrane potential signal (Nason, 2006). The time-averaged wavelet power (Figure 5.1C) confirmed that the power of the fluctuations within the membrane potential of the Jurkat cells was significantly

larger than the fluctuations of the background noise by several orders of magnitude across all of the frequency intervals tested ($p<0.05$).

The variation in the time-averaged wavelet power (Figure 5.1C with the 25th and 75th quartiles) of the nine membrane potential recordings from the Jurkat cells was significantly larger than the variation from the recordings using the dummy cells. Taken together, these findings suggest that the CWT technique can be used to investigate dynamics of a physiological origin without contamination of non-physiological dynamics.

Figure 5.1

Continuous wavelet transform of the membrane potential of Jurkat cells and electrical signals from dummy cells. Representative membrane potential as seen in the time domain from either **(A)** electrical signal from a dummy cell or **(B)** Jurkat cell. The wavelet transforms seen in the time-frequency domain are shown directly below the membrane potential recordings and the colour key to the wavelet power is shown on the far right (highlighted by an *). The wavelet power shows the magnitude of the oscillations and it translates to the change in the maximum and minimum membrane potential values during one oscillatory cycle. The frequency of the oscillatory cycle is shown on the Y axis of the wavelet transform whilst the X axis corresponds to the time at which the oscillation occurred within the membrane potential recording. For example, the membrane potential recording on A has no oscillations and as such the wavelet transform shows no oscillatory activity. On the other hand, the membrane potential recording on B has oscillatory activity occurring throughout the recording. To highlight this, at the 15 minute mark of recording B (shown by **) there are several different oscillations which have frequencies ranging from 0.001 to 10 Hz. **(C)** The median wavelet power from the time-frequency domain plotted as a function of the frequency from the membrane potential signal from either nine Jurkat cells (solid blue line) or 18 different electrical signals from a dummy cell (solid red line). The dashed lines represent the 25th and 75th quartiles. The level of statistical significance difference between the median time-averaged wavelet power of the Jurkat cells and the electrical signal is shown using the greyscale bar as shown by ***. The greyscale bar represents the level of difference in the statistical significance of the time-averaged wavelet power at that particular frequency. In the case of this figure, the areas of the bar that are black show that the difference between the oscillations between the two groups at those frequencies has a *p* value close to 0.0. A Mann Whitney U test was used to test for the significance level and the key for the *p*-value is shown at the bottom of (C) and is highlighted in the figure with ****.



5.2.2 Longitudinal analysis of the membrane potential recording from Jurkat cells in the frequency domain (using histograms)

In order to investigate the nature of the dynamics (fluctuations and oscillations) of the membrane potential, these membrane potential recordings were investigated in the frequency domain using the mean and standard deviation across the entire time-series. The membrane potential was recorded at a sampling frequency of 20 KHz which equates to measuring the membrane potential every 50 μ s. This measurement at each 50 μ s interval was plotted on a frequency histogram. The standard deviation across the membrane potential time-series provides preliminary information on the variability of the membrane potential whilst the frequency histogram represents the distribution of the membrane potential across the time-series measured.

To understand the nature of the membrane potential dynamics recorded from the Jurkat cells, the membrane potential was recorded in standard extracellular solution (SES) and extracellular solution with changes in the ionic concentration of either K^+ , Cl^- or Na^+ (described as CES followed by either K^+ , Cl^- or Na^+ depending on the ion changed, thus a change in the extracellular concentration is denoted as CES $_K$). These ions were changed as they are the major ion species setting the membrane potential and represent the dominant ions used in the intracellular and extracellular solutions. Furthermore, Chapter 3 showed that the Cl^- and K^+ set the membrane potential of the Jurkat cells used in the present study. Thus, it was envisaged that the membrane potential should also change in response to changes in the extracellular of either $[K^+]$ or $[Cl^-]$.

In experiments wherein the concentration of extracellular K^+ was altered, K^+ was increased from 6 mM to 60 mM in the CES by the addition of 54 mM K gluconate. The concentration of Cl^- was reduced from 162 mM to 12 mM in experiments altering the concentration of Cl^- by substituting the concentration of extracellular KCl and NaCl with equimolar concentrations of K gluconate and Na gluconate, respectively. In experiments investigating Na^+ , the extracellular concentration of Na^+ was reduced from 150 mM to 10 mM by replacing 140 mM NaCl with 140 mM choline Cl.

5.2.3 Investigating the effect of ionic changes on the static resting membrane potential

The Jurkat cells were grouped based on the response of the resting membrane potential to the extracellular (CES) perturbations in the concentration of either K⁺, Cl⁻ or Na⁺ (Figure 5.2). The membrane potentials of cells which were responsive to a change in extracellular K⁺ were grouped into cohort 1 whilst cells that were responsive to a change in Cl⁻ were grouped into cohort 2. Cells which had a membrane potential that were sensitive to a change in the extracellular concentration of Na⁺ were grouped into cohort 3. The average membrane potential over a ten minute time period was considered as the static membrane potential.

The effect of ionic changes on the membrane potential time-series

The membrane potential time-series were investigated by analysing the mean, standard deviation and the distribution of the entire time-series. Recall that the sampling frequency of the membrane potential was 20 KHz, however, the membrane potential time-series was (down)sampled during the analysis to 20 Hz (which is equivalent to a sampling interval of 50 ms). Therefore, in a 10 minute recording of the membrane potential, the membrane potential was measured 12000 times. The mean ± SEM and the mean of the standard deviations ± SEM of these 12000 measurements of the membrane potential time-series was calculated for each membrane potential recording present in each of the three cohorts. The data are presented as means and are described simply as either mean membrane potential or mean standard deviation. Similarly, the frequency distribution of the entire membrane potential time-series (the mean and the standard deviation of the entire time-series) was also investigated. The standard deviations of the membrane potential recording provides an insight into the membrane potential dynamics whereby the power of the fluctuations is proportional to the standard deviation of the entire time-series. The histograms also provide an insight into the distribution of the membrane potential which is seen by the spread of the histogram.

Figure 5.3A shows the mean membrane potential of the Jurkat cells belonging to cohort 1. In SES, this mean membrane potential was -28.6 ± 6 mV and significantly depolarised to -8.7 ± 2 mV in CES_k (n=8) ($p<0.005$). Concurrently, the mean standard deviation of the membrane potential time-series also changed from 2.1 ± 1 in SES to

0.59 ± 1 in CES_k ($p<0.005$) (Figure 5.3B). In agreement, the frequency histograms of the membrane potential recordings from the Jurkat cells belonging to cohort 1 also showed that the membrane potential became depolarised i.e. less negative in response to increasing the extracellular concentration of K⁺ from 6 mM to 60 mM. This change in the membrane potential is evident by the shift in the red coloured histogram on Figure 5.3D. The magnitude of this change varied between cells (from the same cohort) but the largest change was observed in the cells expressing the most negative membrane potential in the SES. Likewise, the smallest change in the membrane potential within the same cohort in response to increasing the extracellular concentration of K⁺ was observed in a cell which had a membrane potential that was the least negative i.e. closest to 0 mV. Similar to the findings of the mean standard deviation, there was a concomitant decrease in the spread of the histogram with an increase in the extracellular concentration of K⁺. Upon the change from SES to CES_k, the frequency histogram of the membrane potential from the different cells in cohort 1 also changed roughly from a bell shaped curve to a sharp peak. Taken together, these results suggest that there was a decrease in the membrane potential dynamics of the Jurkat cells upon increasing the concentration of extracellular K⁺.

The mean resting membrane potential of the Jurkat cells from cohort 2 depolarised from -4.1 ± 2 mV in SES to 16 ± 6 mV in CES_{Cl} ($p<0.05$) whilst the standard deviation increased significantly from 1.0 ± 1 in SES to 1.7 ± 1 in CES_{Cl} ($p<0.05$) (Figure 5.3A). The histograms of the membrane potential recordings from the cells in this cohort shifted to more positive potentials in response changing from CES to CES_{Cl} (Figure 5.3B). This was expected as the theoretical E_{Cl}- shifted to more positive potentials upon a reduction in the extracellular [Cl⁻]. In this cohort of cells, the difference in the shape and spread of the frequency histogram of the membrane potential was difficult to ascertain by eye (Figure 5.3E).

Jurkat cells from cohort 3 had a mean membrane potential of -7.2 ± 3 mV in SES which was not significantly different from the mean membrane potential of cells belonging to cohort 2 (Figure 5.3A). Upon a reduction in the extracellular [Na⁺] i.e. CES_{Na}, the mean membrane potential hyperpolarised to -14 ± 5 mV, however, this change was not statistically significant. Nevertheless, the mean standard deviation of the membrane potential from the cells in cohort 3 decreased significantly from 2.0 ± 1

in SES to 0.8 ± 1 in CES_{Na} ($p < 0.0005$) (Figure 5.3B). The frequency histograms of the membrane potential recordings of cells in cohort 3 showed that the membrane potential of the cells shifted to more negative potentials upon reducing extracellular [Na⁺], however, it was difficult to ascertain the difference between the spread of the histograms in SES and CES_{Na} (Figure 5.3F).

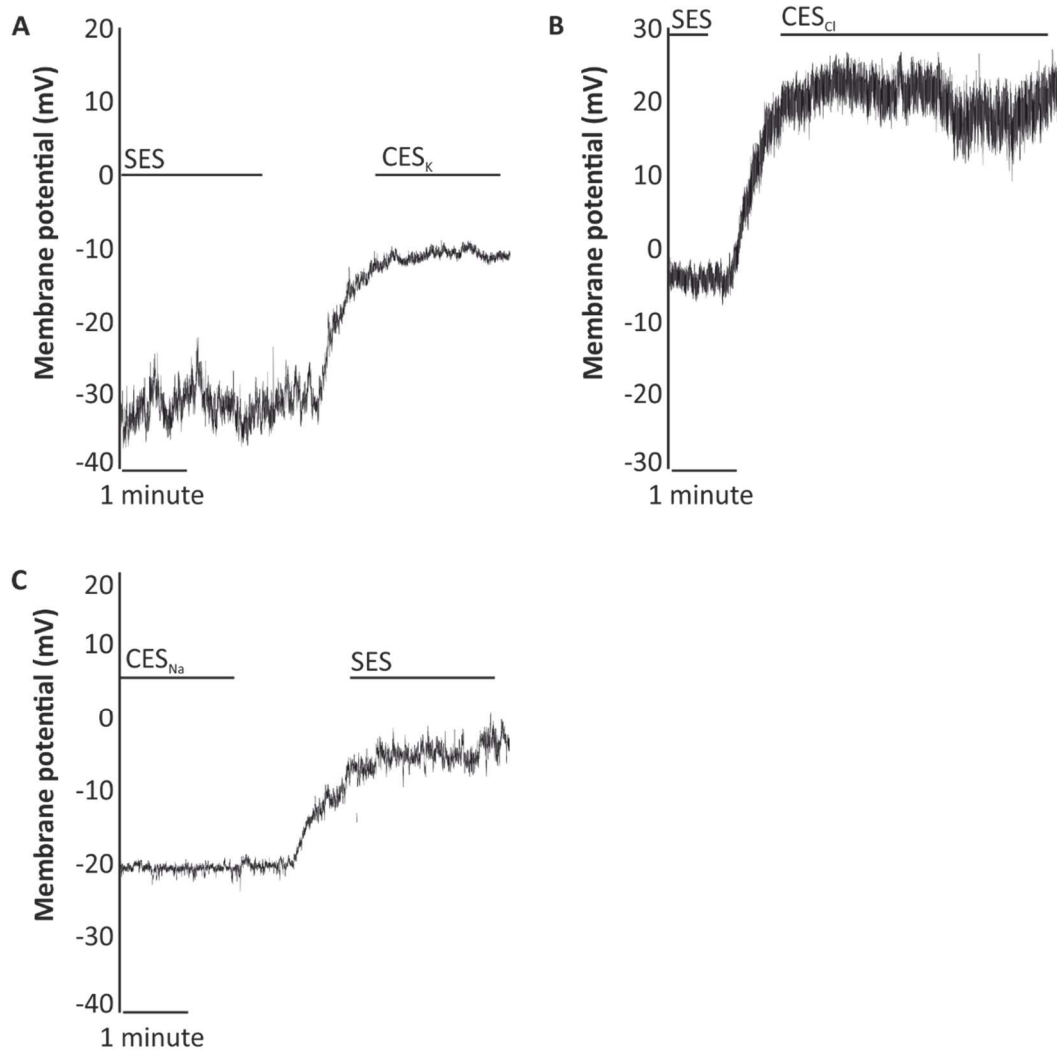
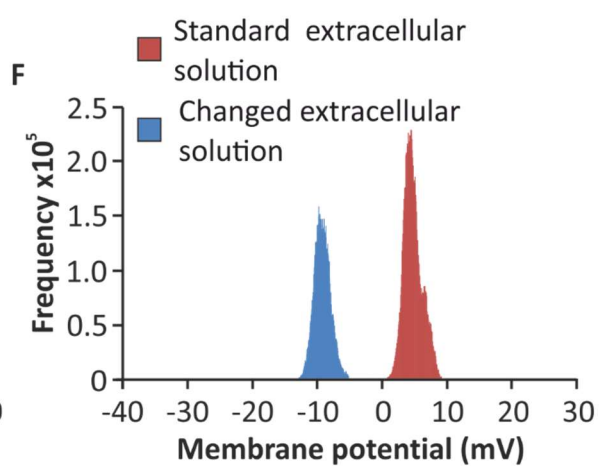
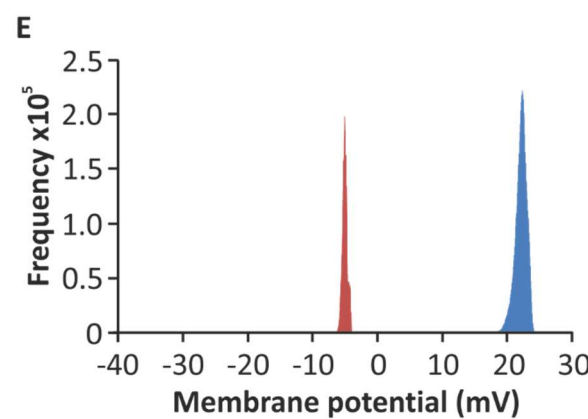
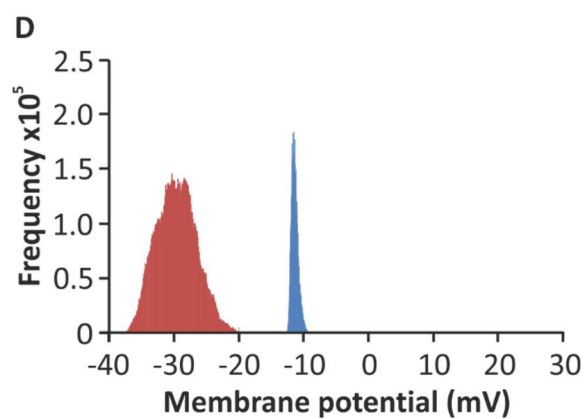
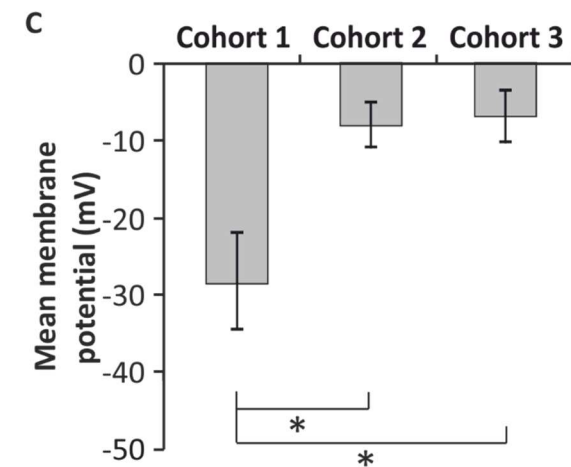
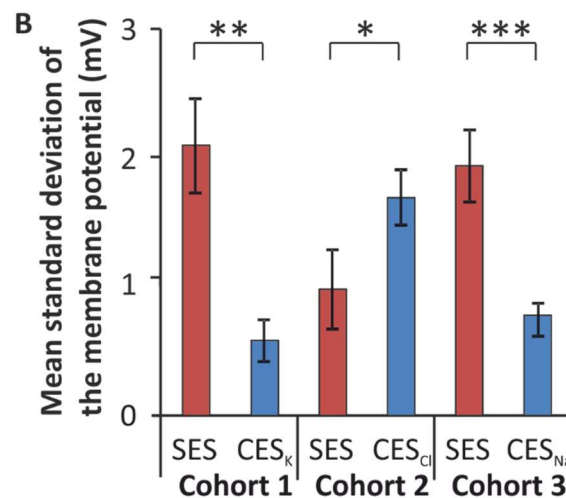
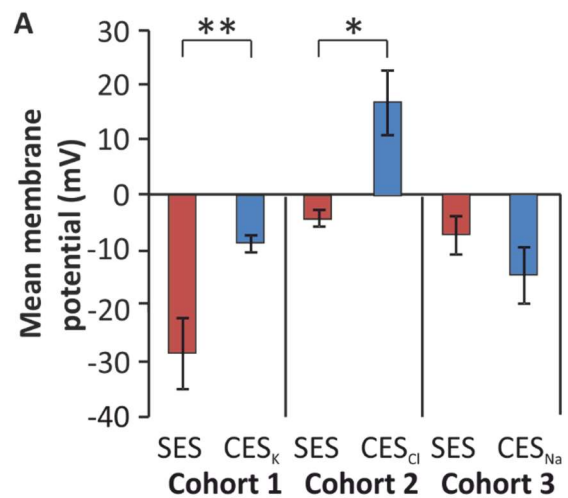


Figure 5.2

The effect of the membrane potential of Jurkat cells in extracellular solution containing different ionic concentrations. Representative membrane potential recordings from different Jurkat cells with either (A) standard extracellular solution (SES) containing 6 mM K⁺ or elevated extracellular K⁺ solution (CES_K) which contained 60 mM K⁺, (B) standard extracellular solution (SES) containing 162 mM Cl⁻ or low extracellular Cl⁻ solution (CES_{Cl}) which contained 12 mM Cl⁻ or (C) low extracellular Na⁺ solution (CES_{Na}) containing 150 mM Na⁺ or standard extracellular solution (SES) which contained 10 mM Na⁺. The membrane potentials recorded in SES were recorded in solution E1 whilst the intracellular solution was solution I1. The changed extracellular solution CES_K was E1K whilst CES_{Cl} was E1Cl or CES_{Na} was E1Na.

Figure 5.3

Investigating the membrane potential in the frequency domain. Bar chart showing **(A)** mean and **(B)** standard deviation of the membrane potential from the cells belonging to either cohort 1, cohort 2 or cohort 3 in either standard extracellular solution (SES) or changed extracellular solution (CES). The bar chart in **(C)** shows the mean membrane potential of cells belonging to either cohort 1, cohort 2 or cohort 3 in standard extracellular solution. Representative frequency histogram of the membrane potential recording from a single cell belonging to either **(D)** cohort 1, **(E)** cohort 2 or **(F)** cohort 3 in either SES (red histograms) or CES (blue histograms). The bar chart in **(A)** is plotted as the mean \pm SEM of the mean of the entire membrane potential recording from each cell in the respective cohort. Similarly, the bar chart in **(B)** is plotted as the mean standard deviation \pm SEM of the mean of the standard deviation from each membrane potential recording in the respective cohorts. The statistical significance of the mean membrane potential and mean standard deviation within each cohort was ascertained using the paired Student's T-test and a level of significance with a $p<0.05$ between the SES and CES is highlighted with *, whilst a level of $p<0.005$ is highlighted with ** and the significance level of $p<0.0005$ is highlighted with ***. The sample size was a minimum of 7.



In summary, the mean membrane potential of the Jurkat cells belonging to either cohort 1, cohort 2 or cohort 3 was sensitive to changes in the extracellular concentration of either K^+ , Cl^- or Na^+ , respectively. The standard deviations and the frequency histogram of the membrane potential time-series also suggest changes in the dynamics of the membrane potential (induced through changes in the extracellular concentration of either K^+ , Cl^- or Na^+). These findings suggest the necessity of further investigations of the membrane potential signal in the time-frequency domain using the CWT technique.

5.2.4 Investigating the membrane potential of Jurkat cells in the time-frequency domain using the continuous wavelet transform

The results from the investigation of the membrane potential time-series suggest that the dynamics of the cell membrane potential change in response to changes in the concentration of extracellular ions. Consequently, CWT was applied to the membrane potential time-series to investigate the dynamics of the cells in the three cohorts. This also allowed for the application of the CWT technique to the analysis of the membrane potential dynamics technique to be appraised.

Comparing the membrane potential dynamics of the Jurkat cells from different cohorts. The wavelet transforms of the membrane potential recorded in SES showed that fluctuations were present at frequency intervals between approximately 0.01 to 10 Hz in all three cohorts (Figure 5.4). The membrane potential of cells from cohort 1 and cohort 2 recorded in SES showed significant differences in the static membrane potential (see Figure 5.3C) and the properties of the membrane potential dynamics (Figure 5.4A). The differences the membrane potentials point to differences in the active membrane transport proteins. CWT analysis of the membrane potential also showed a significant decrease in the time-averaged wavelet power of the fluctuations across all frequency intervals investigated ($p<0.05$) of cells from cohort 1 and cohort 2 (Figure 5.4A). The simplest explanation of the data is that this reflects differences in the activity of membrane transport proteins.

To ascertain if the differences in the time-averaged wavelet power of the fluctuations are due to the actual membrane potential itself or the activity of the underlying membrane transport proteins, the membrane potential dynamics of cells from cohort 2 and cohort 3 was investigated. The mean membrane potential of the Jurkat cells from cohort 2 and cohort 3 were not significantly different (Figure 5.3C) yet there was significant difference in the power of the fluctuations at the frequency intervals tested ($p<0.05$) (Figure 5.4C). These results suggest that the membrane potential dynamics of the Jurkat cells are likely to be associated with distinct ion channels, pumps or carriers. Furthermore, a comparison of the time-averaged wavelet power of the cells belonging to cohort 1 and cohort 3 did not show significant differences in the membrane potential dynamics (Figure 5.4B) despite significant differences in the

mean membrane potential of the Jurkat cells from these two cohorts (Figure 5.3C) ($p<0.05$).

Comparing the membrane potential dynamics of Jurkat cells from cohort 1 in varying concentrations of extracellular K⁺. The membrane potential of Jurkat cells from cohort 1 was recorded in SES and in CES_K and the membrane potential dynamics was investigated using CWT. The time-averaged wavelet power of the membrane potential of cells recorded in SES showed an increase in the median power of the fluctuations with approximately 0.01 Hz and ranged between approximately 0.1 and 1 Hz (Figure 5.5). The fluctuations with these frequencies appear to be blocked in response to increasing the concentration of extracellular K⁺ ($p<0.05$). In fact, elevated extracellular K⁺ blocked fluctuations at all the frequencies investigated and this can be seen by eye in the membrane potential recording.

Comparing the membrane potential dynamics of Jurkat cells from cohort 2 in varying concentrations of extracellular Cl⁻. The membrane potential dynamics of the cells from cohort 2 showed significantly different dynamics in comparison to cells from cohort 1 and the time-average wavelet power across all the frequencies investigated was very small in comparison to the wavelet power of cells from cohort 1. Nevertheless, Figure 5.6 shows that the time-averaged wavelet power of the membrane potential recordings of Jurkat cells from cohort 2 did not cause a change a change in the time-averaged wavelet power of the fluctuations upon the reduction of extracellular Cl⁻ ($p<0.05$). A large spread in the power of the fluctuations, however, was observed in individual membrane potentials as seen by the large spread between the 25th and 75th quartiles.

Comparing the membrane potential dynamics of Jurkat cells from cohort 3 in varying concentrations of extracellular Na⁺. The membrane potential dynamics of the cells from cohort 3 recorded in SES showed that the fluctuations and dynamics were similar to cells from cohort 1 recorded in SES. Furthermore, similar to the effect observed on the membrane potential dynamics in cells from cohort 1 with elevating extracellular K⁺, a reduction in the concentration of Na⁺ also caused a significant reduction ($p<0.05$) in the time-average wavelet power of the fluctuations. This decrease was observed at ~ 0.01 Hz and between ~ 0.1 and 1 Hz frequencies (Figure

5.7). Unlike CES_K, the reduction of Na⁺ did not completely block the fluctuations at these frequencies.

Figure 5.4

A comparison of the membrane potential dynamics recorded from Jurkat cells from three different cohorts. The median (solid lines) time-averaged wavelet power across the frequency intervals 0.01 and 10 Hz calculated from cells belonging to either **(A)** cohort 1 or cohort 2, **(B)** cohort 1 or cohort 3 or **(C)** cohort 2 or cohort 3 together with the 25th and 75th quartiles shown as dashed lines. The Mann Whitney U test was used to ascertain differences between the membrane potential dynamics of the cells from different cohorts at the specific frequency. The bar (greyscale) above the time-averaged plots represents the *p*-value obtained from this Mann Whitney U test. The number of samples was a minimum of 6 for each cohort. The Mann Whitney U test was used to test for level of significance and is shown by the bar on **(A)**, **(B)** and **(C)**.

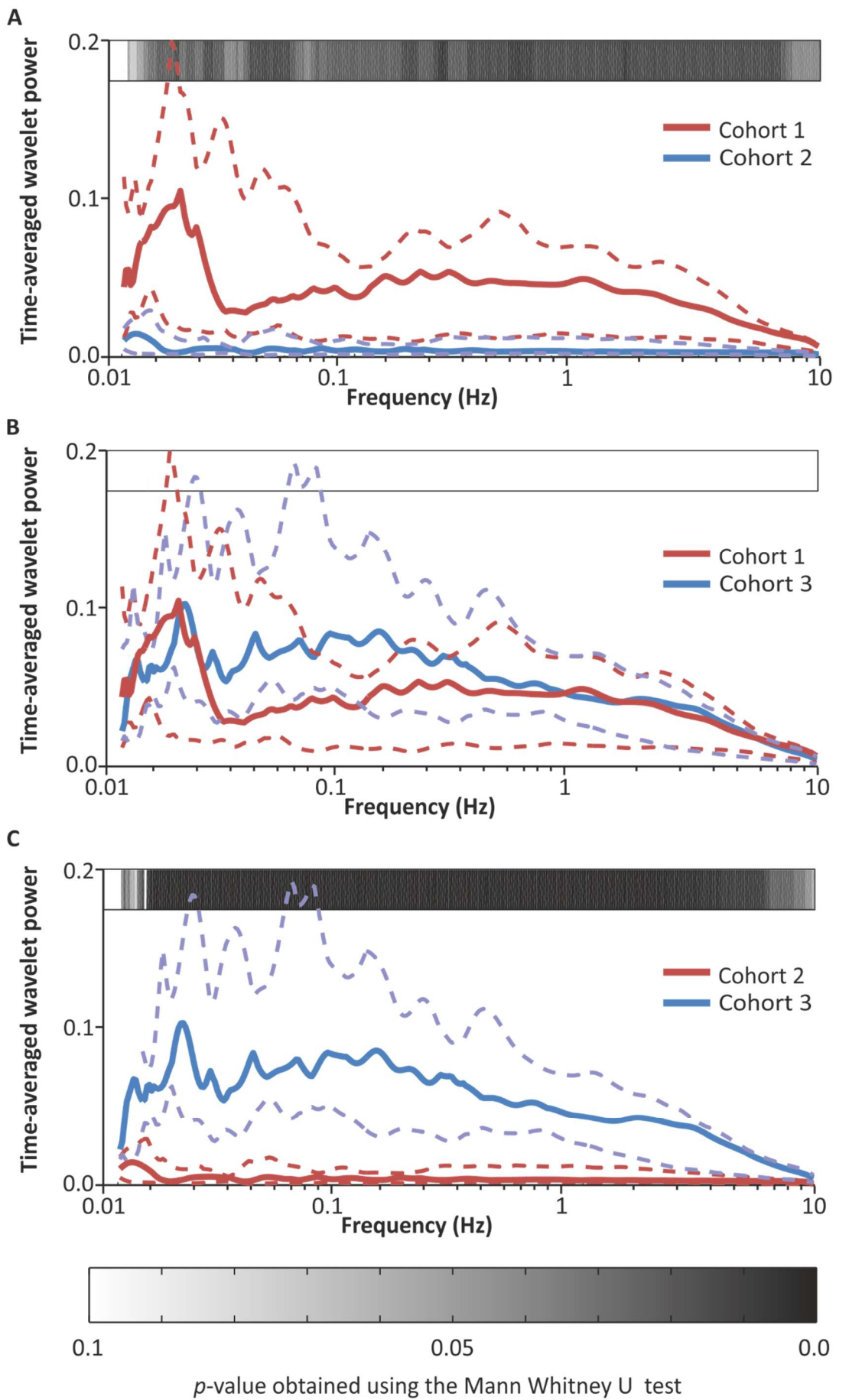


Figure 5.5

A comparison of the membrane potential dynamics of Jurkat cells from cohort 1 recorded in varying concentrations of extracellular K⁺. Representative membrane potential recordings as seen in the time domain from Jurkat cells in either **(A)** standard extracellular solution containing either 6 mM K⁺ or **(B)** changed extracellular solution containing 60 mM K⁺. The wavelet transform of the representative membrane potential time-series is shown directly below the membrane potential recording. **(C)** The median time-averaged wavelet power across the frequency intervals between 0.01 to 10 Hz of the membrane potential from all the cells in either **(A)** or **(B)**. The Mann Whitney U test was used to ascertain the degree of statistical difference between the membrane potential dynamics recorded in either standard extracellular solution (SES) or reduced extracellular K⁺ solution (CES_K) at the specific frequency. The bar (greyscale) above the time-averaged plot represents the *p*-value obtained from this Mann Whitney U test. The dashed lines represent the 25th and 75th quartiles. The number of recordings was a minimum of 7 for each cohort.

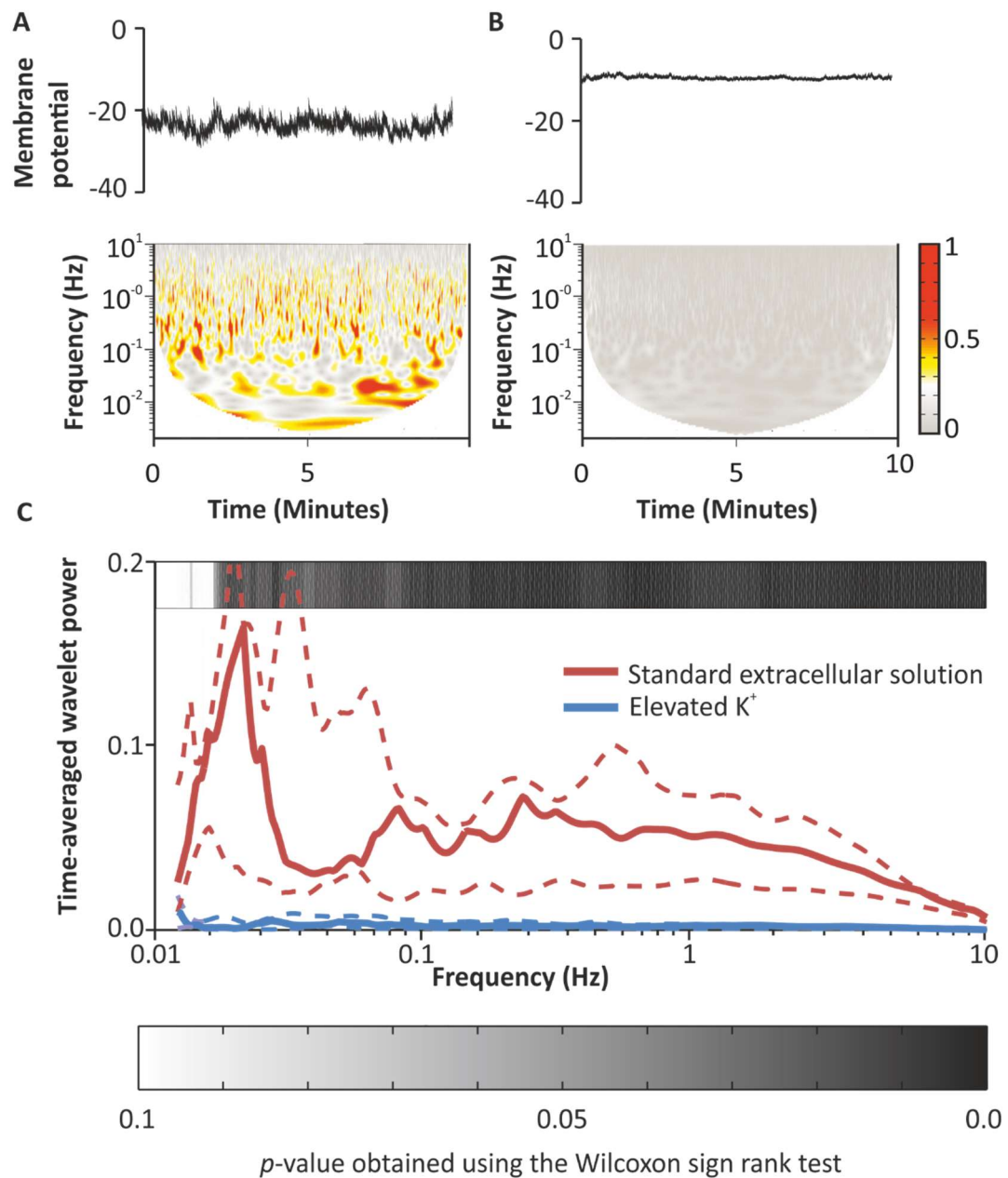


Figure 5.6

A comparison of the membrane potential dynamics of Jurkat cells belonging to cohort 2 recorded in varying concentrations of extracellular Cl⁻. Representative membrane potential recording as seen in the time domain from Jurkat cells in either (A) standard extracellular solution containing 162 mM Cl⁻ or (B) changed extracellular solution containing 12 mM Cl⁻. The wavelet transform of the representative membrane potential time-series is shown directly below the membrane potential recording. (C) The median time-averaged wavelet power across the frequency intervals between 0.01 to 10 Hz of the membrane potential from all the cells in either (A) or (B). The Mann Whitney U test was used to ascertain the degree of statistical difference between the membrane potential dynamics recorded in either standard extracellular solution (SES) or reduced extracellular Cl⁻ solution (CES_{cl}) at the specific frequency. The bar (greyscale) above the time-averaged plot represents the *p*-value obtained from this Mann Whitney U test. The dashed lines represent the 25th and 75th quartiles. The number of recordings was a minimum of 7 for each cohort.

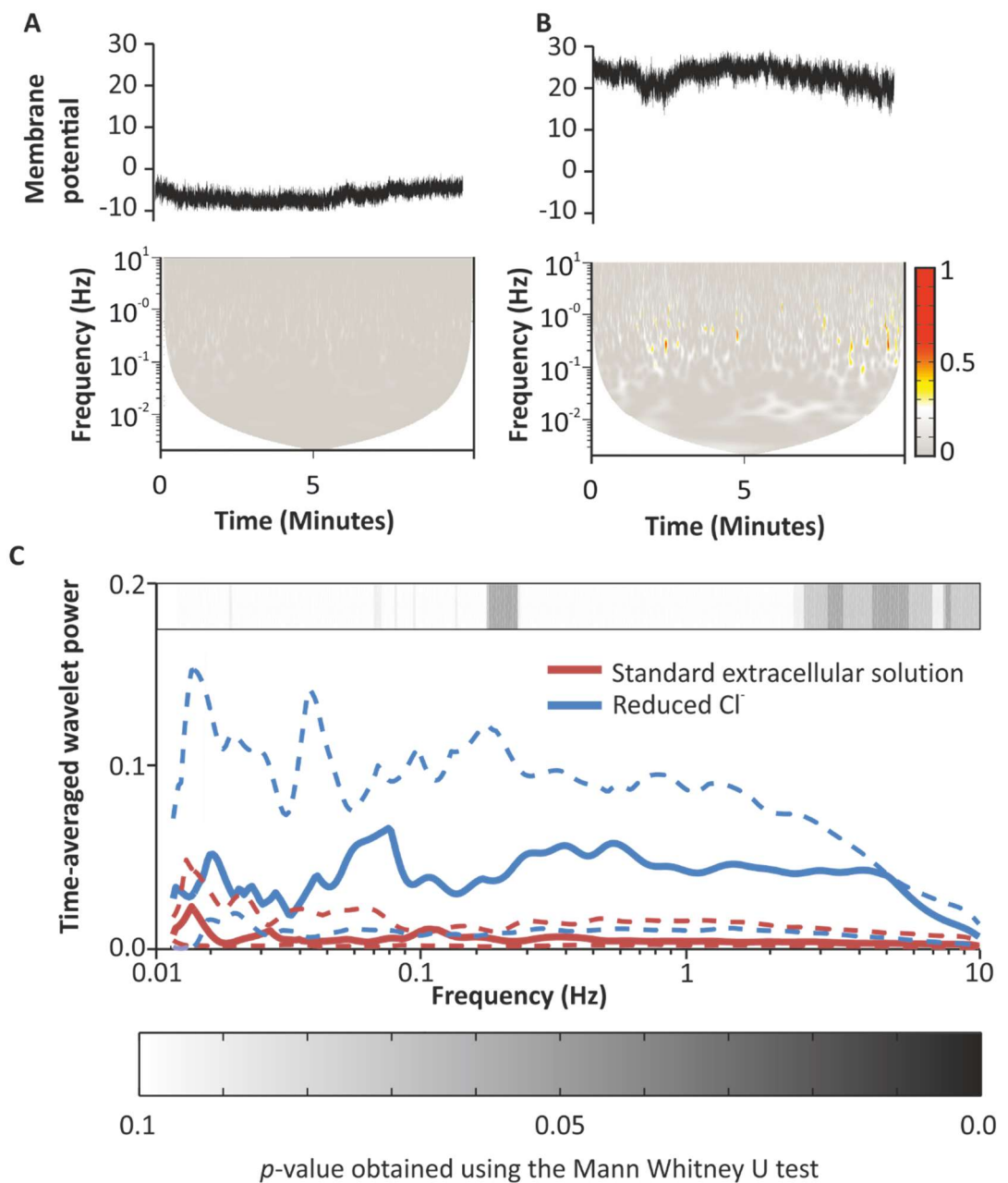
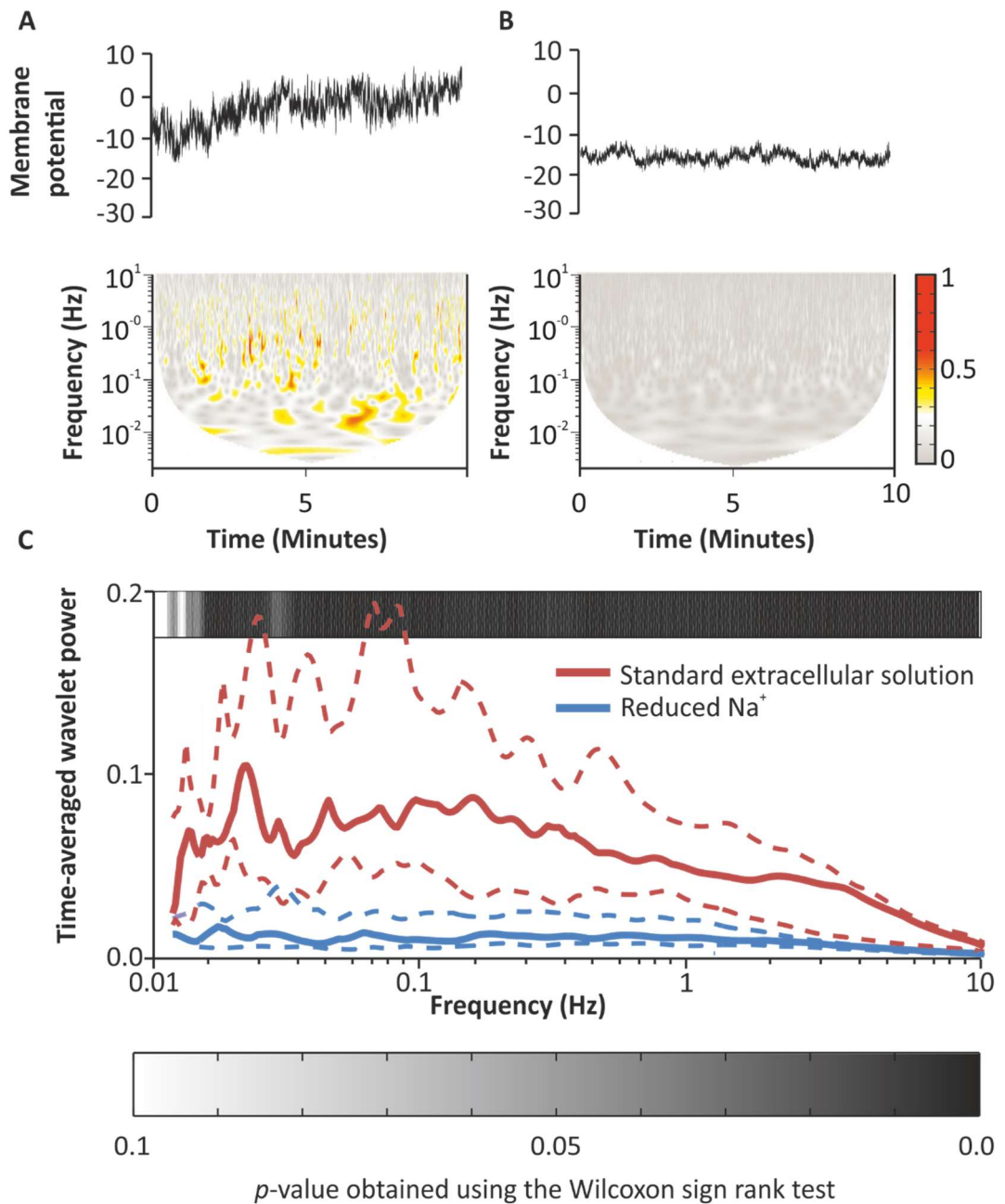


Figure 5.7

A comparison of the membrane potential dynamics of Jurkat cells from cohort 3 recorded in varying concentrations of extracellular Na^+ . Representative membrane potential recording as seen in the time domain from Jurkat cells in either (A) standard extracellular solution containing either 150 mM Na^+ or (B) changed extracellular solution containing 10 mM Na^+ . The wavelet transform of the representative membrane potential time-series is shown directly below the membrane potential recording. (C) The median time-averaged wavelet power across the frequency intervals between 0.01 to 10 Hz of the membrane potential from all the cells in either (A) or (B). The Mann Whitney U test was used to ascertain the degree of statistical difference between the membrane potential dynamics recorded in either standard extracellular solution (SES) or reduced extracellular Na^+ solution (CES_{Na}) at the specific frequency. The bar (greyscale) above the time-averaged plot represents the p -value obtained from this Mann Whitney U test. The dashed lines represent the 25th and 75th quartiles. The number of recordings was a minimum of 8 for each cohort.



In summary, analysis of the membrane potential of Jurkat cells using the CWT technique identified the presence of fluctuations and these fluctuations were affected by changes in the extracellular ion concentrations. Changes in the extracellular concentration of either K^+ , Cl^- or Na^+ have different effects on the membrane potential dynamics. The membrane potential dynamics were significantly altered in response to changes in the extracellular $[K^+]$ suggesting an important role of K^+ channel in the membrane potential dynamics. Consequently, as the voltage-gated K^+ channel was observed in the Jurkat cells (Chapter 3), the effect of this channel on the membrane potential dynamics was investigated. The effect of Cl^- channels on the membrane potential dynamics could not be investigated due to the rundown of Cl^- channel activity (see Figure 3.14) observed in the Jurkat cells. The effects of Na^+ channels on the membrane potential dynamics could not be investigated either as specific Na^+ channels were not observed in the Jurkat cells used. The effect of intracellular Ca^{2+} on the membrane potential dynamics was also investigated.

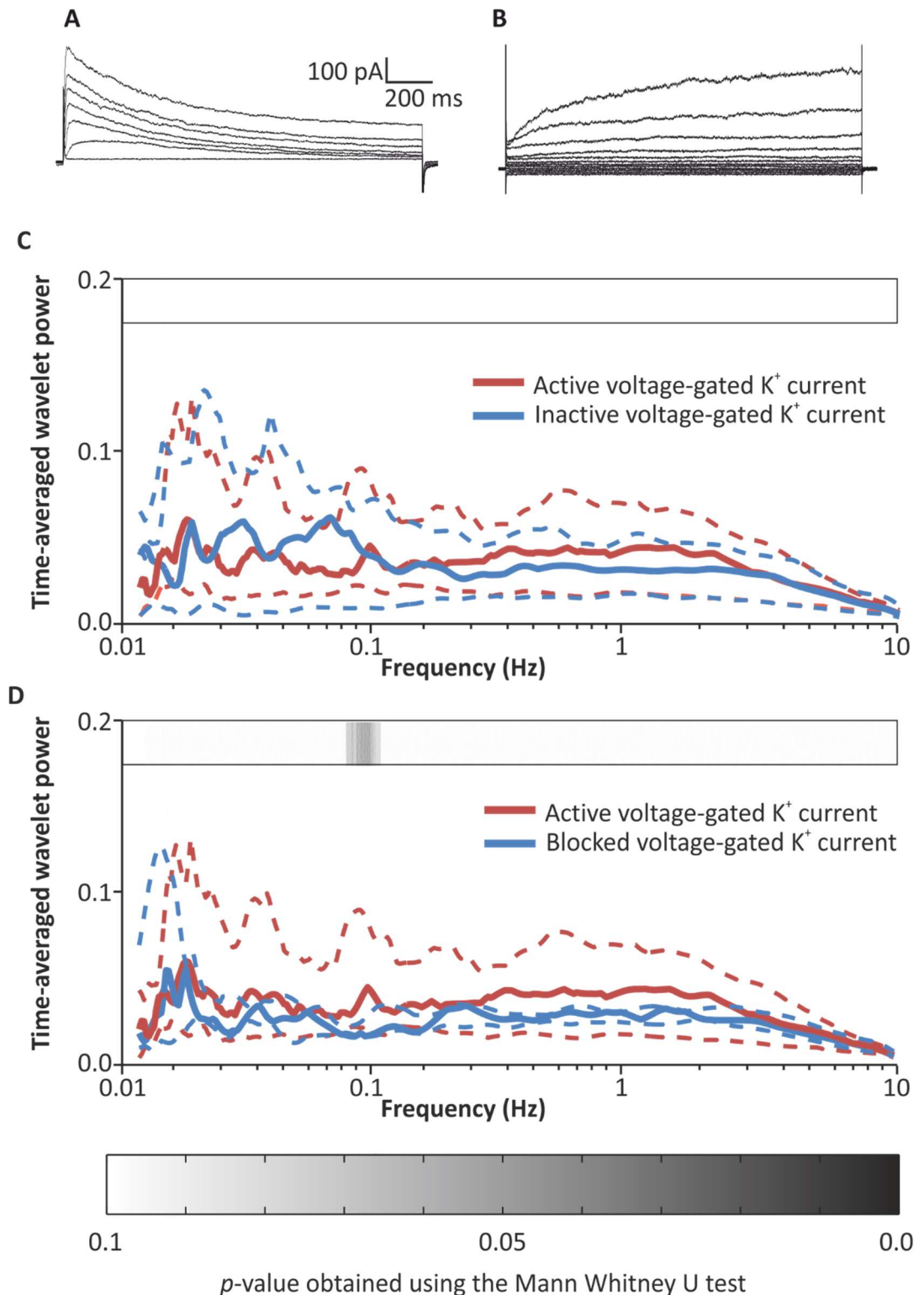
5.2.5 Investigating the role of voltage-gated K⁺ channels on the membrane potential dynamics of Jurkat cells

Voltage-gated K⁺ channels have been identified in the Jurkat cells used in the present study (see Chapter 3), therefore, the possibility that the activity of these channels could be contributing to the observed membrane potential dynamics was investigated. As the activity of ion channels determines the membrane potential, it is also possible that the activity of these channels could be the origin of the observed fluctuations in the membrane potential dynamics. Consequently, the membrane potential of Jurkat cells with the active voltage-gated K⁺ current was compared to the membrane potential recordings of Jurkat cells that lacked activity of this channel. In addition, the membrane potential dynamics of Jurkat cells with the active voltage-gated K⁺ channel was compared to the with cells wherein this K⁺ channel was blocked using 4-AP.

The membrane potential dynamics did not show significant differences between Jurkat cells with an active voltage-gated K⁺ channel and cells which did not have an active voltage-gated K⁺ channel (Figure 5.8). A slight decrease, however, was observed in the median time-averaged wavelet power in the cells which did not show activity of this voltage-gated K⁺ channel. To confirm if the voltage-gated K⁺ channels were not involved in the observable membrane potential dynamics, the K⁺ channels were blocked with 1 mM 4-AP. This concentration of 4-AP completely blocked the voltage-gated K⁺ currents (Figure 3.11). In the presence of 1 mM 4-AP, the membrane potential dynamics failed to show significant differences in comparison to the membrane potential recorded in the absence of 4-AP (Figure 5.8D). Notwithstanding, there was a slight decrease in the median time-averaged wavelet power at most of the frequency intervals investigated, albeit this was not statistically significant. These results suggest that the voltage-gated K⁺ channel do not play a major role in the observed membrane potential dynamics of the Jurkat cells.

Figure 5.8

The influence of the activity of voltage-gated K⁺ channels on the membrane potential dynamics of Jurkat cells. Representative whole cell currents from a Jurkat cell with **(A)** voltage-gated K⁺ current and **(B)** a cell without the voltage-gated K⁺ current. The median time- averaged wavelet power as a function of the frequency from either **(C)** 27 Jurkat cells showing the voltage-gated K⁺ current and 12 cells without the activity of the voltage-gated K⁺ current in the voltage clamp mode or **(D)** 27 Jurkat cells expressing the voltage-gated K⁺ current and 8 different Jurkat cells wherein the voltage-gated K⁺ current was blocked by 1 mM 4-AP. The whole cell currents were induced using test potentials between 80 mV to -20 mV in -20 mV intervals with 30 seconds between each test pulse. The dark red line in (C) and (D) represents the median wavelet power of Jurkat cells with activity of the voltage-gated K⁺ current whilst the dashed lines represent the 25th and 75th quartiles. The dark blue line in (C) represents the median wavelet power of Jurkat cells without activity of the voltage-gated K⁺ current whilst in (D) it represents the blocked voltage-gated K⁺ channel. The dashed lines represent the 25th and 75th quartiles. The Mann Whitney U test was used to ascertain the degree of statistical difference between the membrane potential dynamics recorded in the different conditions at the specific frequency. The bar (greyscale) above the time-averaged plots in (C) and (D) represents the *p*-value obtained from this Mann Whitney U test.



5.2.6 Investigating the influence of intracellular Ca^{2+} on the static membrane potential

Oscillations in intracellular $[\text{Ca}^{2+}]$ have been observed in a number of different cell types and these oscillations cause oscillations in the membrane potential through the activation of Ca^{2+} -activated ion channels (Akagi et al., 1999; Berridge et al., 2003). Therefore, the effects of intracellular Ca^{2+} was investigated on the membrane potential dynamics of the Jurkat cells from the three cohorts recorded in SES and either CES_K, CES_{Cl} or CES_{Na} (as described earlier). Recall, these three cohorts were identified in the previous section of this thesis and the Jurkat cells were grouped according to the response of the membrane potential to changes in the extracellular concentration of either K^+ , Na^+ or Cl^- . Increasing the free intracellular $[\text{Ca}^{2+}]$ from nominally free to 1 μM did not significantly change the static resting membrane potential of cells belonging to either cohort 1 or cohort 2 in SES (Figure 5.9A).

5.2.7 Investigating the effect of intracellular Ca²⁺ on the membrane potential of Jurkat cells in the time domain

As the presence of intracellular Ca²⁺ can affect the membrane potential by modulating the activity of ion carriers, it is possible that the intracellular Ca²⁺ could alter the membrane potential dynamics. Indeed, oscillations in the intracellular concentration of Ca²⁺ have been reported in a wide number of cell types (Akagi et al., 1999; Dolmetsch et al., 1998; Dupont et al., 2011). As such, preliminary investigations on the membrane potential dynamics was undertaken in the presence of intracellular Ca²⁺. The membrane potential dynamics in these investigations were ascertained by the standard deviation of the entire membrane potential time-series recorded in either SES or CES.

Analysis of the standard deviation can highlight differences related to the dynamics of the time-series. The results showed that the membrane potential recorded with an elevated intracellular [Ca²⁺] failed to significantly affect the standard deviation of the membrane potential of Jurkat cells from either cohort 1 or cohort 2, though there was evidence of some differences (see Figure 5.9B).

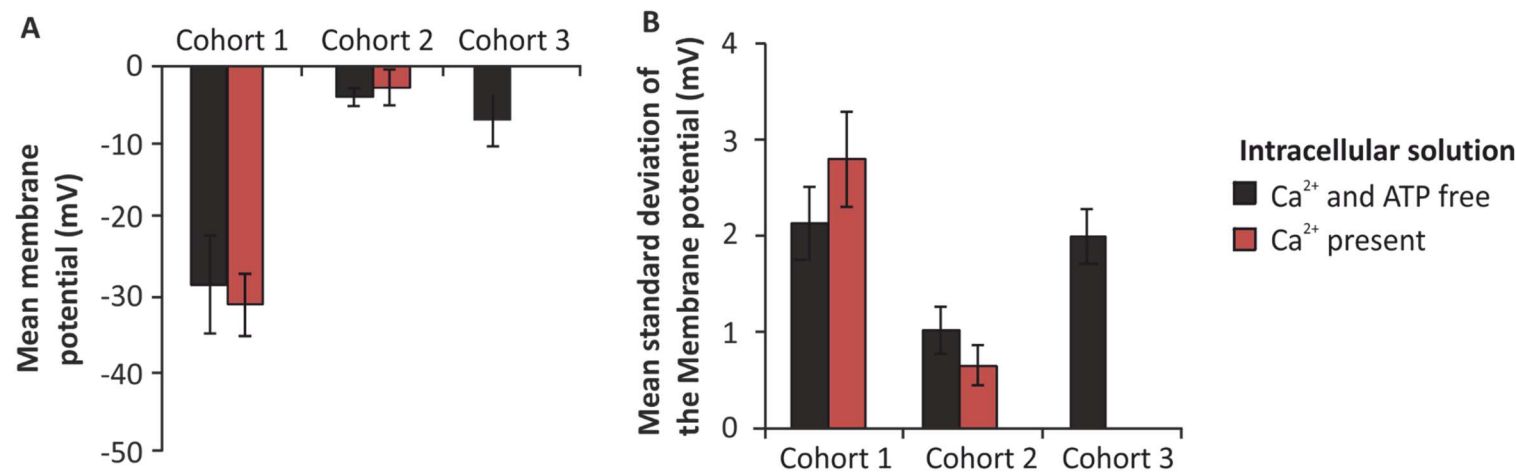


Figure 5.9

Investigating the membrane potential in the frequency domain. Bar chart showing (A) mean and (B) standard deviation of the membrane potential from the cells belonging to the three different cohorts patched with presence or absence of intracellular Ca^{2+} . The bar charts in (A) is plotted as the mean \pm SEM of the mean. The bar chart in (B) is plotted as the standard deviation of the time-series from all the cells in the three cohorts. The statistical significance of the mean membrane potential and mean standard deviation within each cohort was ascertained using the paired Student's T-test. The sample size was a minimum of 6.

5.2.8 Investigating the effect of intracellular Ca^{2+} on the membrane potential of Jurkat cells in the time-frequency domain using the continuous wavelet transform

Analysis of the standard deviation of the membrane potential from the Jurkat cells suggested that the presence of intracellular Ca^{2+} could affect the membrane potential dynamics. To investigate this further, CWT analysis was applied to the membrane potential of Jurkat cells recorded in the presence of intracellular Ca^{2+} .

The results of the CWT analysis of the membrane potential of cells belonging to cohort 1 did not show differences in the membrane potential dynamics in the presence of the elevated intracellular Ca^{2+} in comparison to membrane potential recordings in nominally free Ca^{2+} (Figure 5.10A). Despite non-significant differences in the median time-averaged wavelet power in the presence of 1 μM intracellular Ca^{2+} , there was an increase in the spread of the time-averaged wavelet power between the individual recordings (as seen by the 25th and 75th quartiles in Figure 5.10). This suggests that intracellular Ca^{2+} could have altered the membrane potential dynamics of some Jurkat cells but not others. As such more samples are required to confirm if Ca^{2+} could have affected the membrane potential dynamics of the Jurkat cells. The large deviation was most obvious on the 75th quartile which showed increased power of the fluctuations with frequency intervals spanning approximately 0.024 to approximately 3 Hz.

Increasing the intracellular $[\text{Ca}^{2+}]$ failed to significantly alter the membrane potential dynamics of the cells from cohort 2 (Figure 5.10B). Unlike the results from cohort 1, the elevated concentration of intracellular Ca^{2+} failed to affect the spread of the time-averaged wavelet power between the individual recordings. On the contrary, in the presence of 1 μM intracellular Ca^{2+} , the spread between the recordings decreased in comparison to the spread of the wavelet power observed in nominally free Ca^{2+} .

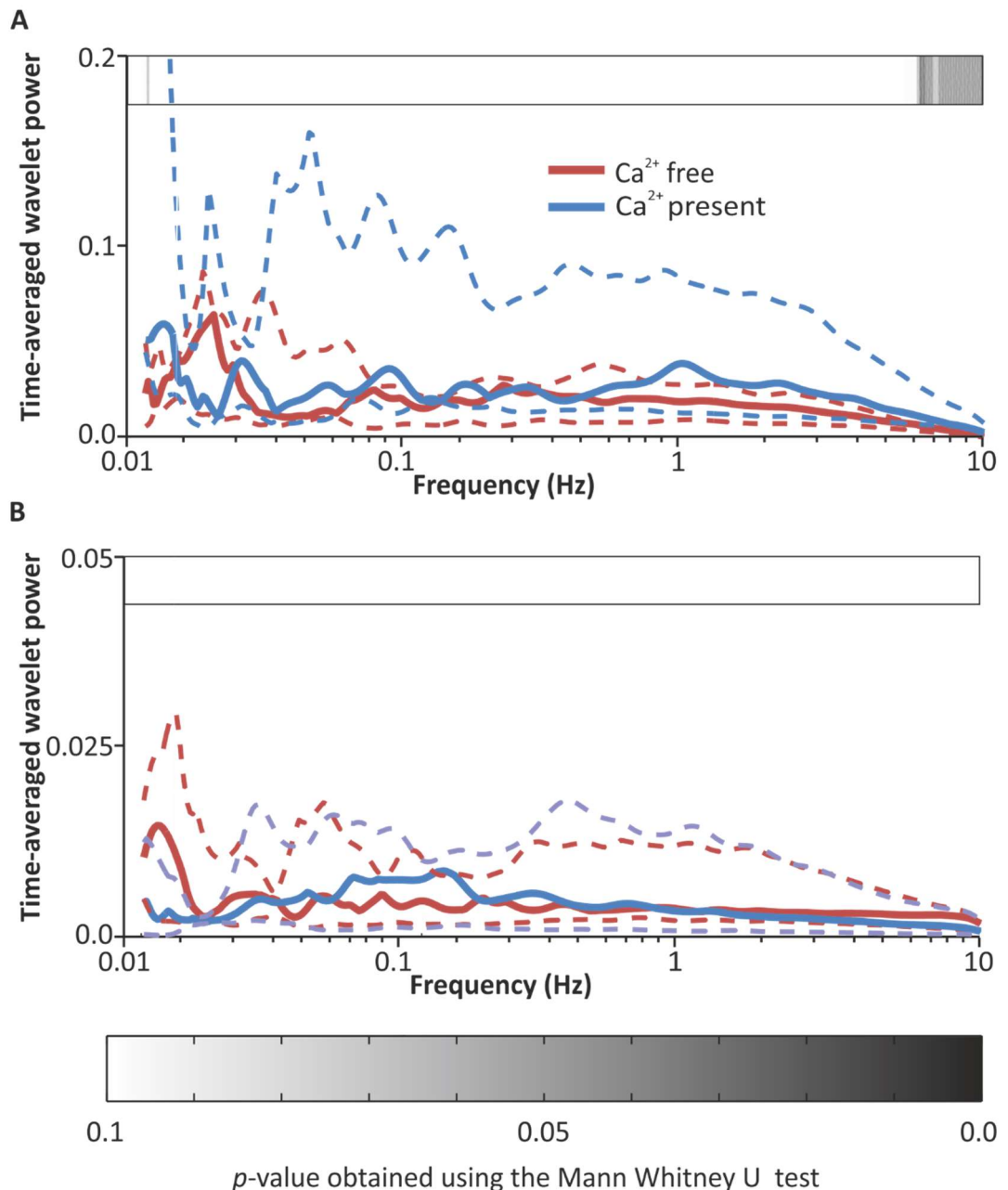


Figure 5.10

The influence of intracellular Ca²⁺ on the membrane potential dynamics of Jurkat cells. The median time-averaged wavelet power as a function of frequency of Jurkat cells patched in the presence or absence of 1 μ M intracellular Ca²⁺ in either (A) cohort 1 or (B) cohort 2. The dashed lines represent the 25th and 75th quartiles. The Mann Whitney U test was used to ascertain differences between the membrane potential dynamics recorded in the different conditions at the specific frequencies. The bar (greyscale) above the time-averaged plots in (A) and (B) represents the *p*-value obtained from this Mann Whitney U test. The number of samples was a minimum of 6.

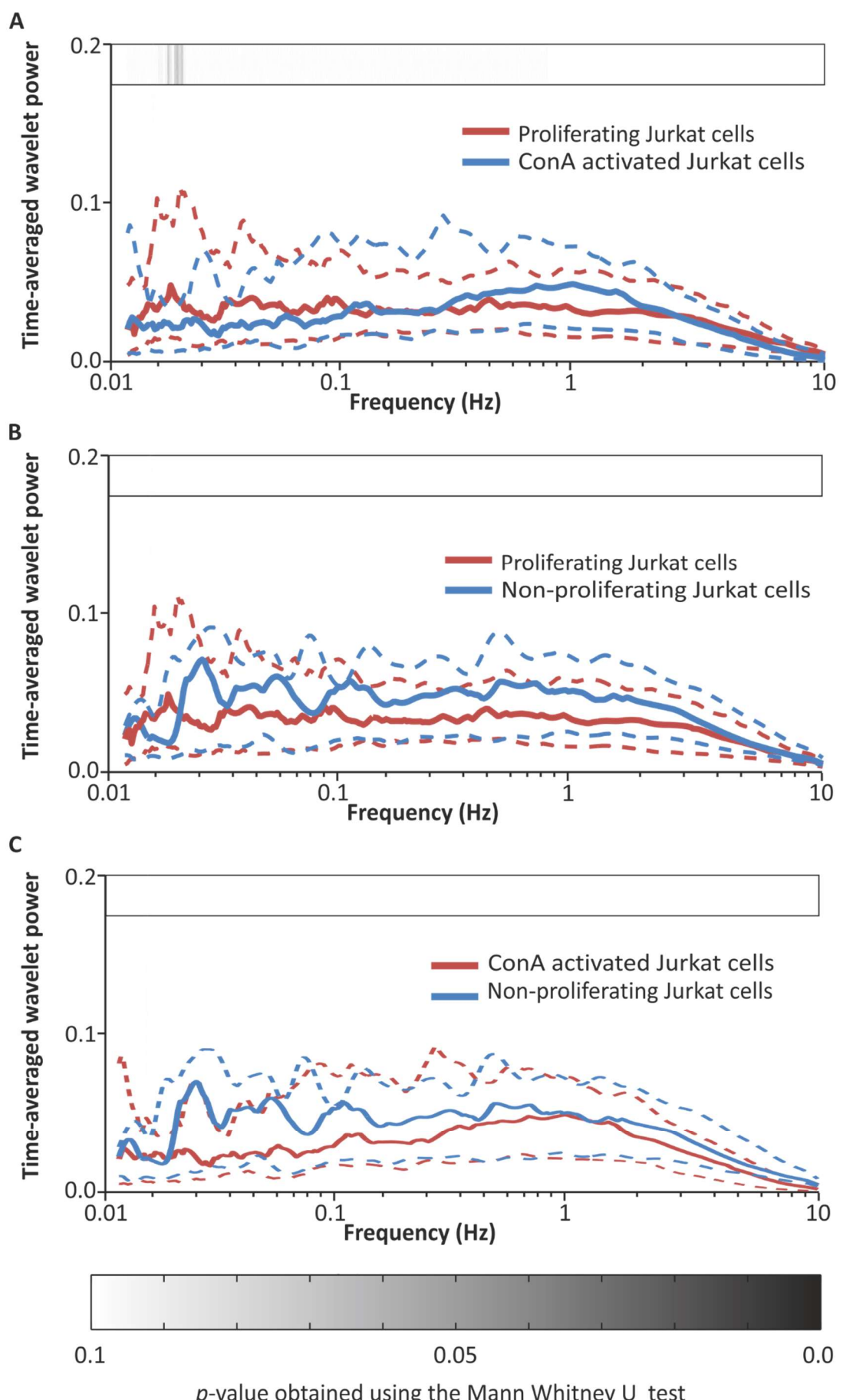
5.2.9 Investigating the membrane potential of Jurkat cells in different states in time-frequency domain using the continuous wavelet transform

One of the aims of this project was to investigate the role of temporal changes in the membrane potential which could potentially be involved in bioelectrical signalling mechanisms associated with either proliferation or activation. Consequently, the membrane potential dynamics of the Jurkat cells that were in either a non-proliferative state, state of log growth or an activated state by the techniques described in Chapter 3 or 4 were investigated using the CWT technique.

The membrane potential dynamics investigated using the CWT technique failed to show significant differences in the time-averaged wavelet power between Jurkat cells in the log phase of growth and ConA activated Jurkat cells (Figure 5.11A). Similarly, Jurkat cells in a non-proliferative state failed to alter the membrane potential dynamics in comparison to Jurkat cells in a proliferative state or an activated state (Figure 5.11B). These results suggest that the membrane potential dynamics of Jurkat cells do not change irrespective of the state of the Jurkat cells.

Figure 5.11

Analysis of the membrane potential time-series from Jurkat cells in different states. Time-averaged wavelet power of the membrane potential of Jurkat cells in either **(A)** Jurkat cells in either the log phase of proliferation or ConA activated state. **(B)** Jurkat cells in either the log phase of proliferation or a non-proliferative state. **(C)** Jurkat cells in the non-proliferative state or ConA activated state. The dashed lines represent the 25th and 75th quartiles. The Mann Whitney U test was used to ascertain differences between the membrane potential dynamics recorded in the different conditions at the specific frequency. The bar (greyscale) above the time-averaged plots represents the *p*-value obtained from this Mann Whitney U test. The number of samples was a minimum of 9.



5.3 Discussion

The dynamic nature of the membrane potential is generally overlooked and as a result it is often reported as a static signal (the magnitude of the membrane potential at a single time point) and thus, only one value for the membrane potential value is quoted. This approach overlooks temporal changes in the membrane potential and the nonstationary dynamics of the membrane potential signal.

The aim of this chapter was to ascertain if the CWT technique could be used to investigate the membrane potential in the time-frequency domain. It is also possible that the time-frequency domain encodes information for regulating cell behaviours that are associated with bioelectric signalling. Consequently, understanding the membrane potential dynamics could shed light on potential bioelectric signalling pathways.

Analysis of the membrane potential in the time-frequency domain using CWT showed the presence of fluctuations rather than continuous oscillations. In other words, the changes in the membrane potential did not occur in a repeatable manner with time. This is seemingly contradictory to the findings of Lang et al., (1991), Enomoto et al., (1986), Pandiella et al., (1989) and Swann et al., (1989). In the aforementioned studies, high amplitude oscillations in the membrane potential of either fibroblasts, mammary epithelial cells or hamster eggs were observed. The oscillations in the membrane potential, however, were observed upon treatment with either bradykinin, epidermal growth factor (EGF) or fertilisation. The magnitude of the oscillations in the membrane potential of those cells were at least 10 mV and the frequency of the oscillations were approximately 0.01 Hz which made them observable in the membrane potential recordings by eye without the need of more complex analytical techniques.

It is possible that oscillations of a similar frequency to the frequency observed in the fibroblasts and epithelial cells but with a lower magnitude were present in the membrane potential of the Jurkat cells used in the present study but were hidden within the membrane potential signal and therefore not obvious by eye. This, however, is unlikely as the wavelet transform analysis failed to highlight the presence

of continuous oscillations at any of the frequency intervals investigated. The high magnitude oscillations seen in the previous studies may not have been present in the membrane potential of the Jurkat cells in the current study due to the treatment of the cells, the type of cells used or the whole cell patch clamping technique used to measure the membrane potential. Alternatively, the high magnitude oscillations may just not exist in the Jurkat cells.

The absence of oscillations in the membrane potential of the Jurkat cells could reflect the fact that oscillations in the membrane potential are cell specific as Enomoto et al., (1986) used mammary epithelial cells whilst Lang et al., (1991) used fibroblasts cells. Furthermore, the fibroblasts and mammary epithelial cells were treated with either bradykinin or EGF which could have affected metabolic processes (Enomoto et al., 1986). In turn, this could have had intracellular effects which manifested in the observed membrane potential dynamics. For example, bradykinin can indirectly cause the release of intracellular Ca^{2+} by stimulating the formation of 1,4,5-inositol triphosphate (Yano et al., 1985). In line with this hypothesis, fibroblasts and mammary epithelial cells which were untreated did not have oscillations in the membrane potential that were obvious by eye. It is still possible that oscillations or fluctuations with similar characteristics observed in the present study were present in the membrane potential of the cells used in their studies. They may have been hidden within the membrane potential recording and not evident without complex analysis (Enomoto et al., 1986; Lang et al., 1991).

The oscillations observed in the membrane potential of fibroblasts and mammary epithelial cells were only observed in the treated cells and thus cells that were not in a resting state. One of the aims of the present study was to investigate the membrane potential dynamics of Jurkat cells in a resting state using complex analytical methods. The fact that the Jurkat cells were in a resting untreated state could have contributed to the absence of large amplitude oscillations in the membrane potential of the Jurkat cells. Perhaps the difference in the measurement technique lead to the differences in the observance of membrane potential oscillations.

The whole cell patch clamping technique was used in the present study whilst electrical impalements were used in the studies by Lang et al., and Enomoto et al., To the contrary, the whole cell patch clamping technique was used by Pandiella et al., yet oscillations in the membrane potential were still observed. The electrode impalement technique does not cause washout of the cytosol and thus, regulatory molecules needed for the functioning of intracellular organelles unlike the whole cell patch clamping technique which was used in the current study (Sarantopoulos, 2007). Consequently, washout of molecules from the cytosol could have affected the functional state of intracellular organelles. As a result, the possible role of functional organelles in the oscillations of the membrane potential could be disrupted from the whole cell patch clamping technique.

The findings from the study conducted by Pandiella et al., showed that at least in fibroblasts cells, oscillations occur in the absence of cytosolic factors indicating that membrane associated factors are sufficient to drive oscillations. Indeed, if oscillations in the membrane potential are driven by oscillations in cytosolic Ca^{2+} then the patch clamping technique would not be able record them due to cytosolic washout caused by the whole cell patch clamping technique (Dupont et al., 2011; Hess et al., 1993). Nevertheless, interplay between cytosolic Ca^{2+} mobilisation from intracellular stores and the extracellular medium occurs in an oscillatory manner which could in turn cause oscillatory changes in the membrane potential by activating ion channels in an oscillatory manner, thus, ultimately leading to membrane potential oscillations (Uhlen and Fritz, 2010). This was, in fact, suggested to be the cause of the oscillations in the membrane potential of fibroblast cells (Pandiella et al., 1987; Peres and Giovannardi, 1990). Consequently, understanding the membrane potential dynamics in and of itself is imperative before adding additional layers of complexities arising from the presence of organelles and other metabolic components. Washout of the cytosolic components could be avoided using the perforated patch clamping technique (Spruston and Johnston, 1992).

Moreover, using the electrode impalement technique to measure the membrane potential has additional difficulties. The technique is more suited to cells which have a diameter larger than 50 μM (Ince et al., 1986; Ogden, 1994). In the case of measuring

the membrane potential of cells with a smaller diameter, the membrane potential is not reliable due to electrode induced transmembrane shunts. These shunts occur due to the lack of a tight seal between the electrode and the plasma membrane (Ince et al., 1984; Li et al., 2004; Svirskis et al., 1997). These transmembrane shunts are thought to arise due to the presence of a water layer between the microelectrode and the plasma membrane. These transmembrane shunts have even been considered to be the cause of membrane potential oscillations observed in membrane potential recordings using impalements (Ince et al., 1986).

The membrane potential could have been recorded using membrane potential dyes such as indo-carbocyanines (Wilson et al., 1985). Although, dyes would overcome the issue of cytosolic washout, as discussed in the introduction, a major drawback with fluorescent dyes is that additional calibration is required to ascertain the precise membrane potential which is an important requirement of the current project (Cohen and Salzberg, 1978).

While continuous oscillations in the membrane potential of Jurkat cells were not identified in the present study, CWT analysis of the membrane potential did highlight fluctuations which had frequencies that spanned between approximately 0.01 and 1 Hz. Evidence for the presence of fluctuations in the membrane potential recordings were seen in the time-frequency domain of the membrane potential of all Jurkat cells recorded in the SES. The presence of fluctuations in all recordings investigated provides preliminary evidence that these fluctuations are deterministic rather than stochastic, although this requires further study to confirm. Nevertheless, the wavelet transform also showed the membrane potential has nonstationary dynamics i.e. the membrane potential changes with time, therefore, this could explain the differences in the quoted membrane potential of a given cell type and also raises questions about citing a single static membrane potential.

The membrane potential fluctuations were affected by either K^+ , Cl^- or Na^+ in the absence of intracellular Ca^{2+} . An increase in the concentration of extracellular K^+ completely blocked the fluctuations whilst a reduction in the concentration of extracellular Na^+ reduced the power i.e. the magnitude of the fluctuations but failed to

completely block them. On the other hand, a reduction in the concentration of extracellular Cl^- caused an increase in the power of the fluctuations. Was the change in the membrane potential dynamics a consequence of the change in the membrane potential itself, or was it due to the change in the ionic concentration and the change in the conductance of these ions? The membrane potential changed significantly in response to changes in the ionic concentration of either extracellular K^+ , Cl^- or Na^+ , concurrently, the membrane potential dynamics also changed. If the membrane potential dynamics was dependent on the membrane potential of the Jurkat cells then a correlation between the membrane potential of a cell and the power of the fluctuations would have been evident in the cells prior to changes in the extracellular concentration of either K^+ , Cl^- or Na^+ . Such correlations were not evident suggesting that the membrane potential dynamics were not voltage dependent. In line with this hypothesis, a comparison between the membrane potential dynamics of the three different cohorts recorded in SES showed that the dynamics were significantly different depending on which ion dominated to determine the membrane potential rather than the membrane potential per se. These results support the hypothesis that the membrane potential dynamics are not dependent on the membrane potential. A similar hypothesis was also made by Enomoto et al., (1986).

An increase the ionic concentration of extracellular K^+ has been shown to reduce the magnitude of oscillatory changes in the membrane potential of fibroblasts and T-lymphocytes (Lang et al., 1991; Maltsev, 1990). These studies are in agreement with the findings of the present study wherein changes in the conductance of K^+ manifested in the altered membrane potential dynamics. It is difficult to relate the membrane potential dynamics to the activity of a specific K^+ channel from the results in the present study. However, the dynamics have been linked to voltage-gated K^+ channels and Ca^{2+} activated K^+ channels in T-lymphocytes and fibroblasts, respectively (Maltsev, 1990; Pandiella et al., 1987). Nevertheless, in the present study, inhibition of the voltage-gated K^+ channels reduced the power of the fluctuations with a frequency of approximately 0.1 Hz but failed to completely inhibit the fluctuations. This suggests that the membrane potential dynamics were not associated solely with the activity of a specific type of voltage-gated K^+ channels. As an increase in the extracellular concentration of K^+ blocked fluctuations in the membrane potential, it is

possible that these fluctuations could have been associated with the conductance of K⁺ through other channels or transport mechanisms or even the conductance of other ions. In agreement with this, there were insignificant differences between the membrane potential dynamics of Jurkat cells belonging to cohort 1 and cohort 3 despite significant differences in the membrane potential. The significantly different membrane potentials likely reflects the activity of different ions channels, pumps and carriers. Several other lines of evidence also support this hypothesis.

First, the power of the fluctuations were also reduced through a reduction of extracellular Na⁺ even though there was no evidence of specific Na⁺ channels in the Jurkat cells used in the current study. Second, the membrane potential of the Jurkat cells was not determined exclusively by K⁺ conductance since the theoretical E_{K+} in the present study was -75 mV and the mean membrane potential of the Jurkat cells in all three cohorts was significantly depolarised in comparison. Third, application of exogenous 4-AP failed to significantly alter the membrane potential despite inhibiting the voltage-gated K⁺ channel.

Although the power of the fluctuations were reduced through the reduction of extracellular Na⁺. It is unlikely that the altered dynamics were due to the conductance of Na⁺ through specific Na⁺ ion channels since the only specific Na⁺ channel observed in lymphocytes (the voltage-gated Na⁺ channel) was not observed in the present study (Fraser et al., 2004). Nevertheless, the conductance of Na⁺ could have occurred through non-specific cation channels or the Na⁺/Ca²⁺ exchanger. If the conductance of Na⁺ was through the Na⁺/Ca²⁺ exchanger then it is possible that a decrease in the concentration of extracellular Na⁺ could cause cytosolic Na⁺ extrusion and Ca²⁺ entry via this exchanger. The increase in the intracellular Ca²⁺ could have activated Ca²⁺ activated channels and contributed to the observed fluctuations in the membrane potential (Lang et al., 1991).

Due to the difficulty in isolating the different current types and thus identifying specific channel types in the Jurkat cells used, it is difficult to link specific channel activity and any dynamics associated with the activity of specific channels. It is

envisioned that future studies will investigate the dynamic signatures of specific channel types.

The wavelet transforms of the membrane potential showed frequent occurrence of the fluctuations in all of the membrane potential recordings suggesting that the membrane potential dynamics is indeed regulated (i.e. deterministic). The regulating factors for these fluctuations, however, remain ill understood. Although changes in the ionic concentration of either K^+ , Cl^- , or Na^+ produced changes in the membrane potential dynamics, it is unlikely that the mere conductance of these ions was the deterministic factor. If the conductance of these ions was the determining factor then the membrane potential dynamics should have been unaffected by changes in the ionic concentrations as the conductance of these ions determined the membrane potential of the Jurkat cells whilst they were in SES. The origin of the fluctuations observed in the membrane potential could be due to the activity of ion channels, pumps and carriers. Although ion channel gating mechanisms are poorly understood, their activity contributes to the conductance of ions, therefore, it could be involved in the origin of the deterministic fluctuations. For instance, hydrophobic gating mechanisms may be involved in voltage-gating K^+ channels (Aryal et al., 2015). In this hydrophobic model of gating, water molecules transition between wet and dry states leading to changes in the pore diameter ultimately acting as gates. The transition between the wet and dry states could be the underlying deterministic factor for the change in the membrane potential dynamics.

Jurkat cells in an activated state or a non-proliferative state failed to show significant differences in the membrane potential dynamics in comparison to Jurkat cells in the log phase of growth. The channels observed in the three different states were also similar and only differed on the proportion of cells expressing the voltage-gated K^+ channel. As the membrane potential is determined by the activity of the ion channels, it is therefore unsurprising that there were no significant differences in the membrane potential dynamics. These results also provide further evidence that the fluctuations in the membrane potential are not simply due to the activity of the voltage-gated K^+ channel.

In the present study, the membrane potential dynamics of the Jurkat cells were investigated on single cells by changing either the concentration of extracellular K⁺, Cl⁻ or Na⁺. The membrane potential of Jurkat cells belonging to either cohort 1, 2 or 3 failed to match the theoretical E_{K+}, E_{Cl-} or E_{Na+} respectively, which suggests that the membrane potential was determined by the conductance of more than one of these ions. It would have been interesting to investigate the voltage sensitivity of the membrane potential dynamics by changing the concentration of more than one ion on a single cell rather than using different cells as was the case in the present study. This could be considered as a limitation of the present series of investigations, however, the current study design was chosen based on the fact that the tight seal between the glass microelectrode and the cell membrane required for the whole cell configuration could not be maintained for a period of 90 minutes.

In summary, the CWT technique can be applied to the membrane potential time-series recorded using the patch clamping technique to investigate the membrane potential in the time-frequency domain in a novel manner. The application of the CWT analysis on the membrane potential time-series highlighted nonstationary dynamics. Furthermore, membrane potential dynamics which are probably deterministic were also identified and these dynamics can be distinguished from dynamics associated with the patch clamping hardware. The results also highlighted the possibility that the membrane potential dynamics of the Jurkat cells is dependent on the activity of ion channels and transport mechanisms rather than the static magnitude of the membrane potential per se. As the CWT technique can be used to investigate membrane potential dynamics, in the next chapter, the CWT technique will be used to investigate oscillations and fluctuations in the membrane potential of endothelial cells. The membrane potential dynamics of endothelial cells were investigated as low frequency oscillations in the cardiovascular system ascertained using the CWT technique have been linked to the activity of endothelial cells.

6 ELECTROPHYSIOLOGICAL CHARACTERISATION AND ANALYSIS OF THE MEMBRANE POTENTIAL DYNAMICS OF HMEC-1 ENDOTHELIAL CELLS

6.1 Introduction

Complex analytical techniques, namely, the CWT technique can be applied to investigate the membrane potential dynamics of Jurkat cells (see Chapter 5). The CWT technique has also been used to investigate the time-frequency domain of blood flow measurements recorded from humans (Stefanovska et al., 1999). The results from studies suggest that the blood flow signal has at least six different oscillatory frequencies (Kvandal et al., 2003; Kvernmo et al., 1999). These oscillatory frequencies range from 0.005 to 2 Hz and are thought to correspond to different aspects of the cardiovascular system (Stefanovska, 2007b). Studies with Nitric oxide dependent and nitric oxide independent vasoactive compounds altered the

characteristics of the two lowest oscillatory frequency ranges i.e. 0.005 – 0.0095 Hz and 0.0095 – 0.021 Hz. This indicates that these two low frequency intervals are related to the activity of microvascular endothelial cells (Bernjak et al., 2008; Kvandal et al., 2006).

The physiological relevance of these oscillations are only starting to be realised. Emerging evidence has shown that the characteristics of the blood flow dynamics at the low frequency intervals is altered in individuals with heart disease in comparison to healthy age-matched controls (Bernjak et al., 2008). Consequently, a thorough understanding of these low frequency oscillations present in the cardiovascular system could provide additional insights into human health.

It is well documented that the membrane potential has an influencing role in a diverse range of cell behaviours (as discussed in Chapter 1). It is possible that the low frequency oscillations in the cardiovascular system which are associated with the behaviour of endothelial cells have their origins in the oscillations of membrane potential. This is also an attractive proposition because the membrane potential is a tractable parameter which would allow further investigation and understanding of the physiological significance of the low frequency oscillations associated with endothelial cell behaviour.

Aims of the chapter

The aim of this chapter is to apply the CWT technique used in Chapter 5 to a physiologically relevant system wherein the membrane potential dynamics are known to be important i.e. blood flow dynamics. More specifically, the blood flow dynamics related to the activity of microvascular endothelial cells which occupy the lowest two frequency intervals i.e. 0.005 – 0.0095 Hz and 0.0095 – 0.021 Hz will be investigated within the membrane potential recordings. The membrane potential of HMEC-1 cells (see Chapter 1 for a detailed discussion on the selection of the HMEC-1 cell line) will be investigated using the patch clamping technique. It is envisaged that this approach will allow understanding of the membrane potential dynamics with respect to any dependence on ion channels, pumps and transporters.

Briefly, the HMEC-1 cell line is a microvascular endothelial cell line which exhibits several characteristics and markers of endothelial cells *in vivo*. In turn, making the HMEC-1 cells more akin to primary microvascular endothelial cells. Consequently, the findings of this chapter should be physiologically relevant.

The findings from Chapter 5 suggested a role for intracellular Ca^{2+} in the membrane potential dynamics, therefore, the effect of Ca^{2+} will also be investigated in the HMEC-1 cells. Moreover, the physiological role of intracellular Ca^{2+} elevations is well documented in endothelial cells adding the physiological relevance of this series of experiments (Berridge et al., 2000; Tran et al., 2000). To investigate oscillations with a minimum frequency of 0.005 Hz, the membrane potential of microvascular endothelial cells were recorded for 30 minutes which will allow identification of oscillations with this minimum frequency.

6.2 Results

6.2.1 The membrane potential of proliferating HMEC-1 cells

In the first instance, the membrane potential of proliferating HMEC-1 cells in the log phase of growth was investigated and the effect of intracellular ATP and intracellular Ca^{2+} on the membrane potential was established. The membrane potential was determined using the current clamp mode of the patch clamping technique.

In the presence of intracellular ATP, the mean immediate membrane potential (recorded within two seconds of achieving the whole cell configuration) for the HMEC-1 cells used in the present study was -4.5 ± 1 mV ($n=50$). The membrane potential of these cells ranged from 18 mV to -25 mV (Figure 6.1). The average resting membrane potential (after two minutes of achieving the whole cell configuration) of these HMEC-1 cells was not significantly different from the mean immediate membrane potential ($n=90$).

The presence of intracellular ATP stimulates active transport mechanisms and together with ion channels, they combine to set the membrane potential of mammalian cells (Wright, 2004). Active transport mechanisms require intracellular ATP to function, therefore, ATP was omitted from the intracellular solution and the contribution of active transport mechanisms to setting the resting membrane potential of the HMEC-1 cells was investigated. In the absence of ATP, the mean resting membrane potential of the HMEC-1 cells was 3.8 ± 2 mV ($n=11$) and was significantly different to the mean resting membrane potential of cells patched in the presence of intracellular ATP which was -5.7 ± 1 mV ($n=90$) ($p<0.05$) (Figure 6.1). The difference between the resting membrane potentials likely reflects the presence of intracellular ATP which would activate ATP dependent ion transport processes.

Studies have shown the presence of Ca^{2+} activated ion channels in HMEC-1 cells (Grgic et al., 2005; Zuidema et al., 2010). It was therefore envisaged that an increase in the concentration of intracellular Ca^{2+} from nominally free to 1 μM free would activate Ca^{2+} activated channels, if they are present on the plasma membrane of the HMEC-1 cells used in the current study. The activation of any Ca^{2+} activated channels could potentially alter the resting membrane potential of the HMEC-1 cells. The

results showed that the average resting membrane potential of the HMEC-1 cells patched in the presence of 1 μ M free intracellular Ca^{2+} was -23 ± 4 mV ($n=25$) ($p<0.05$). The large difference in the membrane potential of the HMEC-1 cells in the presence of intracellular Ca^{2+} indicates the presence of Ca^{2+} -activated ion channels in the HMEC-1. In the next section, the contribution of either Cl^- , Na^+ or K^+ to the resting membrane potentials of the HMEC-1 cells will be investigated. These three ions were investigated as their conductance are the major determinants of the membrane potential (Wright, 2004).

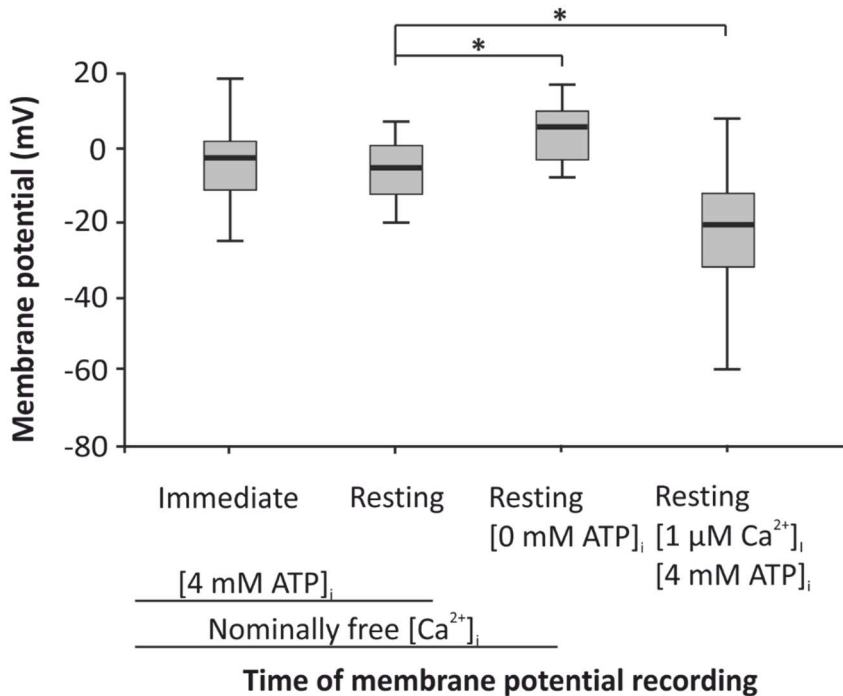


Figure 6.1

The distribution of the membrane potentials of proliferating HMEC-1 cells. The membrane potential of the HMEC-1 cells was measured either immediately (within two seconds of achieving the whole cell configuration or in a resting state (after two minutes of achieving the whole cell configuration). The immediate membrane potential of the HMEC-1 cells was recorded in the presence of 4 mM ATP and nominally free intracellular Ca^{2+} ($n=50$). The resting membrane potentials of the cells was recorded in either 4 mM ($n=90$) or 0 mM ATP and nominally free intracellular Ca^{2+} ($n=11$), or 4 mM ATP and 1 μM free intracellular Ca^{2+} ($n=25$). A Student's T-test was used to compare the level of significance between the conditions and the * denotes $p<0.05$. Note, although the mean resting membrane potential of HMEC-1 cells in the presence of 1 μM free Ca^{2+} and ATP in the intracellular solution was significantly different to the resting membrane potential of the HMEC-1 cells in the absence of 1 μM free Ca^{2+} and presence of intracellular ATP, the assumption of homogeneity of variances as tested by Levene's test of equality of variances was violated. The HMEC-1 cells were patched in extracellular solution HE1 and the intracellular solution was either HI1, HI1.2 or HI1.3. Solution HI1 contained nominally free Ca^{2+} and 4mM ATP. Solution HI1.2 was similar to HI1 but contained 1 μM free CaCl_2 without ATP. Solution HI1.3 contained 1 μM free CaCl_2 and 4mM ATP.

6.2.2 Ionic conductance's regulating the membrane potential of the HMEC-1 cells

The membrane potential of mammalian cells is primarily regulated by the ionic conductance's of K^+ , Cl^- , and Na^+ (Wright, 2004). Consequently, the individual contribution of these three ions to setting the resting membrane potential of the HMEC-1 cells was investigated in nominally free intracellular Ca^{2+} solutions. Channels selective for all of these three ions have been observed in endothelial cells (Nilius et al., 1996; Nilius and Riemann, 1990; Wang et al., 2009a; Zuidema et al., 2010).

The contribution of Cl^- to setting the observed resting membrane potential of the HMEC-1 cells was investigated by reducing the extracellular concentration of Cl^- from 162 mM to 6 mM. The Cl^- concentration was reduced by replacing KCl and NaCl with equimolar concentrations of K gluconate and Na gluconate, respectively. The reduction in the concentration of Cl^- caused the theoretical E_{Cl^-} changed from -33 mV to 48 mV. As such, a change in the observed membrane potential was expected if the conductance of Cl^- contributed to setting the resting membrane potential of the HMEC-1 cells. The HMEC-1 cells could be grouped into two different populations based on the resting membrane potential recorded in the standard extracellular solution (HE1). The mean resting membrane potential of the HMEC-1 cells from population 1 was -0.8 ± 1 mV (10 out of the 23 cells investigated) whilst the resting membrane potential of the HMEC-1 cells from population 2 was -11.4 ± 1 mV (13 out of the 23 cells). The change in the membrane potential of the cells in response to the reduction of extracellular $[Cl^-]$ also produced two different responses. The membrane potential of the cells from population 1 (-0.8 ± 1 mV) did not significantly change ($n=10$) whilst in population 2, the membrane potential of the HMEC-1 cells depolarised from an average of -11.4 ± 1 mV to 20.5 ± 1 mV ($n=13$) ($p<0.0005$) (Figure 6.2A).

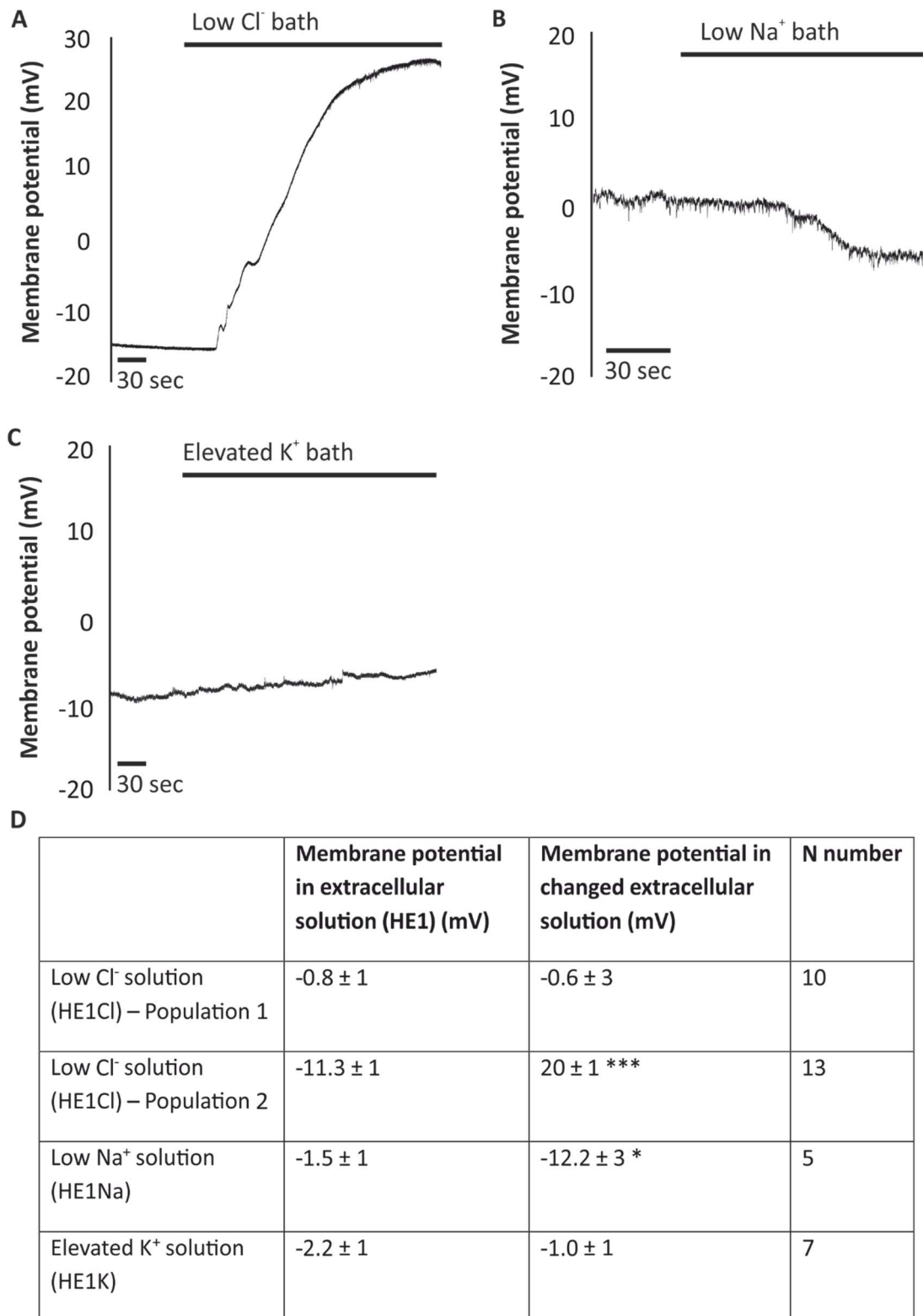
Next, the contribution of Na^+ to setting the resting membrane potential of the HMEC-1 cells was ascertained as Na^+ channels have observed in endothelial cells (Wang et al., 2009a). Extracellular Na^+ was reduced from 150 mM to 10 mM by replacing 140 mM NaCl with equimolar concentrations of NMDG-Cl. This reduction caused the

theoretical E_{Na^+} to change from 91 mV to 5 mV. In response to the decrease in the extracellular Na^+ , the membrane potential of the HMEC-1 cells hyperpolarised from a mean resting membrane potential of -1.5 ± 3 mV to -12.2 ± 7 mV ($n=5$) (Figure 6.2). Unlike the varied response observed in response to the reduction of extracellular Cl^- , all the HMEC-1 cells showed a uniform hyperpolarizing response to the reduction of extracellular Na^+ .

A variety of K^+ channels have been described in HMEC-1 cells in the literature and the conductance of K^+ also plays a role in determining the membrane potential of mammalian cells in general (Grgic et al., 2005; Tran et al., 2000; Zuidema et al., 2010). It was therefore predicted that a change in the extracellular concentration of K^+ would change the membrane potential of the HMEC-1 cells in the present study. As such, the extracellular concentration of K^+ was increased from 6 mM to 30 mM through the addition of 24 mM K gluconate. This change in the concentration of K^+ caused the theoretical E_{K^+} to change from -79 mV to -38 mV. Surprisingly, this increase in the extracellular concentration of K^+ failed to significantly change the membrane potential of the HMEC-1 cells ($n=7$) (Figure 6.2).

Figure 6.2

The membrane potential of HMEC-1 cells in response to changes in the extracellular concentration of either Cl⁻, Na⁺ or K⁺. Representative membrane potential recording of a HMEC-1 cell from **(A)** population 2 exhibiting a depolarising change in response to the reduction of extracellular concentration of Cl⁻ from 162mM to 6mM (n=13) or **(B)** a HMEC-1 cell exhibiting a hyperpolarizing change in response to the reduction of extracellular Na⁺ from 150mM to 10mM (n=5). **(C)** Representative membrane potential recording of a HMEC-1 cell which was unresponsive to the elevation of extracellular concentration of K⁺ from 6mM to 30mM (n=7). **(D)** The mean membrane potential in the standard extracellular solution (solution HE1) and the membrane potential in the changed extracellular solution. The HMEC-1 cells were patched in intracellular solution HI1 and the standard extracellular solution was HE1. The low Cl⁻ extracellular solution in (A) was HE1Cl which was similar to HE1 but the KCl and NaCl were replaced with equimolar concentrations of K gluconate and Na gluconate, respectively. The extracellular bath solution in (B) was changed to HE1Na which was similar to HE1 but the [Na⁺] was reduced to 10 mM. The extracellular bath solution HE1K in (C) contained an extra 24 mM K⁺ rather than 6 mM K⁺ through the addition of 24 mM K gluconate. The data in (D) is presented as mean \pm SEM. A paired Student's T-test was used to ascertain the statistical significance of the difference between the mean membrane potential in standard extracellular solution and the changed extracellular solution shown in (D) and the * denotes a significance level of $p<0.05$ whilst *** represents $p<0.0005$.



In summary, the mean immediate membrane potential of the HMEC-1 cells used in this study was -4.6 ± 1 mV in the presence of intracellular ATP. This membrane potential did not significantly change after two minutes of achieving the whole cell configuration i.e. the resting membrane potential. In the absence of intracellular ATP, the membrane potential stabilised to slightly more depolarised potentials in comparison to the resting membrane potential recorded in the presence of intracellular ATP. Furthermore, the resting membrane potential of the HMEC-1 cells was determined by the conductance of Cl^- and Na^+ although the conductance of Cl^- appeared to have the stronger influence on the resting membrane potential. The next section will investigate the whole cell currents recorded from these HMEC-1 cells using the voltage clamp mode of the patch clamping technique.

6.2.3 Analysis of the whole cell currents of proliferating HMEC-1 cells

The results suggested that Cl⁻ conductance had a large influence in setting the resting membrane potential of some of the HMEC-1 cells used in the present study. Consequently, to further understand the underlying nature of the Cl⁻ conductance, the whole cell currents of these HMEC-1 cells were characterised using the voltage clamp mode of the patch clamping technique.

Analysis of the whole cell currents recorded from HMEC-1 cells that were sensitive to changes in the concentration of extracellular Cl⁻

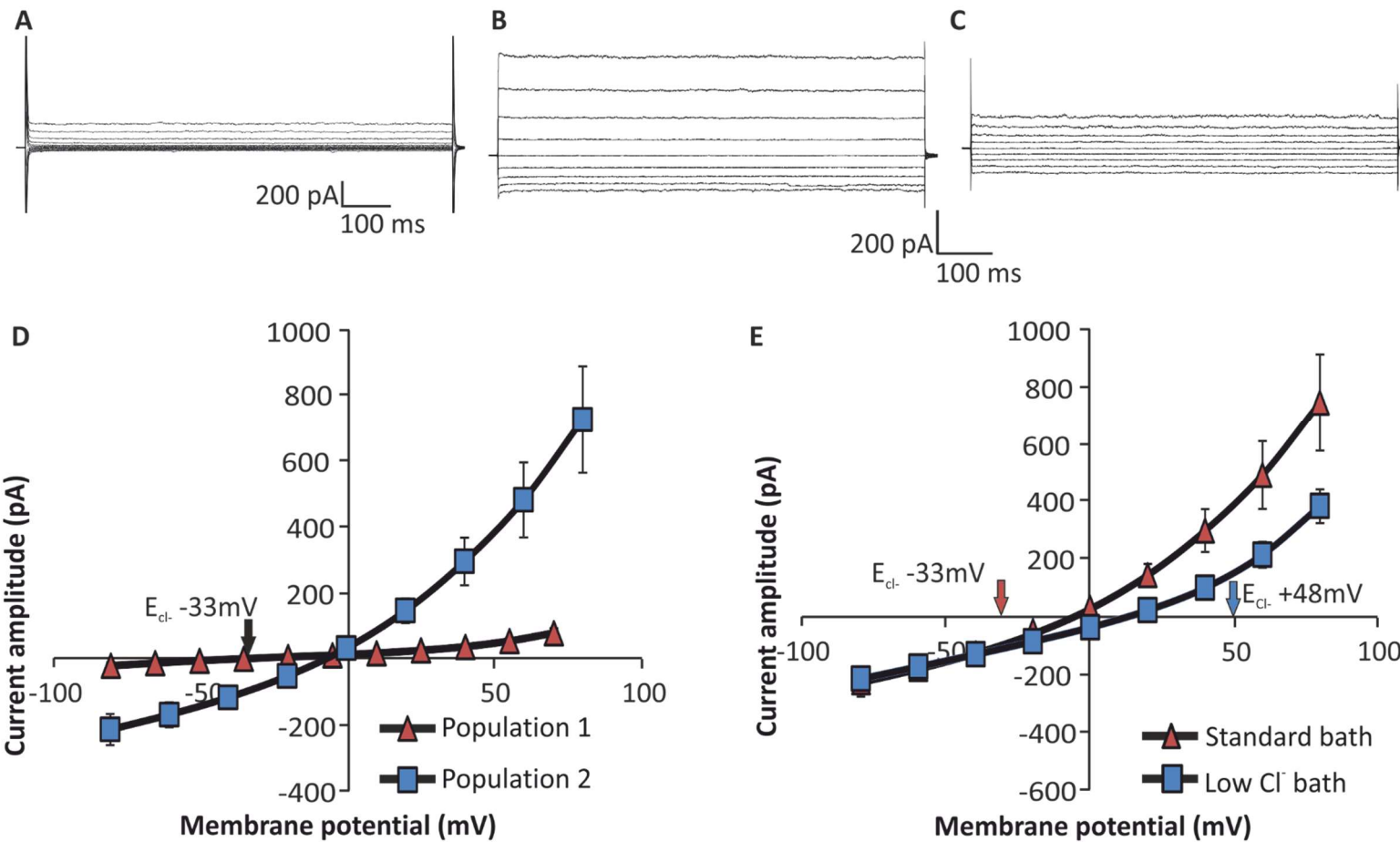
Cells were grouped into either population 1 or population 2 according to the response of the membrane potential to a reduction in extracellular [Cl⁻] (Figure 6.2). The whole cell currents of the HMEC-1 cells belonging to population 1 showed significant differences in the current amplitude and the observed E_{rev} in comparison to cells belonging to population 2 ($p<0.0005$) (Figure 6.3). The mean observed E_{rev} of the whole cell currents of the HMEC-1 cells from population 1 was -2.15 ± 1 mV (n=10) whilst the mean observed E_{rev} of the whole cell currents recorded from population 2 was -7.4 ± 1 mV (n=6). The Cl⁻ selectivity of the whole cell currents of these two populations of HMEC-1 cells was investigated by reducing the extracellular [Cl⁻] from 162 mM to 6 mM. This decrease in the concentration of Cl⁻ changed the theoretical E_{Cl-} from -33 mV to 48 mV.

The mean observed E_{rev} of the whole cell currents and the amplitude of the whole cell currents of the cells from population 1 did not significantly change in response to the reduction of the extracellular concentration of Cl⁻ from 162 mM to 6 mM (n=10). On the other hand, Figure 6.3E shows that the whole cell current amplitude of the cells from population 2 significantly changed in response to the reduction in extracellular [Cl⁻]. The observed E_{rev} of the whole cell currents also depolarised in response to the reduction in the extracellular [Cl⁻] (n=5) ($p<0.005$) in comparison to the observed E_{rev} of the whole cell currents recorded in HE1 (solution contained 162 mM Cl⁻). Although this change in the E_{rev} of the whole cell currents reflected the change in the theoretical E_{Cl-} between standard extracellular solution and the reduced Cl⁻ solution, the magnitude of the change in the observed E_{rev} of the whole cell currents was only 24.2 mV which was significantly less than the magnitude of change in the theoretical E_{Cl-}.

(81 mV). These results hint at the presence of additional conductance's which kept the observed E_{rev} of the whole cell currents away from the theoretical E_{Cl^-} . Nevertheless, the change in the whole cell current amplitude and the observed E_{rev} was compatible with the change in the equilibrium potential for Cl^- in response to the reduction of extracellular $[Cl^-]$ concentration i.e. there was a significant decrease in the inward anion current (outward current) at all positive test potentials investigated.

Figure 6.3

Cl⁻ selectivity of the whole cell currents from the HMEC-1 cells belonging to two different populations. Representative whole cell current traces from the HMEC-1 cells from (A) population 1 and (B) population 2. (C) Representative whole cell currents of a cell belonging to population 2 recorded in low extracellular [Cl⁻] (6mM Cl⁻). The whole cell currents were recorded after ten minutes of achieving the whole cell configuration. The currents in (A) were induced by test potentials between +80 and -100 mV in -15 mV steps whilst the currents in (B) and (C) were induced by test potentials between +80 and -80 mV in -20 mV steps. The currents in (A-C) were induced from a holding potential of 0 mV with 1 second intervals between test pulses. (D) The average current amplitude of the whole cell currents plotted as a function of the membrane potential. (E) The average current amplitude of the whole cell currents in standard extracellular solution (HE1) and low Cl⁻ extracellular solution (HE1Cl) plotted as a function of the membrane potential (n=11). The standard extracellular bath solution was HE1 (which contained 162mM Cl⁻) and the intracellular pipette solution was HI1 whilst the low Cl⁻ extracellular solution was HE1Cl which contained 6mM Cl⁻. The data in (D) is plotted as the mean ± SEM of a minimum of 5 experiments.



Several lines of evidence suggested that the whole cell currents of the HMEC-1 cells from population 2 were largely carried by Cl⁻. The E_{rev} of these currents, however, were closer to 0 mV rather than completely reflecting the theoretical E_{Cl-} of -33 mV. This suggests that other ions were also carrying some of the observed whole cell current and consequently forcing the observed E_{rev} away from the theoretical E_{Cl-}. As such, to minimise contamination of the Cl⁻ currents, the extracellular and intracellular solutions were redesigned and the concentration of intracellular gluconate ions were replaced with equimolar concentrations of Cl⁻ and the extracellular concentration of Na⁺ was reduced from 150 mM to 40 mM. The redesigned intracellular solution was called HI2 whilst the redesigned extracellular solution was called HE2. The whole cell currents of HMEC-1 cells were investigated in these redesigned solutions.

The whole cell current amplitude of the HMEC-1 cells in these redesigned solutions were significantly larger than the whole cell currents of the HMEC-1 cells patched in solutions containing gluconate ions and an elevated concentration of extracellular Na⁺ (extracellular solution HE1 and intracellular solution HI1) (Figure 6.4). In addition, the heterogeneity observed in the amplitude of the whole cell currents in solution HE1 and HI1 (see Figure 6.3) was not observed in the in the whole cell currents recorded in the redesigned intracellular and extracellular solutions.

To investigate the ions responsible for carrying this large amplitude current in these redesigned solutions, Cl⁻ and K⁺ selectivity of the whole cell currents were investigated. The selectivity of the whole cell currents to these two ions was investigated as K⁺ and Cl⁻ currents have been observed in HMEC-1 cells (Grgic et al., 2005). Cl⁻ selectivity of the whole cell currents were investigated by increasing the extracellular concentration of Cl⁻ from 56 mM to 156 mM through the addition of either 100 mM KCl or 100 mM MgCl₂. K⁺ selectivity of the whole cell currents were investigated through the addition of either 100 mM KCl or 100 mM K gluconate in the extracellular solution.

The increase in the extracellular concentration of Cl⁻ from 56 mM to 156 mM through the addition of 100 mM MgCl₂ caused the observed E_{rev} of the whole cell currents to follow the change in the theoretical E_{Cl-}. The observed E_{rev} in the standard

extracellular solution (solution HE2) was $10.2 \pm 1\text{mV}$ ($n=11$) and shifted to $-0.1 \pm 1\text{mV}$ ($n=11$) in the presence of elevated extracellular Cl^- (extracellular solution HE2MgCl). This change was similar to the change in the theoretical E_{Cl^-} between solution HE2 (24 mV) and HE2MgCl (-2 mV). Moreover, the change in the inward and outward current amplitudes were completely consistent with the change in the driving force of Cl^- conductance. Next, the selectivity of the whole cell currents to both K^+ and Cl^- was investigated through the addition of 100 mM KCl in the extracellular solution (solution HE2KCl) (Figure 6.5). The change in both, the whole cell current amplitude and the observed E_{rev} of these currents were consistent with the hypothesis that the large amplitude currents in the redesigned solutions were carried by Cl^- rather than K^+ . Furthermore, when the extracellular concentration of K^+ was increased by 100 mM through the addition of 100 mM K gluconate in the extracellular solution (solution HE2KG) the whole cell currents and the observed E_{rev} of these whole cell currents remained unchanged (Figure 6.5).

Taken together, these results suggest that the whole cell currents were carried by Cl^- rather K^+ , therefore, the nature of this Cl^- conductance was investigated through the addition of exogenous 100 μM NPPB; a widely used Cl^- channel blocker (Myssina et al., 2004). 100 μM NPPB caused a significant decrease in the current amplitude of the whole cell currents ($p<0.005$) confirming the presence of a Cl^- channel in these HMEC-1 cells (Figure 6.5).

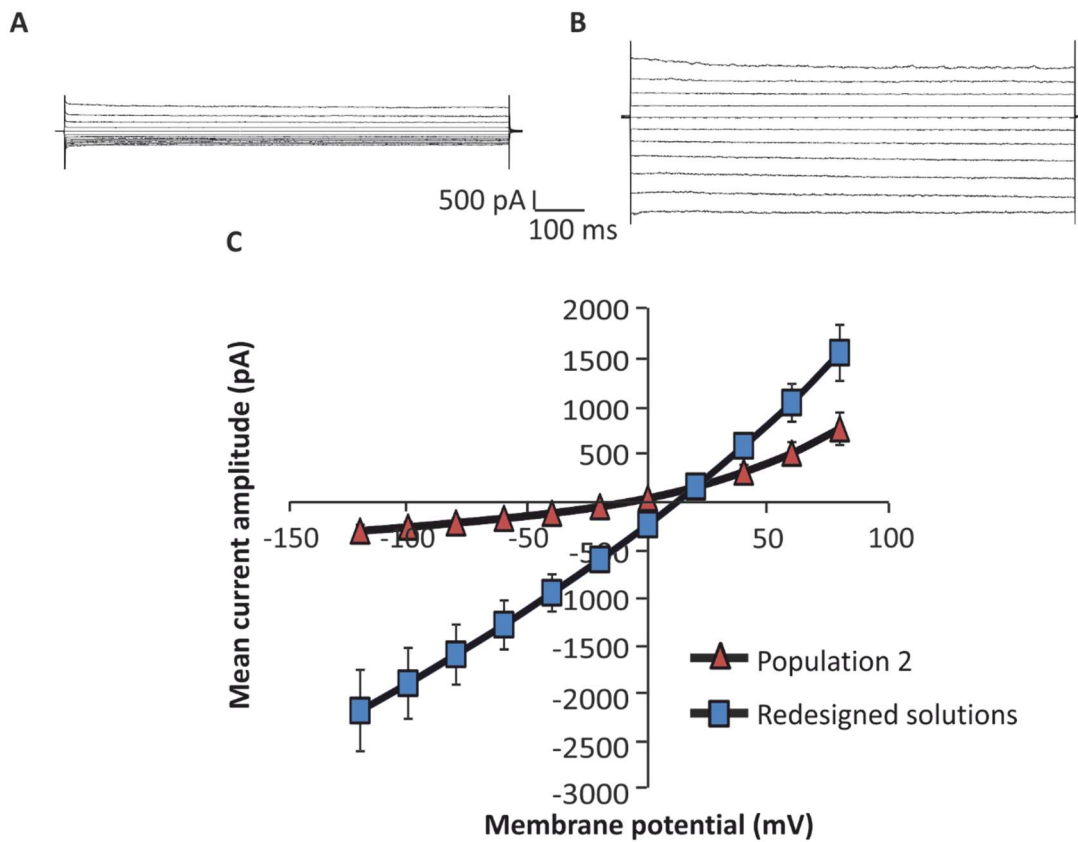
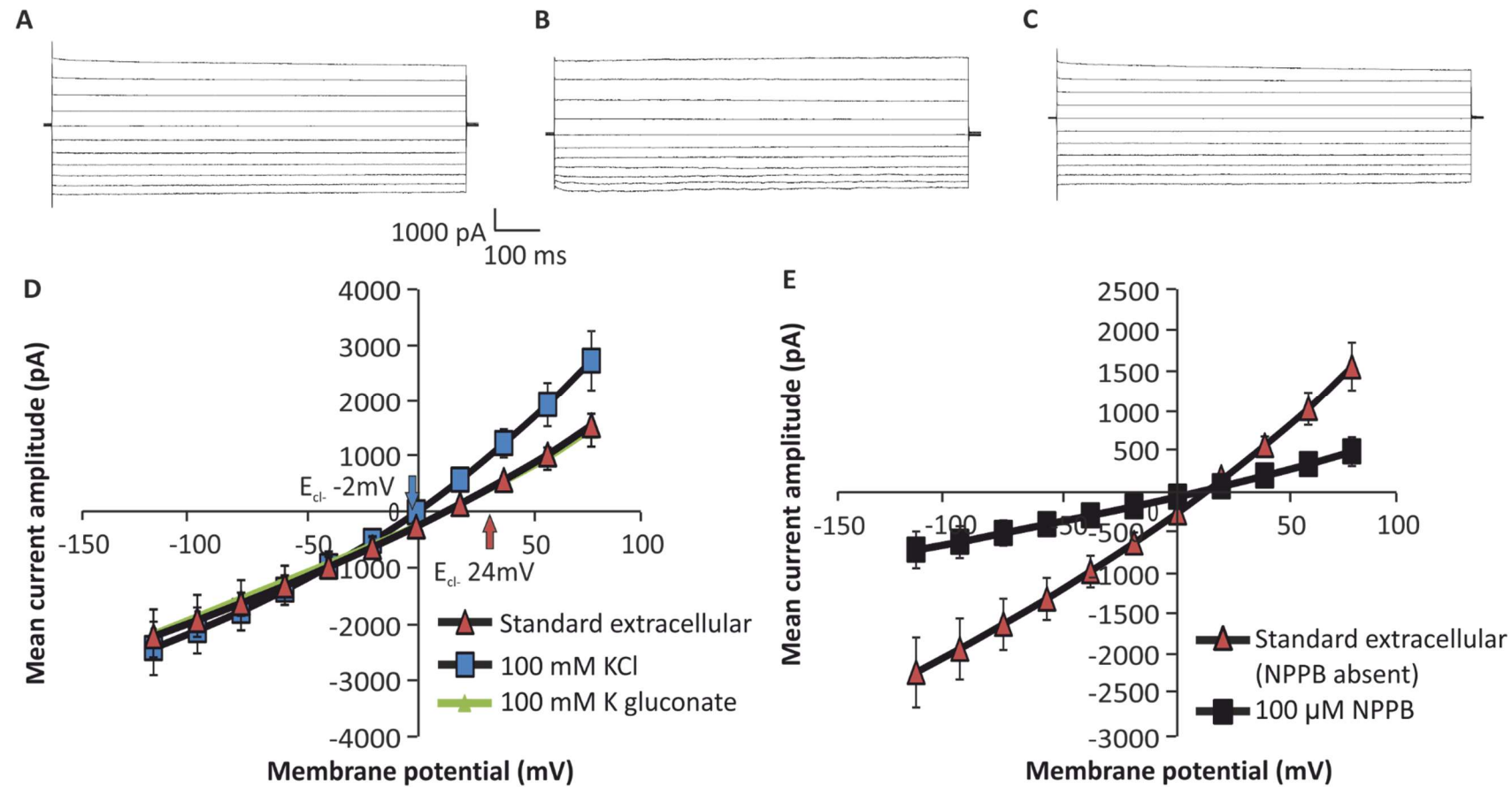


Figure 6.4

Whole cell currents from HMEC-1 cells recorded in two different solutions. Representative whole cell current traces from a HMEC-1 cell recorded in (A) extracellular solution HE1 and intracellular solution HI1 or (B) the redesigned solutions (HE2 and HI2). The whole cell currents were recorded after ten minutes of achieving the whole cell configuration. The currents were induced by test potentials between +80 and -85 mV in -15 mV steps from a holding potential of 0 mV with 1 second intervals between test pulses. (C) The average current amplitude of the whole cell currents is plotted as a function of the membrane potential between +80 and -85mV. The whole cell currents in (A) were recorded in standard extracellular solution HE1 and the intracellular pipette solution HI1. The whole cell currents in (B) were recorded in the redesigned intracellular solution HI2 while the redesigned extracellular was HE2. The data in (C) is plotted as the average \pm SEM of a minimum of 5 experiments.

Figure 6.5

Cl⁻ selectivity and NPPB sensitivity of the whole cell currents recorded from the HMEC-1 cells. Representative whole cell current traces from HMEC-1 cells in **(A)** the redesigned extracellular solution (HE2) which contained a final concentration of 6 mM K⁺ and 56 mM Cl⁻. **(B)** Whole cell currents recorded in elevated KCl solution (HE2KCl) that contained a final concentration of 106 mM K⁺ and 156 mM Cl⁻ and **(C)** elevated K gluconate solution (solution HE2KG) which contained a final concentration of 106 mM K. The whole cell currents were recorded after ten minutes of achieving the whole cell configuration. The currents were induced by test potentials between +80 and -120 mV in -20 mV steps from a holding potential of 0 mV with a 1 second interval between the test pulses. **(D)** The mean current amplitude of the whole cell currents recorded in various extracellular solutions plotted as a function of the membrane potential between +80 and -120 mV. **(E)** The mean current amplitude of the whole cell currents recorded in absence and presence of 100 µM NPPB in the standard extracellular solution (HE2). The HMEC-1 cells were patched in intracellular solution HI2 whilst the extracellular solution was either HE2, HE2KCl, or HE2KG. The data in **(D)** and **(E)** is plotted as the mean ± SEM of a minimum of 5 experiments.



Ca²⁺ sensitivity of the Cl⁻ channel

Next, the Ca²⁺ sensitivity of this Cl⁻ current was investigated by elevating the intracellular free Ca²⁺ concentration from nominally free (Solution HI2) to 100 nM (Solution HI2.1). The presence of the elevated intracellular Ca²⁺ did not change the amplitude of the whole cell current and the observed E_{rev} in comparison to the absence of intracellular Ca²⁺ (Figure 6.6).

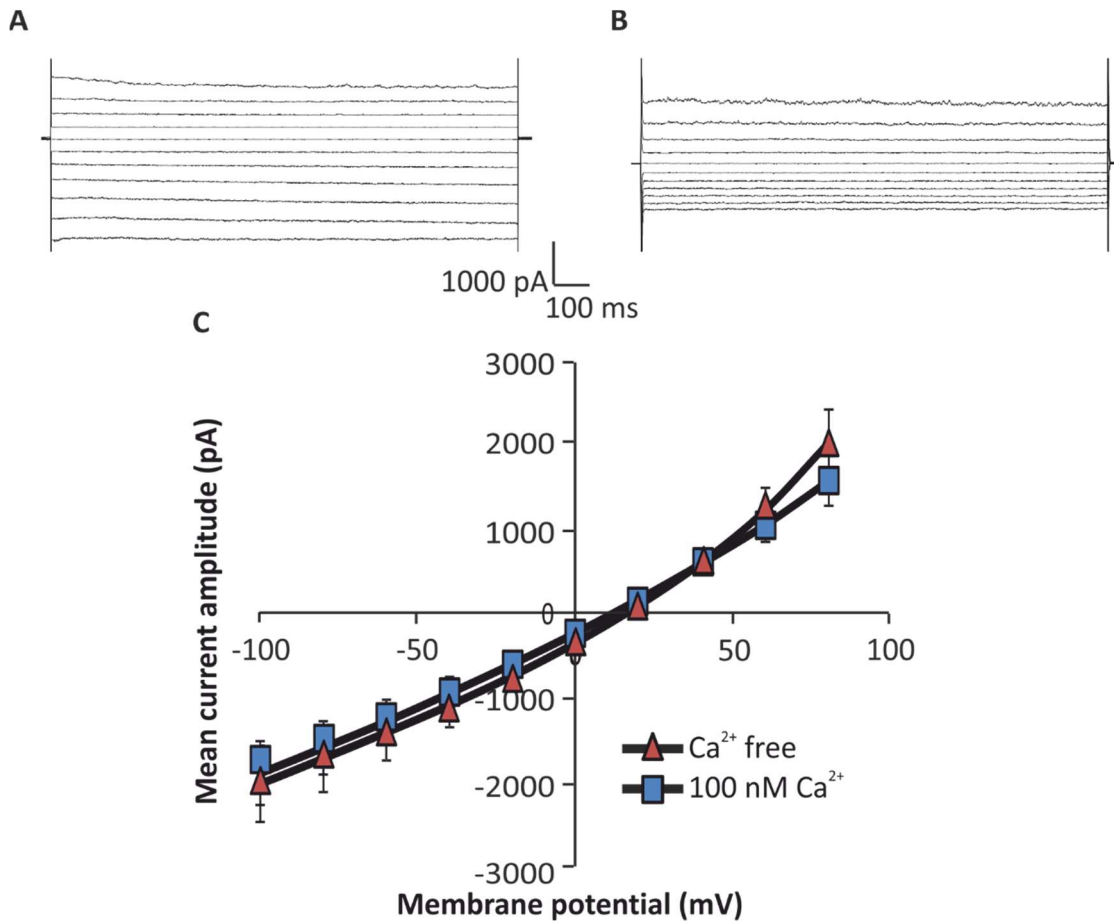


Figure 6.6

Ca^{2+} sensitivity of the Cl^- selective whole cell currents recorded from the HMEC-1 cells. Representative whole cell current traces from HMEC-1 cells recorded in the **(A)** absence of intracellular Ca^{2+} (solution HI2) and **(B)** presence of 100 nM free intracellular Ca^{2+} (solution HI2.1). The whole cell currents were recorded after ten minutes of achieving the whole cell configuration. The currents were induced by test potentials between +80 and -100 mV in -15 mV steps from a holding potential of 0 mV with a 1 second interval between test pulses. **(C)** The mean current amplitude of the whole cell currents plotted as a function of the membrane potential between +80 and -120 mV. The standard extracellular bath solution was HE2 and the intracellular pipette solution was either HI2 or HI2.1. Solution HI2.1 was similar to HI2 but contained 100 nM free Ca^{2+} . The data in **(C)** is plotted as the average \pm SEM of a minimum of 8 experiments.

In summary, the HMEC-1 cells patched with redesigned solutions expressed whole cell current amplitudes that were a significantly larger in comparison to HMEC-1 cells from either population 1 or 2 which were patched in the presence of intracellular gluconate and elevated extracellular $[Na^+]$. The increased current amplitude in these redesigned solutions were carried by Cl^- which was likely to be conducted, at least in part, through a NPPB sensitive Cl^- channel. This Cl^- current was not sensitive to an increase in the intracellular Ca^{2+} concentration to 100 nM free Ca^{2+} .

6.2.4 Investigating the effect of K⁺ conductance on the membrane potential of HMEC-1 cells in the presence of elevated concentrations of intracellular Ca²⁺

The presence of 1 µM intracellular Ca²⁺ caused the resting membrane potential of the HMEC-1 cells to become significantly more hyperpolarised (-23 ± 4 mV) in comparison to Ca²⁺ free intracellular solutions which was -4.5 ± 1 mV (see Figure 6.1). As the resting membrane potential moved towards theoretical E_{K+}, it was hypothesised that the resting membrane potential in the presence of intracellular Ca²⁺ was influenced by the conductance of K⁺. In line with this hypothesis, Ca²⁺-activated K⁺ channels have also been described in HMEC-1 cells (Zhang et al., 2011; Zuidema et al., 2010). To investigate this hypothesis, the response of the membrane potential to elevated extracellular [K⁺] was investigated in the presence of 1 µM intracellular Ca²⁺. The extracellular [K⁺] was increased from 6 mM to 30 mM through the addition of 24 mM K gluconate to the extracellular bath solution. In response to the increase in extracellular [K⁺], the membrane potential of the HMEC-1 cells depolarised by an average of 23.8 ± 3 mV and the mean membrane potential changed from -24 ± 4 mV to -0.8 ± 4 mV (n=11) ($p<0.0005$) (Figure 6.7).

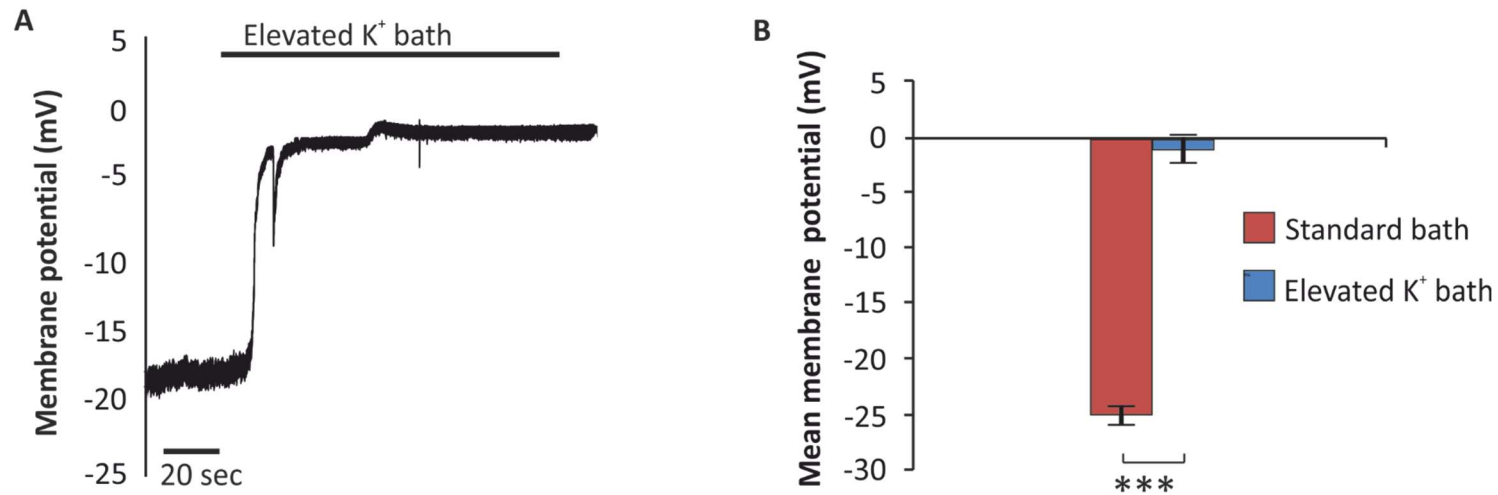


Figure 6.7

The response of the membrane potential of the HMEC-1 cells to an increase in the extracellular concentration of K⁺ in the presence of 1 μM free intracellular Ca²⁺. (A) A representative membrane potential recording of a HMEC-1 cell patched in the presence of 1 μM intracellular Ca²⁺ showing a depolarising change in the membrane potential upon an increase in the extracellular concentration of K⁺ from 6 mM to 30 mM. (B) The mean membrane potential of the seven HMEC-1 cells patched in standard bath (6 mM K⁺) solution and elevated K⁺ bath solution (30 mM K⁺). The HMEC-1 cells were patched in intracellular solution HI1.3 and the standard extracellular bath solution was HE1 which was changed to HE1K. Solution HE1K contained a total concentration of 30 mM K⁺ rather than 6 mM K⁺. The bar graph in (B) is shown as the mean ± SEM. A paired Student's T-test was used to ascertain the statistical significance between the different conditions in (B) and the *** in (B) represents a $p < 0.005$.

6.2.5 Analysis of the whole cell currents of HMEC-1 cells in response to elevated concentrations of intracellular Ca^{2+}

The increase in the intracellular $[\text{Ca}^{2+}]$ from nominally free to 1 μM free resulted in the membrane potential of the HMEC-1 cells becoming hyperpolarised (see Figure 6.1). In addition, the membrane potential was responsive to changes in the concentration of extracellular K^+ in the presence of the elevated intracellular Ca^{2+} (see Figure 6.7). These findings suggest that there are Ca^{2+} -activated channels present in the plasma membrane of the HMEC-1 cells used in the present study. These Ca^{2+} -activated channels are likely to be K^+ channels. To further investigate the Ca^{2+} sensitivity of the membrane potential, whole cell currents from the HMEC-1 cells were investigated in the presence of intracellular Ca^{2+} ranging from 0 and 10 μM (Solution HI3 to HI3.5).

The whole cell currents of the HMEC-1 cells exhibited inactivation in the first few milliseconds at all test potentials. These current kinetics were observed at all of the intracellular $[\text{Ca}^{2+}]$ investigated (Figure 6.8A). This inactivating current, however, was not investigated in detail. The amplitude of the whole cell outward current increased as the intracellular concentrations of Ca^{2+} was increased from nominally free to 600 nM (Figure 6.8D). The amplitude of this outward current did not increase with further increases in the intracellular $[\text{Ca}^{2+}]$. With the exception of 600 nM intracellular Ca^{2+} , the inward current amplitude was not significantly different between the different $[\text{Ca}^{2+}]$ investigated. Furthermore, the observed E_{rev} of the whole cell currents moved towards the theoretical E_{K^+} (-67 mV) as the intracellular $[\text{Ca}^{2+}]$ was increased suggesting that these Ca^{2+} -activated currents were carried by K^+ (Figure 6.8E). This hypothesis was investigated by increasing the extracellular $[\text{K}^+]$ by 100 mM through the addition of 100 mM KCl to the standard extracellular solution with the intracellular $[\text{Ca}^{2+}]$ ranging from nominally free to 10 μM free. The increase in the extracellular $[\text{KCl}]$ caused the theoretical E_{K^+} to change from -67 mV to 6 mV. With the exception of the currents recorded in the nominally free intracellular Ca^{2+} solution, the observed E_{rev} of the whole cell currents followed the change in the theoretical E_{K^+} i.e. the observed E_{rev} moved to less negative potentials. Concomitantly, the inward current significantly increased when the extracellular $[\text{K}^+]$ was increased by 100 mM suggesting that the Ca^{2+} -activated currents were indeed carried by K^+ . In the elevated

$[K^+]$ solution, there was an increase in the magnitude of the inward current as the intracellular $[Ca^{2+}]$ was increased, probably due to the activation of more Ca^{2+} -activated K^+ channels. In fact, Ca^{2+} -activated K^+ channels have been described in HMEC-1 cells (Grgic et al., 2005; Zuidema et al., 2010).

Interestingly, in the presence of Na^+ containing intracellular and extracellular solutions containing 600 nM intracellular Ca^{2+} , the whole cell inward current amplitude was significantly larger than the inward current amplitude observed in the presence of the other concentrations of intracellular Ca^{2+} (Figure 6.8D). This inward current was not observed in the Na^+ free solutions (in the presence of 600 nM intracellular Ca^{2+}) suggesting that this inward current was carried by Na^+ . Furthermore, the observed E_{rev} of the whole cell currents in these Na^+ free solutions was also significantly more hyperpolarised in comparison to the observed E_{rev} in the presence of the Na^+ containing intracellular and extracellular solutions (with 600 nM intracellular Ca^{2+}) (Figure 6.8E). The rapidly inactivating current that was observed in the first few milliseconds in solutions containing Na^+ was also evident in the Na^+ free solutions.

In the presence of the elevated intracellular Ca^{2+} , the initial experiments suggested that the whole cell currents were carried by K^+ . These results however, also indicate the presence of currents carried by Na^+ , therefore, the K^+ selectivity of the Ca^{2+} -activated currents were further investigated in the presence Na^+ free intracellular and extracellular solutions (Solution HI3.4 and HE3.1). K^+ selectivity was investigated through the addition of either exogenous 100 mM K gluconate, 100 mM KCl or 100 mM CsCl. In addition, Cl^- selectivity of the whole cell currents was also investigated as previous results suggested the presence of a Cl^- current (see Figure 6.5).

In response to the exogenous increase in the $[K^+]$ through the addition of either 100 mM K gluconate or 100 mM KCl, the whole cell outward current amplitude decreased at test potentials between 0 and 80 mV whilst the current amplitude increased at test potentials between -160 and 0 mV (Figure 6.9). Furthermore, the observed E_{rev} of the whole cell currents in the presence of the elevated extracellular $[K^+]$ also became more depolarised which mirrored the depolarising change in the theoretical E_{K^+} .

(theoretical E_{K^+} changed from -67 mV to -6 mV). The magnitude of the change in the experiment, however, was not as large as the theoretical E_{K^+} . Interestingly, the inward current was larger when the extracellular solution contained 100 mM KCl in comparison to extracellular solutions containing 100 mM K gluconate suggesting Cl^- also carried some of the whole cell currents. The amplitude of the whole cell currents, however, only increased slightly at test potentials of 60 and 80 mV and -160 and -140 mV when the extracellular $[Cl^-]$ was increased by 100 mM CsCl. The observed E_{rev} of the whole cell currents did not significantly change despite the change in theoretical E_{Cl^-} from 37 mV to 6 mV (Figure 6.9).

Figure 6.8

Ca²⁺ sensitivity of the whole cell currents recorded from HMEC-1 cells. Representative whole cell current traces from HMEC-1 cells recorded in the presence of either **(A)** 200 nM intracellular Ca²⁺, (solution HI3.2), **(B)** 600 nM intracellular Ca²⁺ (solution HI3.3) or **(C)** 600 nM free intracellular Ca²⁺ in Na⁺ free solutions (solution HI3.4). The whole cell currents were recorded after ten minutes of achieving the whole cell configuration. The currents were induced by test potentials between +80 and -120 mV in -20 mV steps from a holding potential of 0 mV with a 1 second interval between test pulses. **(D)** The mean current amplitude of the whole cell currents plotted as a function of the membrane potential between +80 and -120 mV in the presence of different concentrations of intracellular Ca²⁺. The current amplitude was measured between 600 and 800 ms and plotted as the average between these time points. **(E)** The observed E_{rev} of the whole cell currents shown in (D). The standard extracellular bath solution was either HE3 or HE3.1. The intracellular solution was either HI3, HI3.1, HI3.2, HI3.3, HI3.4 or HI3.5. The data in (D) is plotted as the average ± SEM of a minimum of 5 experiments.

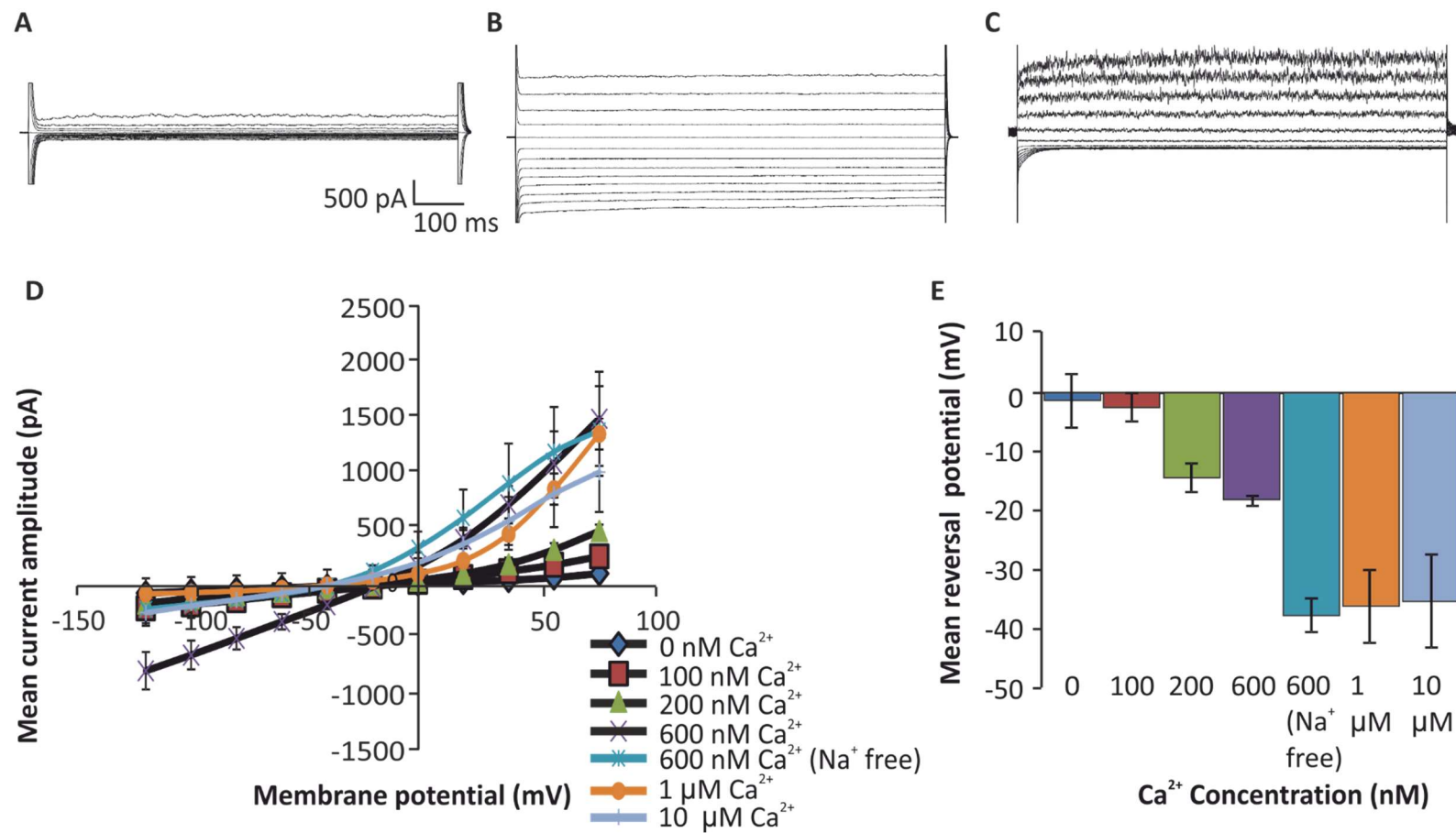
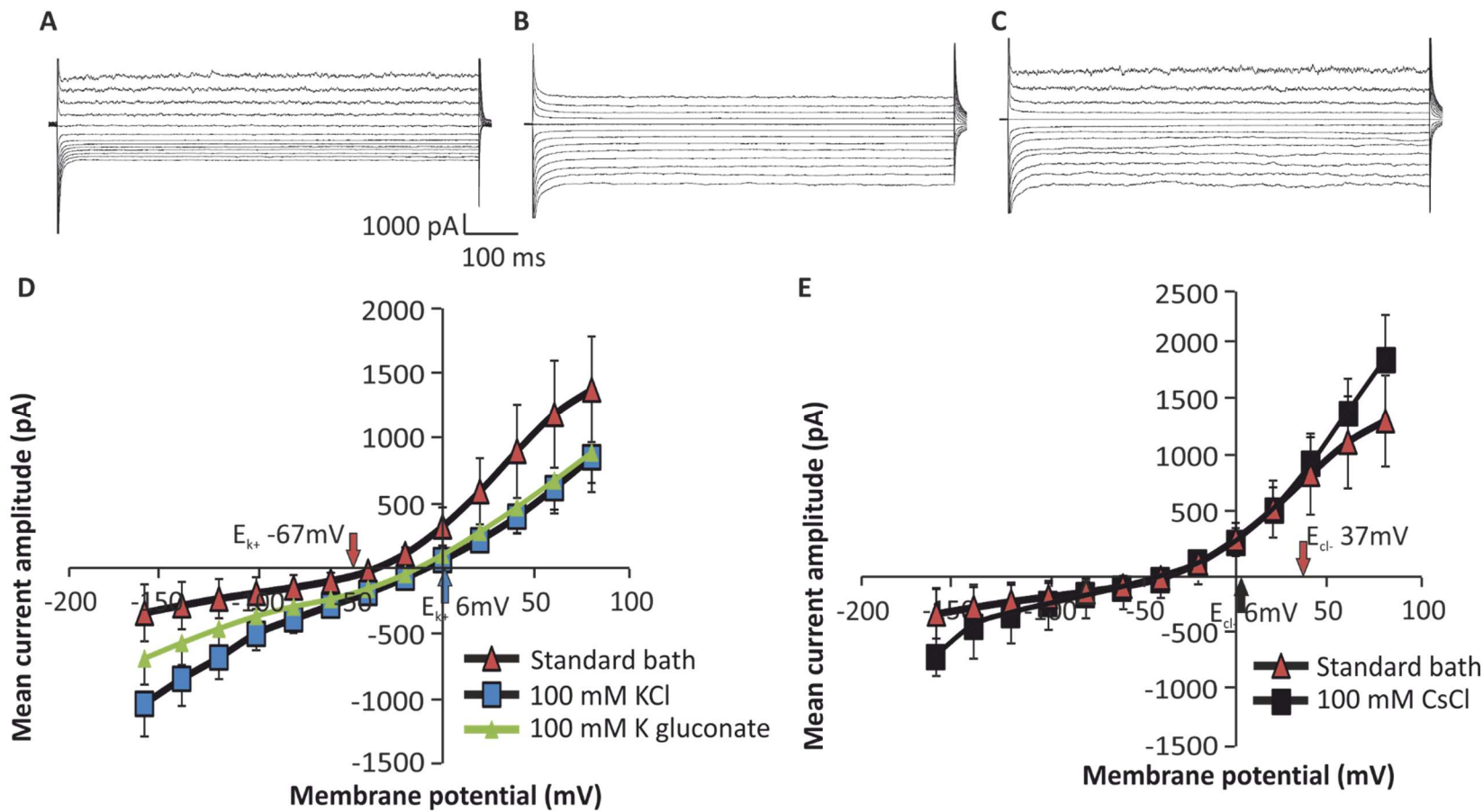


Figure 6.9

K⁺ selectivity of the whole cell currents recorded from HMEC-1 cells. Representative whole cell current traces from HMEC-1 cells recorded in either **(A)** standard extracellular solution (Solution HE3.1), **(B)** extracellular solution containing 100 mM K gluconate (Solution HE3.1KG) or **(C)** extracellular solution containing 100 mM KCl (HE3.1K). The whole cell currents were recorded after ten minutes of achieving the whole cell configuration. The currents were induced by test potentials between +80 and -160 mV in -20 mV steps from a holding potential of 0 mV with a 1 second interval between test pulses. **(D and E)** The mean current amplitude of the whole cell currents plotted as a function of the membrane potential between +80 and -160 mV. The current amplitude was measured between 600 and 800 ms and plotted as the average between these time points. The extracellular bath solution was either HE3.1, HE3.1KG, HE3.1K or HE3.1Cs and the intracellular solution was HI3.4. The data in (D) is plotted as the average ± SEM of a minimum of 6 experiments.



To summarise, the whole cell currents of the HMEC-1 cells used in the present study showed a Ca^{2+} sensitive current wherein the amplitude of the outward whole cell currents increased as the intracellular $[\text{Ca}^{2+}]$ was increased. These Ca^{2+} -activated currents were conducted by K^+ channels. In line with the aims of this chapter, the membrane potential recordings were investigated in the time-frequency domain using the CWT technique.

6.2.6 Analysis of the membrane potential dynamics of HMEC-1 cells

An aim of this chapter was to investigate the membrane potential recordings of the HMEC-1 cells to identify the presence of oscillations and fluctuations that may not be apparent by eye. As such, 30 minute recordings of the membrane potential signal were analysed using the CWT technique. Recall the CWT technique was used to analyse the membrane potential of the Jurkat cells in Chapter 5. The membrane potential was recorded for 30 minutes to allow identification of oscillations and fluctuations with a minimum frequency of 0.005 Hz. Although 17 membrane potential recordings were made for analysis using the CWT technique, nine recordings had to be excluded from the CWT analysis due to the presence of sharp transients which would compromise the reliability of the CWT analysis.

The CWT technique did not show the presence of oscillations, however, fluctuations in the membrane potential signal were identified (Figure 6.10) These fluctuations had different frequencies and ranged from ~0.01 and 1 Hz with a low power, in other words, the amplitude of the fluctuations were small.

The results from the present study suggested that in the presence of intracellular ATP the magnitude of the static resting membrane potential was different in comparison to the absence of intracellular ATP (see Figure 6.1). The contribution of intracellular ATP on the membrane potential dynamics were therefore investigated by recording the membrane potential in the absence and presence of intracellular ATP. The amplitude of the fluctuations were significantly smaller than the fluctuations within the membrane potential in the presence of intracellular ATP (Figure 6.10).

As an increase in the concentration of intracellular Ca^{2+} caused a significant change in the magnitude of the static resting membrane potential of the HMEC-1 cells used in the current study (see Figure 6.1), it was decided to investigate the effect of 200 nM free intracellular Ca^{2+} on the membrane potential dynamics of the HMEC-1 cells. The results of the time frequency analysis hinted at an increase in the power of fluctuations that had a frequency of ~0.1 and 1 Hz in the presence of 200 nM intracellular Ca^{2+} (Figure 6.11).

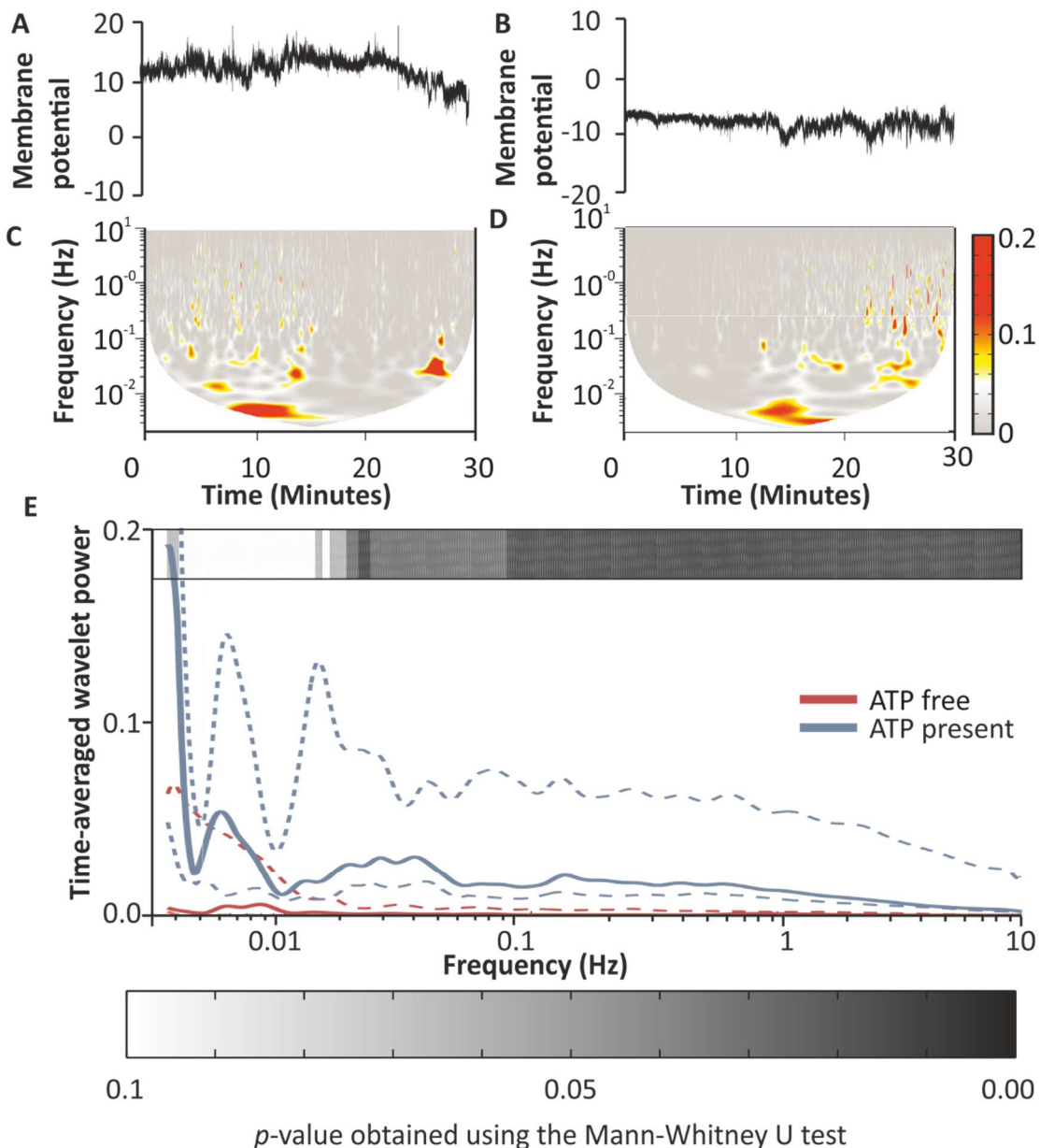


Figure 6.10

The effect intracellular ATP on the membrane potential dynamics of HMEC-1 cells
 Representative membrane potential recordings as seen in the time domain from HMEC-1 cells recorded in either (A) the presence of 4 mM ATP or (B) absence of intracellular ATP. The wavelet transforms seen in the time-frequency domain is shown directly below the membrane potential recordings. (D) The median (solid lines) time-averaged wavelet power across the frequency intervals 0.01 and 10 Hz calculated from cells belonging in the presence and absence of ATP together with the 25th and 75th quartiles shown as dashed lines. The bar above the plot represents the *p*-value obtained from the Mann-Whitney U test for differences between the different conditions at the specific frequency. Each experiment was done a minimum of 4 times.

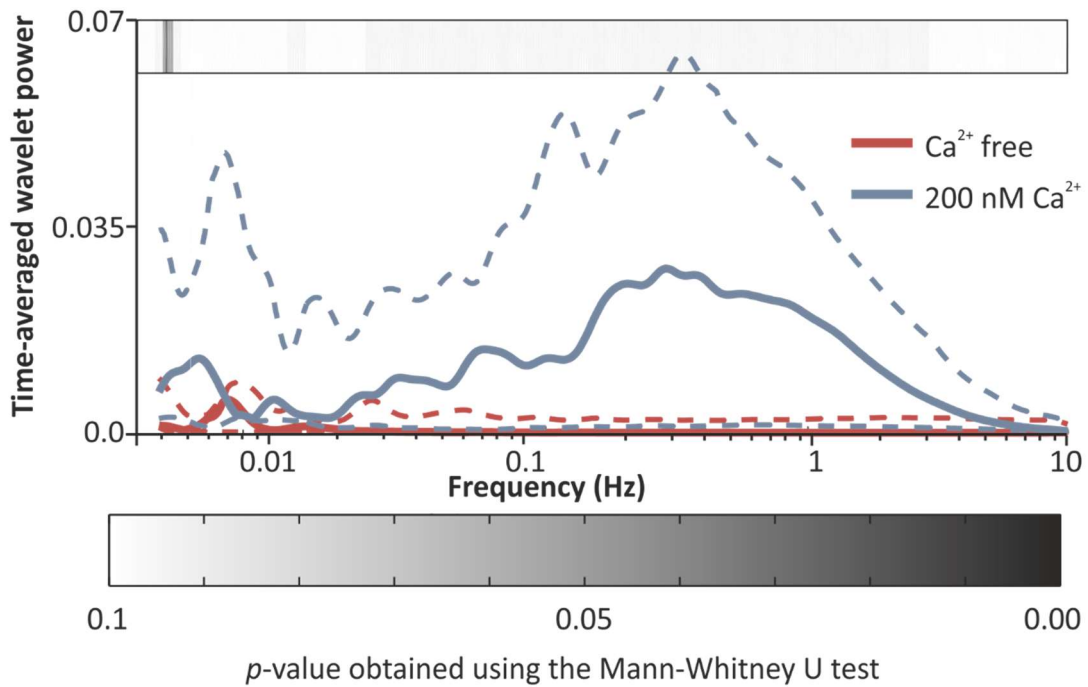


Figure 6.11

The effect of intracellular Ca^{2+} on the membrane potential dynamics of the HMEC-1 cells. The time-averaged wavelet power of the fluctuations in the membrane potential signal as a function of the frequency derived from the wavelet transform analysis of HMEC-1 cells in the absence and presence of 200 nM free intracellular Ca^{2+} . The plot is presented as the median of a minimum of 3 recordings with the 25th and 75th quartiles. The bar above the plot represents the p -value obtained from the Mann-Whitney U test for differences between the different conditions at the specific frequency. Each experiment was done a minimum of 3 times.

In summary, the wavelet transform technique failed to highlight oscillations in the membrane potential signal of the HMEC-1 cells, however, fluctuations were observed. These fluctuations appear to be driven by mechanisms dependent on ATP. The results also suggested that intracellular Ca^{2+} can alter the power and frequency dynamics of these fluctuations.

6.3 Discussion

The aim of this chapter was to investigate the membrane potential dynamics of the HMEC-1 cells with a view to linking them with low frequency oscillations in the cardiovascular system which were found to be related to the activity of endothelial cells. The membrane potential dynamics and the underlying currents determining the membrane potential of the HMEC-1 was also investigated.

The immediate static membrane potential of the HMEC-1 cells. The magnitude of the static “immediate” membrane potential of the HMEC-1 cells (in the presence of nominally free Ca^{2+} and intracellular ATP), which was recorded within two seconds of achieving the whole cell configuration was -4.5 ± 1 mV. The magnitude of the static “resting” membrane potential (recorded after two minutes of achieving the whole cell configuration) of these cells failed to significantly change in comparison to the immediate resting membrane potential in the presence of intracellular ATP.

The HMEC-1 cells were perfused with the extracellular solution for 10 minutes before a cell was patched, therefore, it was possible that the membrane potential of the cells began to change during this 10 minute period. The change in the membrane potential could have been induced by the difference in the ionic composition of the extracellular solution and the culture medium. Unfortunately, the immediate static membrane potential was not recorded in the absence of intracellular ATP or in the presence of intracellular Ca^{2+} which would have provided further information on the immediate membrane potential of the HMEC-1 cells used in the present study.

The static resting membrane potential of the HMEC-1 cells has been shown to be approximately -30 mV (Zhang et al., 2011; Zuidema et al., 2010). The difference in the resting membrane potential of the HMEC-1 cells patched in the present study and those observed by Zhang et al., and Zuidema et al., could be due to reasons associated with the treatment of the cells during the cell culture. The characteristics of endothelial cells are highly malleable and can vary with culture and growth conditions (Hewett et al., 1993). In addition, the membrane potential of cells in general vary with different stages of the cell cycle due to changes in the activity of the underlying ion channels (Gericke et al., 1993), therefore, the HMEC-1 could be at different stages of

the cell cycle. In support of this hypothesis, the HMEC-1 cells in the present study were patched 24 hours after splitting the cells using trypsin treatment. On the other hand, Zuidema et al., (2010) patched the HMEC-1 cells one hour after trypsin treatment. In addition, both Zuidema et al., and Zhang et al., cultured the HMEC-1 cells in MCDB-131 medium supplemented with bicarbonate. Bicarbonate has been found to increase the open probability of K^+ channels in rabbit corneal endothelium (Rae et al., 1990). In fact, K^+ channels were dominant in the HMEC-1 cells used by both, Zuidema et al., and Zheng et al., As such, it is possible that the bicarbonate present in MCDB-131 culture medium influenced the membrane potential by altering the phenotype of the active ion channels on the plasma membrane of the HMEC-1 cell used in those studies.

The differences in the static resting membrane potential of the HMEC-1 cells in the present study and the study conducted by Zuidema et al., could be associated with the presence of 600 nM intracellular Ca^{2+} used by Zuidema et al., (2010). In support for this theory, the static resting membrane potential of the HMEC-1 cells in the present study was closer to 0 mV in the absence of intracellular Ca^{2+} but this static resting membrane potential depolarised to -23.6 ± 4 mV in the presence of 1 μM free intracellular Ca^{2+} . The membrane potential in the presence of Ca^{2+} was closer to -37 mV observed by Zuidema et al., and the -32 mV observed by Zhang et al., It is possible that the combination of the reasons discussed contributed to the differences in the resting membrane potential of the HMEC-1 cells and those published in literature.

The influence of ATP on setting the membrane potential of the HMEC-1 cells. In the absence of intracellular ATP, the resting membrane potential of the HMEC-1 cells in the present study was significantly more depolarised in comparison to the resting membrane potential in the presence of intracellular ATP, albeit by only 8 mV. This finding suggests that active transport processes could have contributed to setting the membrane potential of the HMEC-1 cells used in the present study by approximately -8 mV. In fact, the activity of the Na^+/K^+ ATPase pump has been shown to contribute approximately -8 mV to the resting membrane potential of endothelial cells (Daut et al., 1994; Oike et al., 1993). It is also possible that the presence of intracellular ATP increased the activity of unknown ion channels, thus causing a change in the

membrane potential of the cells (Janigro et al., 1996; Wilson et al., 1998). For example, the activity of Ca^{2+} -activated K^+ channels has been shown to increase in the presence of active Na^+/K^+ ATPase pumps which itself requires intracellular ATP (Gerlach et al., 2001; Tajima et al., 2011).

The heterogeneity of the HMEC-1 cells. The results from changing the extracellular concentration of either Cl^- , Na^+ or K^+ highlighted heterogeneity in the HMEC-1 cells. The response of the membrane potential to a changes in the extracellular concentration of Cl^- highlighted two populations of HMEC-1 cells. In population 1, the membrane potential was not affected by the change in the extracellular $[\text{Cl}^-]$, whilst in population 2, both, the membrane potential and the observed E_{rev} of the whole cell currents followed the change in the theoretical E_{Cl} . The observed change in the membrane potential, however, was not as large as the theoretical E_{rev} (see Figure 6.2). Nevertheless, investigations on Cl^- selectivity of the whole cell currents indicated that the whole cell currents were carried by Cl^- . Furthermore, this current was also sensitive to NPPB which is a Cl^- channel blocker suggesting that this Cl^- conductance was through Cl^- channels (Myssina et al., 2004). A number of different types of Cl^- channels have been observed in endothelial cells which include swelling-activated Cl^- channels, glycine-gated Cl^- channels and Ca^{2+} -activated Cl^- channels (Nilius et al., 1997b; Yamashina et al., 2001). It is unlikely that the whole cells currents in the present study were conducted through glycine-gated Cl^- channels as these channels are activated by glycine and glycine was not present in either the intracellular or extracellular solutions (Yamashina et al., 2001).

The membrane transport proteins conducting Cl^- . Swelling-activated Cl^- channels and Ca^{2+} -activated Cl^- channels have been observed in endothelial cells and both channel types show outward current rectification (Nilius et al., 1997b). A small degree of outward rectification was observed in some of the HMEC-1 cells. It was possible, however, that more obvious outward rectification was not apparent for a number of reasons. Firstly, the presence of the inward current could have blunted the appearance of the outward rectification. Secondly, both, swelling-activated Cl^- channels and Ca^{2+} -activated Cl^- channels exhibit different degrees of outward rectification and both channel types are co-expressed in endothelial cells. If both channels were active in the

HMEC-1 cells used in the present study then the degree of outward rectification may be complicated (Nilius et al., 1997b). Thirdly, it is possible that other channels, pumps and transporters were also active which could have confused the whole cell current picture. In favour of this third hypothesis, the observed E_{rev} of the whole cell currents was not the same as the theoretical E_{Cl^-} (see Figure 6.3D and Figure 6.5E) and the membrane potential was also sensitive to changes in extracellular Na^+ (see Figure 6.2). The precise Cl^- channel in the HMEC-1 cells used in the present study remains unknown.

The membrane transport proteins conducting Na^+ . A reduction in the concentration of extracellular Na^+ caused the membrane potential to hyperpolarise, (the magnitude of this change was relatively minor) indicating the presence of Na^+ conductance. It is possible that this Na^+ conductance was through either Na^+ selective channels, nonselective cation channels or pumps and carriers conducting Na^+ such as the Na^+/K^+ ATPase pump. In fact, the contribution of Na^+ conductance to setting the resting membrane of endothelial cells has been shown to range between 3 to 30% through non-specific cation channels (Himmel et al., 1993; Miao et al., 1993). Interestingly, in the voltage clamp mode, a large inward current was only observed in the presence of 600 nM intracellular Ca^{2+} in the standard extracellular solution (Solution HI3) which was not observed in Na^+ - free solutions suggesting that this large inward current was carried by Na^+ . On the other hand, it is possible that the large inward current which was only observed at 600 nM intracellular Ca^{2+} represented a heterogeneous population of HMEC-1 cells. Notwithstanding, Na^+ specific channels i.e. amiloride-sensitive Na^+ channels and epithelial Na^+ channels have been observed in the endothelium but it seems unlikely that this large inward current in the presence of 600 nM intracellular Ca^{2+} was conducted by the amiloride-sensitive Na^+ channel. This hypothesis is based on findings which showed that the open probability of the amiloride-sensitive Na^+ channel increased with elevations in the intracellular $[Ca^{2+}]$ between 100 nM and 1 μM and this was not the case in the present study (Benos and Stanton, 1999; Golestaneh et al., 2001; Hillebrand et al., 2007; Kusche-Vihrog et al., 2008; Marunaka et al., 1999; Perez et al., 2009).

The membrane transport proteins conducting K⁺. The membrane potential of the HMEC-1 cells was not sensitive to the elevation of extracellular [K⁺] in nominally free intracellular Ca²⁺ (see Figure 6.2). On the other hand, the membrane potential was sensitive to perturbations in [K⁺] when the intracellular [Ca²⁺] was increased to 1 μM suggesting the presence of Ca²⁺-activated K⁺ channels. Several lines of evidence support this hypothesis, firstly, in the presence of 1 μM intracellular Ca²⁺, the membrane potential also shifted towards the theoretical E_{K+}. Secondly, the observed E_{rev} of the whole cell currents moved towards the theoretical E_{K+} of -67 mV, concurrently, there was also a significant increase in the outward whole cell current amplitude as the intracellular [Ca²⁺] was increased from nominally free to 600 nM. Several types of Ca²⁺-activated K⁺ channels such as the small-conductance, intermediate-conductance and large-conductance family of Ca²⁺-activated K⁺ channels have been observed in HMEC-1 cells (Grgic et al., 2005; Zhang et al., 2011; Zuidema et al., 2010). Furthermore, the large-conductance Ca²⁺-activated channels can be activated by 600 nM intracellular Ca²⁺ and these channels exhibit outward rectification with slow time-dependent activation (Zuidema et al., 2010). In this study, similar current kinetics i.e. outward rectification and slow time-dependent activation was also observed in 70% (7 out of 10 cells patched) in the presence of 600 nM intracellular Ca²⁺ and Na⁺ free intracellular and extracellular solutions. The degree of time-dependent activation of the outward current in these conditions was more obvious in some current traces than others but this could be due to the large amplitude current that exhibited rapid time-dependent inactivation at the start of each test potential. This large amplitude current could have masked the rising phase of the slow time-dependent activating current. Although the exact Ca²⁺-activated K⁺ channel remains unidentified, it is possible that the HMEC-1 cells used in the present study had co-activated small, intermediate and large-conductance Ca²⁺-activated channels due to the variation in the outward current amplitude in the presence of 600 nM intracellular Ca²⁺ and the abundance of these channel types in endothelial cells (Coleman et al., 2004).

Whole cell currents of the HMEC-1 cells in the presence of reduced concentrations of Na⁺ and gluconate. The whole cell current amplitude of the HMEC-1 cells were significantly larger than the whole cell current amplitude of HMEC-1 cells when

intracellular gluconate was replaced with equimolar concentrations of Cl^- with a reduction in the extracellular $[\text{Na}^+]$. This increase in the magnitude of the whole cell currents could have been due to either the increase in Cl^- or the reduction of extracellular Na^+ . It is also possible that the intracellular gluconate ions had an inhibitory effect on the Cl^- channels (Ueda et al., 1990). It is unlikely that the extracellular concentration of Na^+ had a blocking effect on the Cl^- conductance as no published reports of Na^+ block on Cl^- conductance was found. The increase in the $[\text{Cl}^-]$ could have activated Cl^- channels or the increase in the $[\text{Cl}^-]$ could have provided more substrate for the Cl^- channels, thus, resulting in an increase in the whole cell outward current amplitude. In fact, volume-activated currents in HeLa cells have been shown to be modulated by external Cl^- (Stutzin et al., 1997).

The presence of membrane transport proteins conducting ions besides K^+ or Cl^- . The evidence from the present study provides strong evidence for the presence of K^+ and Cl^- channels, however, it is possible that other channel types were also present but overlooked. Several lines of evidence support this hypothesis, the observed E_{rev} of the whole cell currents failed to completely reflect the theoretical E_{Cl^-} or E_{K^+} . Furthermore, the observed E_{rev} of the whole cell currents moved closer to the theoretical E_{K^+} (-67 mV) in Na^+ free intracellular and extracellular solutions (see Figure 6.8). The membrane potential was also sensitive to perturbations in the extracellular $[\text{Na}^+]$. A non-specific cation current has been described in endothelial cells derived from human umbilical vein (Nilius et al., 1993). The non-specific current described by Nilius et al., (1993) had similar characteristics i.e. Ca^{2+} sensitivity of the current and the effect of the absence of extracellular Na^+ . In the absence of extracellular Na^+ , Nilius et al., like the present study, observed a decrease in the inward current with a hyperpolarising shift in the observed E_{rev} of the whole cell currents. Nilius et al., (1993) did not ascertain the type of the non-specific channel, however, a number of non-specific cation channels, namely, the TRP channels have recently been identified which could be potential candidates for conducting the non-specific current in the HMEC-1 cells used in the present study (Gees et al., 2010; Nadler et al., 2001; Schmitz et al., 2003; Voets et al., 2004).

The role of K⁺ channels in HMEC-1 cells. The precise ion channels in the HMEC-1 cells were not ascertained but the results suggest the presence of calcium-activated K⁺ channels and Cl⁻ channels. Notwithstanding, Ca²⁺-activated K⁺ channels, such as BKCa and IKCa have been implicated in cell proliferation of endothelial cells such as HMEC-1 cells, in addition to other cell types (Grgic et al., 2005; Wiecha et al., 1998). In HMEC-1 cells expressing both BKCa and IKCa channels, BKCa channel inhibition failed to inhibit mitogenesis suggesting IKCa channels, rather than BKCa channels play a role in the proliferation of HMEC-1 cells (Grgic et al., 2005). On the contrary, in HUVEC endothelial cells, the BKCa channel rather than the IKCa channel was associated with proliferation (Wiecha et al., 1998). These findings suggest that K⁺ channel types involved with proliferation varies with cell type. Nevertheless, similar to the mechanism associated with K⁺ channels and proliferation in lymphocytes, it is speculated that the K⁺ channels in endothelial cells play a role in proliferation through control of the membrane potential which could in turn control Ca²⁺ influx. On the contrary, however, a study conducted by Millership et al., (2011) wherein kidney cells transfected with a nonconducting mutant K⁺ channel showed increased proliferation without Ca²⁺ entry. In these kidney cells, it was hypothesised that the presence of the mutant K⁺ channels were linked to the ERK1/2 or JNK pathways either directly, or indirectly in a currently unknown manner. Similar results on proliferation from transfecting nonconducting mutant K⁺ channels have also been observed in fibroblast cells wherein conformational change in the channel was considered to initiate signalling cascades (Hegle et al., 2006). It is possible that K⁺ channels mediate proliferation through different (possibly even multiple) mechanisms depending on the K⁺ channel type, cell type and the state of the cell.

The membrane potential dynamics of the Jurkat cells. The membrane potential dynamics recorded from the HMEC-1 cells were investigated using the CWT technique discussed in Chapter 5. This technique was used to investigate the presence of low frequency oscillations (0.005 Hz) associated with the activity of microvascular endothelial cells within the cardiovascular system (Kvandal et al., 2006; Kvandal et al., 2003; Kvernmo et al., 1999). Oscillations in the membrane potential were not observed, however, fluctuations within the membrane potential with a low frequency were identified. In the studies conducted Kvandal et al., and Kvernmo et al, vasoactive

compounds were used to investigate the originating source of the oscillations. These vasoactive compounds would ultimately alter blood flow. Consequently, it is possible that the low frequency oscillations identified from the studies were driven by the blood flow itself, rather than activity the activity of the endothelial cells. In the present study, however, flow dynamics were not considered in favour of a simpler system. The aspect of flow dynamics could be added to the model system by culturing tubules and altering the flow rate of the perfusion. In fact, one of the reasons HMEC-1 cells were selected as the model system was due to the fact that they can be grown as tubules.

In the presence of intracellular ATP, these fluctuations had different frequency intervals (~ 0.005 Hz and 0.05 Hz). Interestingly, in the absence of intracellular ATP, there were hints that the membrane potential dynamics changed. Although 17 membrane potential recordings were made to investigate the influence of active transport mechanisms on the membrane potential dynamics, only eight recordings were suitable for analysis in the time-frequency domain using the CWT technique, consequently, further studies are required. Nevertheless, these preliminary results suggests that active transport mechanism could be contributing to the membrane potential dynamics of the HMEC-1 cells.

In the presence of intracellular ATP, the membrane potential dynamics also showed an increase in the time-averaged wavelet power of the fluctuations with a frequency interval of 0.1 Hz and 1 Hz. These results suggest the presence of intracellular Ca^{2+} affected the membrane potential dynamics of the HMEC-1 cells. It has to be remembered that the sample size was only 4 recordings, therefore, further studies on the effect of intracellular Ca^{2+} and the membrane potential dynamics are required. Notwithstanding, the effect of the presence of 200 nM intracellular Ca^{2+} on the whole cell currents and observed E_{rev} of these currents showed significant differences relative to the whole cell currents and the observed E_{rev} of the currents in the absence of intracellular Ca^{2+} . Taken together, these results suggest that the membrane potential dynamics of the HMEC-1 cells are, in part, associated with the activity of the Ca^{2+} -activated non-specific cation channels (see Figure 6.9).

The overriding aim of the current project was to investigate the role of membrane potential dynamics using CWT in cell behaviours such as proliferation. Consequently, the endothelial cells used in the current project were in a proliferative state. The majority of the microvascular endothelial cells *in vivo*, however, are quiescent and are connected to adjacent endothelial cells, therefore, the physiological relevance of the findings from investigations on the HMEC-1 cells is debateable (Staton et al., 2009). The approach for using proliferating HMEC-1 cells in the current study was selected to investigate the role of membrane potential dynamics in proliferation. The role of membrane potential dynamics *in vivo* can be easily investigated using the HMEC-1 cell line by either patching confluent cells rather than individual cells. Moreover, HMEC-1 cells grown as tubules can be patched to reflect vessel structure *in vivo* (Francescone et al., 2011) . It may be possible to use a model system where endothelial cells are surrounded by smooth muscle cells in a co-culture, however, the presence of oscillations in the smooth muscle cells may attenuate and mask oscillations arising from endothelial cells, if indeed the oscillations are driven by the activity of the endothelial cells (Truskey, 2010).

In summary, the findings from investigating the membrane potential dynamics of HMEC-1 cells did not show low frequency oscillations similar to those observed in the cardiovascular system. The results, however, suggested the presence of fluctuations in the membrane potential dynamics of the HMEC-1 cells and these fluctuations could be dependent on the active transport mechanisms and Ca^{2+} -activated non-specific cation channels.

7 CONCLUSION

The primary aim of the current study was to investigate the presence of fluctuations and oscillations in the membrane potential (i.e. the membrane potential dynamics) of Jurkat cells and HMEC-1 endothelial cells using the CWT technique. The application of the CWT technique to investigate membrane potential dynamics provides a novel approach to investigating the membrane potential recorded using the patch clamping technique. It was also hypothesised that the static membrane potential influences cell behaviours such as proliferation and activation.

The magnitude of the static membrane potential and the membrane potential dynamics of Jurkat cells in different proliferative states were investigated. These states included cells in the log phase of growth, cells in a non-proliferative state and activated Jurkat cells. The work in this thesis identified the culture conditions required to produce Jurkat cells in these different states. The Jurkat cells that were either in the log phase of growth or a non-proliferative state were achieved by simply varying the serum concentration in the culture medium; medium containing 10% FBS for Jurkat cells in the log phase of proliferation whilst 1% FBS at 48 hours caused the cells to be in a non-proliferative state. Pharmacological intervention, for example, using cytostatic drugs could have been used to regulate proliferation of the cells. These compounds, however, could have had non-specific effects on the cells, thus compromising the physiological relevance of the results. Likewise, the FBS in the culture medium could

have also had non-specific effects on the cells and thus affected the physiological relevance of the results. In fact, it can be argued that the side effects induced by compounds are more specific than FBS, consequently, the use of compounds to alter proliferation could have been better. Studies were also carried out on activated Jurkat cells which were activated through continuous treatment with ConA.

The literature suggests the magnitude of the static membrane potential of proliferating cells is depolarised in comparison to non-proliferating cells (as shown previously in Figure 1.1). In the present study, it was also shown that the magnitude of the static membrane potential of proliferating Jurkat cells was depolarised whilst the membrane potential of the non-proliferating Jurkat cells was comparatively hyperpolarised. These results are in line with the hypothesis and the literature suggests that the membrane potential could play an influencing role in cell proliferation.

It was hypothesised that the membrane potential is not static and this dynamic nature can be investigated using the CWT technique. The work in this study proves this hypothesis and shows that the membrane potential of Jurkat cells is not static, instead, it is dynamic exhibiting fluctuations. The amplitude of these fluctuations were not completely dependent on the activity of a specific channel type or the magnitude of the static membrane potential per se. Rather, the amplitude of these fluctuations appear to be dependent on the conductance of a particular ion species. For example, in situations where K^+ contributed to the static membrane potential, the fluctuations had larger amplitude in comparison to cells with a membrane potential determined primarily by the conductance of ions besides K^+ , i.e. Cl^- .

The membrane potential dynamics also changed in response to perturbations in the extracellular [ion]. This hints at the importance of ion permeability in the dynamics. An increase in the extracellular $[K^+]$ caused a significant decrease in the amplitude of the fluctuations to the extent of blocking the fluctuations whilst a decrease in the extracellular $[Cl^-]$ caused an increase in the amplitude of the membrane potential fluctuations. Similar to the effect of increasing extracellular $[K^+]$, a decrease in the extracellular $[Na^+]$ also caused a reduction the amplitude of the fluctuations. The fluctuations, however, were not completely blocked.

Although significant changes in the magnitude of the static membrane potential of the Jurkat cells in different states was observed, the membrane potential dynamics i.e. fluctuations, did not show significant differences. It is possible that the differences in the dynamic properties of the cells were not observed due to the lack of intracellular Ca^{2+} in this series of experiments. Ca^{2+} was not added in the intracellular solutions to simplify the membrane potential dynamics. It is envisaged that future studies will investigate the effect of intracellular Ca^{2+} in the membrane potential dynamics of Jurkat cells in the three different states.

Alternatively, it is also possible that the differences in the membrane potential dynamics were not observed due to the patch clamping technique itself. The whole cell patch clamping technique causes cytosolic washout, consequently, other dynamic activities in the cell, such as the metabolic activity which could have impacted the membrane potential dynamics would be lost. The metabolic activity of the cells could have itself been affected by altering the state of the cells, for example, metabolic differences would be expected in proliferating and non-proliferating Jurkat cells due to the Warburg effect (Heiden et al., 2009). Furthermore, the experimental set-up used to record the membrane potential in the present study may not accurately reflect the conditions during cell growth. The temperature, atmospheric conditions and the culture medium in the patch clamping experiment differed from the culture conditions. The experimental setup for future studies could incorporate culture chambers that are designed to control the temperature and the atmospheric conditions (Nikon, 2015).

The membrane potential dynamics of HMEC-1 endothelial cells were also investigated in light of the low frequency oscillations observed in the cardiovascular system that were hypothesised to be related to the activity of endothelial cells. The origins of the low frequency oscillations in the blood flow were associated with endothelial cells as these cells can signal to surrounding cells and influence blood flow i.e. by secreting nitric oxide (Verma et al., 2003). The low frequency oscillations in the blood flow signal had a frequency interval of 0.005 Hz to 0.0095 Hz and 0.0095 to 0.021 Hz. Consequently, to investigate these low frequency oscillations reliably, the membrane potential was recorded continuously for 30 minutes in the present study. The results suggest that fluctuations rather than oscillations were

present in the membrane potential dynamics of these cells. The preliminary data suggests that these membrane potential dynamics were altered by the presence of either ATP or Ca^{2+} in the intracellular solution. It is possible that the low frequency oscillations in the cardiovascular system were observed due to a coupling effect between adjacent endothelial cells. In the current study, only the membrane potential dynamics of single cells were investigated. Despite this, these single HMEC-1 endothelial cells still exhibited low frequency fluctuations, therefore, it is possible that low frequency oscillations are present in the membrane potential of HMEC-1 cells that have been cultured as tubules to replicate vessels *in vitro*.

In summary, analysis of the continuous membrane potential (for more than five minutes) using the CWT technique is a novel application of the CWT technique. Application of this technique in this manner can provide additional information of the membrane potential in the frequency domain. Consequently, the characteristics of fluctuations and oscillations in the membrane potential can also be investigated rather than just the magnitude of the static membrane potential at specific time points. Based on the evidence presented in this thesis, application of the CWT technique to the membrane potential has the capability of distinguishing the dynamics related to an animal cell against background noise that is not of a physiological origin. The CWT technique is a powerful analytical tool, however, a drawback of the CWT technique is that it requires a continuous uninterrupted recording of the membrane potential around a relatively stable baseline without which the results can be unreliable. The membrane potential is nonstationary (due the activation and inactivation of ion channels, pumps and carriers with time), therefore, careful consideration has to be given to normalise the initial experimental set up. The work in this thesis demonstrates that the CWT can be used to investigate the membrane potential dynamics under tightly controlled conditions.

Future Direction

The work in the present thesis provides the first evidence of the application of the CWT technique to investigate long term recordings of the membrane potential to demonstrate the presence of fluctuations in the membrane potential of Jurkat cells and

HMEC-1 cells. It is expected that future work will investigate the origin of these fluctuations and confirm if the observed fluctuations are deterministic or stochastic. It is also envisaged that the physiological role of these fluctuations will be determined in the future work.

The preliminary evidence suggests that intracellular Ca^{2+} and possibly even other intracellular components play a role in the observed fluctuations. It is therefore, expected that studies will investigate these aspects through alternative electrophysiological methodologies which maintain the cells in a more physiologically relevant state. Such techniques will need to be optimised to allow long term recordings of the membrane potential. It is also expected that the conditions used during the membrane potential recordings will reflect the conditions of the cells during cell culture.

The CWT technique in its current form could be applied to other cell types to determine if low frequency oscillatory behaviour is present in their membrane potential recordings. Cell types which have already been shown to exhibit oscillations of a large amplitude that were visible in the recordings without complex analytical techniques could also be investigated using the CWT technique to ascertain the presence of the low frequency oscillations.

It is also envisaged that the membrane potential dynamics from disease states will also be investigated. The current literature suggests that the blood flow dynamics differ with cardiovascular ageing and according to the health status of individuals (Goldberger et al., 2002; Lancaster et al., 2015; Shiogai et al., 2010).

8 GLOSSARY

Bioelectric signalling = A term used to describe cell behaviours induced by ion channel activity or the membrane potential.

ConA = A plant mitogen used to activate lymphocytes

PHA = A plant mitogen used to activate lymphocytes

Continuous wavelet transform = A technique used to analyse the frequency over time

Cytostatic = A substance that inhibits proliferation without inducing cell death

Deterministic = In the context of dynamics, it describes dynamics that are not random

Dynamic membrane potential = The membrane potential which is continually changing with time

E_{Rev} = reversal potential. The membrane potential at which point there is no net movement of an ion.

Fluctuations = Changes in the signal which do not have a predictable cycle over a time period

Frequency domain = The analysis of a signal with respect to the frequency of a characteristic

HMEC-1 = A immortalised model cell line of microvascular endothelial

IV = Current voltage plot– used to analyse the whole cell currents

Jurkat cells = An immortalised model cell line of T-lymphocytes

Mitogen = A substance that induces cell behaviour

Non stationary time signal = A signal wherein the characteristics change in a random fashion with time

NPPB = A non-specific Cl⁻ channel blocker.

Oscillations = Changes in the signal which have a predictable cycle over a time period

Patch clamping = An electrophysiological technique to record ion channel activity

Static membrane potential = The membrane potential at a single time point

TEA = A non-specific K⁺ channel blocker

4AP = A non-specific K⁺ channel blocker

Time frequency domain = The analysis of a signal with variation in time

9 REFERENCES

- Abdullaev, I.F., Rudkouskaya, A., Mongin, A.A., and Kuo, Y.-H. (2010). Calcium-activated potassium channels BK and IK1 are functionally expressed in human gliomas but do not regulate cell proliferation. In Plos One.
- Accardi, A., and Miller, C. (2004). Secondary active transport mediated by a prokaryotic homologue of ClC Cl- channels. Nature 427, 803-807.
- Adams, D.S., and Levin, M. (2012). Measuring resting membrane potential using the fluorescent voltage reporters DiBAC4(3) and CC2-DMPE. Cold Spring Harbor protocols 2012, 459-464.
- Ades, E.W., Candal, F.J., Swerlick, R.A., George, V.G., Summers, S., Bosse, D.C., and Lawley, T.J. (1992). HMEC-1 - Establishment of an immortalized human microvascular endothelial cell line. Journal of Investigative Dermatology 99, 683-690.
- Akagi, K., Nagao, T., and Urushidani, T. (1999). Correlation between Ca²⁺ oscillation and cell proliferation via CCKB/gastrin receptor. Biochimica Et Biophysica Acta-Molecular Cell Research 1452, 243-253.
- Aldrich, S. (2015). Lecin from Phaseolus Vulgaris (red kidney bean) (Sigma-Aldrich), pp. Product Specification.
- Amigorena, S., Choquet, D., Teillaud, J.L., Korn, H., and Fridman, W.H. (1990). Ion channel blockers inhibit B-cell activation at a precise stage of the G1-phase of the cell-cycle - possible involvement of K⁺ channels. Journal of Immunology 144, 2038-2045.
- Arcangeli, A., and Bechetti, A. (2006). Complex functional interaction between integrin receptors and ion channels. Trends in Cell Biology 16, 631-639.

Arcangeli, A., Bianchi, L., Becchetti, A., Faravelli, L., Coronello, M., Mini, E., Olivotto, M., and Wanke, E. (1995). A novel inward-rectifying K⁺ current with a cell-cycle dependence governs the resting potential of mammalian neuroblastoma cells. *Journal of Physiology-London* *489*, 455-471.

Aryal, P., Sansom, M.S.P., and Tucker, S.J. (2015). Hydrophobic gating in ion channels. *Journal of Molecular Biology* *427*, 121-130.

ATCC (2015). Jurkat, Clone E6-1 (ATCC® TIB-152™) (ATCC).

Azmitia, E.C. (2001). Modern views on an ancient chemical: Serotonin effects on cell proliferation, maturation, and apoptosis. *Brain Research Bulletin* *56*, 413-424.

Bading, H. (2013). Nuclear calcium signalling in the regulation of brain function. *Nature Reviews Neuroscience* *14*, 593-608.

Bartkova, J., Lukas, J., Muller, H., Lutzhoft, D., Strauss, M., and Bartek, J. (1994). Cyclin D1 protein expression and function in human breast-cancer. *International Journal of Cancer* *57*, 353-361.

Beckstein, O. (2004). Principles of gating mechanisms of ion channels. In *Laboratory of Molecular Biophysics and Merton College* (Oxford: University of Oxford), pp. 241.

Benichou, G., and Leca, G. (1989). T cell chemiluminescence a novel aspect of T cell membrane activation studied with Jurkat tumor cell line. *Journal of Cellular Biochemistry Supplement*, 253-253.

Benos, D.J., and Stanton, B.A. (1999). Functional domains within the degenerin/epithelial sodium channel (Deg/ENaC) superfamily of ion channels. *Journal of Physiology-London* *520*, 631-644.

Bernjak, A., Clarkson, P.B.M., McClintock, P.V.E., and Stefanovska, A. (2008). Low-frequency blood flow oscillations in congestive heart failure and after beta 1-blockade treatment. *Microvascular Research* *76*, 224-232.

Berridge, M.J. (1995). Calcium signalling and cell-proliferation. *Bioessays* *17*, 491-500.

Berridge, M.J., Bootman, M.D., and Roderick, H.L. (2003). Calcium signalling: Dynamics, homeostasis and remodelling. *Nature Reviews Molecular Cell Biology* *4*, 517-529.

Berridge, M.J., Lipp, P., and Bootman, M.D. (2000). The versatility and universality of calcium signalling. *Nature Reviews Molecular Cell Biology* *1*, 11-21.

Bezanilla, F. (2000). The voltage sensor in voltage-dependent ion channels. *Physiological reviews* *80*, 555-592.

Bezanilla, F., and Perozo, E. (2003). The voltage sensor and the gate in ion channels. *Membrane Proteins* *63*, 211-241.

Bhave, G., Hu, H.-J., Glauner, K.S., Zhu, W., Wang, H., Brasier, D.J., Oxford, G.S., and Gereau, R.W. (2003). Protein kinase C phosphorylation sensitizes but does not activate the capsaicin receptor transient receptor potential vanilloid 1 (TRPV1). *Proceedings of the National Academy of Sciences* *100*, 12480-12485.

Binggeli, R., and Cameron, I.L. (1980). Cellular-potentials of normal and cancerous fibroblasts and hepatocytes. *Cancer Res* *40*, 1830-1835.

Binggeli, R., and Weinstein, R.C. (1986). Membrane-potentials and sodium-channels - hypotheses for growth-regulation and cancer formation based on changes in sodium-channels and gap-junctions. *Journal of Theoretical Biology* *123*, 377-401.

Blackiston, D.J., McLaughlin, K.A., and Levin, M. (2009). Bioelectric controls of cell proliferation Ion channels, membrane voltage and the cell cycle. *Cell Cycle* *8*, 3527-3536.

Bootman, M.D. (2012). Calcium signalling. In *Cold Spring Harbor Perspectives in Biology*.

Borowiec, A.-S., Hague, F., Gouilleux-Gruart, V., Lassoued, K., and Ouadid-Ahidouch, H. (2011). Regulation of IGF-1-dependent cyclin D1 and E expression by hEag1 channels in MCF-7 cells: The critical role of hEag1 channels in G1 phase progression. *Biochimica Et Biophysica Acta-Molecular Cell Research* *1813*, 723-730.

Borowiec, A.-S., Hague, F., Harir, N., Guenin, S., Guerineau, F., Gouilleux, F., Roudbaraki, M., Lassoued, K., and Ouadid-Ahidouch, H. (2007). IGF-1 activates hEAG K(+) channels through an AKT-dependent signaling pathway in breast cancer cells: Role in cell proliferation. *Journal of Cellular Physiology* *212*, 690-701.

Bortner, C.D., and Cidlowski, J.A. (2004). The role of apoptotic volume decrease and ionic homeostasis in the activation and repression of apoptosis. *Pflugers Arch* *448*, 313-318.

Bortner, C.D., Hughes, F.M., Jr., and Cidlowski, J.A. (1997). A primary role for K⁺ and Na⁺ efflux in the activation of apoptosis. *The Journal of biological chemistry* *272*, 32436-32442.

Bose, T., Cieslar-Pobuda, A., and Wiechec, E. (2015). Role of ion channels in regulating Ca²⁺ homeostasis during the interplay between immune and cancer cells. *Cell Death Dis* *6*.

Bouis, D., Hospers, G.A.P., Meijer, C., Molema, G., and Mulder, N.H. (2001). Endothelium in vitro: A review of human vascular endothelial cell lines for blood vessel-related research. *Angiogenesis* *4*, 91-102.

Bruggemann, A., Stuhmer, W., and Pardo, L.A. (1997). Mitosis-promoting factor-mediated suppression of a cloned delayed rectifier potassium channel expressed in Xenopus oocytes. *Proceedings of the National Academy of Sciences of the United States of America* *94*, 537-542.

Cahalan, M.D., Chandy, K.G., Decoursey, T.E., and Gupta, S. (1985). A voltage-gated potassium channel in human lymphocytes-T. *Journal of Physiology-London* *358*, 197-237.

- Callahan, M.J., and Korn, S.J. (1994). Permeation of Na⁺ through a delayed rectifier K⁺ channel in chick dorsal-root ganglion neurons. *J Gen Physiol* 104, 747-771.
- Catterall, W.A. (2011). Voltage-gated calcium channels. *Cold Spring Harbor Perspectives in Biology* 3.
- Catterall, W.A., Chandy, K.G., Clapham, D.E., Gutman, G.A., Hofmann, F., Harmar, A.J., Abernethy, D.R., and Spedding, M. (2003). International Union of Pharmacology: Approaches to the nomenclature of voltage-gated ion channels. *Pharmacol Rev* 55, 573-574.
- Chen, L.X., Wang, L.W., Zhu, L.Y., Nie, S.H., Zhang, J., Zhong, P., Cai, B., Luo, H.B., and Jacob, T.J.C. (2002). Cell cycle-dependent expression of volume-activated chloride currents in nasopharyngeal carcinoma cells. *American Journal of Physiology-Cell Physiology* 283, C1313-C1323.
- Chen, L.X., Zhu, L.Y., Jacob, T.J.C., and Wang, L.W. (2007). Roles of volume-activated Cl⁻ currents and regulatory volume decrease in the cell cycle and proliferation in nasopharyngeal carcinoma cells. *Cell Proliferation* 40, 253-267.
- Cheong, A., Bingham, A.J., Li, J., Kumar, B., Sukumar, P., Munsch, C., Buckley, N.J., Neylon, C.B., Porter, K.E., Beech, D.J., *et al.*, (2005). Downregulated REST transcription factor is a switch enabling critical potassium channel expression and cell proliferation. *Molecular cell* 20, 45-52.
- Cherif, A.H., Jedlicka, D.M., Colyer, T.E., Movahedzadeh, F., and Phillips, W.B. (2012). Redesigning human body systems: Effective pedagogical strategy for promoting active learning and STEM education. *Education Research International* 2012, 17.
- Chong, J.H.A., Tapiaramirez, J., Kim, S., Toledooral, J.J., Zheng, Y.C., Boutros, M.C., Altshuller, Y.M., Frohman, M.A., Kraner, S.D., and Mandel, G. (1995). Rest - a mammalian silencer protein that restricts sodium channel gene-expression to neurons. *Cell* 80, 949-957.
- Choquet, D., and Korn, H. (1992). Mechanism of 4-aminopyridine action on voltage-gated potassium channels in lymphocytes. *J Gen Physiol* 99, 217-240.
- Cines, D.B., Pollak, E.S., Buck, C.A., Loscalzo, J., Zimmerman, G.A., McEver, R.P., Pober, J.S., Wick, T.M., Konkle, B.A., Schwartz, B.S., *et al.*, (1998). Endothelial cells in physiology and in the pathophysiology of vascular disorders. *Blood* 91, 3527-3561.
- Clarke, R.J., and Kane, D.J. (1997). Optical detection of membrane dipole potential: Avoidance of fluidity and dye-induced effects. *Biochimica Et Biophysica Acta-Biomembranes* 1323, 223-239.
- Cohen, L.B., and Salzberg, B.M. (1978). Optical measurement of membrane-potential. *Rev Physiol Biochem Pharmacol* 83, 35-88.
- Cohen, P.L., and Eisenberg, R.A. (1991). LPR and GLD - single gene models of systemic autoimmunity and lymphoproliferative disease. *Annual Review of Immunology* 9, 243-269.

Coleman, H.A., Tare, M., and Parkington, H.C. (2004). Endothelial potassium channels, endothelium-dependent hyperpolarization and the regulation of vascular tone in health and disease. *Clinical and Experimental Pharmacology and Physiology* 31, 641-649.

Cone, C.D. (1969). Electroosmotic interactions accompanying mitosis initiation in sarcoma cells in vitro. *Transactions of the New York Academy of Sciences* 31, 404-427.

Cone, C.D. (1971). Unified theory on basic mechanism of normal mitotic control and oncogenesis. *Journal of Theoretical Biology* 30, 151-181.

Cone, C.D., and Cone, C.M. (1976). Induction of mitosis in mature neurons in central nervous-system by sustained depolarization. *Science* 192, 155-158.

Cone, C.D., and Tongier, M. (1971). Control of somatic cell mitosis by simulated changes in transmembrane potential level. *Oncology* 25, 168-182.

Cone, C.D., and Tongier, M. (1973). Contact inhibition of division - involvement of electrical transmembrane potential. *Journal of Cellular Physiology* 82, 373-386.

Craig, T.J., Ashcroft, F.M., and Proks, P. (2008). How ATP inhibits the open K-ATP channel. *J Gen Physiol* 132, 131-144.

Czeisler, C.A., and Klerman, E.B. (1999). Circadian and sleep-dependent regulation of hormone release in humans. In *Recent Progress in Hormone Research*, Vol 54: Proceedings of the 1998 Conference, P.M. Conn, ed., pp. 97-132.

Dahl, S.G., Sylte, I., and Ravna, A.W. (2004). Structures and models of transporter proteins. *Journal of Pharmacology and Experimental Therapeutics* 309, 853-860.

Daut, J., Standen, N.B., and Nelson, M.T. (1994). The role of the membrane-potential of endothelial and smooth-muscle cells in the regulation of coronary blood-flow. *Journal of Cardiovascular Electrophysiology* 5, 154-181.

Day, M.L., Pickering, S.J., Johnson, M.H., and Cook, D.I. (1993). Cell-cycle control of a large-conductance K⁺-channel in mouse early embryos. *Nature* 365, 560-562.

de Queiroz, F.M., Ponte, C.G., Bonomo, A., Vianna-Jorge, R., and Suarez-Kurtz, G. (2008). Study of membrane potential in T-lymphocytes subpopulations using flow cytometry. *Bmc Immunology* 9.

Deane, K.H.O., and Mannie, M.D. (1992). An alternative pathway of B-cell activation - stilbene disulfonates interact with a cl- binding motif on AEN-related proteins to stimulate mitogenesis. *European Journal of Immunology* 22, 1165-1171.

DeCoursey, T.E., Chandy, K.G., Gupta, S., and Cahalan, M. (1984). Voltage-gated K⁺ channels in human T-lymphocytes: a role in mitogenesis? *Nature* 307, 465-468.

DeCoursey, T.E., and Cherny, V.V. (1996). Voltage-activated proton currents in human THP-1 monocytes .2. Journal of Membrane Biology *152*, 131-140.

DeCoursey, T.E., and Cherny, V.V. (1998). Temperature dependence of voltage-gated H⁺ currents in human neutrophils, rat alveolar epithelial cells, and mammalian phagocytes. J Gen Physiol *112*, 503-522.

Defries, R., and Mitsuhashi, M. (1995). Quantification of mitogen-induced human lymphocyte-proliferation - comparison of AlamarBlue assay to H-3 thymidine incorporation assay. Journal of Clinical Laboratory Analysis *9*, 89-95.

Denker, S.P., and Barber, D.L. (2002). Cell migration requires both ion translocation and cytoskeletal anchoring by the Na-H exchanger NHE1. Journal of Cell Biology *159*, 1087-1096.

Dolmetsch, R.E., Xu, K.L., and Lewis, R.S. (1998). Calcium oscillations increase the efficiency and specificity of gene expression. Nature *392*, 933-936.

Downie, B.R., Sanchez, A., Knotgen, H., Contreras-Jurado, C., Gymnopoulos, M., Weber, C., Stuhmer, W., and Pardo, L.A. (2008). Eag1 expression interferes with hypoxia homeostasis and induces angiogenesis in tumors. The Journal of biological chemistry *283*, 36234-36240.

Doyle, D.A., Cabral, J.M., Pfuetzner, R.A., Kuo, A.L., Gulbis, J.M., Cohen, S.L., Chait, B.T., and MacKinnon, R. (1998). The structure of the potassium channel: Molecular basis of K⁺ conduction and selectivity. Science *280*, 69-77.

Du, L.H., Lyle, C.S., Obey, T.B., Gaarde, W.A., Muir, J.A., Bennett, B.L., and Chambers, T.C. (2004). Inhibition of cell proliferation and cell cycle progression by specific inhibition of basal JNK activity - Evidence that mitotic Bcl-2 phosphorylation is JNK-independent. J Biol Chem *279*, 11957-11966.

Dubois, J.M., and Rouzaire-Dubois, B. (2004). The influence of cell volume changes on tumour cell proliferation. European Biophysics Journal with Biophysics Letters *33*, 227-232.

Dupont, G., Combettes, L., Bird, G.S., and Putney, J.W. (2011). Calcium oscillations. In Cold Spring Harbor Perspectives in Biology.

Dupuis, G., and Bastin, B. (1988). Lectin interactions with the Jurkat leukemic T-cell line - quantitative binding-studies and Interleukin-2 production. Journal of Leukocyte Biology *43*, 238-247.

Dupuis, G., Heroux, J., and Payet, M.D. (1989). Characterization of Ca-2+ and K-+ currents in the human Jurkat T-cell line - effects of phytohemagglutinin. Journal of Physiology-London *412*, 135-154.

Duszynski, J., Koziel, R., and Zablocki, K. (2006). Calcium signals are affected by ciprofloxacin as a consequence of reduction of mitochondrial DNA content in Jurkat cells. Febs Journal *273*, 108-108.

- Dutzler, R., Campbell, E.B., Cadene, M., Chait, B.T., and MacKinnon, R. (2002). X-ray structure of a CIC chloride channel at 3.0 angstrom reveals the molecular basis of anion selectivity. *Nature* *415*, 287-294.
- Elledge, S.J. (1996). Cell cycle checkpoints: Preventing an identity crisis. *Science* *274*, 1664-1672.
- Englund, U.H., Gertow, J., Kagedal, K., and Elinder, F. (2014). A voltage dependent non-inactivating Na⁺ channel activated during apoptosis in Xenopus Oocytes. In *Plos One*.
- Enomoto, K., Cossu, M.F., Edwards, C., and Oka, T. (1986). Induction of distinct types of spontaneous electrical-activities in mammary epithelial-cells by epidermal growth-factor and insulin. *Journal of Cell Biology* *103*, A222-A222.
- Evan, G.I., and Vousden, K.H. (2001). Proliferation, cell cycle and apoptosis in cancer. *Nature* *411*, 342-348.
- Fanger, C.M., Hoth, M., Crabtree, G.R., and Lewis, R.S. (1995). Characterization of T-cell mutants with defects in capacitative calcium-entry - genetic-evidence for the physiological roles of CRAC channels. *Journal of Cell Biology* *131*, 655-667.
- Farias, L.M.B., Ocana, D.B., Diaz, L., Larrea, F., Avila-Chavez, E., Cadena, A., Hinojosa, L.M., Lara, G., Villanueva, L.A., Vargas, C., *et al.*, (2004). Ether a go-go potassium channels as human cervical cancer markers. *Cancer Res* *64*, 6996-7001.
- Fernandez-Salas, E., Suh, K.S., Speransky, V.V., Bowers, W.L., Levy, J.M., Adams, T., Pathak, K.R., Edwards, L.E., Hayes, D.D., Cheng, C., *et al.*, (2002). mtCLIC/CLIC4, an organelular chloride channel protein, is increased by DNA damage and participates in the apoptotic response to p53. *Molecular and Cellular Biology* *22*, 3610-3620.
- Fleming, M.R., Singh, V., Jenkins, D.P., Wulff, H., and Kaczmarek, L.K. (2013). Gating modulation of the sodium-activated potassium channel KCa4. 1 (Slack) by bithionol and niclosamide. *The FASEB Journal* *27*, 913.924.
- Flynn, J.T., Westbrooks, M., and Lucas, K.A. (1997). Establishment and characterization of a line of adipose-derived human microvascular endothelial cells (HADMEC-5) transformed by simian virus 40 large T antigen expression: Application to endotoxin research. *Shock* *8*, 45-54.
- Fontaine, B., Pena, J.L., and Brette, R. (2014). Spike-threshold adaptation predicted by membrane potential dynamics in vivo. *Plos Computational Biology* *10*.
- Fontijn, R., Hop, C., Brinkman, H.J., Slater, R., Westerveld, A., Vanmourik, J.A., and Pannekoek, H. (1995). Maintenance of vascular endothelial cell-specific properties after immortalization with an amphotrophic replication-deficient retrovirus containing Human Papilloma-Virus-16 E6/E7 DNA. *Experimental Cell Research* *216*, 199-207.
- Francescone, R.A., Faibis, M., and Shao, R. (2011). A Matrigel-based tube formation assay to assess the vasculogenic activity of tumor cells. *Journal of visualized experiments : JoVE*.

Fraser, S.P., Diss, J.K.J., Lloyd, L.J., Pani, F., Chioni, A.M., George, A.J.T., and Djamgoz, M.B.A. (2004). T-lymphocyte invasiveness: control by voltage-gated Na(+) channel activity. *Febs Letters* 569, 191-194.

Freedman, B.D., Price, M.A., and Deutsch, C.J. (1992). Evidence for voltage modulation of il-2 production in mitogen-stimulated human peripheral-blood lymphocytes. *Journal of Immunology* 149, 3784-3794.

Fukumoto, T., Kema, I.P., and Levin, M. (2005). Serotonin signaling is a very early step in patterning of the left-right axis in chick and frog embryos. *Current Biology* 15, 794-803.

Fukushima, Y., Hagiwara, S., and Henkart, M. (1984). Potassium current in clonal cyto-toxic T-lymphocytes from the mouse. *Journal of Physiology-London* 351, 645-656.

Fulda, S. (2010). Evasion of apoptosis as a cellular stress response in cancer. *International journal of cell biology* 2010, 370835-370835.

Gadsby, D.C. (2009). Ion channels versus ion pumps: the principal difference, in principle. *Nature Reviews Molecular Cell Biology* 10, 344-352.

Gadsby, D.C., Vergani, P., and Csanady, L. (2006). The ABC protein turned chloride channel whose failure causes cystic fibrosis. *Nature* 440, 477-483.

Gali-Muhtasib, H., and Bakkar, N. (2002). Modulating cell cycle: current applications and prospects for future drug development. *Current Cancer Drug Targets* 2, 309-336.

Gallo, V., Zhou, J.M., McBain, C.J., Wright, P., Knutson, P.L., and Armstrong, R.C. (1996). Oligodendrocyte progenitor cell proliferation and lineage progression are regulated by glutamate receptor-mediated K⁺ channel block. *The Journal of neuroscience : the official journal of the Society for Neuroscience* 16, 2659-2670.

Gao, Z., Ure, K., Ding, P., Nashaat, M., Yuan, L., Ma, J., Hammer, R.E., and Hsieh, J. (2011). The master negative regulator REST/NRSF controls adult neurogenesis by restraining the neurogenic program in quiescent stem cells. *Journal of Neuroscience* 31, 9772-9786.

Gees, M., Colsoul, B., and Nilius, B. (2010). The role of transient receptor potential cation channels in Ca²⁺ signalling. In *Cold Spring Harbor Perspectives in Biology*.

Gelfand, E.W., Cheung, R.K., Mills, G.B., and Grinstein, S. (1987). Role of membrane-potential in the response of human T-lymphocytes to phytohemagglutinin. *Journal of Immunology* 138, 527-531.

Gerard, C., and Goldbeter, A. (2014). The balance between cell cycle arrest and cell proliferation: control by the extracellular matrix and by contact inhibition. *Interface Focus* 4.

Gericke, M., Droogmans, G., and Nilius, B. (1993). Thapsigargin discharges intracellular calcium stores and induces transmembrane currents in human endothelial-cells. *Pflugers Arch* 422, 552-557.

Gerlach, A.C., Syme, C.A., Giltinan, L., Adelman, J.P., and Devor, D.C. (2001). ATP-dependent activation of the intermediate conductance, Ca²⁺ activated K⁺ channel, hIK1, is conferred by a C-terminal domain. *J Biol Chem* 276, 10963-10970.

Giles, T.D. (2006). Circadian rhythm of blood pressure and the relation to cardiovascular events. *Journal of Hypertension* 24, S11-S16.

Gillis, S., and Watson, J. (1980). Biochemical and biological characterization of lymphocyte regulatory molecules. Identification of an Interleukin 2-producing human-leukemia T-cell line. *J Exp Med* 152, 1709-1719.

Gimbrone, M.A., Cotran, R.S., and Folkman, J. (1974). Human vascular endothelial cells in culture - growth and DNA-synthesis. *Journal of Cell Biology* 60, 673-684.

Glavinovic, M.I., and Trifaro, J.M. (1988). Quinine blockade of currents through Ca-2+-activated K⁺ channels in bovine chromaffin cells. *Journal of Physiology-London* 399, 139-152.

Goehring, I., Gerencser, A.A., Schmidt, S., Brand, M.D., Mulder, H., and Nicholls, D.G. (2012). Plasma membrane potential oscillations in insulin secreting Ins-1 832/13 cells do not require glycolysis and are not initiated by fluctuations in mitochondrial bioenergetics. *The Journal of biological chemistry* 287, 15706-15717.

Goldberger, A.L., Amaral, L.A.N., Hausdorff, J.M., Ivanov, P.C., Peng, C.K., and Stanley, H.E. (2002). Fractal dynamics in physiology: Alterations with disease and aging. *Proceedings of the National Academy of Sciences of the United States of America* 99, 2466-2472.

Golestaneh, N., Klein, C., Valamanesh, F., Suarez, G., Agarwal, M.K., and Mirshahi, M. (2001). Mineralocorticoid receptor-mediated signaling regulates the ion gated sodium channel in vascular endothelial cells and requires an intact cytoskeleton. *Biochemical and Biophysical Research Communications* 280, 1300-1306.

Golias, C.H., Charalabopoulos, A., and Charalabopoulos, K. (2004). Cell proliferation and cell cycle control: a mini review. *International Journal of Clinical Practice* 58, 1134-1141.

Gonzalez, J.E., Oades, K., Leychkis, Y., Harootunian, A., and Negulescu, P.A. (1999). Cell-based assays and instrumentation for screening ion-channel targets. *Drug Discovery Today* 4, 431-439.

Gonzalez, J.E., and Tsien, R.Y. (1997). Improved indicators of cell membrane potential that use fluorescence resonance energy transfer. *Chemistry & Biology* 4, 269-277.

Gottlieb, E., Armour, S.M., Harris, M.H., and Thompson, C.B. (2003). Mitochondrial membrane potential regulates matrix configuration and cytochrome c release during apoptosis. *Cell Death and Differentiation* 10, 709-717.

Grgic, I., Eichler, I., Heinau, P., Si, H., Brakemeier, S., Hoyer, J., and Kohler, R. (2005). Selective blockade of the intermediate-conductance Ca²⁺-activated K⁺ channel suppresses

proliferation of microvascular and macrovascular endothelial cells and angiogenesis in vivo. *Arteriosclerosis Thrombosis and Vascular Biology* 25, 704-709.

Grinstein, S., and Foskett, J.K. (1990). Ionic mechanisms of cell-volume regulation in leukocytes. *Annu Rev Physiol* 52, 399-414.

Grissmer, S., Nguyen, A.N., and Cahalan, M.D. (1993). Calcium-activated potassium channels in human T-lymphocytes -Expression levels, calcium-dependence, ion selectivity, and pharmacology. *J Gen Physiol* 102, 601-630.

Habela, C.W., Olsen, M.L., and Sontheimer, H. (2008). ClC3 is a critical regulator of the cell cycle in normal and malignant glial cells. *Journal of Neuroscience* 28, 9205-9217.

Hamill, O.P., Marty, A., Neher, E., Sakmann, B., and Sigworth, F.J. (1981). Improved patch-clamp techniques for high-resolution current recording from cells and cell-free membrane patches. *Pflugers Arch* 391, 85-100.

Hanley, P.J., Mussett, B., Renigunta, V., Limberg, S.H., Dalpke, A.H., Sus, R., Heeg, K.M., Preisig-Muller, R., and Daut, J. (2004). Extracellular ATP induces oscillations of intracellular Ca²⁺ and membrane potential and promotes transcription of IL-6 in macrophages. *Proceedings of the National Academy of Sciences of the United States of America* 101, 9479-9484.

Harrison, R.R., Kolb, I., Kodandaramaiah, S.B., Chubykin, A.A., Yang, A., Bear, M.F., Boyden, E.S., and Forest, C.R. (2015). Microchip amplifier for in vitro, in vivo, and automated whole cell patch-clamp recording. *Journal of Neurophysiology* 113, 1275-1282.

Heginbotham, L., Lu, Z., Abramson, T., and Mackinnon, R. (1994). Mutations in the K⁺ channel signature sequence. *Biophys J* 66, 1061-1067.

Hegle, A.P., Marble, D.D., and Wilson, G.F. (2006). A voltage-driven switch for ion-independent signaling by ether-a-go-go K⁺ channels. *Proceedings of the National Academy of Sciences of the United States of America* 103, 2886-2891.

Heiden, V., Cantley, M.G., and Thompson, C.B. (2009). Understanding the Warburg effect: the metabolic requirements of cell proliferation. *science* 324, 1029-1033.

Heimlich, G., and Cidlowski, J.A. (2006). Selective role of intracellular chloride in the regulation of the intrinsic but not extrinsic pathway of apoptosis in Jurkat T-cells. *J Biol Chem* 281, 2232-2241.

Hering, S., Griffin, B.E., and Strauss, M. (1991). Immortalization of human fetal sinusoidal liver-cells by Polyoma-Virus large T-antigen. *Experimental Cell Research* 195, 1-7.

Hess, S.D., Oortgiesen, M., and Cahalan, M.D. (1993). Calcium oscillations in human-t and natural-killer-cells depend upon membrane-potential and calcium influx. *Journal of Immunology* 150, 2620-2633.

Hewett, P.W., Murray, J.C., Price, E.A., Watts, M.E., and Woodcock, M. (1993). Isolation and characterization of microvessel endothelial-cells from human mammary adipose-tissue. In *Vitro Cellular & Developmental Biology-Animal* 29A, 325-331.

Hille, B. (1992). Ion channels of excitable membranes, Third Edition edn.

Hillebrand, U., Schillers, H., Riethmuller, C., Stock, C., Wilhelm, M., Oberleithner, H., and Huasberg, M. (2007). Dose-dependent endothelial cell growth and stiffening aldosterone: endothelial protection by eplerenone (vol 25, pg 639, 2007). *Journal of Hypertension* 25, 901-901.

Himmel, H.M., Whorton, A.R., and Strauss, H.C. (1993). Intracellular calcium, currents, and stimulus-response coupling in endothelial-cells. *Hypertension* 21, 112-127.

Hodgkin, A.L., and Huxley, A.F. (1952). A quantitative description of membrane current and its application to conduction and excitation in nerve. *Journal of Physiology-London* 117, 500-544.

Hodgkin, A.L., and Katz, B. (1949). The effect of sodium ions on the electrical activity of the giant axon of the squid. *Journal of Physiology-London* 108, 37-77.

Hogan, P.G., Chen, L., Nardone, J., and Rao, A. (2003). Transcriptional regulation by calcium, calcineurin, and NFAT. *Genes & Development* 17, 2205-2232.

Hu, H., Li, D.-L., Fan, L., Ren, J., Wang, S.-P., Jia, B., Liu, B.-H., Sun, L., Yu, X.-J., and Zang, W.-J. (2010). Involvement of volume-sensitive Cl⁻ channels in the proliferation of human subcutaneous pre-adipocytes. *Clinical and Experimental Pharmacology and Physiology* 37, 29-34.

Huang, L., Li, B., Li, W., Guo, H., and Zou, F. (2009). ATP-sensitive potassium channels control glioma cells proliferation by regulating ERK activity. *Carcinogenesis* 30, 737-744.

Huang, X., Dubuc, A.M., Hashizume, R., Berg, J., He, Y., Wang, J., Chiang, C., Cooper, M.K., Northcott, P.A., Taylor, M.D., *et al.*, (2012). Voltage-gated potassium channel EAG2 controls mitotic entry and tumor growth in medulloblastoma via regulating cell volume dynamics. *Genes & Development* 26, 1780-1796.

Hughes, F.M., Bortner, C.D., Purdy, G.D., and Cidlowski, J.A. (1997). Intracellular K⁺ suppresses the activation of apoptosis in lymphocytes. *J Biol Chem* 272, 30567-30576.

Huizinga, J.D., Chen, J.-H., Zhu, Y.F., Pawelka, A., McGinn, R.J., Bardakjian, B.L., Parsons, S.P., Kunze, W.A., Wu, R.Y., Bercik, P., *et al.*, (2014). The origin of segmentation motor activity in the intestine. *Nature Communications* 5.

Ince, C., Leijh, P.C.J., Meijer, J., Vanbavel, E., and Ypey, D.L. (1984). Oscillatory hyperpolarizations and resting membrane-potentials of mouse fibroblast and macrophage cell-lines. *Journal of Physiology-London* 352, 625-635.

Ince, C., Vanbavel, E., Vanduijn, B., Donkersloot, K., Coremans, A., Ypey, D.L., and Verveen, A.A. (1986). Intracellular microelectrode measurements in small-cells evaluated with the patch clamp technique *Biophys J* 50, 1203-1209.

Jackson, C.J., Garbett, P.K., Nissen, B., and Schrieber, L. (1990). Binding of human endothelium to Ulex-Europaeus I-coated dynabeads - application to the isolation of microvascular endothelium. *Journal of Cell Science* 96, 257-262.

Jaffe, E.A., Nachman, R.L., Becker, C.G., and Minick, C.R. (1973). Culture of human endothelial cells derived from umbilical veins - identification by morphologic and immunological criteria. *Journal of Clinical Investigation* 52, 2745-2756.

Jang, S.H., Byun, J.K., Jeon, W.-I., Choi, S.Y., Park, J., Lee, B.H., Yang, J.E., Park, J.B., O'Grady, S.M., Kim, D.-Y., *et al.*, (2015). Nuclear localization and functional characteristics of voltage-gated potassium channel Kv1.3. *J Biol Chem* 290, 12547-12557.

Jang, S.H., Choi, S.Y., Ryu, P.D., and Lee, S.Y. (2011). Anti-proliferative effect of Kv1.3 blockers in A549 human lung adenocarcinoma in vitro and in vivo. *European Journal of Pharmacology* 651, 26-32.

Janigro, D., Nguyen, T.S., Gordon, E.L., and Winn, H.R. (1996). Physiological properties of ATP-activated cation channels in rat brain microvascular endothelial cells. *American Journal of Physiology-Heart and Circulatory Physiology* 270, H1423-H1434.

Jaramillo, M.C., and Zhang, D.D. (2013). The emerging role of the Nrf2-Keap1 signaling pathway in cancer. *Genes & Development* 27, 2179-2191.

Javanmoghadam-Kamrani, S., and Keyomarsi, K. (2008). Synchronization of the cell cycle using lovastatin. *Cell Cycle* 7, 2434-2440.

Jentsch, T.J., Friedrich, T., Schriever, A., and Yamada, H. (1999). The CLC chloride channel family. *Pflugers Arch* 437, 783-795.

Jiang, M., Min, Y., Debusk, L., Fernandez, S., Strand, D.W., Hayward, S.W., and Lin, P.C. (2010). Spontaneous immortalization of human dermal microvascular endothelial cells. *World journal of stem cells* 2, 114-120.

Jow, F., Sullivan, K., Sokol, P., and Numann, R. (1999). Induction of Ca²⁺-activated K⁺ current and transient outward currents in human capillary endothelial cells. *Journal of Membrane Biology* 167, 53-64.

Kastan, M.B., Zhan, Q.M., Eldeiry, W.S., Carrier, F., Jacks, T., Walsh, W.V., Plunkett, B.S., Vogelstein, B., and Fornace, A.J. (1992). A mammalian-cell cycle checkpoint pathway utilizing p53 and gadd45 is defective in ataxia-telangiectasia. *Cell* 71, 587-597.

Kaupp, U.B., and Seifert, R. (2002). Cyclic nucleotide-gated ion channels. *Physiological reviews* 82, 769-824.

Kaur, S., Leszczynska, K., Abraham, S., Scarcia, M., Hiltbrunner, S., Marshall, C.J., Mavria, G., Bicknell, R., and Heath, V.L. (2011). RhoJ/TCL regulates endothelial motility and tube formation and modulates actomyosin contractility and focal adhesion numbers. *Arteriosclerosis, thrombosis, and vascular biology* 31, 657-664.

Kim, J.S., Nam, M.H., An, S.S.A., Lim, C.S., Hur, D.S., Chung, C., and Chang, J.K. (2011). Comparison of the automated fluorescence microscopic viability test with the conventional and flow cytometry methods. *Journal of Clinical Laboratory Analysis* 25, 90-94.

Kim, T.-K., Nam, Joo H., Ahn, W.-G., Kim, N.-H., Ham, H.-Y., Hong, C.-W., Nam, J.-S., Lee, J., Huh, S.-O., So, I., et al., (2013). Lys1110 of TRPM2 is critical for channel activation. *Biochemical Journal* 455, 319-327.

Kinet, S., Bernard Fau - Mongellaz, C., Mongellaz C Fau - Perreau, M., Perreau M Fau - Goldman, F.D., Goldman Fd Fau - Taylor, N., and Taylor, N. (2002). gp120-mediated induction of the MAPK cascade is dependent on the activation state of CD4(+) lymphocytes.

Koch, A.E., Polverini, P.J., Kunkel, S.L., Harlow, L.A., Dipietro, L.A., Elner, V.M., Elner, S.G., and Strieter, R.M. (1995). Variability among human umbilical vein endothelial cultures. *Science (Washington D C)* 268, 447-448.

Koch, K.S., and Leffert, H.L. (1979). Increased sodium-ion influx is necessary to initiate rat hepatocyte proliferation. *Cell* 18, 153-163.

Koni, P.A., Khanna, R., Chang, M.C., Tang, M.D., Kaczmarek, L.K., Schlichter, L.C., and Flavell, R.A. (2003). Compensatory anion currents in Kv1.3 channel-deficient thymocytes. *J Biol Chem* 278, 39443-39451.

Koopman, G., Reutelingsperger, C.P.M., Kuijten, G.A.M., Keehnen, R.M.J., Pals, S.T., and Vanoers, M.H.J. (1994). Annexin-V for flow cytometric detection of phosphatidylserine expression on B-cells undergoing apoptosis. *Blood* 84, 1415-1420.

Korn, S.J., and Ikeda, S.R. (1995). Permeation selectivity by competition in a delayed rectifier potassium channel. *Science* 269, 410-412.

Koziel, R., Szczepanowska, J., Magalska, A., Piwocka, K., Duszynski, J., and Zablocki, K. (2010). Ciprofloxacin inhibits proliferation and promotes generation of aneuploidy in Jurkat cells. *Journal of Physiology and Pharmacology* 61, 233-239.

Krammer, P.H., Arnold, R., and Lavrik, I.N. (2007). Life and death in peripheral T cells. *Nature Reviews Immunology* 7, 532-542.

Krump-Konvalinkova, V., Bittinger, F., Unger, R.E., Peters, K., Lehr, H.A., and Kirkpatrick, C.J. (2001). Generation of human pulmonary microvascular endothelial cell lines. *Laboratory Investigation* 81, 1717-1727.

Kuno, M., Kawasaki, J., and Nakamura, F. (1997). A highly temperature-sensitive proton current in mouse bone marrow-derived mast cells. *J Gen Physiol* 109, 731-740.

Kurachi, Y., Terzic, A., and Cohen, M.V. (2001). Heart physiology and pathophysiology, N. Speralakis, ed. (Academic Press), pp. 1261.

Kuriyama, H., Kitamura, K., and Nabata, H. (1995). Pharmacological and physiological significance of ion channels and factors that modulate them in vascular tissues. *Pharmacol Rev* 47, 387-573.

Kusche-Vihrog, K., Sobczak, K., Bangel, N., Wilhelmi, M., Nechyporuk-Zloy, V., Schwab, A., Schillers, H., and Oberleithner, H. (2008). Aldosterone and amiloride alter ENaC abundance in vascular endothelium. *Pflugers Arch* 455, 849-857.

Kvandal, P., Landsverk, S.A., Bernjak, A., Stefanovska, A., Kvernmo, H.D., and Kirkeboen, K.A. (2006). Low-frequency oscillations of the laser Doppler perfusion signal in human skin. *Microvascular Research* 72, 120-127.

Kvandal, P., Stefanovska, A., Veber, M., Kvenmo, H.D., and Kirkeboen, K.A. (2003). Regulation of human cutaneous circulation evaluated by laser Doppler flowmetry, iontophoresis, and spectral analysis: importance of nitric oxide and prostaglandines. *Microvascular Research* 65, 160-171.

Kvernmo, H.D., Stefanovska, A., Kirlteboen, K.A., and Kvernebo, K. (1999). Oscillations in the human cutaneous blood perfusion signal modified by endothelium-dependent and endothelium-independent vasodilators. *Microvascular Research* 57, 298-309.

Lacroix, J., Halaszovich, C.R., Schreiber, D.N., Leitner, M.G., Bezanilla, F., Oliver, D., and Villalba-Galea, C.A. (2011). Controlling the activity of a Phosphatase and Tensin Homolog (PTEN) by membrane potential. *J Biol Chem* 286, 17945-17953.

Lai, W., Chen, S., Wu, H., Guan, Y., Liu, L., Zeng, Y., Zhao, H., Jiang, J., and Chu, Z. (2011). PRL-3 promotes the proliferation of LoVo cells via the upregulation of KCNN4 channels. *Oncology Reports* 26, 909-917.

Lall, N., Henley-Smith, C.J., De Canha, M.N., Oosthuizen, C.B., and Berrington, D. (2013). Viability reagent, Prestoblue, in comparison with other available reagents, utilized in cytotoxicity and antimicrobial assays. *International journal of microbiology* 2013, 420601-420601.

Lallet-Daher, H., Roudbaraki, M., Bavencoffe, A., Mariot, P., Gackiere, F., Bidaux, G., Urbain, R., Gosset, P., Delcourt, P., Fleurisse, L., et al., (2009). Intermediate-conductance Ca²⁺-activated K⁺ channels (IKCa1) regulate human prostate cancer cell proliferation through a close control of calcium entry. *Oncogene* 28, 1792-1806.

Lancaster, G., Stefanovska, A., Pesce, M., Vezzoni, G.M., Loggini, B., Pingitore, R., Ghiara, F., Barachini, P., Cervadoro, G., Romanelli, M., et al., (2015). Dynamic markers based on blood perfusion fluctuations for selecting skin melanocytic lesions for biopsy. *Scientific Reports* 5.

Lang, F., Friedrich, F., Kahn, E., Woll, E., Hammerer, M., Waldegger, S., Maly, K., and Grunicke, H. (1991). Bradykinin-induced oscillations of cell-membrane potential in cells expressing the ha-ras oncogene. *J Biol Chem* *266*, 4938-4942.

Lea, N.C., Orr, S.J., Stoeber, K., Williams, G.H., Lam, E.W.F., Ibrahim, M.A.A., Mufti, G.J., and Thomas, N.S.B. (2003). Commitment point during G(0)→G(1) that controls entry into the cell cycle. *Molecular and Cellular Biology* *23*, 2351-2361.

Lechleiter, J.D., and Clapham, D.E. (1992). Molecular mechanisms of intracellular calcium excitability in *X. laevis* oocytes. *Cell* *69*, 283-294.

Lee, Y., and Shacter, E. (2007). Bcl-2 does not protect Burkitt's lymphoma cells from oxidant-induced cell death.

Lenardo, M., Chan, F.K.M., Hornung, F., McFarland, H., Siegel, R., Wang, J., and Zheng, L.X. (1999). Mature T-lymphocyte apoptosis - Immune regulation in a dynamic and unpredictable antigenic environment. *Annual Review of Immunology* *17*, 221-253.

Lenardo, M.J. (1991). Interleukin-2 programs mouse alpha-beta-T-lymphocytes for apoptosis. *Nature* *353*, 858-861.

Lenzi, D., Radke, K., and Wilson, M. (1991). Clonal cells from embryonic retinal cell-lines express qualitative electrophysiological differences. *Journal of Neurobiology* *22*, 823-836.

Leonard, R.J., Garcia, M.L., Slaughter, R.S., and Reuben, J.P. (1992). Selective blockers of voltage-gated K⁺ channels depolarize human T-lymphocytes - Mechanism of the antiproliferative effect of charybdotoxin. *Proceedings of the National Academy of Sciences of the United States of America* *89*, 10094-10098.

Levy, D.I., and Deutsch, C. (1996a). Recovery from C-type inactivation is modulated by extracellular potassium. *Biophys J* *70*, 798-805.

Levy, D.I., and Deutsch, C. (1996b). A voltage-dependent role for K⁺ in recovery from C-type inactivation. *Biophys J* *71*, 3157-3166.

Lewis, R.S., and Cahalan, M.D. (1988). Subset-specific expression of potassium channels in developing murine T-lymphocytes. *Science* *239*, 771-775.

Lewis, R.S., and Cahalan, M.D. (1995). Potassium and calcium channels in lymphocytes. *Annual Review of Immunology* *13*, 623-653.

Lewis, R.S., Ross, P.E., and Cahalan, M.D. (1993). Chloride channels activated by osmotic-stress in T-lymphocytes. *J Gen Physiol* *101*, 801-826.

Li, W.C., Soffe, S.R., and Roberts, A. (2004). A direct comparison of whole cell patch and sharp electrodes by simultaneous recording from single spinal neurons in frog tadpoles. *Journal of Neurophysiology* *92*, 380-386.

- Lim, H.-H., Shane, T., and Miller, C. (2012). Intracellular proton access in a Cl-/H⁺ antiporter. *Plos Biology* *10*.
- Lin, H., Li, Z., Chen, C., Luo, X., Xiao, J., Dong, D., Lu, Y., Yang, B., and Wang, Z. (2011). Transcriptional and post-transcriptional mechanisms for oncogenic overexpression of Ether A Go-Go K⁺ channel. In *Plos One*.
- Lin, J.Y. (2011). A user's guide to channelrhodopsin variants: features, limitations and future developments. *Experimental Physiology* *96*, 19-25.
- Ling, G., and Gerard, R.W. (1949). The normal membrane potential of Frog Sartorius Fibers. *Journal of Cellular and Comparative Physiology* *34*, 383-396.
- Lipskaia, L., and Lompre, A.M. (2004). Alteration in temporal kinetics of Ca²⁺ signaling and control of growth and proliferation. *Biology of the Cell* *96*, 55-68.
- Lisal, J., and Maduke, M. (2008). The ClC-0 chloride channel is a 'broken' Cl(-)/H(+) antiporter. *Nature Structural & Molecular Biology* *15*, 805-810.
- Lodish, H., Berk, A., Matsudaira, P., Kaiser, C., Scott, M., Krieger, M., Zipursky, S.L., Darnell, J. (2004). *Molecular cell biology*, 5th Edition edn (New York: W. H. Freeman and Company).
- Loew, L.M. (2010). Design and Use of Organic Voltage Sensitive Dyes.
- Loo, D.D.F., Eskandari, S., Hirayama, B.A., and Wright, E.M. (2002). A kinetic model for secondary active transport, Vol 129 (New York: Springer).
- Lotz, M.M., Wang, H., Song, J.C., Pories, S.E., and Matthews, J.B. (2004). K⁺ channel inhibition accelerates intestinal epithelial cell wound healing. *Wound Repair and Regeneration* *12*, 565-574.
- Lynch, K., Fernandez, G., Pappalardo, A., and Peluso, J.J. (2000). Basic fibroblast growth factor inhibits apoptosis of spontaneously immortalized granulosa cells by regulating intracellular free calcium levels through a protein kinase C δ -dependent pathway. *Endocrinology* *141*, 4209-4217.
- Macfarlane, S.N., and Sontheimer, H. (2000a). Changes in ion channel expression accompany cell cycle progression of spinal cord astrocytes. *Glia* *30*, 39-48.
- MacFarlane, S.N., and Sontheimer, H. (2000b). Modulation of Kv1.5 currents by Src tyrosine phosphorylation: Potential role in the differentiation of astrocytes. *Journal of Neuroscience* *20*, 5245-5253.
- Macian, F. (2005). NFAT proteins: Key regulators of T-cell development and function. *Nature Reviews Immunology* *5*, 472-484.
- MacKinnon, R. (2003). Potassium channels. *Febs Letters* *555*, 62-65.

- Madhavan, H. (2007). Simple Laboratory methods to measure cell proliferation using DNA synthesis property. *Journal of stem cells & regenerative medicine* *3*, 12-14.
- Maher, S., Toomey, D., Condron, C., and Bouchier-Hayes, D. (2002). Activation-induced cell death: The controversial role of Fas and Fas ligand in immune privilege and tumour counterattack. *Immunology and Cell Biology* *80*, 131-137.
- Mair, N., Frick, M., Meraner, A., Schramek, H., and Dietl, P. (1998). Long-term induction of a unique Cl⁻ current by endothelin-1 in an epithelial cell line from rat lung: evidence for regulation of cytoplasmic calcium. *Journal of Physiology-London* *511*, 55-65.
- Maltsev, V.A. (1990). Oscillating and triggering properties of t-cell membrane-potential. *Immunology Letters* *26*, 277-282.
- Marek, N., Mysliwska, J., Raczynska, K., and Trzonkowski, P. (2010). Membrane potential of CD4(+) T cells is a subset specific feature that depends on the direct cell-to-cell contacts with monocytes. *Human Immunology* *71*, 666-675.
- Marino, A.A., Morris, D.M., Schwalke, M.A., Iliev, I.G., and Rogers, S. (1994). Electrical potential measurements in human breast-cancer and benign lesions. *Tumor Biology* *15*, 147-152.
- Marom, S., and Levitan, I.B. (1994). State-dependent inactivation of the Kv3 potassium channel. *Biophys J* *67*, 579-589.
- Marunaka, Y., Niisato, H., O'Brodovich, H., and Eaton, D.C. (1999). Regulation of an amiloride-sensitive Na⁺-permeable channel by a beta(2)-adrenergic agonist, cytosolic Ca²⁺ and Cl⁻ in fetal rat alveolar epithelium. *Journal of Physiology-London* *515*, 669-683.
- Matteson, D.R., and Deutsch, C. (1984). K-channels in T-lymphocyte - A patch clamp study using monoclonal-antibody adhesion. *Nature* *307*, 468-471.
- Meyer, R., and Heinemann, S.H. (1998). Characterization of an eag-like potassium channel in human neuroblastoma cells. *Journal of Physiology (Cambridge)* *50*, 49-56.
- Meyer, R., Schonherr, R., Gavrilova-Ruch, O., Wohlrab, W., and Heinemann, S.H. (1999). Identification of ether a go-go and calcium-activated potassium channels in human melanoma cells. *Journal of Membrane Biology* *171*, 107-115.
- Miao, K., Wondergem, R., Hossler, F.E., and Joyner, W.L. (1993). Contributions of K⁺, Na⁺, and Cl⁻ to the membrane-potential of intact Hamster vascular endothelial-cells. *Journal of Cellular Physiology* *156*, 550-559.
- Miller, E.W., Lin, J.Y., Frady, E.P., Steinbach, P.A., Kristan, W.B., Jr., and Tsien, R.Y. (2012). Optically monitoring voltage in neurons by photo-induced electron transfer through molecular wires. *Proceedings of the National Academy of Sciences of the United States of America* *109*, 2114-2119.

Millership, J.E., Devor, D.C., Hamilton, K.L., Balut, C.M., Bruce, J.E., and Fearon, I.M. (2011). Calcium-activated K⁺ channels increase cell proliferation independent of K⁺ conductance. *American Journal of Physiology-Cell Physiology* 300, C792-802.

Ming, L., Sakaida, T., Yue, W., Jha, A., Zhang, L., and Yu, J. (2008). Sp1 and p73 activate PUMA following serum starvation. *Carcinogenesis* 29, 1878-1884.

Miura, R.M. (2002). Analysis of excitable cell models. *Journal of Computational and Applied Mathematics* 144, 29-47.

Molleman, A. (2003). Patch clamping: an introductory guide to patch clamp electrophysiology (Chichester, England: Wiley).

Moller, B., Vaag, A., and Johansen, T. (1990). Ouabain inhibition of the sodium-potassium pump - estimation of ED50 in different types of human-leukocytes invitro. *British Journal of Clinical Pharmacology* 29, 93-100.

Morais-Cabral, J.H., Zhou, Y.F., and MacKinnon, R. (2001). Energetic optimization of ion conduction rate by the K⁺ selectivity filter. *Nature* 414, 37-42.

Morth, J.P., Pedersen, B.P., Toustrup-Jensen, M.S., Sorensen, T.L.M., Petersen, J., Andersen, J.P., Vilse, B., and Nissen, P. (2007). Crystal structure of the sodium-potassium pump. *Nature* 450, 1043-U1046.

Movafagh, A., Heydary, H., Mortazavi-Tabatabaei, S.A., and Azargashb, E. (2011). The significance application of indigenous phytohemagglutinin (PHA) mitogen on metaphase and cell culture procedure. *Iranian Journal of Pharmaceutical Research* 10, 895-903.

Murata, Y., Iwasaki, H., Sasaki, M., Inaba, K., and Okamura, Y. (2005). Phosphoinositide phosphatase activity coupled to an intrinsic voltage sensor. *Nature* 435, 1239-1243.

Murlas, C.G., Gulati, A., Singh, G., and Najmabadi, F. (1995). Endothelin-1 stimulates proliferation of normal airway epithelial cells. *Biochem Biophys Res Commun* 212, 953-959.

Muruganandam, A., Herx, L.M., Monette, R., Durkin, J.P., and Stanimirovic, D.B. (1997). Development of immortalized human cerebromicrovascular endothelial cell line as an in vitro model of the human blood-brain barrier. *Faseb Journal* 11, 1187-1197.

Muto, S., Nemoto, J., Okada, K., Miyata, Y., Kawakami, K., Saito, T., and Asano, Y. (2000). Intracellular Na⁺ directly modulates Na⁺,K⁺-ATPase gene expression in normal rat kidney epithelial cells. *Kidney International* 57, 1617-1635.

Myssina, S., Lang, P.A., Kempe, D.S., Kaiser, S., Huber, S.M., Wieder, T., and Lang, F. (2004). Cl⁻ channel blockers NPPB and niflumic acid blunt Ca²⁺-induced erythrocyte "apoptosis". *Cellular Physiology and Biochemistry* 14, 241-248.

Nadler, M.J.S., Hermosura, M.C., Inabe, K., Perraud, A.L., Zhu, Q.Q., Stokes, A.J., Kurosaki, T., Kinet, J.P., Penner, R., Scharenberg, A.M., *et al.*, (2001). LTRPC7 is a Mg ATP-regulated divalent cation channel required for cell viability. *Nature* *411*, 590-595.

Nanazashvili, M., Li, H., Palmer, L.G., Walters, D.E., and Sackin, H. (2007). Moving the pH gate of the Kir1.1 inward rectifier channel. *Channels (Austin, Tex)* *1*, 21-28.

Nason, G. (2006). Stationary and non-stationary time series (London: Geological Society).

Nelson, B.H. (2004). IL-2, regulatory T cells, and tolerance. *Journal of Immunology* *172*, 3983-3988.

Nguyen, T., and Russell, J. (2001). The regulation of FasL expression during activation-induced cell death (AICD). *Immunology* *103*, 426-434.

Nikon (2015). Culture chambers for live-cell imaging.

Niles, A.L., Moravec, R.A., and Riss, T.L. (2009). In vitro viability and cytotoxicity testing and same-well multi-parametric combinations for high throughput screening. *Current chemical genomics* *3*, 33-41.

Nilius, B., Droogmans, G., Gericke, M., and Schwarz, G. (1993). Nonselective ion pathways in human endothelial cells. In *Experientia Supplementum*, D. Siemen, and J. Hescheler, eds. (Birkhaeuser Verlag, P. O. Box 133, CH-4010 Basel, Switzerland; Birkhaeuser Boston, Inc., 175 Fifth Avenue, New York, New York 10010, USA), pp. 269-280.

Nilius, B., Eggermont, J., Voets, T., and Droogmans, G. (1996). Volume-activated Cl⁻ channels. *General Pharmacology* *27*, 1131-1140.

Nilius, B., Prenen, J., Kamouchi, M., Viana, F., Voets, T., and Droogmans, G. (1997a). Inhibition by mibepradil, a novel calcium channel antagonist, of Ca(2+)- and volume-activated Cl⁻ channels in macrovascular endothelial cells. *Br J Pharmacol* *121*, 547-555.

Nilius, B., Prenen, J., Szucs, G., Wei, L., Tanzi, F., Voets, T., and Droogmans, G. (1997b). Calcium-activated chloride channels in bovine pulmonary artery endothelial cells. *Journal of Physiology-London* *498*, 381-396.

Nilius, B., and Riemann, D. (1990). Ion channels in human endothelial-cells. *General Physiology and Biophysics* *9*, 89-112.

Nimigean, C.M., and Allen, T.W. (2011). Origins of ion selectivity in potassium channels from the perspective of channel block. *J Gen Physiol* *137*, 405-413.

Nisato, R.E., Harrison, J.A., Buser, R., Orci, L., Rinsch, C., Montesano, R., Dupraz, P., and Pepper, M.S. (2004). Generation and characterization of telomerase transfected human lymphatic endothelial cells with an extended life span. *American Journal of Pathology* *165*, 11-24.

Nishimoto, I., Wagner, J.A., Schulman, H., and Gardner, P. (1991). Regulation of Cl⁻ channels by multifunctional CAM kinase. *Neuron* 6, 547-555.

O'Malley, D.M. (1994). Calcium permeability of the neuronal nuclear envelope: evaluation using confocal volumes and intracellular perfusion. *The Journal of neuroscience : the official journal of the Society for Neuroscience* 14, 5741-5758.

Odonnell, M.E., Cragoe, E., and Villereal, M.L. (1983). Inhibition of Na⁺ influx and DNA-synthesis in human-fibroblasts and neuroblastoma-glioma hybrid-cells by amiloride analogues. *Journal of Pharmacology and Experimental Therapeutics* 226, 368-372.

Ogden, D.a.S., P. (1994). Patch clamp techniques for single channel and whole-cell recording (Cambridge: The Company of Biologists Ltd.).

Oike, M., Droogmans, G., Casteels, R., and Nilius, B. (1993). Electrogenic Na⁺/K⁺-transport in human endothelial-cells. *Pflugers Arch* 424, 301-307.

Okada, Y., Tsuchiya, W., and Inouye, A. (1979). Oscillations of membrane-potential in l-cells 4. Role of intracellular Ca²⁺ in hyperpolarizing excitability. *Journal of Membrane Biology* 47, 357-376.

Ooms, L.M., Horan, K.A., Rahman, P., Seaton, G., Gurung, R., Kethesparan, D.S., and Mitchell, C.A. (2009). The role of the inositol polyphosphate 5-phosphatases in cellular function and human disease. *Biochemical Journal* 419, 29-49.

Ouadid-Ahidouch, H., and Ahidouch, A. (2013). K⁺ channels and cell cycle progression in tumor cells. *Frontiers in Physiology* 4.

Ouadid-Ahidouch, H., Le Bourhis, X., Roudbaraki, M., Toillon, R.A., Delcourt, P., and Prevarskaya, N. (2001). Changes in the K⁺ current-density of MCF-7 cells during progression through the cell cycle: Possible involvement of a h-ether.a-gogo K⁺ channel. *Receptors & Channels* 7, 345-356.

Ouadid-Ahidouch, H., Roudbaraki, M., Delcourt, P., Ahidouch, A., Joury, N., and Prevarskaya, N. (2004). Functional and molecular identification of intermediate-conductance Ca²⁺-activated K⁺ channels in breast cancer cells: association with cell cycle progression. *American Journal of Physiology-Cell Physiology* 287, C125-C134.

Ousingsawat, J., Spitzner, M., Puntheeranurak, S., Terracciano, L., Tornillo, L., Bubendorf, L., Kunzelmann, K., and Schreiber, R. (2007). Expression of voltage-gated potassium channels in human and mouse colonic carcinoma. *Clinical Cancer Research* 13, 824-831.

Ousingsawat, J., Spitzner, M., Schreiber, R., and Kunzelmann, K. (2008). Upregulation of colonic ion channels in APC (Min/+) mice. *Pflugers Archiv : European journal of physiology* 456, 847-855.

Palutke, M., Kukuruga, D., and Tabaczka, P. (1987). A flow cytometric method for measuring lymphocyte-proliferation directly from tissue-culture plates using Ki-67 and propidium iodide. *Journal of Immunological Methods* 105, 97-105.

Pandiella, A., Magni, M., Lovisolo, D., and Meldolesi, J. (1989). The effects of epidermal growth-factor on membrane-potential - rapid hyperpolarization followed by persistent fluctuations. *J Biol Chem* 264, 12914-12921.

Pandiella, A., Malgaroli, A., Meldolesi, J., and Vicentini, L.M. (1987). EGF raises cytosolic Ca²⁺ in A431 and Swiss 3T3 cells by a dual mechanism - redistribution from intracellular stores and stimulated influx. *Experimental Cell Research* 170, 175-185.

Panyi, G., Varga, Z., and Gaspar, R. (2004). Ion channels and lymphocyte activation. *Immunology Letters* 92, 55-66.

Pappas, C.A., and Ritchie, J.M. (1998). Effect of specific ion channel blockers on cultured Schwann cell proliferation. *Glia* 22, 113-120.

Pappone, P.A., and Ortiz-Miranda, S.I. (1993). Blockers of voltage-gated potassium channels inhibit proliferation of cultured brown fat cells. *American Journal of Physiology* 264, C1014-C1019.

Pardo, L.A. (2004). Voltage-gated potassium channels in cell proliferation. *Physiology* 19, 285-292.

Pardo, L.A., del Camino, D., Sanchez, A., Alves, F., Bruggemann, A., Beckh, S., and Stuhmer, W. (1999). Oncogenic potential of EAG K⁺ channels. *Embo Journal* 18, 5540-5547.

Pawelec, G., Borowitz, A., Krammer, P.H., and Wernet, P. (1982). Constitutive interleukin-2 production by the Jurkat human-leukemic T-cell line. *European Journal of Immunology* 12, 387-392.

Pearson (2010). The living unit (Pearson Education).

Pender, M.P. (1999). Activation-induced apoptosis of autoreactive and alloreactive T-lymphocytes in the target organ as a major mechanism of tolerance. *Immunology and Cell Biology* 77, 216-223.

Peres, A., and Giovannardi, S. (1990). Mitogen-induced oscillations of membrane-potential and ca-2+ in human fibroblasts. *Febs Letters* 261, 35-38.

Perez, F.R., Venegas, F., Gonzalez, M., Andres, S., Vallejos, C., Riquelme, G., Sierralta, J., and Michea, L. (2009). Endothelial epithelial sodium channel inhibition activates endothelial nitric oxide synthase via phosphoinositide 3-kinase/Akt in small-diameter mesenteric arteries. In *Hypertension*, pp. 1000-1007.

Perl, A., Gergely, P., Puskas, F., and Banki, K. (2002). Metabolic switches of T-cell activation and apoptosis. *Antioxidants & Redox Signaling* 4, 427-443.

Petrenko, A.B., Yamakura, T., Baba, A., and Shimoji, K. (2003). The role of N-methyl-D-aspartate (NMDA) receptors in pain: A review. *Anesthesia and Analgesia* 97, 1108-1116.

Phipps, D.J., Branch, D.R., and Schlichter, L.C. (1996). Chloride-channel block inhibits T-lymphocyte activation and signalling. *Cellular signalling* 8, 141-149.

Picollo, A., and Pusch, M. (2005). Chloride/proton antiporter activity of mammalian CLC proteins CLC-4 and CLC-5. *Nature* 436, 420-423.

Pinton, P., Giorgi, C., Siviero, R., Zecchini, E., and Rizzuto, R. (2008). Calcium and apoptosis: ER-mitochondria Ca²⁺ transfer in the control of apoptosis. *Oncogene* 27, 6407-6418.

Preussat, K., Beetz, C., Schrey, M., Kraft, R., Wolf, S., Kalff, R., and Patt, S. (2003). Expression of voltage-gated potassium channels Kv1.3 and Kv1.5 in human gliomas. *Neuroscience Letters* 346, 33-36.

Prior, I.A., Lewis, P.D., and Mattos, C. (2012). A comprehensive survey of Ras mutations in cancer. *Cancer Res* 72, 2457-2467.

PromoKine (2015). Membrane potential sensitive dyes.

Puro, D.G., Roberge, F., and Chan, C.C. (1989). Retinal glial cell proliferation and ion channels: a possible link. *Investigative ophthalmology & visual science* 30, 521-529.

Quent, V.M.C., Loessner, D., Friis, T., Reichert, J.C., and Hutmacher, D.W. (2010). Discrepancies between metabolic activity and DNA content as tool to assess cell proliferation in cancer research. *Journal of Cellular and Molecular Medicine* 14, 1003-1013.

R&D systems, i. (2015). Quantikine ELISA: Human IL-2 Immunoassay. In R&D Systems.

Rae, J.L., Dewey, J., Cooper, K., and Gates, P. (1990). Potassium channel in rabbit corneal endothelium activated by external anions. *Journal of Membrane Biology* 114, 29-36.

Rao, V.R., Perez-Neut, M., Kaja, S., and Gentile, S. (2015). Voltage-gated ion channels in cancer cell proliferation. *Cancers* 7, 849-875.

Reuss, L. (2011). Ion transport across nonexcitable membranes. In eLS (<http://onlinelibrary.wiley.com/doi/10.1002/9780470015902.a0001264.pub3/full>).

Rizzuto, R., and Pozzan, T. (2006). Microdomains of intracellular Ca²⁺: molecular determinants and functional consequences. *Physiological reviews* 86, 369-408.

Rosenbaum, T., Gordon-Shaag, A., Munari, M., and Gordon, S.E. (2004). Ca²⁺/calmodulin modulates TRPV1 activation by capsaicin. *J Gen Physiol* 123, 53-62.

Rosner, M., Schipany, K., and Hengstschlaeger, M. (2013). Merging high-quality biochemical fractionation with a refined flow cytometry approach to monitor nucleocytoplasmic protein expression throughout the unperturbed mammalian cell cycle. *Nature Protocols* 8, 602-626.

- Ross, P.E., Garber, S.S., and Cahalan, M.D. (1994). Membrane chloride conductance and capacitance in Jurkat T-lymphocytes during osmotic swelling. *Biophys J* 66, 169-178.
- Sarantopoulos, C. (2007). Perforated patch-clamp techniques. In *Neuromethods*, W. Walz, ed., pp. 253-293.
- Sarkadi, B., Tordai, A., and Gardos, G. (1990). Membrane depolarization selectively inhibits receptor-operated calcium channels in human-T (Jurkat) Lymphoblasts. *Biochimica Et Biophysica Acta* 1027, 130-140.
- Schilling, T., Gratopp, A., DeCoursey, T.E., and Eder, C. (2002). Voltage-activated proton currents in human lymphocytes. *Journal of Physiology-London* 545, 93-105.
- Schlichter, L.C., Sakellaropoulos, G., Ballyk, B., Pennefather, P.S., and Phipps, D.J. (1996). Properties of K⁺ and Cl⁻ channels and their involvement in proliferation of rat microglial cells. *Glia* 17, 225-236.
- Schmid, A., Blum, R., and Krause, E. (1998). Characterization of cell volume-sensitive chloride currents in freshly prepared and cultured pancreatic acinar cells from early postnatal rats. *Journal of Physiology-London* 513, 453-465.
- Schmitz, C., Perraud, A.L., Johnson, C.O., Inabe, K., Smith, M.K., Penner, R., Kurosaki, T., Fleig, A., and Scharenberg, A.M. (2003). Regulation of vertebrate cellular Mg²⁺ Homeostasis by TRPM7. *Cell* 114, 191-200.
- Schneider, U., Schwenk, H.U., and Bornkamm, G. (1977). Characterization of EBV-genome negative null and T-cell lines derived from children with acute lymphoblastic leukemia and leukemic transformed non-Hodgkin lymphoma. *International Journal of Cancer* 19, 621-626.
- Schoenherr, C.J., and Anderson, D.J. (1995). The neuron-restrictive silencer factor (NRSF) - a coordinate repressor of multiple neuron-specific genes. *Science* 267, 1360-1363.
- Schreiber, M., and Salkoff, L. (1997). A novel calcium-sensing domain in the BK channel. *Biophys J* 73, 1355-1363.
- Schumacher, P.A., Sakellaropoulos, G., Phipps, D.J., and Schlichter, L.C. (1995). Small-conductance chloride channels in human peripheral T-lymphocytes. *Journal of Membrane Biology* 145, 217-232.
- Schutz, M., Teifel, M., and Friedl, P. (1997). Establishment of a human placental endothelial cell line with extended life span after transfection with SV 40 T-antigens. *European Journal of Cell Biology* 74, 315-320.
- Segal, S.S., Welsh, D.G., and Kurjiaka, D.T. (1999). Spread of vasodilatation and vasoconstriction along feed arteries and arterioles of hamster skeletal muscle. *Journal of Physiology-London* 516, 283-291.

Seltman, H. (2012). Experimental Design for Behavioral and Social Sciences (Carnegie Mellon University).

Sen, C.K., Roy, S., and Packer, L. (1996). Involvement of intracellular Ca²⁺ in oxidant-induced NF-kappa B activation (vol 385, pg 58, 1996). *Febs Letters* 390, 241-241.

Shao, R., and Guo, X. (2004). Human microvascular endothelial cells immortalized with human telomerase catalytic protein: a model for the study of in vitro angiogenesis. *Biochemical and Biophysical Research Communications* 321, 788-794.

Shiogai, Y., Stefanovska, A., and McClintock, P.V.E. (2010). Nonlinear dynamics of cardiovascular ageing. *Physics Reports-Review Section of Physics Letters* 488, 51-110.

Sigel, H. (1983). Metal ions in biological systems: Calcium and its role in biology, Vol 17 (New York: Marcel Dekker, Inc.).

Spruston, N., and Johnston, D. (1992). Perforated patch-clamp analysis of the passive membrane-properties of 3 classes of hippocampal-neurons. *Journal of Neurophysiology* 67, 508-529.

Stanford, J.S., Lieberman, S.L., Wong, V.L., and Ruderman, J.V. (2003). Regulation of the G2/M transition in oocytes of *Xenopus tropicalis*. *Developmental Biology* 260, 438-448.

Starkus, J.G., Kuschel, L., Rayner, M.D., and Heinemann, S.H. (1997). Ion conduction through C-type inactivated Shaker channels. *J Gen Physiol* 110, 539-550.

Staton, C.A., Reed, M.W., and Brown, N.J. (2009). A critical analysis of current in vitro and in vivo angiogenesis assays. *International journal of experimental pathology* 90, 195-221.

Stefanovska, A. (2007a). The brain, the heart and the vasculature: Complex but uncomplicated interactions. *Inflammation Research* 56, S231-S232.

Stefanovska, A. (2007b). Coupled oscillators - Complex but not complicated cardiovascular and brain interactions. *Ieee Engineering in Medicine and Biology Magazine* 26, 25-29.

Stefanovska, A., and Bracic, M. (1999). Physics of the human cardiovascular system. *Contemporary Physics* 40, 31-55.

Stefanovska, A., Bracic, M., and Kvernmo, H.D. (1999). Wavelet analysis of oscillations in the peripheral blood circulation measured by laser Doppler technique. *IEEE Trans Biomed Eng* 46, 1230-1239.

Stern, R.G., Milestone, B.N., and Gatenby, R.A. (1999). Carcinogenesis and the plasma membrane. *Medical hypotheses* 52, 367-372.

Sterratt, D.C. (2014). Nomenclature of Ion Channels (IUPHAR Scheme).

Stillwel, E.F., Cone, C.M., and Cone, C.D. (1973). Stimulation of DNA-synthesis in CNS neurons by sustained depolarization. *Nature-New Biology* 246, 110-111.

Strober, W. (2001). Trypan blue exclusion test of cell viability. Current protocols in immunology / edited by John E Coligan [et al] Appendix 3, 3B-Appendix 3B.

Stuart, G.J., and Palmer, L.M. (2006). Imaging membrane potential in dendrites and axons of single neurons. *Pflugers Arch* 453, 403-410.

Stutzin, A., Eguiguren, A.L., Cid, L.P., and Sepulveda, F.V. (1997). Modulation by extracellular Cl⁻ of volume-activated organic osmolyte and halide permeabilities in HeLa cells. *American Journal of Physiology-Cell Physiology* 273, C999-C1007.

Suh, K.S., Mutoh, M., Gerdes, M., Crutchley, J.M., Mutoh, T., Edwards, L.E., Dumont, R.A., Sodha, P., Cheng, C., Glick, A., et al., (2005). Antisense suppression of the chloride intracellular channel family induces apoptosis, enhances tumor necrosis factor alpha-induced apoptosis, and inhibits tumor growth. *Cancer Res* 65, 562-571.

Sukul, N.C., and Sukul, A. (2006). High Dilution Effects: Physical and Biochemical Basis (New York: Kluwer Academic Publishers), pp. 90-91.

Sumpio, B.E., Riley, J.T., and Dardik, A. (2002). Cells in focus: endothelial cell. *International Journal of Biochemistry & Cell Biology* 34, 1508-1512.

Sundelacruz, S., Levin, M., and Kaplan, D.L. (2009). Role of Membrane Potential in the Regulation of Cell Proliferation and Differentiation. *Stem Cell Reviews and Reports* 5, 231-246.

Svirskis, G., Gutman, A., and Hounsgaard, J. (1997). Detection of a membrane shunt by DC field polarization during intracellular and whole cell recording. *Journal of Neurophysiology* 77, 579-586.

Swann, K., Igusa, Y., and Miyazaki, S. (1989). Evidence for an inhibitory effect of protein kinase-C on G-protein-mediated repetitive calcium transients in hamster eggs. *Embo Journal* 8, 3711-3718.

Tajima, N., Itokazu, Y., Korpi, E.R., Somerharju, P., and Kakela, R. (2011). Activity of BKca channel is modulated by membrane cholesterol content and association with Na⁺/K⁺-atpase in human melanoma IGR39 cells. *J Biol Chem* 286, 5624-5638.

Takahashi, A., Yamaguchi, H., and Miyamoto, H. (1994). Change in density of K⁺ current of HeLa cells during the cell cycle. *The Japanese journal of physiology* 44 Suppl 2, S321-324.

Tang, Y.B., Liu, Y.J., Zhou, J.G., Wang, G.L., Qiu, Q.Y., and Guan, Y.Y. (2008). Silence of ClC-3 chloride channel inhibits cell proliferation and the cell cycle via G(1)/S phase arrest in rat basilar arterial smooth muscle cells. *Cell Proliferation* 41, 775-785.

Tao, Y.M., Yan, D., Yang, Q.Y., Zeng, R., and Wang, Y.Z. (2006). Low K⁺ promotes NF-kappa B/DNA binding in neuronal apoptosis induced by K⁺ loss. *Molecular and Cellular Biology* 26, 1038-1050.

Taub, M. (1978). Isolation of amiloride-resistant clones from dog kidney epithelial-cells. *Somatic Cell Genetics* 4, 609-616.

Terri Sundquist, M.S., Rich Moravec, B.S., Andrew Niles, M.S., Martha O'brien, Ph.D., and Terry Riss, Ph.D (2006). Time Apoptosis Assays. In *Cell Notes* (Promega Corporation), pp. 18-21.

Thompson, G.J., Langlais, C., Cain, K., Conley, E.C., and Cohen, G.M. (2001). Elevated extracellular K⁺ inhibits death-receptor- and chemical-mediated apoptosis prior to caspase activation and cytochrome c release. *Biochemical Journal* 357, 137-145.

Timmerman, L.A., Clipstone, N.A., Ho, S.N., Northrop, J.P., and Crabtree, G.R. (1996). Rapid shuttling of NF-AT in discrimination of Ca²⁺ signals and immunosuppression. *Nature* 383, 837-840.

Tran, Q.K., Ohashi, K., and Watanabe, H. (2000). Calcium signalling in endothelial cells. *Cardiovascular Research* 48, 13-22.

Truskey, G.A. (2010). Endothelial cell vascular smooth muscle cell co-culture assay for high throughput screening assays for discovery of anti-angiogenesis agents and other therapeutic molecules. *International journal of high throughput screening* 2010, 171-181.

Tsien, R.Y., Pozzan, T., and Rink, T.J. (1982). T-cell mitogens cause early changes in cytoplasmic free Ca²⁺ and membrane-potential in lymphocytes. *Nature* 295, 68-71.

Ueda, S., Lee, S.L., and Fanburg, B.L. (1990). Chloride efflux in cyclic AMP-induced configurational change of bovine pulmonary-artery endothelial-cells. *Circulation Research* 66, 957-967.

Uhlen, P., and Fritz, N. (2010). Biochemistry of calcium oscillations. *Biochemical and Biophysical Research Communications* 396, 28-32.

Ullrich, N. (1999). The role of ion channels in cell proliferation. *Neuroscientist* 5, 70-73.

Ullrich, N., and Sontheimer, H. (1996). Biophysical and pharmacological characterization of chloride currents in human astrocytoma cells. *American Journal of Physiology-Cell Physiology* 270, C1511-C1521.

Urrego, D., Tomczak, A.P., Zahed, F., Stuhmer, W., and Pardo, L.A. (2014). Potassium channels in cell cycle and cell proliferation. *Philos Trans R Soc B-Biol Sci* 369.

Vasiliou, V., Vasiliou, K., and Nebert, D.W. (2009). Human ATP-binding cassette (ABC) transporter family. *Human Genomics* 3, 281-290.

- Vay, L., Gu, C., and McNaughton, P.A. (2012). The thermo-TRP ion channel family: properties and therapeutic implications. *British Journal of Pharmacology* *165*, 787-801.
- Venetsanakos, E., Mirza, A., Fanton, C., Romanov, S.R., Tlsty, T., and McMahon, M. (2002). Induction of tubulogenesis in telomerase-immortalized human microvascular endothelial cells by glioblastoma cells. *Experimental Cell Research* *273*, 21-33.
- Verma, S., Buchanan, M.R., and Anderson, T.J. (2003). Endothelial function testing as a biomarker of vascular disease. *Circulation* *108*, 2054-2059.
- Vermeulen, K., Van Bockstaele, D.R., and Berneman, Z.N. (2003). The cell cycle: a review of regulation, deregulation and therapeutic targets in cancer. *Cell Proliferation* *36*, 131-149.
- Vicente, R., Escalada, A., Coma, M., Fuster, G., Sanchez-Tillo, E., Lopez-Iglesias, C., Soler, C., Solsona, C., Celada, A., and Felipe, A. (2005). Differential voltage-dependent K⁺ channel responses during proliferation and activation in macrophages. *J Biol Chem* *280*, 13204-13204.
- Vitaterna, M.H., Takahashi, J.S., and Turek, F.W. (2001). Overview of circadian rhythms. *Alcohol Research & Health* *25*, 85-+.
- Voets, T., Nilius, B., Hoefs, S., van der Kemp, A., Droogmans, G., Bindels, R.J.M., and Hoenderop, J.G.J. (2004). TRPM6 forms the Mg²⁺ influx channel involved in intestinal and renal Mg²⁺ absorption. *J Biol Chem* *279*, 19-25.
- Voya, J.C., Via, D.P., Butterfield, C.E., and Zetter, B.R. (1984). Identification and isolation of endothelial-cells based on their increased uptake of acetylated-low density lipoprotein. *Journal of Cell Biology* *99*, 2034-2040.
- Voytik-Harbin, S.L., Brightman, A.O., Waisner, B., Lamar, C.H., and Badylak, S.F. (1998). Application and evaluation of the alamarBlue assay for cell growth and survival of fibroblasts. *In Vitro Cellular and Developmental Biology Animal* *34*, 239-246.
- Walev, I., Reske, K., Palmer, M., Valeva, A., and Bhakdi, S. (1995). Potassium-inhibited processing of IL-1-beta in human monocytes. *Embo Journal* *14*, 1607-1614.
- Wang, K., Xue, T., Tsang, S.Y., Van Huizen, R., Wong, C.W., Lai, K.W., Ye, Z.H., Cheng, L.Z., Au, K.W., Zhang, J., et al., (2005). Electrophysiological properties of pluripotent human and mouse embryonic stem cells. *Stem Cells* *23*, 1526-1534.
- Wang, S., Meng, F., Mohan, S., Champaneri, B., and Gu, Y. (2009a). Functional ENaC channels expressed in endothelial cells: a new candidate for mediating shear force. *Microcirculation* *16*, 276-287.
- Wang, Y.F., Jia, H.J., Walker, A.M., and Cukierman, S. (1992). K-current mediation of prolactin-induced proliferation of malignant (NB2) lymphocytes. *Journal of Cellular Physiology* *152*, 185-189.

Wang, Z., Wong, N.C., Cheng, Y., Kehl, S.J., and Fedida, D. (2009b). Control of voltage-gated K⁺ channel permeability to NMDG(+) by a residue at the outer pore. *J Gen Physiol* 133, 361-374.

Whiteaker, K.L., Gopalakrishnan, S.M., Groebe, D., Shieh, C.C., Warrior, U., Burns, D.J., Coghlann, M.J., Scott, V.E., and Gopalakrishnan, M. (2001). Validation of FLIPR membrane potential dye for high throughput screening of potassium channel modulators. *Journal of Biomolecular Screening* 6, 305-312.

Wiecha, J., Munz, B., Wu, Y., Noll, T., Tillmanns, H., and Waldecker, B. (1998). Blockade of Ca²⁺-activated K⁺ channels inhibits proliferation of human endothelial cells induced by basic fibroblast growth factor. *J Vasc Res* 35, 363-371.

Wilson, G.F., and Chiu, S.Y. (1993). Mitogenic factors regulate ion channels in Schwann-cells cultured from newborn rat sciatic-nerve. *Journal of Physiology-London* 470, 501-520.

Wilson, G.F., Magoski, N.S., and Kaczmarek, L.K. (1998). Modulation of a calcium-sensitive nonspecific cation channel by closely associated protein kinase and phosphatase activities. *Proceedings of the National Academy of Sciences of the United States of America* 95, 10938-10943.

Wilson, H.A., Seligmann, B.E., and Chused, T.M. (1985). Voltage-sensitive cyanine dye fluorescence signals in lymphocytes: plasma membrane and mitochondrial components. *J Cell Physiol* 125, 61-71.

Wolff, C., Fuks, B., and Chatelain, P. (2003). Comparative study of membrane potential-sensitive fluorescent probes and their use in ion channel screening assays. *Journal of Biomolecular Screening* 8, 533-543.

Wonderlin, W.F., Woodfork, K.A., and Strobl, J.S. (1995). Changes in membrane-potential during the progression of MCF-7 human mammary-tumor cells through the cell-cycle. *Journal of Cellular Physiology* 165, 177-185.

Worrell, R.T., Butt, A.G., Cliff, W.H., and Frizzell, R.A. (1989). A volume-sensitive chloride conductance in human colonic cell line T84. *American Journal of Physiology* 256, C1111-1119.

Wright, S.H. (2004). Generation of resting membrane potential. *Advances in Physiology Education* 28, 139-142.

Wu, J., Zhong, D., Fu, X., Liu, Q., Kang, L., and Ding, Z. (2014). Silencing of Ether à Go-Go 1 by shRNA inhibits osteosarcoma growth and cell cycle progression. *International Journal of Molecular Sciences* 15, 5570-5581.

Xiao, B., Coste, B., Mathur, J., and Patapoutian, A. (2011). Temperature-dependent STIM1 activation induces Ca²⁺ influx and modulates gene expression. *Nature Chemical Biology* 7, 351-358.

Xu, B., Mao, J., Wang, L., Zhu, L., Li, H., Wang, W., Jin, X., Zhu, J., and Chen, L. (2010). ClC-3 chloride channels are essential for cell proliferation and cell cycle progression in nasopharyngeal carcinoma cells. *Acta Biochimica Et Biophysica Sinica* 42, 370-380.

Yamashina, S., Konno, A., Wheeler, M.D., Rusyn, I., Rusyn, E.V., Cox, A.D., and Thurman, R.G. (2001). Endothelial cells contain a glycine-gated chloride channel. *Nutrition and Cancer-an International Journal* 40, 197-204.

Yang, J.W., Chang, E., Cherry, A.M., Bangs, C.D., Oei, Y., Bodnar, A., Bronstein, A., Chiu, C.P., and Herron, G.S. (1999). Human endothelial cell life extension by telomerase expression. *J Biol Chem* 274, 26141-26148.

Yang, M., and Brackenbury, W.J. (2013). Membrane potential and cancer progression. *Frontiers in physiology* 4.

Yang, S.J., Liang, H.L., Ning, G., and Wong-Riley, M.T.T. (2004). Ultrastructural study of depolarization-induced translocation of NRF-2 transcription factor in cultured rat visual cortical neurons. *European Journal of Neuroscience* 19, 1153-1162.

Yano, K., Higashida, H., Hattori, H., and Nozawa, Y. (1985). Bradykinin-induced transient accumulation of inositol trisphosphate in neuron-like cell-line NG108-15 cells. *Febs Letters* 181, 403-406.

Yasuda, T., Bartlett, P.F., and Adams, D.J. (2008). Kir and Kv channels regulate electrical properties and proliferation of adult neural precursor cells. *Molecular and Cellular Neuroscience* 37, 284-297.

Yin, S., Hu, Q., Luo, J., Li, Y., Lu, C., Chen, X., and Hu, H. (2014). Loureirin B, an essential component of Sanguis Draxonis, inhibits Kv1.3 channel and suppresses cytokine release from Jurkat T cells. *Cell & Bioscience* 4.

Yoshida, M., Giocomo, L.M., Boardman, I., and Hasselmo, M.E. (2011). Frequency of subthreshold oscillations at different membrane potential voltages in neurons at different anatomical positions on the dorsoventral axis in the rat medial entorhinal cortex. *Journal of Neuroscience* 31, 12683-12694.

Ypey, D.L., and Clapham, D.E. (1984). Development of a delayed outward-rectifying K⁺ conductance in cultured mouse peritoneal-macrophages. *Proceedings of the National Academy of Sciences of the United States of America-Biological Sciences* 81, 3083-3087.

Yu, S.P., and Choi, D.W. (2000). Ions, cell volume, and apoptosis. *Proceedings of the National Academy of Sciences of the United States of America* 97, 9360-9362.

Yu, S.P., Yeh, C.H., Strasser, U., Tian, M., and Choi, D.W. (1999). NMDA receptor-mediated K⁺ efflux and neuronal apoptosis. *Science* 284, 336-339.

Zagotta, W.N., and Siegelbaum, S.A. (1996). Structure and function of cyclic nucleotide-gated channels. *Annual Review of Neuroscience* 19, 235-263.

- Zhang, H., Zhang, J., Zha, R., Hu, M., and Wang, Y. (2011). Magnesium lithospermate B decreases Ca^{2+} (1) in endothelial cells by inhibiting K^+ currents. European Journal of Pharmacology 650, 285-289.
- Zhang, Y.Y., Yue, J., Che, H., Sun, H.Y., Tse, H.F., and Li, G.R. (2014). BKCa and hEag1 channels regulate cell proliferation and differentiation in human bone marrow-derived mesenchymal stem cells. J Cell Physiol 229, 202-212.
- Zhao, N., Dong, Q., Du, L.-L., Fu, X.-X., Du, Y.-M., and Liao, Y.-H. (2013). Potent Suppression of Kv1.3 Potassium Channel and IL-2 Secretion by Diphenyl Phosphine Oxide-1 in Human T Cells. Plos One 8.
- Zheng, F., Li, H., Du, W., and Huang, S. (2011). Role of hERG1 K^+ channels in leukemia cells as a positive regulator in SDF-1a-induced proliferation. Hematology 16, 177-184.
- Zheng, Y.J., Furukawa, T., Ogura, T., Tajimi, K., and Inagaki, N. (2002). M phase-specific expression and phosphorylation-dependent ubiquitination of the ClC-2 channel. J Biol Chem 277, 32268-32273.
- Zhou, Q.S., Zhao, J., Wiedmer, T., and Sims, P.J. (2002). Normal hemostasis but defective hematopoietic response to growth factors in mice deficient in phospholipid scramblase 1. Blood 99, 4030-4038.
- Zhu, Y., and Ikeda, S.R. (1993). Anomalous permeation of Na^+ through a putative K^+ channel in rat superior cervical-ganglion neurons. Journal of Physiology-London 468, 441-461.
- Zuidema, M.Y., Yang, Y., Wang, M., Kalogeris, T., Liu, Y., Meininger, C.J., Hill, M.A., Davis, M.J., and Korthuis, R.J. (2010). Antecedent hydrogen sulfide elicits an anti-inflammatory phenotype in postischemic murine small intestine: role of BK channels. American Journal of Physiology-Heart and Circulatory Physiology 299, H1554-H1567.